UNIVERSIDADE D
COIMBRA

Luciana Carolina Lopes Ferreira

Pathophysiology of Doxorubicin Cardiotoxicity: From Mitochondrial Homeostasis to Biological Clocks

Tese no âmbito do Doutoramento em Ciências Farmacêuticas, especialidade Toxicologia, orientada pelo Professor Doutor Paulo Jorge Oliveira e pelo Professor Doutor João Laranjinha e apresentada à Faculdade de Farmácia da Universidade de Coimbra.

Novembro de 2018

Faculdade de Farmácia
da Universidade de Coimbra

Pathophysiology of Doxorubicin Cardiotoxicity: From Mitochondrial Homeostasis to Biological Clocks

Luciana Carolina Lopes Ferreira

Tese de Doutoramento em Ciências Farmacêuticas,
ramo de Toxicologia, orientada pelo Professor Doutor Paulo Jorge Oliveira e pelo Professor Doutor João Laranjinha, apresentada à Faculdade de Farmácia da Universidade de Coimbra.

Novembro de 2018

UNIVERSIDADE D
COIMBRA

This work was conducted under the scientific supervision of Professor Paulo J. Oliveira, PhD, Center for Neurosciences and Cell Biology, Coimbra, Portugal; and Professor Paolo Sassone-Corsi, PhD, Center for Epigenetics and Metabolism, University of California, Irvine, CA, USA. The internal supervision was provided by Professor João Laranjinha, PhD, Center for Neurosciences and Cell Biology, Faculty of Pharmacy, University of Coimbra, Coimbra, Portugal.

The work presented in this dissertation was supported by a PhD fellowship from the Portuguese Foundation for Science and Technology (FCT) addressed to the author (SFRH/BD/52429/2013), the research grant from FCT addressed to Paulo J. Oliveira (PTDC/DTP-FTO/1180/2012), and by an institutional grant (POCI-01-0145-FEDER-007440).

UNIÃO EUROPEIA
Fundo Europeu
de Desenvolvimento Regional

Part of this work resulted from a collaboration with Professor Paolo Sassone-Corsi
from the Center for Epigenetics and Metabolism,
University of California, Irvine, CA, USA.

ACKNOWLEDGEMENTS/ AGRADECIMENTOS

Fundação Portuguesa para a Ciência e a Tecnologia pelo apoio financeiro concedido na forma de bolsa individual (PD/BD/52429/2013) e projeto financiado no âmbito deste estudo, que permitiu desenvolver o trabalho apresentado nesta tese.

Programa Doutoral em Bioquímica e Biofísica Médicas (M2B), por me permitir embarcar neste projeto e Dr. João Laranjinha pelo apoio prestado.

Dr. Paulo Oliveira, pela orientação ao longo destes anos, por me dar condições para desenvolver o meu trabalho e, não menos importante, por incentivar um bom ambiente de laboratório. Agradeço a sua disponibilidade, correções e partilha de entusiasmo, assim como por me permitir desenvolver o meu projeto com bastante independência e autonomia.

Dr. Paolo Sassone-Corsi for accepting me in his lab. During the past four years, this experience was, without a doubt, the most challenging and enriching. I am thankful for the high demand for quality and knowledge sharing. I extent my acknowledgements to all the lab members that kindly made me feel so welcomed: Carolina, Emilie, Paola, Marlene, Jonathan, Mari, Ken, Leonardo, Shogo and Elizabeth.

Todas as pessoas com quem, independentemente de por períodos mais ou menos longos, tive a oportunidade de trabalhar e privar no laboratório. Todas elas contribuíram para o meu crescimento. Um especial obrigada à Cláudia, Susana, Ana Maria, Tatiana, Teresa Serafim, José, Ricardo, Guida, Vilma, Rui, Liljana e Caroline. Obrigada à Teresa Oliveira por ter acompanhado de perto o meu percurso e pelos seus aconselhamentos e correções.

Funcionários do UC-Biotech, em especial à D. Alda, D. Adelaide e Leonor, pelo bom humor, pela disponibilidade em ajudar em todas as situações, e por nos facilitarem o nosso trabalho diário.

Fran and Alex for welcomed me with open arms in their house and for introducing me to the real american culture. It was wonderful to meet so many different people and having them has my house mates. A special thanks to Karen, for trying to make me feel at home since the first day.

Minhas amigas do coração, não são muitas mas são as melhores. Diva, Lara, Andreia e Noémi. Sempre presentes, mesmo quando a presença física nem sempre é fácil. Um enorme obrigada.

Diogo, meu companheiro e melhor amigo, por conseguires tornar leve o que parece pesado e por ao teu lado me fazeres sentir em casa.

Minha família, sem a qual nada disto teria sido possível. Aos meus avós, aos que estão cá e aos que já partiram, obrigada pelos valores e pelo carinho. Às minhas tias e primos. Ao Gil. À minha irmã, a prenda que sempre quis. E principalmente às pessoas mais importantes da minha vida, os meus pais.

PUBLISHED WORK

Part of the work included in this thesis is already published or submitted to international peer-reviewed scientific journals or published as book chapters, as follows:

Teresa Cunha-Oliveira*, Luciana L. Ferreira*, Ana Raquel Coelho, Cláudia C. M. Deus, Paulo J. Oliveira, (2018) **Doxorubicin triggers bioenergetic failure and p53 activation in mouse stem cell-derived cardiomyocytes**. *Toxicol Appl Pharmacol*, 348:1-13 **these authors contributed equally to this work*

Luciana L. Ferreira, Teresa Cunha-Oliveira, Caroline D. Veloso, Cláudio F. Costa, Kendall B. Wallace, Paulo J. Oliveira, **Single nanomolar doxorubicin exposure triggers compensatory mitochondrial responses in H9c2 cardiomyoblasts**. *Food Chem Toxicol*, (*under second round review)*

Luciana L. Ferreira*, Ana Raquel Coelho*, Paulo J. Oliveira, Teresa Cunha-Oliveira, **Mitochondrial Toxicity Induced by Chemotherapeutic Drugs**, ed. Yvonne Will and James A. Dykens, 593-612. New Jersey, NJ: John Wiley & Sons, Inc. ISBN: 9781119329725 (2018) **these authors contributed equally to this work*

Luciana L. Ferreira, Paulo J. Oliveira, Teresa Cunha-Oliveira, **Epigenetics in doxorubicin cardiotoxicity**, ed. Ramón Cacabelos, Elsevier, ISBN 9780128139394, *in press*.

Results presented in this thesis have been presented in national and international scientific meetings in the form of oral and poster communications.

CONTENTS

LIST OF FIGURES

LIST OF TABLES

ABBREVIATIONS

AceCS1	acetyl-CoA synthetase 1
Acetyl Co-A	acetyl coenzyme A
ACLY	ATP-citrate lyase
ADP	adenosine diphosphate
AIF	apoptosis-inducing factor
AMPK	AMP-activated protein kinase
ANP	atrial natriuretic peptide
ANT	adenine nucleotide translocase
ATP	adenosine triphosphate
BAK	BCL-2 homologous antagonist/killer
BAX	BCL-2 associated X protein
BCL-2	B-cell CLL/lymphoma 2
BID	BH3 interacting-domain death agonist
Bmal1	brain and muscle ARNT-Like 1
BNP	brain natriuretic peptide
CCG	clock controlled gene
CHF	congestive heart failure
CLOCK	circadian locomotor output cycles kaput
CRY	cryptochrome
CsA	cyclosporin A
CypD	cyclophilin D
DBP	D-box binding protein
DCA	dichloroacetate
DEX	dexamethasone
DISC	death-inducing signaling complex
DNA	deoxyribonucleic acid
DOX	doxorubicin
DOXol	doxorubicinol
DRZ	dexrazoxane
EMA	European Medicines Agency
eNOS	endothelial isoform of nitric oxide synthase
ETC	electron transport chain
FAD	flavin adenine dinucleotide
FADD	Fas-Associated protein with death domain
FAO	fatty acid oxidation

FCCP	trifluorocarbonylcyanide phenylhydrazone
FDA	Food and Drug Administration
GPX	glutathione peroxidase
H_2O_2	hydrogen peroxide
HAT	histone acetyltransferase
$HO^{\cdot}$	hydroxyl radical
IMM	inner mitochondrial membrane
iNOS	inducible isoform of nitric oxide synthase
iPSC	induced-pluripotent stem cell
kb	kilobase
LVEF	left ventricular ejection fraction
miRNA	microRNA
mPTP	mitochondrial permeability transition pore
mtDNA	mitochondrial DNA
NAD^+	nicotinamide adenine dinucleotide, oxidized form
NADH	nicotinamide adenine dinucleotide, reduced form
NAM	nicotinamide
NAMPT	nicotinamide phosphoribosyltransferase
NMN	nicotinamide mononucleotide
NO	nitric oxide
Noxa	phorbol-12-myristate-13-acetate-induced protein 1
$O_2^{\cdot -}$	superoxide radical
OMM	outer mitochondrial membrane
$ONOO^-$	peroxynitrite
OXPHOS	oxidative phosphorylation
PARP	poly-ADP ribose polymerase
PDC	pyruvate dehydrogenase complex
PDH	pyruvate dehydrogenase enzyme
PDK	pyruvate dehydrogenase kinase
PER	period protein
PGC-1α	peroxisome proliferator-activated receptor gamma coactivator 1α
PRX	peroxiredoxin
PUMA	p53-upregulated modulator of apoptosis
RNA	ribonucleic acid
ROR	retinoic acid-related orphan receptor
ROS	reactive oxygen species

SAM	s-adenosyl-L-methionine
SCN	suprachiasmatic nucleus
SIRT	sirtuin
SMAC/Diablo	second mitochondria-derived activator of caspases
SOD	superoxide dismutase
SRB	sulforhodamine B assay
TCA	tricarboxylic acid
TEF	thyrotroph embryonic factor
TFAM	mitochondrial transcription factor A
TopII	topoisomerase II
ULK1	UNC-51–like kinase 1
VDAC	voltage-dependent anion channel
ZT	zeitgeber time
ΔΨm	mitochondrial transmembrane potential

ABSTRACT

Doxorubicin is one of the most widely used chemotherapeutic agents due to its effectiveness against a broad-spectrum of malignancies. However, its clinical use is hampered by severe dose-dependent and cumulative cardiotoxic side effects that lead to cardiomyopathies and congestive heart failure. Importantly, late-onset symptoms of cardiac toxicity have been observed in childhood cancer survivors. Despite the advances in the field in terms of preventive measures and doxorubicin delivery mechanisms, the cardiotoxicity is still a treatment bottleneck. Mitochondrial dysfunction and DNA damage are the mechanisms that better explain the toxicity of doxorubicin, but it is believed that is a combination of effects that leads to the life-threatening heart problems. Therefore, it is important to elucidate the various aspects of the pathophysiology of doxorubicin-associated cardiotoxicity in order to establish targeted interventions that could minimize the side effects without interfering with the anticancer capacity.

The present dissertation aims to contribute for the understanding of mechanisms underlying acute and chronic forms of doxorubicin-induced cardiotoxicity, and several research questions related with this subject are addressed. The first question was whether preconditioning of myoblastic H9c2 cell line with sub-clinical doses of doxorubicin would lead to an increase of cellular defenses and overall resistance against a further and higher dose exposure of doxorubicin (Chapter 5). We observed that doxorubicin pre-treatment, in low doses, was able to protect cell viability and mitochondrial activity from further damage by higher concentrations, without, apparently, interfering with the anticancer capacity. Even though the mechanisms were not completely elucidated, the results suggest the induction of a beneficial and possibly epigenetic-based mitochondrial adaptation. Multiple studies in doxorubicin field have been performed with H9c2 cardiomyoblasts over the past years. However, other *in vitro* models have gained interest due to their resemblance with mature cardiomyocytes, including induced-pluripotent stem cell (iPSC)-derived

cardiomyocytes. Thus, our next aim was to conduct acute doxoxubicin-exposure experiments to investigate the morphological, functional and biochemical changes occurring in the iPSC-derived mouse cardiomyocytes and validate these cells as a model to study doxorubicin-induced cardiotoxicity (Chapter 6). Our results reinforced the dose-dependent nature of doxorubicin cardiotoxicity. From the two different concentrations of doxorubicin tested (0.5 and 1 μM), the highest dose of drug induced a high degree of apoptosis, while the lowest dose led to early apoptotic events, decreased mitochondrial oxygen consumption rates and inhibition of pyruvate dehydrogenase by PDK4. The effects were partially prevented upon pre-treatment with the PDK inhibitor dichloroacetate. Lastly, it was hypothesized that doxorubicin exposure early in life could induce long-term cardiac dysfunction and compromise the normal transcriptional and signaling circadian homeostasis (Chapter 7). This assumption relied on the fact that the circadian clock, an important system for the maintenance of cardiac functions, is driven by the interplay with cellular metabolism and energy status. To test this hypothesis, juvenile C57BL/6J male mice (4 weeks age) were subjected to a sub-chronic doxorubicin treatment and several cardiac parameters were analyzed after a long period of recovery time. We observed that doxorubicin induced long-term cardiac dysfunction and interfered with oscillatory molecular mechanisms including gene expression rhythmicity and acetylation profiles of histone 3 (H3) and Bmal1. The molecular mechanisms behind doxorubicin detrimental effects were also supported by studies with synchronized murine embryonic fibroblasts (MEFs) and HEK293 cells.

Overall the results presented in this thesis not only reinforce previous observations regarding doxorubicin impact on mitochondrial function, metabolic remodeling and long-term transcriptional homeostasis but also describe, for the first time, other mechanisms of doxorubicin toxicity including the impact on pyruvate dehydrogenase complex and circadian rhythms. Furthermore, we demonstrated that doxorubicin preconditioning could be an interesting strategy during anticancer therapies. In

conclusion, our data helped to clarify several aspects of doxorubicin impact on cardiac cells and hopefully contribute to a better understanding of its pathogenesis and development of more effective interventions.

Keywords: Doxorubicin, Cardiotoxicity, Heart, Mitochondria, Apoptosis, Circadian rhythm

RESUMO

A doxorubicina é um dos fármacos antineoplásicos mais amplamente utilizados devido à sua eficácia no tratamento de um vasto espectro de cancros. No entanto, a sua utilização clínica é limitada por graves efeitos secundários associados à cardiotoxicidade cumulativa dependente da dose que pode levar ao desenvolvimento de cardiomiopatias e insuficiência cardíaca. Um aspeto particularmente importante é o facto de sintomas persistentes da toxicidade cardíaca terem sido observados em sobreviventes de cancros infantis. Apesar dos avanços em medidas preventivas e mecanismos de administração controlados, a cardiotoxicidade continua a ser o maior obstáculo à eficácia do tratamento. A disfunção mitocondrial e os danos ao nível do DNA são os mecanismos que melhor explicam a toxicidade da doxorubicina. No entanto, acredita-se que é uma combinação de fatores que contribuem para os problemas cardíacos que podem pôr em causa a vida do paciente. Assim sendo, é importante elucidar os vários aspetos da fisiopatologia da cardiotoxicidade associada à doxorubicina de forma a estabelecer intervenções específicas que possam minimizar os efeitos secundários sem interferir com a capacidade anticancerígena.

Esta dissertação tem como principal objetivo contribuir para a compreensão dos mecanismos subjacentes à cardiotoxicidade aguda e crónica induzida pela doxorubicina, sendo abordados vários aspetos no âmbito desta temática. A primeira questão que se colocou foi se o pré-condicionamento da linha celular mioblástica H9c2 com doses subclínicas de doxorubicina induziria o aumento das defesas celulares e a resistência contra uma segunda exposição à doxorubicina em doses mais elevadas (Capítulo 5). O pré-tratamento com doses baixas de doxorubicina permitiu proteger a viabilidade celular e a atividade mitocondrial após uma segunda exposição a concentrações mais elevadas, sem que, aparentemente, a capacidade anticancerígena tenha sido afetada. Apesar de os mecanismos não terem sido completamente elucidados, os resultados sugerem a indução de uma adaptação mitocondrial, possivelmente relacionada com regulação epigenética. Nos últimos anos, vários

estudos têm utilizado as células H9c2 como modelo de cardiotoxicidade induzida pela doxorubicina. No entanto, outros modelos *in vitro* têm ganho interesse devido à sua maior semelhança com cardiomiócitos maduros, incluindo cardiomiócitos derivados de células estaminais pluripotentes induzidas (iPSC). O nosso objetivo seguinte foi expôr cardiomiócitos de murganho derivados de iPSC a tratamentos agudos com doxorubicina, analisando as subsequentes alterações morfológicas, funcionais e bioquímicas e validar estas células como um modelo adequado para estudar a cardiotoxicidade associada à doxorubicina (Capítulo 6). Os nossos resultados reforçaram a dependência dose-efeito. Das duas concentrações de doxorubicina utilizadas (0.5 e 1 μM), a dose mais elevada induziu apoptose, enquanto que a dose mais baixa levou à ocorrência de fenómenos precedentes à apoptose, diminuição das taxas de consumo de oxigénio mitocondrial e inibição da piruvato desidrogenase pela PDK4. Os efeitos foram parcialmente prevenidos após pré-tratamento com o inibidor de PDK, dicloroacetato. Por último, colocou-se a hipótese de que a exposição à doxorubicina numa fase precoce poderia induzir, a longo prazo, disfunção cardíaca e comprometer a normal homeostasia de fenómenos de transcrição e sinalização circadianos (Capítulo 7). Este pressuposto baseou-se no facto de o relógio circadiano, um sistema importante na manutenção das funções cardíacas, ser dependente da interação entre o metabolismo e o estado energético celular. De modo a testar esta hipótese, murganhos C57BL/6J machos juvenis (4 semanas) foram sujeitos a um tratamento sub-crónico com doxorubicina e, após um período de recuperação, vários parâmetros cardíacos foram avaliados. Observou-se que a doxorubicina induziu disfunção cardíaca persistente e interferiu com mecanismos moleculares oscilatórios, incluindo ritmicidade da expressão genética e perfis de acetilação da histona 3 (H3) e Bmal1. Os mecanismos moleculares foram também suportados por estudos utilizando fibroblastos embrionários de murganho (MEFs) sincronizados e células HEK293.

Os resultados apresentados nesta tese reforçam observações anteriores relativas ao impacto da doxorubicina na função mitocondrial e remodelação metabólica e

transcriptómica, mas também descrevem, pela primeira vez, outros mecanismos da toxicidade da doxorubicina, incluindo o impacto no complexo piruvato desidrogenase e nos ritmos circadianos. Além disso, demonstrou-se que o pré-condicionamento com doxorubicina poderá ser uma estratégia relevante durante o processo de terapia anticancerígena. Em conclusão, os nossos resultados ajudaram a clarificar vários aspetos do impacto da doxorubicina em células cardíacas e possivelmente contribuir para uma melhor compreensão da sua patogénese e desenvolvimento de intervenções clínicas mais eficazes.

Palavras chave: Doxorubicina, Cardiotoxicidade, Coração, Mitocôndria, Apoptose, Ritmo Circadiano

GENERAL INTRODUCTION

Chapter 1

1. Doxorubicin: from anti-cancer to cardiotoxicant

Doxorubicin (DOX; Adriamycin) belongs to the anthracycline family of antibiotics and was first isolated in 1969 from *Streptomyces peucetius* var. *caesius* [1]. Since its approval by the US Food and Drug Administration (FDA) in 1974, DOX emerged as one of the most frequently used antineoplastic agents prescribed for cancer chemotherapy. Malignant neoplasms in which DOX is mostly used include leukemias, lymphomas, bladder, breast and thyroid cancers, multiple myeloma and others [2, 3]. Molecularly, DOX possesses a rigid planar tetracyclic structure with adjacent quinone and hydroquinone moieties and an aminosugar attached to one of the rings by a glycosidic bond. Large advances were achieved in cancer medicine since the initial use of DOX in the treatment of malignant neoplasms. This is particularly evident in pediatric oncology, where its important role on hematological cancer treatments soon turned it into one of the most prescribed drugs. In fact, over the last 50 years, the 5-years survival rate for pediatric cancers improved from about 50% to 80%, whereas it is estimated that over 50% of the childhood cancer regimens incorporated anthracyclines [4, 5]. However, the effectiveness of the treatment is variable, often determined by either the dosage administered, the type of tumor or the individuality of the patient. Typically, DOX adult dose range used in treatments is 40-75 mg/m^2 every 21 to 28 days and can be used as single agent or in combination with other chemotherapeutic agents [6]. Passive diffusion is the main DOX transmembrane transport mechanism, leading to much higher intracellular concentrations than in the extracellular milieu [7, 8]. In terms of pharmacokinetics, DOX plasma concentration-time curve can be described

by a biexponential model. During the first hours after infusion DOX concentration declines rapidly to nanomolar concentrations, and is then followed by a second phase presenting a slower rate of elimination, contributing to a terminal half-life of about 20-30 hours [9, 10]. Plasma clearance in mostly mediated by hepatic metabolism and biliary excretion [9]. In the liver, one of the principal organs responsible for detoxification in the body, cytosolic enzymes – carbonyl reductases and aldo-keto reductases – reduce DOX into its main circulating alcohol metabolite, doxorubicinol (DOXol). Other products resulting from DOX and DOXol metabolization, the aglycones, were also detected in plasma and human cardiac cytosol [9, 11]. It is estimated that 40-50% of the administered dosage is excreted predominantly via bile in faeces within 7 days, while 5-10% of the drug and its metabolites appear in urine within 5 days [12].

For a long time, DOX precise mode of anticancer action was not well defined. The first proposed mechanism for the cytotoxicity on cancer cells was based on DNA intercalation. This process is initiated when DOX enters the cell by diffusion and binds to the proteasome in the cytoplasm. Later, DOX is translocated through the nuclear pores into the nucleus where it binds to nuclear DNA due to the higher affinity for the DNA over the proteasome [13]. When DNA is physically constrained, the separation of the double strand induces DNA supercoils and, as consequence, torsional stress and dysregulation of processes such as replication and transcription [14]. DOX was found to intercalate not only with nuclear DNA but also with mitochondrial DNA (mtDNA) [15]. Coldwell and colleagues measured DOX-DNA adducts using accelerator mass spectrometry and found that treatment with clinically relevant DOX concentrations resulted in the formation of adducts within an hour of drug treatment [16]. The formation of more DOX-DNA adducts may contribute to an increased effectiveness of the drug in tumor cells. However, today is commonly accepted that the inhibition of topoisomerase IIα (TopIIα) is the main mechanism of DOX antitumor action. Topoisomerases are highly conserved enzymes present in all types of living

organisms. More specifically, topoisomerases II constitute a family of nuclear enzymes essentials to all life forms, capable of cleaving and rejoining DNA strands in a controlled manner [17], existing in two isoforms in humans: alpha and beta, which are encoded by different genes. TopIIα is predominantly present in actively replicating cells (such as cancer cells) and it works by untangling DNA duplexes after replication or transcription, introducing transient double strand breaks into DNA segments resulting on the relaxation of the over-coiled DNA and, finally, resealing the break [17]. DOX belongs to a class of drugs that increases the levels of TopII:DNA covalent complexes, stabilizing the cleavage complex and impeding the DNA resealing, leading to an increase in double strand breaks and apoptosis [18]. Moreover, the generation of free radicals, causing oxidative damage to cellular membranes, proteins and DNA (explored in more detail in section 1.2.1.2) is also a mechanism of cytotoxicity on malignant cells [19, 20].

Despite the efficiency against tumor cells, DOX clinical use soon proved to be hampered by serious liabilities, including the development of resistance in tumor cells and off-target complications, namely dose-dependent and cumulative cardiotoxicity [21]. Basically, "dose-dependent" means that incremental, and partially irreversible damage occurs with each administration of the drug and that the second administration adds a sequential adverse effect to the organ already damaged from the first exposure. These adverse cardiac effects can range from sub-clinical ventricular dysfunction, usually quantified through the measurement of left ventricular ejection fraction (LVEF), to chronic cardiomyopathy and congestive heart failure (CHF). It was reported that DOX-related CHF was detected in around 26% of patients treated with a cumulative DOX dose of 550 mg/m^2 [22]. It is known that the likelihood of developing cardiomyopathy and the response of the patient to the treatment are associated with gender [23], age [22], ethnicity [24], cumulative doses [21] or even body size, which influences the pharmacokinetics and metabolism of the drug. The response of patients to drugs is not linear and, in fact, some patients are

more tolerant to high doses of DOX while others present cardiac events at low doses [25]. Importantly, the published reports usually focus on different populations and follow-up periods and, sometimes, different definitions of cardiotoxicity, contributing for the variability of results. DOX cardiotoxicity can usually be categorized into acute and chronic forms, with the latter being presented as early- or late- onset manifestations. Acute cardiotoxicity occurs shortly after initiation of a DOX regimen (usually within a few hours of infusion or during the course of the treatment), but with the current treatment protocols, acute cardiac alterations became infrequent, occurring in no more than about 1% of patients, being usually reversible [24, 26]. Acute effects are manifested usually as reversible myopericarditis, left ventricular dysfunction or arrhythmias [27]. The early-onset form is developed several weeks or months after the treatment. It is characterized, usually, by the development of left ventricular systolic dysfunction that can progress toward dilated cardiomyopathy and CHF [24]. The late-onset (or delayed) form, can arise years or even decades after completing the regimens and is associated with abnormal left ventricle structure and function, echocardiographic and pathologic changes and CHF [28]. The latter was first described in the 1990's, mainly among survivors of childhood cancers [29-31]. The effects of DOX administration can eventually be hampered by other factors, synergizing with unfavorable lifestyle and health conditions such as hypertension, diabetes, obesity, exposure to other cytotoxic drugs or prior heart problems [32]. Structurally, DOX-induced cardiotoxicity involves cardiomyocyte hypertrophy, mitochondrial swelling, cytoplasm vacuolization, nuclear enlargement, loss of myofibrils, and fibrosis [33-35]. The early detection and prevention of treatment-related cardiotoxicity is challenging and the treatment of DOX-induced CHF is still limited to the normal approaches for the treatment of regular chronic heart failure [36]. Echocardiography is commonly used in the short- and long-term monitoring, together with serum biomarkers of cardiotoxicity (cardiac troponin I, brain natriuretic peptide [BNP], atrial natriuretic peptide [ANP]) [27]. However, the cardiovascular monitoring

is still challenging and the limitation of cumulative DOX doses (400 to 550 mg/m^2) is usually the preferred approach, although lower doses may represent lower cancer response rates [37].

1.1. The heart of the problem

Most of the drugs used in chemotherapy act by inhibiting the exacerbated proliferative profile observed in cancer cells. Inevitably, other body cells with high division rates are also damaged. Cardiomyocytes possess a very limited proliferation rate, but they are particularly vulnerable to long-term exposure and damage caused by anthracyclines. Although not exclusively (hepato- and nephron-toxicity were also reported [38-40]), the greatest target of DOX-induced toxicity is, in fact, the heart. Many authors have explained this unique susceptibility of the myocardium and many hypotheses originated. Drug distribution measurements soon proved different accumulation in rat organs [41]. After the exposure to one dose of DOX (1 or 4 mg DOX/kg, intra-peritoneal injection in rats), the liver was the organ exhibiting higher levels of the drug, but cumulative doses did not produce higher levels than a single dose. In contrast, the cardiac tissue showed a slower but constant DOX accumulation, reaching much higher levels than the other tissues analyzed [41].

It is also believed that the heart is particularly vulnerable to DOX because of the high density of mitochondria in cardiomyocytes (35% of the total cell volume), which are highly dependent on mitochondrial ATP [42]. Cardiolipins, mitochondrial negatively-charged phospholipids present mostly in the inner membrane, have an increased affinity for anthracyclines contributing to increased mitochondrial accumulation [43]. There, DOX undergoes redox cycling with the production of superoxide radicals, which lead to cellular damage and death. In addition, the heart apparently shows a less active antioxidant defense network when compared to liver, leaving the former

organ less protected against free radical and oxidative stress [44]. DOX itself also causes the depletion of glutathione peroxidase activity [44]. Additionally, the heart is commonly considered a terminally differentiated organ composed mostly by cardiomyocytes, fibroblasts and endothelial cells and it has a very restricted regenerative capacity [45]. The limited pool of stem cells found in the heart are thought to be quiescent under normal conditions, but essential for cardiac homeostasis and creation of new cardiomyocytes and vascular cells after injury [45-47]. In a pediatric animal model of late-onset DOX cardiotoxicity, mice exposed to DOX presented impaired vascular development and decreased capillary density [48]. Moreover, these animals were extremely more susceptible to myocardial infarction, presenting a survival rate of 25%, compared with saline treated animals (80%), and a much lower number of progenitor cells were observed in the border zone of the infarcted heart [48]. These results reinforce that early-life exposure to DOX decreases heart resistance to further stresses even though no obvious cardiac abnormalities were observed during adult life, one explanation is by reducing the pool of cardiac and endothelial progenitor cells.

1.2. Mechanisms of DOX-induced cardiotoxicity

The pathogenesis of DOX is complex and multidirectional and the mechanisms on the basis of cardiotoxicity are usually considered independent from the anticancer mechanisms. Evidences suggest that oxidative stress and TopIIβ inhibition are the prime sources of cardiac dysfunction but multiple other deleterious mechanisms have also been proposed. In the following sections some of the molecular mechanisms behind DOX-related cardiotoxicity that can ultimately lead to cardiomyocytes death and heart failure will be discussed.

1.2.1. Role of mitochondria and oxidative stress

1.2.1.1. Mitochondria: an overview

Mitochondria are essential dynamic organelles with a central role on many cellular pathways, being the production of ATP through oxidative phosphorylation (OxPhos) process its most recognized task. These organelles are present in almost all eukaryotic cells and act actively in cell homeostasis, from the synthesis of intermediary metabolites to the modulation of cell signaling and death pathways. According to the endosymbiotic theory, mitochondria arose from an alpha-proteobacterium engulfed by an archeal cell host, and this event seemed to be the main driving force for the eukaryogenesis, even though there are still remaining open questions [49]. The symbiotic and mutually beneficial relationship experienced by both living forms allowed a profound rearrangement of the eukaryotic cell host energy production, that shifted from the cell membrane to the mitochondrial membrane. One evidence for the endosymbiotic theory is the fact that many copies of a circular mitochondrial genome (mtDNA) are still present in mitochondria. However, the mitochondrial genome suffered many transformations over time, with most of the bacterial genes being lost or transferred to the nuclear genome. In the majority of the eukaryotic organisms, the mtDNA is a circular molecule with ~16 kb and encodes 13 proteins that are part of the mitochondrial OxPhos complexes, two ribosomal RNAs and 22 tRNAs, necessary for the semi-autonomous mitochondrial gene expression processes. More recently, regulatory peptides encoded as short reading frames (sORFs) were also identified in the mitochondrial genome, including humanin and MOTS-c [50, 51]. Although essential for mitochondrial function, the proteins encoded by the mitochondrial DNA are a minority compared to the mitochondrial proteins encoded by the nuclear DNA (more than 1,000), which requires a harmonious crosstalk between both genomes [52-54]. The nuclear control over mitochondrial activity and biogenesis is referred as "anterograde regulation", while the capacity of mitochondria to control the expression

of nuclear genes through the reprogramming of the cellular metabolism is called "retrograde response" [55]. Both contribute for the cellular normal function and plasticity.

Structurally, mitochondria possess two separate and functionally distinct outer (OMM) and inner (IMM) membranes that delimitates an intermembrane space and the mitochondrial matrix. Five complexes which participate in OxPhos are embedded in the IMM: NADH/ubiquinone oxireductase (or NADH dehydrogenase, complex I), succinate dehydrogenase (complex II), cytochrome *c* reductase (complex III), cytochrome *c* oxidase (complex IV) and ATP synthase (complex V), but only complexes I-IV belong to the electron transport chain (ETC) (Fig. 1.1). Although is still debatable, many authors defend that some complexes are organized in the IMM into larger structures called supercomplexes or respirasomes, in order to increase the efficiency in electron transport and reduce the overproduction of reactive oxygen species (ROS) [56-58].

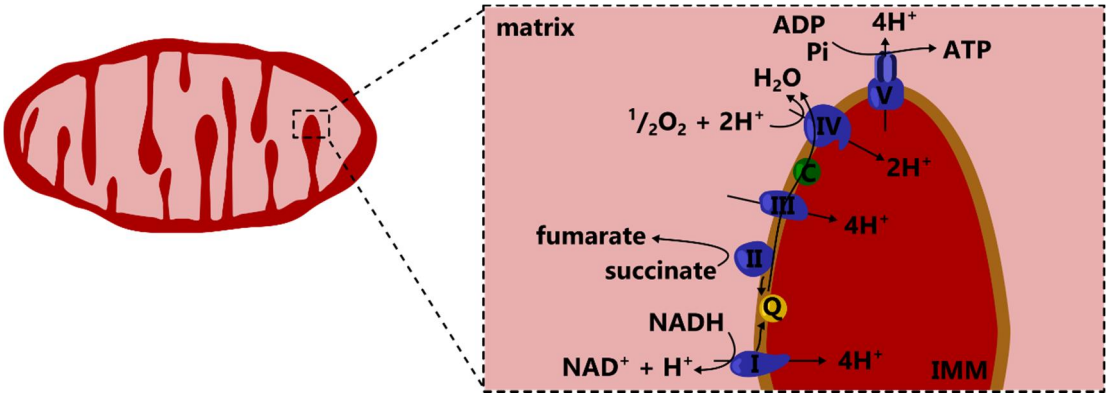

Figure 1.1: Schematic representation of the oxidative phosphorylation in mitochondria. Electrons derived from NADH and succinate are transported through the electron transport chain (complexes I, II, III and IV) and protons are pumped from the matrix to the intermembrane space. The established gradient is then used by ATP synthase (complex V) to phosphorylate ADP and form ATP. C, cytochrome *c*; H+, proton; Pi, inorganic phosphate; Q, ubiquinone (coenzyme Q).

The tricarboxylic acid (TCA) cycle, another essential pathway in mitochondria, generates reduced molecules (NADH and succinate) that donate electrons and fuel the sequential redox reactions and conformational changes in the ETC, with the consequent pumping of protons from the matrix to the intermembrane space. Complex II is also a component of the TCA cycle, functioning as a linker between the two important pathways, but while in the TCA cycle it oxidizes succinate to fumarate, in the context of OxPhos it transfers the electrons from succinate to ubiquinone [59]. In addition, complex II is the only ETC component that does not pump protons. Sequentially, NADH and succinate enter the ETC through complex I and II, respectively, and the electrons are transferred to ubiquinone and then from there to complex III, cytochrome *c* and complex IV, which finally transfers them to molecular oxygen (Fig. 1.1). The proton gradient, namely its electric component ($\Delta\Psi$), formed in this process is then used by complex V to synthesize ATP, through the phosphorylation of ADP. Complex V is preferably found at the edge of the mitochondrial cristae, with the other complexes along the side, and it was suggested that this placement is fundamental for the creation of the proton gradient and accumulation of protons in the concave side of the cristae [60, 61]. Complexes II and III, but mostly complex I, are known to mediate the production of ROS which work in the homeostatic signaling pathways but, when exacerbated, can damage key cellular components [62, 63]. In order to keep ROS levels under control, the cell needs to maintain a balance between ROS production and ROS neutralizers. However, if the balance sways to excessive ROS production, a condition of oxidative stress develops, which can extend from enzyme inactivation by thiol cross-linking to global macromolecular damage [64]. To fight the oxidative stress, cells have an antioxidant machinery composed by enzymes such as superoxide dismutases (SODs), gluthatione peroxidases (GPXs), catalase, glutathione reductase, peroxiredoxins and non-enzymatic molecules including the glutathione/ glutathione disulfide redox couple [65]. The mitochondrial inner membrane $\Delta\Psi$ is a very critical factor, because when too

high it favors electron leak and excessive ROS production, but if it is very low, the ATP production is reduced. Thus, a very thin line separates a healthy from a stressed state. Moreover, in mitochondria, long chain fatty acids can be converted to acetyl-CoA, through the fatty acid β-oxidation pathway, and many cellular metabolites can be produced. In fact, some cofactors and substrates of important epigenetic enzymes are mitochondrially-regulated and the mitochondrial metabolism impacts the epigenetic dynamics of histone modifications such as acetylation and methylation or DNA methylation [55]. Acetyl-CoA and NAD^+, for instance, are cofactors of histone acetyltransferases and NAD^+-dependent histone deacetylases (sirtuins, SIRTs), respectively. More recently, mtDNA itself was found to be epigenetically regulated [66, 67].

Mitochondria also participate in calcium (Ca^{2+}) homeostasis [68, 69]. The accumulation of Ca^{2+} in mitochondria occurs via the mitochondrial Ca^{2+} uniporter (MCU) and is driven by the mitochondrial $\Delta\Psi$ (-180 mV under physiological conditions), being counteracted by the mitochondrial Na^+/Ca^{2+} and H^+/Ca^{2+} exchangers. Despite the low affinity of MCU to Ca^{2+}, the proximity of mitochondria to the endoplasmic or sarcoplasmic reticulum, where the Ca^{2+} levels are high, stimulates the uptake [70, 71]. The increase of Ca^{2+} in mitochondria is a transient process that stimulates Ca^{2+}-sensitive dehydrogenases and consequently respiration, but Ca^{2+} overload may lead to mitochondrial damage, opening of the mitochondrial permeability transition pore and apoptosis [69, 70, 72]. Morphologically, mitochondria are extremely dynamic organelles and it is believed that they barely exists as independent bean-shaped structures as accepted for many years. Instead, they exist in an interconnected network and shift from elongated to fragmented organelles, via fusion and fission events [73, 74]. More recently, mitochondrial nanotunnels were also described as tubular double-membrane protrusions that connect the matrices of non-adjacent mitochondria and participate in intermitochondrial communication [75].

1.2.1.2. The oxidative stress-based mechanism

Due to its chemical structure, DOX is easily reduced to a semiquinone free radical by several enzymes, including NADH dehydrogenase (or complex I), NADPH oxidase, cytochrome P450 reductase, nitric oxide synthase or xanthine oxidase [76, 77]. These enzymes have the capacity of accepting electrons from NADH or NADPH and transfer them to DOX. Even though many cellular compartments were described as potential sites of ROS production, mitochondria have a prominent role since mitochondrial NADH dehydrogenase is the main responsible for DOX redox cycling [78]. The process starts with one-electron reduction of the quinone ring of DOX-tetracyclic structure (**eq. 1**) (Fig. 1.2), which leads to the formation of the semiquinone free radical ($DOX^{\bullet-}$). $DOX^{\bullet-}$ can reduce molecular oxygen forming the superoxide radical $O_2^{\bullet-}$ [79]. DOX can then again undergo redox cycle, being alternatively reduced and oxidized through the reaction with electron donors and acceptors, functioning as an intermediate and leading to the generation of even more $O_2^{\bullet-}$ (**eq. 2**). This oxygen radical has a short lifetime in aqueous solution due to the fast reaction with another $O_2^{\bullet-}$ and producing hydrogen peroxide (H_2O_2) (**eq. 3**). Alternatively, $O_2^{\bullet-}$ can be converted by superoxide dismutases (SODs) to H_2O_2. H_2O_2 is much more stable and less reactive than $O_2^{\bullet-}$ and, under physiological conditions, its excess is eliminated by catalase or glutathione peroxidase. However, $O_2^{\bullet-}$ and H_2O_2 can also interact producing a hydroxyl radical ($HO^{\bullet}$), much more cytotoxic than the parent compounds (**eq. 4**). In the presence of a transition metal catalyst, particularly iron, the interaction of $O_2^{\bullet-}$ with H_2O_2 is accelerated and can be divided into two parts, with iron being reduced and then oxidized (**eq. 4.1** and **eq. 4.2**) (Haber-Weiss reaction, 1934) [80, 81]. Interestingly, it was later described that $DOX^{\bullet-}$, through the generation of $O_2^{\bullet-}$, could mediate a rapid release of iron from ferritin, the major intracellular iron storage protein [82].

$DOX + e \rightarrow DOX^{\bullet -}$ **(equation 1)**

$DOX^{\bullet -} + O_2 \leftrightarrow DOX + O_2^{\bullet -}$ **(equation 2)**

$O_2^{\bullet -} + O_2^{\bullet -} + 2H^+ \rightarrow H_2O_2 + O_2$ **(equation 3)**

$O_2^{\bullet -} + H_2O_2 \rightarrow O_2 + HO^- + HO^{\bullet}$ **(equation 4)**

$O_2^{\bullet -} + Fe^{3+} \rightarrow O_2 + Fe^{2+}$ **(equation 4.1)**

$H_2O_2 + Fe^{2+} \rightarrow HO^- + HO^{\bullet} + Fe^{3+}$ **(equation 4.2)**

Moreover, DOX can complex with iron and, in the presence of a reducing system, the complexes can be reduced from DOX-Fe^{3+} to DOX-Fe^{2+} and later react with O_2 or H_2O_2, ultimately leading to $HO^{\bullet}$. When no reducing system is available, the complex DOX-Fe^{3+} can still suffer a self-redox reaction [83]. In accordance, dexrazoxane (DRZ, a cardioprotectant with iron-chelating properties) is currently the only FDA-approved agent used to reduce the cardiac toxicity of anthracyclines [84-86]. At physiological conditions of pH and temperature, DRZ undergoes hydrolysis, ultimately leading to the formation of its ring-opened metal ion-binding form, ADR925, which has a structure similar to EDTA, and can then either remove iron from the iron-DOX complexes or bind free iron, preventing oxygen radical formation [87]. However, more recently DRZ-induced TopIIβ depletion was also suggested as essential for an effective cardioprotection against anthracycline cardiotoxicity [88].

DOX also disturbs the nitric oxide (NO) network, reported as essential for the integrity of the cardiovascular system under physiological conditions [89]. It has been shown that the endothelial isoform of nitric oxide synthase (eNOS) reduces DOX with the subsequent production of $O_2^{\bullet -}$ and decreased production of NO [90]. Excessive $O_2^{\bullet -}$ reacts with NO leading to the formation of peroxynitrite ($ONOO^-$), a potent oxidant, and contributing to the progression of cardiovascular disease [91]. Additionally, $ONOO^-$ has been implicated in the nitration/inactivation of manganese-superoxide

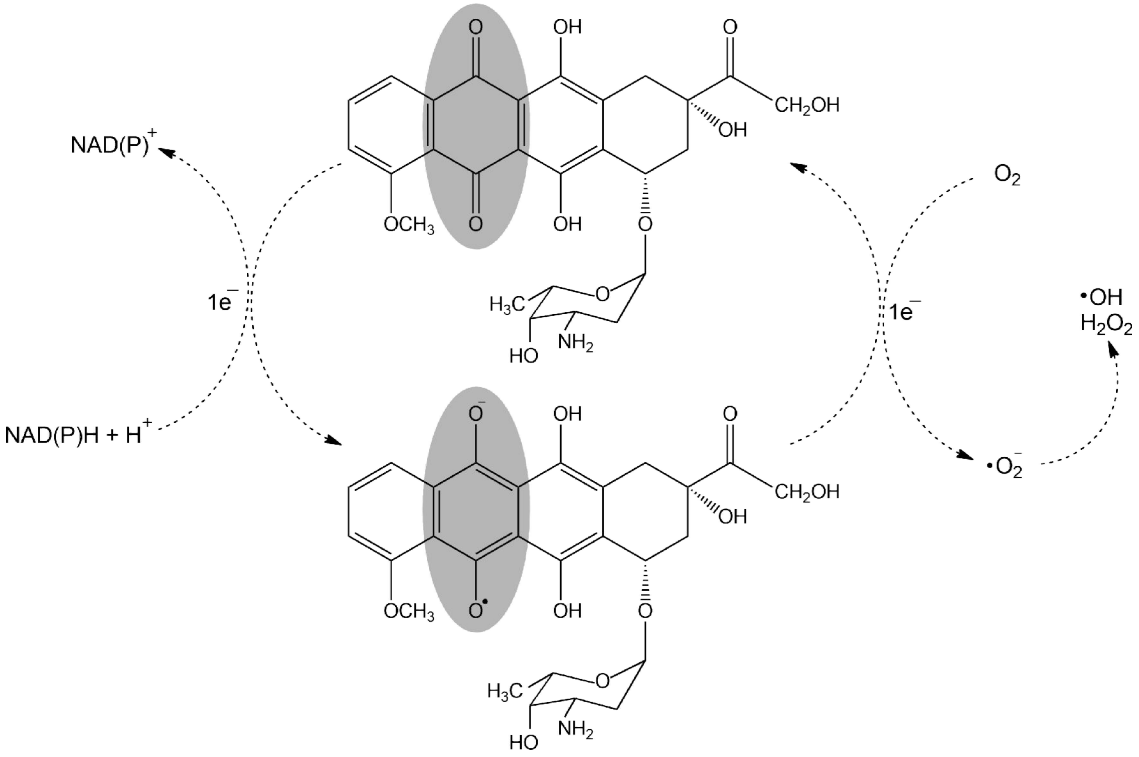

Figure 1.2: Schematic representation of the formation of ROS through reduction of DOX into DOX-semiquinone. DOX accepts electrons from NAD(P)H-dependent oxidoreductases generating a semiquinone form. Molecular oxygen can accept the electron from semiquinone, forming a superoxide radical ($O_2^{\bullet -}$). Subsequent mechanisms based on free iron and antioxidant enzymes may induce the generation of other ROS (H_2O_2 and $HO^{\bullet}$).

dismutase (Mn-SOD) with the consequent accumulation of $O_2^{\bullet -}$ [92, 93]. Similarly, DOX treatment *in vivo* induced increased inducible NOS (iNOS) levels and myocardial nitrotyrosine formation, which is a footprint for nitrative stress [94, 95].

In several *in vitro* and *in vivo* models of DOX cardiotoxicity, disruption of calcium homeostasis was also observed [96-98]. Particularly in cardiomyocytes, Ca^{2+} is essential as a key regulator of muscle contraction and fundamental for the function of important mitochondrial enzymes such as pyruvate dehydrogenase, isocitrate dehydrogenase, α-ketoglutarate dehydrogenase and ATP synthase [99]. Thus, Ca^{2+} is proposed as a link between the cardiac excitation-contraction coupling and oxidative phosphorylation and ATP production [100]. Mitochondrial Ca^{2+} overload was

observed after DOX exposure, even before changes in cytosolic Ca^{2+} could be detected [97]. DOX and its metabolites were described as inhibitors of several cationic pumps that directly or indirectly regulate cell Ca^{2+} flux [101, 102]. Thus, increased cytoplasmic Ca^{2+} accumulation was suggested to contribute to the augment of mitochondrial Ca^{2+} accumulation [103].

The combination of oxidative stress with Ca^{2+} overload is determinant for the opening of mitochondrial permeability transition pores (mPTP), protein complexes that create nonselective channels (Fig. 1.3). The molecular identity of the pore is still not clear and over the past years many were the discussions and hypotheses. The initial mPTP complex was believed to be formed by three main proteins: the IMM adenine nucleotide translocator (ANT), the OMM voltage-dependent anion channel (VDAC) and cyclophilin D (CypD), located in the mitochondrial matrix [104]. However, recent molecular knock-out studies proved the limitations of this model. Mitochondrial-dependent cell death and Ca^{2+}/oxidative stress-induced mPTP were found to be similar between *Vdac*-deficient and wild-type mitochondria, confirming the dispensable role of VDAC for mPTP [105]. Similarly, ANT, a translocator which exchanges mitochondrial ATP for cytosolic ADP, was found to be a non-essential component of the mPTP, although it might contribute to its regulation [106]. On the other hand CypD seems to have a regulatory role in the activation of mPTP, supported by its interaction with cyclosporine A (CsA), a pharmacological agent proved to efficiently inhibit the formation of mPTP [107-109]. More recently, CypD was shown to interact with ATP synthase (through the δ/OSCP subunit of the catalytic core F1), modulating ATP synthesis and hydrolytic capacity [110]. In fact, more recent proposals about the structure of the pore suggest that ATP synthase is involved. Whether the channel is formed in the membrane interface of two adjacent ATP synthase monomers (forming dimers), or in the ATP synthase c-subunit that might expand in response to prolonged high matrix Ca^{2+} concentration, it is still not clear [111-113]. Functionally, the permeabilization of the inner membrane leads to the free

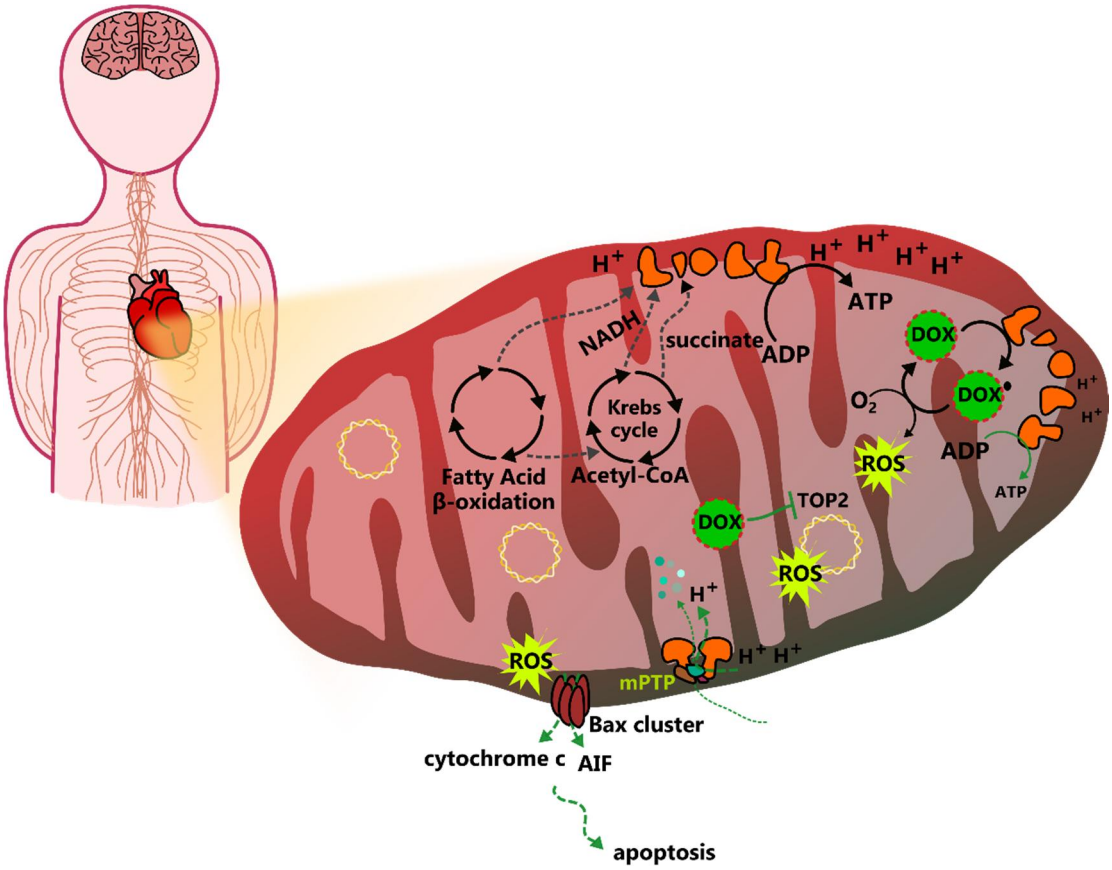

Figure 1.3: Overview of molecular reactions and mitochondrial alterations associated with development of DOX cardiotoxicity. DOX accepts electrons from NADH dehydrogenase generating a semiquinone form. Molecular oxygen can accept the electron from this semiquinone, forming $O_2^{\bullet-}$. Subsequent mechanisms based on free iron and antioxidant enzymes may induce the generation of other ROS (H_2O_2 and $HO^{\bullet}$). AIF, apoptosis inducing factor; $DOX^{\bullet}$, doxorubicin semiquinone radical; mPTP, mitochondrial permeability transition pore; ROS, reactive oxygen species; Top2, topoisomerase II.

passage of molecules with molecular weights smaller than approximately 1.5 kDa (including Ca^{2+} itself), osmotic unbalance, depolarization of the mitochondrial membrane due to the leakage of protons, dysregulation of oxidative state and, ultimately, mitochondrial swelling and disruption [114, 115]. Uncoupling of OxPhos also causes the reversal of ATP-synthase that hydrolyses ATP rather than synthesizing it. These effects are usually related with long-lasting pore opening, while brief openings may be related with physiological regulation of Ca^{2+} and ROS homeostasis [116]. DOX-induced mPTP opening has been observed by many groups [96, 114] and

DOX cardiac toxic effects were ameliorated with the inhibition of mPTP by CsA [117, 118]. Furthermore, DOX was reported to induce a reduction in the amount of functional ANT after a sub-chronic treatment, reinforcing the effects of DOX in the reduction of bioenergetic capacity but also in the dysregulation of mPTP [119].

1.2.2. DOX and cardiomyocyte cell death

Cell death occurs usually after damaging events and can generally be divided into three main types: apoptosis, necrosis and autophagic cell death. Apoptosis is the best characterized form of regulated cell death. Morphologically, it is defined by cell shrinkage, pyknosis and generation of apoptotic bodies [120] and it can be triggered by two major signaling pathways: the mitochondrial (intrinsic) pathway and the death receptor (extrinsic) pathway. While the extrinsic pathway involves the binding of "death ligands" to cell surface receptors, the intrinsic pathway is mediated by OMM permeabilization, and both mechanisms activate a caspase cascade. A class of very important proteins participate in the mitochondrial apoptotic process: the BCL-2 family. This family comprises proteins responsible for induction (proapoptotic) and inhibition (antiapoptotic or prosurvival) of apoptosis, and also a third group of proteins (BH-3 only) that regulate apoptosis by either directly activating the proapoptotic proteins or by suppressing the antiapoptotic proteins [121, 122]. The functional balance between these proteins determines cell fate.

BAX and BAK are two proapoptotic proteins from BCL-2 family required for the mitochondrial-mediated apoptosis. For mitochondrial participation, the OMM needs to be permeabilized in order to allow the release of another proapoptotic molecules such as cytochrome *c*, Omi/HtrA2 or Smac/DIABLO for further caspase cascade

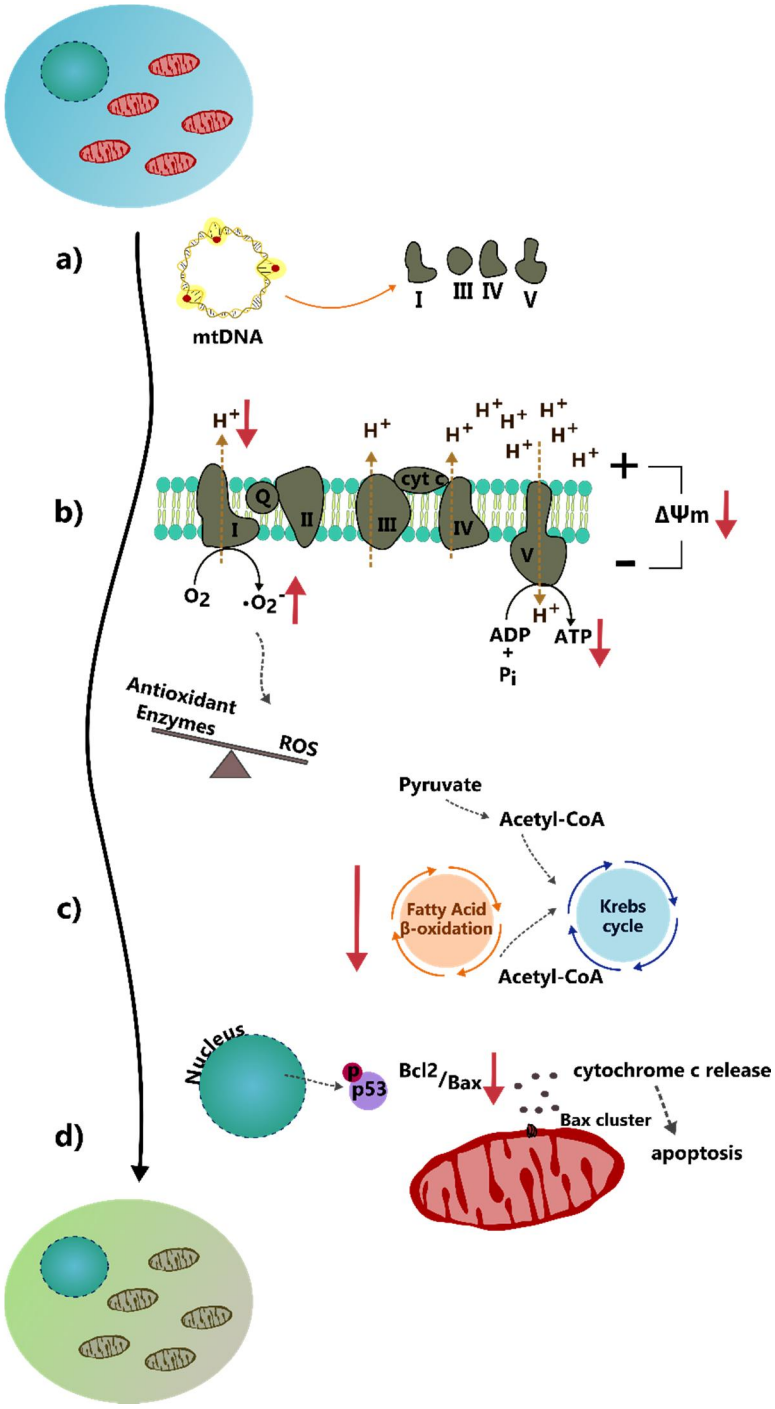

Figure 1.4: Main mechanisms by which DOX affects mitochondrial related functions. Some of the consequences of the chemotherapeutic treatment include a) decrease in mtDNA content and quality causing disturbance in protein synthesis and defective respiratory chain elements, b) increased oxidative stress, leading to the oxidation of mitochondrial membranes and other structures such as proteins from electron transport chain resulting in electron leak and even more mtROS production, collapse of ΔΨ and decreased ATP content, c) decline of fatty acid β-oxidation efficiency, d) increased p53-mediated apoptosis, cytochrome *c* release from intermembrane space, caspase activation, and apoptosis. ΔΨm, mitochondrial transmembrane electric potential; cyt *c*, cytochrome *c*; mtDNA, mitochondrial DNA; Q, coenzyme Q.

activation, or AIF (apoptosis-inducing factor) that triggers a caspase-independent cell death (Fig. 1.5). This is accomplished upon activation of BAX and BAK that oligomerize and form openings in the OMM [123, 124]. The BH-3 only proteins, including BIM, BID, Puma and Noxa, regulate BAX/BAK activation. On the other hand, the antiapoptotic members (BCL-2, BCL-XL, BCL-W, MCL-1) prevent the pore formation by inhibiting the proapoptotic proteins or by sequestering the BH-3 only activator proteins [125]. Caspases are cysteine proteases with specificity for aspartic acid residues and the most relevant caspases in the apoptotic programming are usually divided into initiator (caspase-2, -8, -9) or executioner (caspase-3, -6, -7) caspases. The caspase-dependent mitochondrial pathway usually relies on the apoptotic protease-activating factor 1 (Apaf-1)-apoptosome that is mediated by cytochrome *c* release and leads to the activation of caspase-9 [126, 127]. Once activated, caspase-9 cleaves and activates caspase-3 and -7. In the extrinsic pathway, these two caspases are activated by caspase-8 [126]. When active, executioner caspases cleave more than 1000 substrates which leads to cellular changes associated with apoptosis [126]. An alternative to the BAX/BAK-dependent pore formation is the mPTP, but this OMM permeabilization is usually related with necrotic cell death due to the swelling and complete rupture of OMM. However, some studies suggest the involvement of BAX and BAK in the mPTP regulation [128].

An important regulator of the apoptotic process is the transcription factor p53. The p53 activation is induced by diverse forms of stimuli, including oxidative stress and DNA-damage, and can either induce cell cycle arrest and stimulate DNA-repair mechanisms when exposed to weak or moderate stress insults, or initiate an apoptotic response or cellular senescence after a more intense and damaging stress. p53 is a short-lived protein that requires post-translational modifications such as phosphorylation and acetylation to be stabilized and activated. As a result, it may work as a DNA-binding transcription factor, controlling the expression of several p53-responsive genes such as Puma, Noxa, BAX and Apaf1. Additionally, in response to

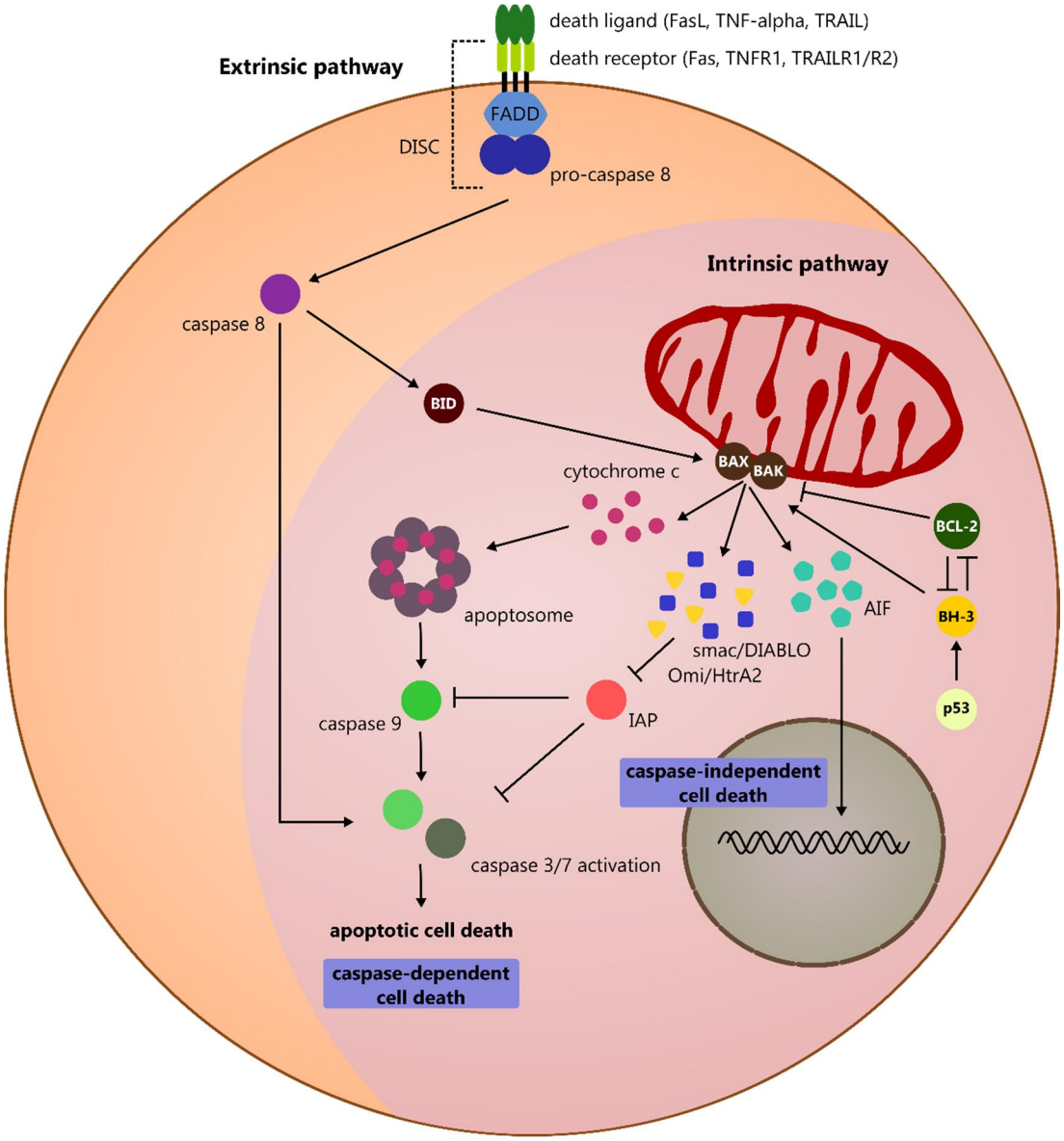

Figure 1.5: Extrinsic and intrinsic apoptotic pathways. In response to cellular stresses including DNA damage and oxidative stress, p53 and other cellular damage sensors activate BH-3 only proteins that induce the permeabilization of the OMM through the activation of the proapototic members of the BCL-2 family (BAX and BAK). The antiapoptotic members (BCL-2) try to prevent the pore formation by inhibiting the proapoptotic proteins or by sequestering the BH-3 only activator proteins. From these openings, cytochrome *c* is released with the subsequent formation of the apoptosome and activation of caspase-9 that activates the effector caspases-3 and -7. Smac/Diablo and Omi/HtrA2 are also released and anthagonize the IAP (inhibitor of apoptosis protein) caspase inhibitors. In doing so, they potentiate the caspase activation by the apoptosome. In a caspase-independent process, AIF (apoptosis-inducing factor) translocates from mitochondria to the nucleus triggering chromatin condensation and DNA fragmentation. In the extrinsic pathway, death ligands engage cell membrane receptors and lead to the formation of death-inducing signaling complex (DISC) that further activates caspase-8. Then, caspase-8 can either activate caspase-3 and -7 or activate BID, which also leads to the permeabilization of the OMM by BAX and BAK, coordinating the cross-regulation between extrinsic and intrinsic apoptotic pathways.

stress, p53 can induce transcription-independent apoptosis by behaving like a BH3-only protein, inhibiting antiapoptotic proteins and activating the proapoptotic members [129, 130]. Numerous studies reported DOX-induced cardiomyocyte apoptosis. *In vitro*, the apoptotic phenomenon has been commonly described; still, some concerns exist regarding the *in vivo* contribution of apoptosis to the development of chronic cardiomyopathy [131-135]. DOX is known for p53 activation [136-138] and the exposure to 0.5-1 μM DOX for 24 hours was demonstrated to induce BAX clusters and release of cytochrome *c* into the cytoplasm in H9c2 cardiomyoblasts [136] (Fig. 1.3 and 1.4). Interestingly, in the same *in vitro* model, caspase inhibition did not fully prevent DOX toxicity [139], and AIF, a flavoprotein normally located within the mitochondrial intermembrane space, was shown to translocate to the nucleus, triggering chromatin condensation and DNA fragmentation in a caspase-independent mechanism [140]. AIF cleavage and release from mitochondria is regulated by particular proteases including Ca^{2+}-dependent calpains [141] whose activity is increased in many condition associated with calcium overload including ischemia-reperfusion [142] and DOX exposure [143]. Additionally, *in vitro* and *in vivo* models have shown that DOX induces cytochrome *c* release [144], increased caspase-9 and -3 activity [138, 145, 146], and BCL-2/BAX decreased ratio [147, 148] (Fig. 1.3 and 1.4).

The activation of p53 may also be induced by the genotoxic stress caused by TopIIβ inhibition. This isoform, contrary to TopIIα, is found predominantly in non-proliferating cells, such as cardiomyocytes [149]. Likewise, DOX promotes the formation of protein-linked DNA double strand breaks by the induction of stable TopIIβ:DOX:DNA structures. Lyu et al. demonstrated that mouse embryonic fibroblasts from Top2β$^{-/-}$ embryos presented decreased markers of DNA damage (γ-H2AX) compared with Top2β$^{+/+}$ [150]. In a group of anthracycline-sensitive patients, the level of TopIIβ was found to be increased compared with the resistant group, suggesting the importance of TopIIβ to the cardiotoxicity risk [151]. Some authors actually support that TopIIβ is the primary target of DOX and that mitochondrial

dysfunction is secondary to TopIIβ-related double-strand breaks [152]. DOX was found to downregulate PGC-1α and PGC-1β in Top2β$^{+/+}$ but not in Top2β$^{\Delta/\Delta}$ hearts and similar results were obtained for OxPhos transcripts and oxygen consumption, with Top2β$^{+/+}$ showing more deleterious effects and suggesting that TopIIβ is required for DOX-induced functional changes in cardiac mitochondria [153].

The intrinsic and the extrinsic apoptosis pathways are not independent, but rather interconnected as can be observed in mitochondrial-mediated apoptosis induced by BID upon cleavage by caspase-8 (Fig. 1.5) [154]. The extrinsic apoptotic process onset is mediated by ligands such as FasL, TRAIL and TNF-α that through cell surface receptors lead to the formation of a death-inducing signaling complex (DISC). Caspase-8 is then activated and either mediates the activation of the effector caspase-3 and -7 or, as previously referred, the cleavage and activation of BID that promotes the formation of BAX/BAK-induced openings in the OMM [155]. Fas pathway was evoked as participating on DOX-induced cardiomyocytes death. *In vivo* DOX administration during 5 weeks translated into extensive myocardial apoptosis and fibrosis, and increased oxidative-nitrosative stress [156]. Cardiac-targeted sFas overexpression, a competitive inhibitor of FasL and attenuator of Fas-mediated apoptosis, improved overall the DOX-associated cardiotoxicity, as well as alleviated the overexpression of the proinflammatory cytokines [156]. Fas overexpression was previously reported in response to DOX exposure [157].

DOX treatment has also been related with necrotic cell death [131]. This particular type of death is characterized by plasma membrane rupture and cellular swelling. The inner mitochondrial membrane integrity and the formation of mPTP have been linked to necrosis as well. Initially considered an unprogrammed process, necrosis is now considered another regulated form of cell death (being necroptosis the best characterized subtype of regulated necrosis) [158, 159]. A recent study proposes a mechanism of PARP-1 mediated necrosis following DOX-induced DNA damage

[160]. Other authors also demonstrated the increase of markers of necrotic cell injury (eg. LDH release) in DOX-treated animals and suggested the link between mitochondrial damage, necrotic cell death and Bnip3 mitochondrial regulation [161].

Lastly, autophagy is a controlled and conserved process of self-elimination that works in the maintenance of the cellular homeostasis. The autophagic process allows removing damaged organelles or protein aggregates before they compromise the cell function. In this process, the unwanted cellular components are engulfed, forming the autophagosome that later is fused with lysosomes and degraded by lysosomal enzymes. Additionally, this process has important roles on organelle biogenesis and turnover, since degraded lipids and proteins are recycled to be consumed for the production of ATP and synthesis of new proteins during stress conditions, such as starvation, oxidative stress or calcium overload [162]. Autophagy, for instance, was described as critical for the maintenance of normal cardiac function during starvation [163].

Stimulation of autophagy before DOX treatment using rapamycin, an mTOR inhibitor and autophagy inducer, seemed to alleviate the cardiotoxic symptoms [164]. Also, a starvation period before DOX administration seemed to mitigate the DOX-induced impairment of cardiac function, but under normal feeding conditions DOX seems to impair the autophagic process, probably through the inactivation of AMPK and ULK1 [165]. However, autophagy is a double-edged sword whose consequences can be beneficial but also harmful, depending on the extension of the process. Extreme levels of autophagy may lead to cell death and the crosstalk between autophagy and other cell death pathways such as necrosis and apoptosis have been reported [162, 166, 167]. In this regard, discrepant results have been described, since some studies reported DOX-induced stimulation of autophagy [168, 169] while others observed the opposite [138, 165].

1.2.3. Metabolic remodeling in the heart

The mammalian heart is a very energy-demanding organ [42, 170]. A mature mammalian heart is structurally organized in four chambers and composed mostly by cardiomyocytes and supportive fibrovascular connective tissue [45]. The cardiac excitation-contraction coupling goes from the electrical excitation of the cardiomyocytes to the contraction of the heart and pumping of blood to the rest of the body. Sequentially, the contraction process starts with an electrical activation based on Na^+ influx that leads to cell depolarization and entry of Ca^{2+} through the sarcolemma. When Ca^{2+} enters the cardiomyocytes via L-type voltage-dependent Ca^{2+} channels, ryanodine receptors in the sarcoplasmic reticulum open, eliciting the release of Ca^{2+} to the cytoplasm [171]. The binding of Ca^{2+} to troponin C in the myofilaments triggers the contraction process. For relaxation, Ca^{2+} is dissociated from troponin and taken from the cytosol, either back to the sarcoplasmic reticulum or out of the cell through Na^+/Ca^{2+} exchangers or Ca^{2+}-ATPases [172, 173]. The constant contraction of the heart requires a constant fueling of the ATP-production mechanisms. In fact, it was suggested that the heart cycles around 6 kg of ATP per day, which is 20 to 30 times its own weight [174]. In this context, mitochondria (as referred in section 1.2.1.1) are the main cellular factories where the conversion of substrates to ATP occurs.

In an adult heart most of the ATP is generated in OxPhos from the oxidation of fatty acids, contrasting with a fetal heart that is mostly based on the oxidation of carbohydrate substrates, partially because of the relatively low oxygen environment [175]. Cardiac mitochondria uses preferentially fatty acids for ATP production, but mitochondria are also very flexible and can use many other substrates including carbohydrates, amino acids and ketone bodies [176, 177]. This versatility confers an advantage under a variety of physiological conditions such as intense exercise (oxidation of lactate)[178] or prolonged fasting/ketogenic diets (oxidation of ketone bodies)[179].

The mechanism of ATP production in a normal heart occurs mainly in a very controlled manner: fatty acyl-CoA and pyruvate, from fatty acids and glucose conversion, respectively, are transported across the IMM and transformed into acetyl-CoA. Pyruvate conversion is regulated by pyruvate dehydrogenase (PDH) complex, while fatty acyl-CoA undergoes fatty acid beta oxidation (FAO), and the resulting acetyl-CoA enters the TCA cycle forming NADH and succinate that posteriorly fuel the ETC. The mitochondrial dysfunction and consequent alterations in myocardial energy play an important role in the onset of DOX-cardiotoxicity. Significant reductions of intracellular ATP were observed with DOX [145, 165, 180-182], and many authors demonstrated disturbances in the fatty acid and glucose metabolism [183-187], even though many contradictory results have been described probably due to the multiplicity of models and experimental setups. Some authors, for instance, support the hypothesis that cardiomyocytes try to compensate the decreased ATP production with increased efficiency in the conversion of pyruvate into acetyl-CoA, even though decreased glycolytic activity was observed (10 and 20 nM DOX, HL-1 cardiomyocytes) [186]. Others reported the increased expression of glycolytic rate-limiting enzymes with DOX, accompanied by a decrease in transcripts associated with fatty acid metabolism, suggesting a switch in substrate utilization (total 14 mg/kg DOX, 6 weeks, rats) [188]. In an attempt to confirm these transcriptional results, another study used the same rat model and ^{13}C NMR isotopomer analysis to measure cellular substrates, and observed inhibition of long-chain fatty acid oxidation and increased glucose oxidation [184]. On the contrary, other authors observed decreased utilization of both glucose and fatty acid substrates in rats (total 12 - 40 mg/kg DOX, sub-chronic model) and in isolated adult rat cardiomyocytes (1 mM DOX, acute model) [187, 189]. The decline in oxidation of fatty acids was suggested to be related with impaired mitochondrial function and reduced PPARα and PGC-1α transcriptional-activation [134, 190].

1.3. Delayed and persistent DOX cardiotoxicity

For a long time, it was assumed that the number of cardiomyocytes did not change significantly during physiological postnatal growth in humans because their proliferation stops soon after birth [191]. As a consequence, stressful events lead to cell death and no compensatory cell renewal mechanism is observed, resulting in progressive loss of myocardium, fibrotic scarring and declining cardiac function. However, some recent studies suggested that, even though limited in an adult mammalian heart, new cardiomyocytes arise through life and most of them come from preexisting cardiomyocytes [192, 193]. Thus, the human myocardial growth during the first years of life would be based not only in cardiomyocytes enlargement but also, to some extent, in cell proliferation [193]. Very recently, Patterson el al. identified mononuclear diploid cardiomyocytes (MNDCMs) as one proliferative population of cardiomyocytes in adult hearts and demonstrated their contribution for heart functional recovery [192]. These cells are abundant during embryonic heart development but their number starts declining after birth. Other works reinforced the importance of the first weeks of life in animal models for the setting of the number of cardiomyocytes in the heart [194, 195]. The existence of endogenous cardiac progenitor cells capable of differentiating into cardiomyocytes has also been questioned over the past years [196, 197]. Still, the importance of cardiac stem cells in the support of cardiac function and homeostasis, neovascularization and cardiac endothelial cells regeneration is recognized [198]. Cardiac stem cells were found in adult hearts, but a negative correlation with age was reported, meaning that the pool of stem cells is reduced with age [199]. In addition, human neonatal cardiac stem cells were shown to have higher regenerative ability when compared with adult-derived cardiac stem cells [200]. Altogether these facts impose critical constraints on the treatment of young patients, whose hearts may still not be totally and terminally developed and may contain important cellular pools for the regenerative process.

The vulnerability of children for the development of DOX-induced chronic and persistent cardiotoxicity is known [27, 30, 201]. Children are in many aspects different from adults, not only in cardiac development and composition but also in drug metabolism including absorption, metabolism and excretion [202]. DOX treatment can lead to the loss of myocytes and impaired cardiac growth, resulting in inadequate left ventricular mass, myofiber disarray, myocardial fibrosis and declining cardiac systolic function [30, 203]. Changes in cardiac transcription in response to DOX may also contribute for a more severe response in young hearts compared to adult hearts. Cardiac Adriamycin-Responsive Protein (CARP) is mainly present in heart tissues during the earliest stages of cardiac morphogenesis since it functions as a transcriptional regulator of cardiac muscle genes important in growth and morphogenesis. CARP levels, apart from being age-dependent (higher levels in neonatal hearts compared with adult hearts), are highly susceptible to DOX, likely through a DOX-mediated generation of H_2O_2, which may contribute to more severe DOX cardiotoxicity in young hearts [204, 205]. Another cause for the differential age-dependent action of DOX may be the different expression of apoptotic signaling molecules in the hearts of children and adults. In fact, some studies support the idea that postmitotic cells possess a reduced apoptotic potential and that immature cardiac cells have a more active intrinsic apoptotic pathway, being more sensitive to DOX-induced injury [131, 144]. Comparing the response of adult rat cardiomyocytes, neonatal rat cardiomyocytes and H9c2 cardiomyoblasts to DOX, it was observed that adult cardiomyocytes were considerably more resistant to DOX-induced apoptosis, reinforcing the detrimental role of DOX exposure in pediatric patients [144]. Still, these results do not totally explain why late-onset cardiotoxicity, that is normally associated with childhood-cancer patients, can appear many years or decades after the end of the treatment. The heart of pediatric patients may not be completely developed at the time of the exposure, which affects further cardiac development and the capacity to deal with increased workloads and stresses. This is very important since DOX persistent

cardiotoxic effects are particularly evidenced after a second-hit stress, such as a further drug exposure, or a cardiac-demanding condition including exercise or pregnancy [206]. Additionally, another explanation could be related with the induction of mtDNA lesions caused by DOX, disturbing the normal process of protein synthesis and resulting in a defective respiratory chain [207]. In turn, this failure of the mitochondrial machinery would lead to an inability to respond to high energy demands, producing a higher leakage of electrons and, consequently, increasing ROS production which perpetuates these cyclic events. It was also proposed that the epigenetic modulation can be in the basis of the persistent "memory" observed in these patients. By using animal models of long-term DOX cardiotoxicity (5 to 10-week drug-free period), persistent alterations of gene expression and increased oxidative stress were observed [188, 208]. Moreover, a decrease in global cardiac DNA methylation in DOX-treated animals *versus* their saline counterparts was observed, with 50 genes presenting statistically significant differences in methylation status [209]. DOX-induced decreased global DNA methylation in the heart has also been reported elsewhere, as well as altered activity of histone deacetylases [210]. The hypothesis is that the deleterious mitochondrial effects caused by DOX could lead to metabolite-mediated long-lasting alterations in the epigenome [211].

1.4. Clinical and experimental interventions to reduce DOX cardiotoxicity

During the last years several attempts were made to overcome the cardiac side-effects of DOX. The first approach usually involves reducing the dosages or decrease the number of cycles of the chemotherapeutic regimen but these strategies compromise the efficiency of the treatment [212]. Over the past years multiple drug delivery systems have been tested in order to overcome the systemic toxicity observed during and after anthracycline treatment. The different systems include polymers, liposomes,

amphiphilic peptides, hydrogels, micelles or nanoparticles that can be organized into nanosized structures (reviewed in [6, 12]). Some nanotechnology-based DOX delivery systems have been FDA and EMA (European Medicines Agency) approved in the last years, including PEGylated liposomal Doxil®/Caelyx®, Lipodox® and liposomal Myocet®, and others are being tested in ongoing Phase II/III clinical trials (Fig. 1.6) [6]. Another explored strategy was the synthesis of modified anthracyclines in order to get compounds equality efficient in terms of anticancer action but with reduced cardiotoxicity. From the most promising compounds, epirubicin, idarubicin and mitoxantrone have been considerably more explored due to their apparent reduced risk of clinical cardiotoxicity, even though the results have not been always conclusive [213-215]. Preventively, mitochondrial-targeting pharmacological strategies have been studied aiming to prevent deleterious effects by protecting these organelles. One example is the use of antioxidants in the prevention of the oxidative stress, one of the primary causes of mitochondrial dysfunction. The antioxidant coenzyme Q10 prevented the decrease of interventricular septum wall thickening observed in an anthracycline-treated group of children with acute lymphoblastic leukemia or non-Hodgkin lymphoma [216]. Furthermore, carvedilol, a neurohormonal antagonist that blocks adrenoreceptors and has vasodilating properties, also showed promising results by preventing the inhibitory effects of DOX on mitochondrial respiratory complexes and the decrease in mitochondrial calcium loading capacity [217, 218]. In patients undergoing anthracycline therapy, carvedilol seemed to be an interesting protector of left ventricle function [219]. Similarly, the prophylactic use of statins, drugs with anti-inflammatory and antioxidative properties and well established as cardio-protectants [220], was proposed to be effective in the maintenance of LVEF in anthracycline-treated patients [221-223]. However, DRZ is currently the only FDA-approved method for anthracycline cardiotoxicity prevention with many clinical trials supporting its beneficial action [84, 224, 225]. In a study from Lipshultz et al., children

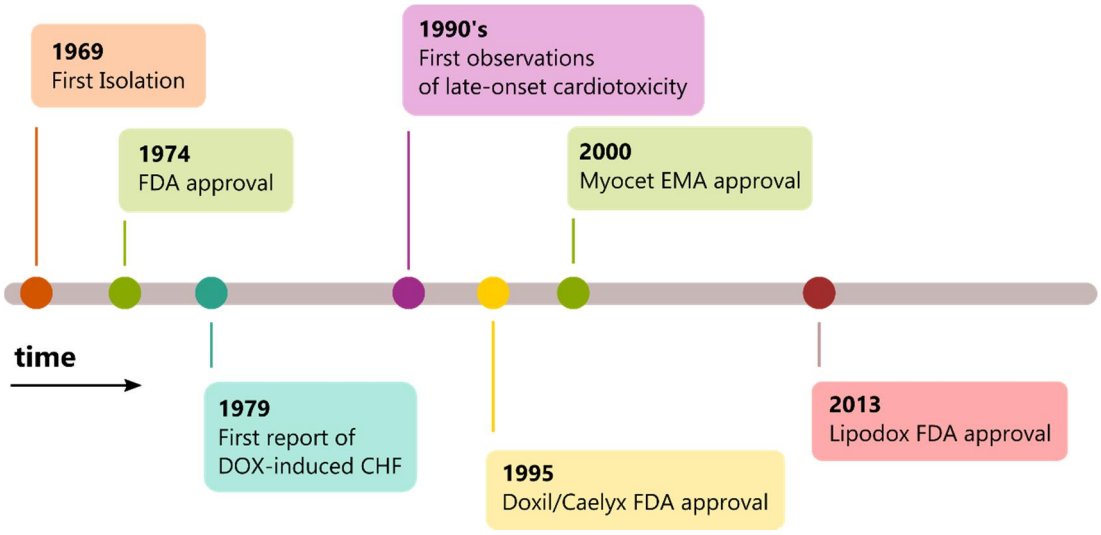

Figure 1.6: Timeline of key landmarks on the history of DOX research. Five years after DOX first isolation from *S. peucetius* var. *caesius* in 1969, Adryamicin® was approved by FDA. The following observations of DOX-associated cardiotoxicity encouraged the development of new nanotechnological formulations. In 1995, the PEGylated liposomal Doxil®/Caelyx® was the first DOX-based nanosystem to reach the market. Since then, a restricted number of other formulations have been approved and others are present in clinical trials. FDA, US Food and Drug Administration; CHF, cardiac heart failure; EMA, European Medicines Agency

with acute lymphoblastic leukemia were followed during the treatment with DOX alone or DOX combined with DRZ. The control group treated only with DOX showed a higher increase in serum levels of cardiac troponin T after the treatment, compared to the group receiving the combined therapy [85]. Moreover, DRZ also reduced the incidence and severity of early and late cardiotoxicity in children with solid tumours receiving DOX [86]. Cardiac function was measured based on fractional shortening and systolic and diastolic left ventricular diameter, and the DOX plus DRZ group presented significant fewer cardiac events (27.7% *vs*. 52.4%) and less severe congestive heart failure (6.4% *vs*. 14.3%), compared to the group treated with DOX alone [86]. In addition, DRZ seemed not to affect the response rates to chemotherapy [224, 226]. As previously referred (section 1.2.1.2), the proposed mechanisms for DRZ

cardioprotection rely on its ability to chelate intracellular iron, decreasing ROS formation, and on depleting cardiac TopII [87, 227].

Chapter 2

2. Epigenetics and the circadian clock

2.1. Epigenetics: a dynamic machinery

Epigenetic regulation of gene expression occurs at three different levels: post-translational modifications of histones, covalent DNA modifications and non-coding RNA regulation. Despite the conserved nature that is broadly associated to epigenetics, the epigenome retains plasticity and is dynamically regulated in response to endogenous and exogenous stimuli, such as environmental signals [228]. The identified covalent modifications that take place on histones and DNA (including methylation, phosphorylation and acetylation) usually require enzymes whose activity is mediated by the availability of sub-products of the cellular metabolism. Mitochondria, in particular, provide (directly or indirectly) a number of critical metabolites that link the metabolic status and epigenetics, including NAD^+, ATP, α-ketoglutarate, succinate, acetyl-CoA and SAM (s-adenosyl-L-methionine).

For example, the addition of a methyl group at position 5 of cytosine (5-mc) is a highly conserved epigenetic process known as DNA methylation [229]. This mark is normally associated with repression of gene transcription, although it also has important roles in transposon silencing, genomic imprinting, cell differentiation or X-chromosome inactivation [230, 231]. The regulation of gene expression can be achieved either by directly blocking the binding of transcription factors or by the recruitment of chromatin-associated methyl-CpG-binding domain (MBD) proteins which in turn interact with remodeling complexes and histone deacetylases [232]. In mammals DNA

methylation is preferentially found on cytosine-phosphate-guanine (CpG) dinucleotides, which are commonly found in clusters called CpG islands or in repetitive sequences in the genome. Globally, the CpG island fraction normally accounts for around 1% of the genome and frequently coincides with promoter regions. DNA methylation reaction is catalyzed by a family of DNA methyltransferases (DNMTs). Three main DNMTs are associated with DNA methylation in mammals: DNMT1, DNMT3A and DNMT3B. While DNMT1 works in the maintenance of the established DNA methylation pattern in new synthesized DNA molecules during cell DNA replication, DNMT3A and DNMT3B are responsible for *de novo* DNA methylation during embryonic development [233]. The universal methyl-donor in mammals is SAM, an intermediate of one-carbon metabolism, constituted by two interconnected cycles, the methionine and the folate cycles [234]. On the other hand, the process of reverse DNA methylation is controlled by ten-eleven translocation (TET) family enzymes and is dependent on α-ketoglutarate and Fe(II) [235]. α-ketoglutarate is a key metabolite produced in mitochondria either via TCA cycle or the catabolic metabolism of the amino acid glutamine. Succinate and fumarate, in turn, compete with α-ketoglutarate for the binding to the active site of TET enzymes, working as inhibitors and exposing a clear connection between mitochondrial metabolism and DNA methylation [236-239].

Histone acetylation is among the most well-understood covalent modifications identified on chromatin. Chromatin is very dynamic and can be condensed or relaxed depending on many factors. In particular, a high level of histone acetylation is characterized by a transcriptionally active and competent euchromatin, whereas hypoacetylation represses gene transcription through the accumulation of silent heterochromatin domains [240, 241]. These processes occur because the addition of an acetyl group to the amino groups of lysines converts these positively charged residues to uncharged acetyl-lysines, decreasing the electrostatic interactions between the negatively charged DNA and histone tails and, consequently, facilitating the access

of transcription factors to the target sequences. Additionally, members of the family of bromodomains and extraterminal (BET) proteins can read this kind of histone modification, regulating gene expression, cell cycle and development [242]. The equilibrium between acetylation and deacetylation is kept by enzymes with either histone acetyltransferase (HATs) or histone deacetylase (HDACs) activity [243]. While HATs use mostly acetyl-CoA as donor of acetyl groups, a group of HDACs, called sirtuins (SIRTs), is nicotinamide adenine dinucleotide (NAD^+)-dependent. Thus, the availability of both metabolites can modulate the efficacy and specificity of the reactions.

2.2. Introduction to the circadian clock

The endogenous circadian clock evolved in response to the challenging daily cycles resultant from the ~24 h Earth's rotation. The light/dark cycles led the living forms to adapt in response to the external stimuli. From cyanobacteria to plants, birds, rodents or humans, the obedience to temporal niches is controlled by a molecular circadian clock [244]. The term circadian is derived from the latin words for about (circa) a day (diem). In mammals, physiological processes including sleep-wake cycles, feeding behavior, hormone secretion or body temperature oscillate exhibiting a circadian pattern and assuring that the biochemical and behavior processes occur at the appropriate time of the day. These internal timers enable to predict and adapt to environmental fluctuations. In the body, the circadian clock is hierarchically organized in a network that regulates endocrine and metabolic functions. The master clock resides in the suprachiasmatic nucleus (SCN) of the hypothalamus and orchestrates the peripheral circadian clocks, existing in nearly all cells in the body [245]. While the master clock is mostly controlled by the photic inputs of the light/dark cycles through the retinohypothalamic tract, the peripheral clocks are kept synchronized not only by the neuroendocrine signals from the SCN but also, for

instance, by the timing of nutrient availability. Even though the peripheral clocks are self-sustained, the SCN is essential for mastering the phases among tissues. Lesions in the SCN in rodents lead to the disruption of circadian rhythms of drinking, locomotor activity, temperature and sleep/wake cycles [246, 247] and the transplant of fetal SCN tissue is capable of restoring circadian behaviours in SCN-lesioned rats, supporting the role of SCN as a central pacemaker [248]. Mostly light, but also food intake, temperature, exercise or social cues are important stimuli, referred as zeitgebers (from the german "time-givers") (Fig. 2.1). However, even in conditions of constant darkness and *ad libitum* standard chow, mice are capable to entrain the SCN clock, only with slight shifts from the 24 hours period [249]. In humans subjected to a forced desynchrony protocol, the intrinsic period was shown to be longer than the 24 hours (24 hours 9 min ± 12 min) [250]. Therefore, the intrinsic clock is self-sustained but it still requires the daily outside photoperiod adjustment to be in harmony with the external conditions. In addition, the rhythms are temperature-compensated, which means that they do not run faster or slower with different environmental temperatures. The robustness of the master clock and flexibility of certain local peripheral clocks were confirmed by several studies in which restricted feeding (eg. during the day, when mice are typically asleep) changed the circadian phase in peripheral clocks such as liver but left the SCN cycles unaffected [251, 252].

Circadian desynchrony and loss of coordination between the internal rhythms and the external environment has a negative impact on the homeostasis of the organism. In fact, evidences suggest that the disruption of the circadian clock may affect the incidence of multiple disorders, including cancer and chronic diseases, mostly cardiovascular, metabolic and neuropsychiatric [253]. This is particularly evident for sleeping disorders in night shift workers [254]. Strikingly, mice under time-restricted high-fat diet were protected against metabolic disorders such as obesity, hepatic steatosis or inflammation, conditions observed in animals under *ad libitum* high-fat

diet [255], thereby enhancing the importance of metabolic cycles for the body homeostasis.

2.2.1. The molecular clock

The molecular function of the circadian clocks is based on negative transcription-translation auto-regulatory feedback loops. It is believed that around 10% of the mammalian transcriptome may be under circadian control and oscillate in a circadian manner [256]. The core clock proteins include transcriptional activators (*Circadian Locomotor Output Cycles Kaput* – CLOCK; *Brain and Muscle ARNT-Like 1* – Bmal1) and transcriptional repressors (*Cryptochromes* - CRY, *Period* - PER, REV-ERB) that act in concert to generate daily rhythms of their own protein levels and of thousands of other clock-controlled proteins. CLOCK (or NPAS2 in the brain) interacts with Bmal1 forming a heterodimer that binds to E-boxes in clock controlled gene (CCG) promoters, including Per (*Per1*, *Per2* and *Per3*), Cry (*Cry1* and *Cry2*) and *Rev-erbα/β* genes, and activate their transcription [257](Fig. 2.1). PER and CRY proteins heterodimerize and translocate to the nucleus where they inhibit CLOCK-Bmal1-mediated transcription, including their own transcription, in a negative feedback loop. The stability of the PER/CRY complex is posttranslationally regulated leading to a time-controlled clearance of the complex and initiation of a new transcriptional cycle [258-260]. Bmal1 and CLOCK also activate RORα and REV-ERBα that are involved in Bmal1 transcription activation or inhibition, respectively [261, 262](Fig. 2.1). D-box binding protein (*DBP*) and thyrotroph embryonic factor (*TEF*) are other CCG whose protein products bind to D-boxes and regulate the expression of downstream genes. The circadian machinery is also tightly regulated by posttranslational modifications (eg. acetylation, phosphorylation and ubiquitination) that help to regulate oscillations in gene expression and support the phase alternation [263]. CLOCK itself works as a histone acetyltransferase of the histones H3 and H4 [264] and, together with other

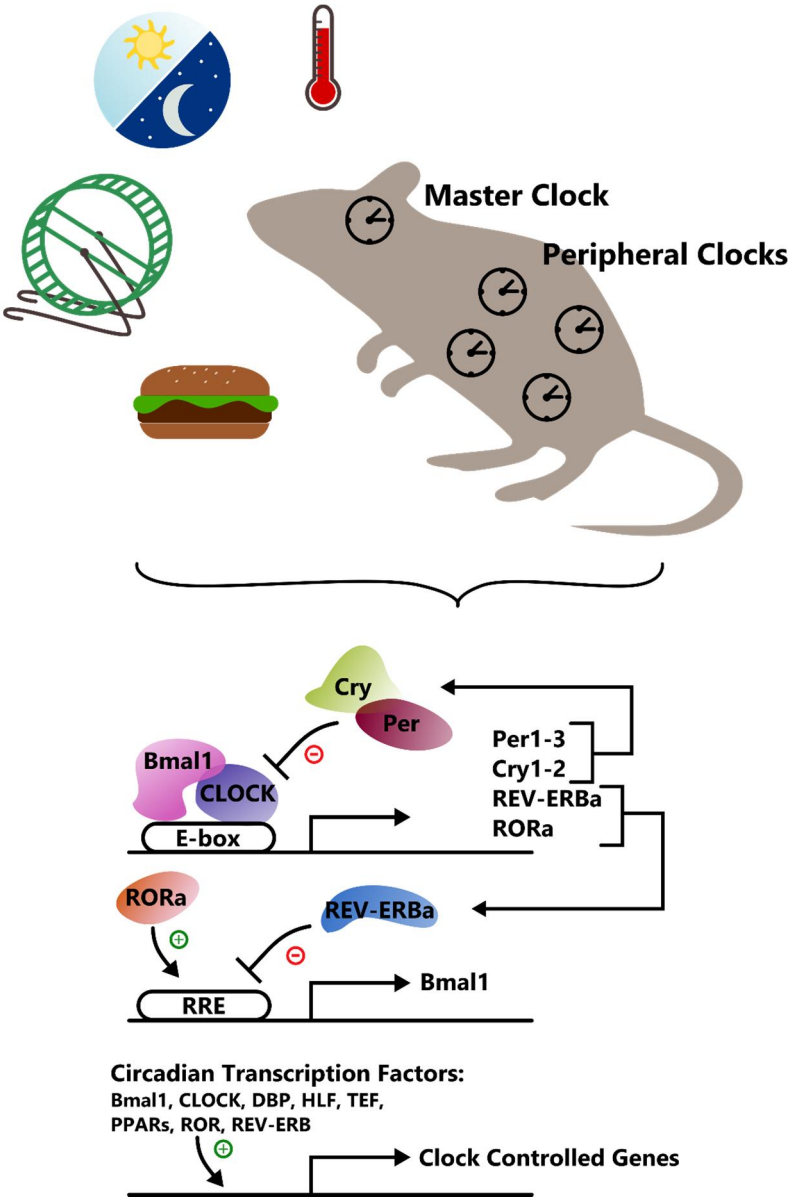

Figure 2.1: Schematic diagram of the mammalian circadian clock machinery. External zeitgebers including light/darkness, temperature, food intake and exercise entrain the master (SCN) and peripheral clocks. Molecularly, the Bmal1-CLOCK heterodimer binds to E-boxes at promoters of certain target genes including *Per*, *Cry*, *Rev-erb* and *Ror*. Upon transcription, PER and CRY proteins heterodimerize and translocate to the nucleus where they inhibit Bmal1-CLOCK mediated transcription and therefore their own transcription. ROR and REV-ERB are involved in the second feedback loop. In the nucleus, ROR and REV-ERB activate/repress Bmal1 transcription via competitive binding to the REV-ERB/ROR response (RRE) element. The main molecular machinery but also clock controlled transcriptional factors regulate the expression of the clock controlled genes that accounts for approximately 10% of the genome. +, activates transcription; -, represses transcription; DBP, D-box binding protein; HLF, hepatic leukemia factor; TEF, thyrotroph embryonic factor.

histone acetyltransferases, works in maintaining the cycles of histone acetylation and chromatin remodeling necessary for the cyclic transcriptional events [265]. For example, promoter regions of CCG exhibit circadian histone acetylation at H3K9 and H3K14 attributed to the HATs CLOCK and p300 [264, 265]. This activity is counterbalanced by the NAD^+-dependent histone deacetylase SIRT1, known for deacetylating H3K9/K14 at the promoters of CCG [266]. CLOCK and SIRT1 do not target only histones, but also circadian proteins (eg. Bmal1 and PER2) and metabolic, inflammatory and transcriptional regulators [266-269]. The trimethylation of H3 Lys4(K4) by the histone methyltransferase MLL1 was also reported to follow a circadian profile and to be required for chromatin remodeling and promoting transcriptional activation [270].

2.2.2. Reciprocal connection between the circadian clock and metabolism

Multiple metabolic pathways have been shown to be regulated by the circadian clock [271, 272]. Under controlled conditions, ~15% of metabolites identified in human plasma and saliva were found to be circadian [273]. Glucose, lipids and amino acids metabolism, DNA synthesis and repair, mitochondrial energy metabolism, and the cellular redox state are examples of metabolic processes known to be regulated by the circadian clock [274, 275]. Mice liver circadian metabolome was previously reported, showing that metabolites present disparate temporal peaks, with nucleotides and carbohydrates generally peaking around ZT 9 (zeitgeber time 9, equivalent to nine hours after light onset), whereas amino acids and xenobiotic-related metabolites peaked at night (ZT 15-ZT 21) [276]. Moreover, the posttranslational regulation of clock proteins and histones requires cofactors provided by cell energy metabolism, revealing a close interdependence between circadian regulation and cellular metabolism. The most well-characterized pathway interconnecting both processes is

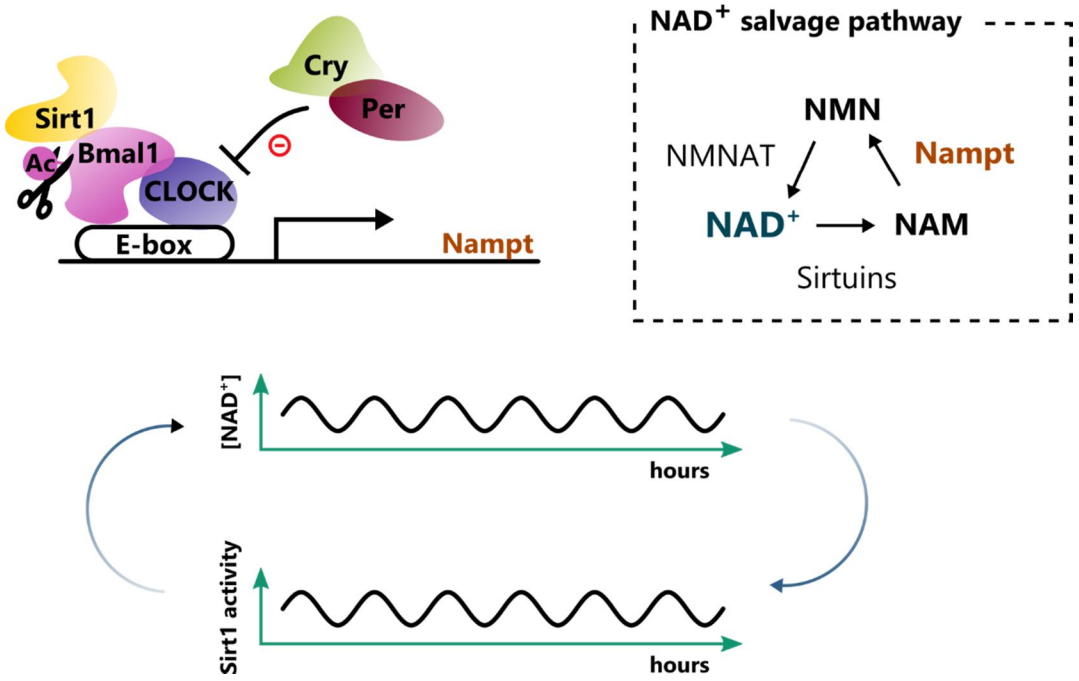

Figure 2.2: Crosstalk between transcriptional and enzymatic feedback loops. The circadian machinery regulates the transcription of *Nampt* (NAM phosphoribosyl transferase), an essential enzyme that participates in the NAD+ salvage pathway, and, by consequence, the intracellular levels of NAD+. The activity of the NAD+-dependent deacetylase SIRT1 is clock-controlled and SIRT1 itself controls the oscillatory synthesis of its own coenzyme by association with CLOCK-Bmal1 in the CLOCK chromatin complex. The metabolites and enzymes involved are: nicotinamide (NAM), nicotinamide adenine dinucleotide (NAD), nicotinamide mononucleotide (NMN) and nicotinamide mononucleotide adenylyl transferases (NMNAT). -, represses transcription; Ac, acetyl group.

the NAD+ metabolism (Fig. 2.2). NAD+ is used as co-substrate by SIRTs for acetyl group removal from protein substrates. Thus, the energy state of the cell and the amount of NAD+ is a crucial determinant for SIRTs activity and protein acetylation. Additionally, NAD+ is a circadian metabolite. This happens because one of the two metabolic pathways of NAD+ synthesis, the salvage pathway, operates in a circadian manner. Along this pathway, nicotinamide (NAM) is converted into nicotinamide mononucleotide (NMN) by the enzyme nicotinamide phosphoribosyltransferase (NAMPT), a rate limiting enzyme. Later NMN is converted by the enzyme NAM/nicotinic mononucleotide adenylytransferase into NAD+ (Fig. 2.2). The circadian clock controls the *Nampt* transcription through the binding of Bmal1,

CLOCK and SIRT1 to *Nampt* promoter (Fig. 2.2). As a consequence of Nampt oscillation, NAD^+ levels and SIRTs activity (but not the protein abundance) show a circadian rhythmicity [277]. SIRT1 plays important roles in energy metabolism, proliferation, apoptosis and transcriptional regulation but is also a regulator of both central and peripheral circadian clocks [278, 279]. SIRT1 ablation results in altered circadian expression and increased cellular NAD^+ levels through the overexpression of *Nampt* [280]. On the other hand, activation of SIRT1 is implicated with repressed CLOCK:Bmal1-driven gene expression by reducing H3 acetylation at CCG promoters [280]. Furthermore, SIRT1 and NAD^+ levels regulate H3K4 trimethylation by clock-controlled MLL1 acetylation [281].

In addition, hepatic SIRT6, localized constitutively in nuclear chromatin, regulates the circadian expression of genes implicated in fatty acid and cholesterol metabolism [282], while free fatty acids themselves were shown to stimulate SIRT6 catalytic efficiency [283], linking the circadian transcription with diet-induced metabolic regulation. Other NAD^+ dependent chromatin regulatory enzymes are poly-ADP ribose polymerases (PARPs). PARP-1 activity was shown to oscillate daily following feeding-fasting cycles and to modulate CLOCK-Bmal1 binding to DNA [284]. Interestingly, PARP-1 and SIRT1 activities seem to be related and linked by NAD^+ content, since PARP-1 deletion increases NAD^+ availability and SIRT1 activity [285].

As previously referred, another important metabolite that links cellular metabolism and epigenetics is acetyl-CoA. Acetyl-CoA is derived mainly from glucose, fatty acids and branched amino acids catabolism and it occupies a central role in multiple cellular processes including TCA cycle, fatty acids, steroids and specific amino acids biosynthesis [286, 287]. Also, acetyl-CoA provides the transfer of the acetyl group into proteins during acetylation reactions, including to histones. The regulation of protein acetylation is highly dependent on the distribution of acetyl-CoA inside the cell and two separate acetyl-CoA pools are known: the mitochondrial and the nuclear/cytosolic

pool [286, 288]. In mitochondria, acetyl-CoA is mainly produced from the oxidative decarboxylation of pyruvate by pyruvate dehydrogenase complex (PDC) and from fatty acid oxidation. The nuclear/cytosolic pool derives either from citrate by ATP citrate-lyase (ACLY) or from acetate, produced by acetyl-CoA synthetase 1 (AceCS1). Interestingly, SIRT1 is required for the control of AceCS1 activity and the cyclic acetylation of AceCS1 contributes to the rhythmicity of acetyl-CoA levels [269]. Murine protein levels of ACLY were also found to be cyclic in the liver [289].

The continuous demonstrations of the relation between the circadian clock and metabolism place mitochondria in a central position of interface between energy regulation, redox state and the circadian cycle. Indeed, oxygen consumption, OxPhos subunits activity, and ATP levels exhibit a circadian oscillation [290-293]. Also, mitochondrial dynamics and network morphology appear to be Bmal1-dependent [294]. Another very interesting study demonstrated that both mitochondrial rhythmic transcripts and proteins are predominantly gated to accumulate at specific ZTs in mice liver, rather than equally distributed through the day [293]. Still in this study, ~38% of mitochondrial proteins were described to oscillate daily, with most of them reaching their peak at ZT 4 [293]. Furthermore, clock-driven acetylation is particularly important in mitochondrial proteins involved in metabolic pathways (eg. fatty acid beta-oxidation, urea cycle, TCA cycle) [295]. In mitochondria, protein acetylation is vital for the regulation of the metabolic reactions, given that ~63% of mitochondrially localized proteins contain acetylation sites, even though the functional consequence of these acetylations have not been totally established [296]. Disruption of the clock in the liver resulted in a number of changes in the levels of acetylation of multiple proteins, including acetyl-CoA acyltransferase 2, hydroxyacyl-CoA dehydrogenase alpha, glutathione-S transferase, or succinate dehydrogenase protein complex subunit A [295].

As mitochondria are the prime organelle for ROS production, and oxygen exhibits a circadian consumption rate, it has been suggested that oscillations in cellular redox state could derive from rhythmic ROS production, as well as from the oscillatory activity of antioxidant proteins [297]. Conversely, critical oxidative stress caused by H_2O_2 resets circadian clocks *in vitro* [298]. Accumulating evidences illustrate the importance of the redox state for the maintenance of oscillatory rhythms. In human red blood cells, that possess no nucleus and therefore no transcriptional oscillations, it was found that peroxiredoxins (PRX), antioxidant proteins that help in the control of intracellular H_2O_2 levels, undergo 24 hours redox cycles suggesting that transcription cycles may not be totally essential for the persistence of some molecular clocks [299]. In some particular tissues, heart included, the activity of PRX is modulated by the reversible hyperoxidation of its active site. In mitochondria, when the levels of hyperoxidized PRX III (PRX III-SO_2H) reach a certain threshold, H_2O_2 starts being released into the cytosol. It is believed that this release happens in a circadian manner and with a downstream effect on mitochondrial sulfiredoxin levels and PRX reduction [300, 301].

One of the players responsible for the mitochondrial rhythmicity is mitochondrial SIRT3. NAD^+ is required in glycolysis and TCA cycle as electron carrier and is fundamental for the activity of SIRT3 and other SIRTs. This mitochondrial sirtuin has a key role in several mitochondrial pathways including lipid metabolism and oxidative phosphorylation. The transcriptional regulation of the master regulator of mitochondrial biogenesis, PGC-1α, can be modulated by SIRTs, including SIRT3 [302]. SIRT3 was also found to regulate fatty-acid oxidation under fasting conditions as well as the acetylation state and activity of long-chain acyl coenzyme A dehydrogenase [303]. As a NAD^+ dependent enzyme, SIRT3 generates rhythms in the acetylation and activity of oxidative enzymes influencing the oxidative phosphorylation [290]. Circadian disruption impaired SIRT3 activity with downstream effects on the

acetylation levels of SIRT3 targets including manganese superoxide dismutase and isocitrate dehydrogenase 2 [290].

AMPK is regulated by the ATP/AMP balance, thus, it is influenced by the oscillatory levels of ATP along the day. Since AMPK is known for phosphorylating CRY proteins and regulating their degradation [304], it has an intercommunication function between mitochondrial function, energy state and the circadian regulation. The PPAR family (PPAR$\alpha/\gamma/\delta$), that regulates lipid metabolism and energy homeostasis, also showed circadian expression profiles [305, 306].

2.3. Circadian disruption and heart disease

It is recognized the importance of intact circadian rhythms to the maintenance of cardiovascular health. Cardiac function and physiology are highly dependent of the daily rhythmicity; heart rate, blood pressure and cardiac contractility all peak in the wake hours and are lower during sleep [307, 308]. These differences are associated with the different physiological demands during the day. Non-dipping pattern of circadian blood pressure (failure to decrease blood pressure at night) is an important pathophysiological factor that is associated with increased cardiovascular risk [309]. Similarly, adverse cardiovascular effects do not happen randomly along the day. Instead, they are more prone to occur during the morning as happens with myocardial infarction that is most likely to occur between 6:00 am and noon or sudden cardiac death whose incidence peaks in the midmorning [308]. Both, physiological parameters and pathological conditions are associated. For example, the pressure load verified during the morning combined with risk factors such as cardiac hypertrophy, endothedial dysfunction or atherosclerosis may predispose to higher incidences of cardiovascular events. On the other hand, disturbances in the circadian rhythms as a consequence of the modern lifestyle, where people experience jet-lag, constant

electrical lightening or shift work, have a profound impact on cardiovascular diseases. Cortisol and melatonin that peak at morning and nighttime, respectively, and work together in setting the daily circadian rhythms, were observed to be desynchronized in night shift workers [310, 311]. This group of workers has previously been described to have a higher propensity to develop ischaemic heart disease [312]. Melatonin was suggested to be cardioprotective by acting as antioxidant and stimulating transcription of antioxidant enzymes [313-315].

Several works focused their attention on the cardiac circadian patterns of gene expression. It was estimated, in murine models, that around 8-13% of cardiac genes show circadian regulation [316, 317]. Interestingly, while the circadian transcriptome in the liver shows a broad distribution of phases, in the heart most of the genes show a synchronized peak of expression at ZT 4 [316]. The heart mostly relies on mitochondria for the production of ATP and it is curious to observe that this concentration of transcription peak around one particular ZT follows the same pattern observed for mitochondrial rhythmic proteins [293]. Heart-specific Bmal1 knockout mice presented progressive heart failure, ventricular dilation, thinner myocardial walls and myocardial fibrosis [318]. In addition, multiple genes regulating fatty acid metabolism, TCA cycle, OxPhos and mitochondrial biogenesis were mainly downregulated [318]. Considering that the heart has the ability to shift from fatty acid metabolism to other sources of energy when required, the lack of flexibility caused by circadian disruption is a problem for the cardiac homeostasis. Mice with *clock* mutant cardiomyocytes that were fed with a high fat diet exhibited metabolic and transcriptomic alterations, including attenuated oscillations of triglycerides and lipolysis, that reinforced the role of the clock in the regulation of myocardial fatty acid metabolism [319]. Circadian disruption by exposure to disrupted light/dark cycle regimens also altered the oscillatory expression of cardiac clock and metabolic genes [318]. Furthermore, mice carrying a mutation in *Per2* showed attenuated dipping of blood pressure and heart rate, and presented shorter circadian periods under constant

darkness [320]. PER2 was also related with fatty acid metabolism and inflammation during myocardial ischemia and reperfusion [321] and it was described to be essential in the maintenance of endothelial progenitor cells and angiogenesis [322].

Highly energy demanding organs, such as the heart, are supported by the oxidative metabolism of a wide range of fuels in mitochondria. The metabolism of these substrates is tied to the NAD^+ pathway for energy production. Depletion of NAD^+ levels were associated to heart pathological conditions [323], while elevating NAD^+ levels seems to be a strategy with potential therapeutic effects in cardiac diseases [324]. In addition, the synthesis of NAD^+ in the heart is almost exclusively based on the salvage pathway (described on section 2.1.2) in opposite to the *de novo* synthesis [325]. While ischemia and ischemia/reperfusion downregulate *Nampt* and increase apoptotic markers, the overexpression of *Nampt* increases NAD^+ and ATP concentrations and attenuated myocardial injury [326].

2.4. Chronopharmacology: drug input to the circadian clock

The importance of the time of the day for the efficiency of drugs and treatments has been known for decades. It is not by chance that certain medications are taken during fasting, after meals or before bedtime. Important parameters including drug's absorption, distribution, metabolism, elimination or the side effects are taken in consideration when determining the time of drug administration. The term chronopharmacology emerged from this observation that the administration of medication should be synchronized with the body's circadian clock to maximize the effectiveness of the drug and minimize the side effects. Most anticancer medications, for instance, display different tolerability and efficacy as a result of different circadian timing of drug administration [327]. Moreover, many enzymes involved in liver detoxification and drug metabolism, including P450-oxidoreductase, aldehyde

dehydrogenases or members of drug transporter families are regulated by DBP, TEF and HLF in a circadian manner [328]. Another example of a clock-controlled process is drug conjugation, which is relevant in converting xenobiotics into a more hydrophilic form, facilitating their excretion. In male mice, the hepatic glutathione S-transferase, a conjugation enzyme, shows higher activity in the light phase [329]. The circadian fluctuations also modulate the pharmacokinetics of intravenously administered drugs, such as the anticancer DOX [330]. In a mammary adenocarcinoma mice model, DOX was administered at 6 different circadian stages (three during the resting phase, after light onset and three during the active phase, during darkness) and a significant best tolerability and efficacy were observed near the middle of the resting phase (ZT 7), in opposite to ZT 19, where higher toxicity was detected [331]. A previous study also demonstrated DOX maximal benefit and minimal toxic effects with administration in the middle-end of the daily resting phase [332]. In contrast, repeated DOX administration in rats at ZT 9 led to higher toxic death numbers, as well as higher levels of cardiotoxicity markers including creatine kinase, malondialdehyde (lipid peroxidation indicator) and glutathione peroxidase [333]. Inflammatory responses to DOX were also demonstrated to be under circadian influence [334]. More recently, it was observed that human embryonic stem cell-derived cardiomyocytes possess a significant circadian pattern of apoptotic response when exposed to DOX [335]. Altogether, these evidences are crucial in the understanding of how the circadian system affects drug pharmacology.

Many drugs have also been investigated in order to specifically target the circadian machinery and be used in the case of clock-linked metabolic disorders. One such example is melatonin that is taken to decrease the effects of jetlag or sleeping problems [336, 337]. Other molecules have been found to modulate the central and peripheral clocks [338], as well as specifically modulate clock proteins such as Bmal1 and CRY [339, 340]. The authors speculated that these new molecules can be a promising strategy in treating circadian rhythm-related diseases.

As previously referred, circadian rhythms disruption can be the cause of chronic diseases. External cues, including therapeutic drugs, have been shown to contribute to the adverse pathological consequences by affecting core properties of the circadian clock as was observed with mitomycin C (used in chemotherapy and ophthalmology) [341] or carbachol [342]. Furthermore, the consumption of drugs of abuse [343], alcohol [344, 345] or the exposure to tobacco/cigarette smoke [346] were described to affect not only the expression of clock controlled genes but also locomotor activity and behavior. Additionally, *in vivo* studies demonstrated the increased lengthening and phase shift of peripheral clocks in mice exposed to caffeine [347] and phase delay of circadian melatonin rhythm in humans, possibly by increasing cyclic AMP levels, an active player of the cellular circadian clock [348]. The fact that the exposure to environmental stresses and xenobiotics has the capacity to modulate peripheral circadian clocks is alarming for the homeostatic balancing of the body. An appropriate maintenance of the circadian clocks, the awareness of the desynchronization caused by drugs and the respect for the internal rhythms are important for the improvement of pharmacotherapeutics to delineate future protective measures.

Chapter 3

3. Objectives and Experimental Approaches

3.1. Hypothesis and Aims

Doxorubicin treatment often results in severe cardiotoxic effects (as described on Chapter 1). The multiplicity of dysregulated pathways and cell functions after DOX exposure makes it difficult to clearly understand the pathophysiology of the disease and to plan strategies to ameliorate the balance between toxicity against cancer *versus* cardiac cells.

Three different specific aims were addressed in the present thesis, which were divided in three independent chapters:

a) The first objective was to evaluate the role of DOX preconditioning in the resistance against a further DOX exposure in H9c2 cardiomyoblasts. It is known that DOX induces persistent changes in the cardiac tissue, most of the times deleterious. However, the occurrence of hormesis-like effects have been reported in the field of toxicology and it has been described that low/moderate levels of ROS may have a beneficial role by upregulating defenses against oxidative stress and leading to cellular adaptation. Thus, our hypothesis was that exposing cardiac-derived cells to sub-clinical concentrations of DOX would trigger cellular resistance against a subsequent clinical-relevant DOX exposure. To test this hypothesis we used proliferating H9c2 cardiomyoblasts in order to be able to maintain viable cells in culture for a long period after the

first DOX incubation. Several morphological, transcriptional and bioenergetics parameters were evaluated in combination with the cell viability assays.

b) The impact of DOX on the H9c2 cell line has been extensively studied by several groups, including ours, over the years [34, 136-138, 140, 349]. However, this cell line possess some limitations and other *in vitro* models with features more similar to mature cardiomyocytes have been preferred. Thus, the second goal was to investigate the effects of DOX exposure on non-proliferating and beating iPSC-derived mouse cardiomyocytes in terms of response to stress and cellular/ mitochondrial metabolism. The presence of the contractile component makes these cells more bioenergetically demanding, which allows to obtain a better understanding of the toxicity of DOX in beating cardiomyocytes.

c) The last specific aim was to improve the knowledge on the persistence of the effects when DOX treatment is performed early in life (during childhood). Our hypothesis was that the early exposure to DOX, which is known for interfering with the cell redox state and metabolism, could alter the normal circadian regulation of the heart. We also aimed to understand if sirtuins, SIRT1 in particular, could be the bridge between energy status and circadian homeostasis. To clarify these questions we used juvenile C57BL/6J male mice for the early-life DOX treatment, and complementary experiments were performed with MEFs and HEK293. The effects of DOX on total and circadian gene expression, as well as key acetylation patterns were evaluated.

With these several lines of study we hope to provide new insights and highlight relevant information on the distinct responses of cardiac models to different DOX treatments and concentrations. Ultimately, the obtained results will contribute for a better management of the anticancer treatment and help in the research for preventive measures.

3.2. Biological Models

3.2.1. H9c2(2-1) cell line

H9c2(2-1) (frequently referred just as H9c2) cell line is a subclone of the original clonal cell line H9c2 (Fig. 3.1 A), obtained by serial passaging of cells from embryonic rat heart [350]. This cardiomyoblast cell line is one of the most popular *in vitro* models in cardiovascular research and cardiotoxicity studies, extensively used by our group [34, 136, 138, 349, 351]. This cell model is regularly used as a model of cardiomyocytes, however, in opposition to the latter, H9c2 are proliferating cells and possess some features of skeletal muscle, resembling immature myogenic cells [350, 352]. The attractiveness of H9c2 relies on the facility of being kept in culture, the lack of ethical issues related with using experimental animals and the longer lifespan that allows their use for multiple passages. Additionally, H9c2 have the ability to differentiate either into skeletal or cardiac muscle when differently stimulated. It has been reported that the reduction of serum in the culture media leads to an adult skeletal muscle phenotype, while low serum culture media supplemented with retinoic acid shifts to an adult cardiac muscle phenotype [350, 351, 353, 354]. Furthermore, when reaching confluence, H9c2 start to fuse into multinucleated tubular structures and exhibiting skeletal muscle properties [350]. Importantly, neither in their undifferentiated state nor with the differentiated cardiac phenotype the cells possess contractile activity. However H9c2 still possess features of cardiac tissue including cardiac L-type Ca^{2+} channels [355, 356] and are a validated model for *in vitro* studies of cardiac hypertrophy [357].

3.2.2. Cor.At™ cardiomyocytes

Cor.At™ cells (Axiogenesis, NCardia, Germany) are pure primary-like cardiomyocytes derived from induced-pluripotent stem cells (iPSCs), through a

puromycin selection process (Fig. 3.1 B) [358, 359]. Primary cardiomyocytes are obviously an informative model, however, the technical difficulties often observed in primary culture management, including low yields and impure cultures, represent a significant obstacle. Similarly to primary cardiomyocytes, Cor.At cells have limited proliferative capacity and a contraction machinery that allows them to beat synchronously about 48 hours after culture and with a progressive increase with time [360, 361]. In addition, Cor.At cells express cardiac marker genes (eg. troponins, tropomyosins, myosins, Nppa, Nppb, Gata4 and Gata6), ions channels and connexins involved in gap junctions formation and contraction; with the presence of cardiac α-actin and connexin 43 confirmed by immunofluorescence experiments [359, 361]. Structural and functionally, Cor.At present a mature myofibrillar architecture, characterized by uniformly distributed α-actin-rich striations [362] and display cardiac voltage-gated ion currents which include sodium, potassium and L-type calcium currents [361]. These features typical from developed cardiomyocytes make them a useful tool for cardiac toxicity screening assays of compounds interfering not only with ion channels function and contractility but also with the highly bioenergetically demanding cardiomyocytes metabolism [360, 361].

3.2.3. C57BL/6J mice

The C57BL/6J mouse is a substrain of the C56BL/6 mouse inbred strain that is one of the mice models most commonly used in animal studies (Fig. 3.1 C). The cardiovascular physiology within mammalian species does not differ greatly, and the ventricular structure of mouse and human heart are considered very similar [363]. Mice hearts possess higher resting heart rates and higher energetic requirements comparing with larger animals with lower resting heart rates. Therefore, they exhibit increased oxidative capacity, myosin ATPase activity and sarcoplasmic reticulum ATPase activity, which is compliant with the increased mitochondrial density in the

myocardium [364, 365]. For being such energy demanding organs, mice hearts can be very informative in regard to the understanding of the impact of cardiac challenges in cellular homeostasis and metabolic remodeling. As an example, C56BL/6 mice have been used for many groups as model of sub-chronic and acute DOX-induced heart injury including when investigating dilated cardiomyopathy [95, 366-370].

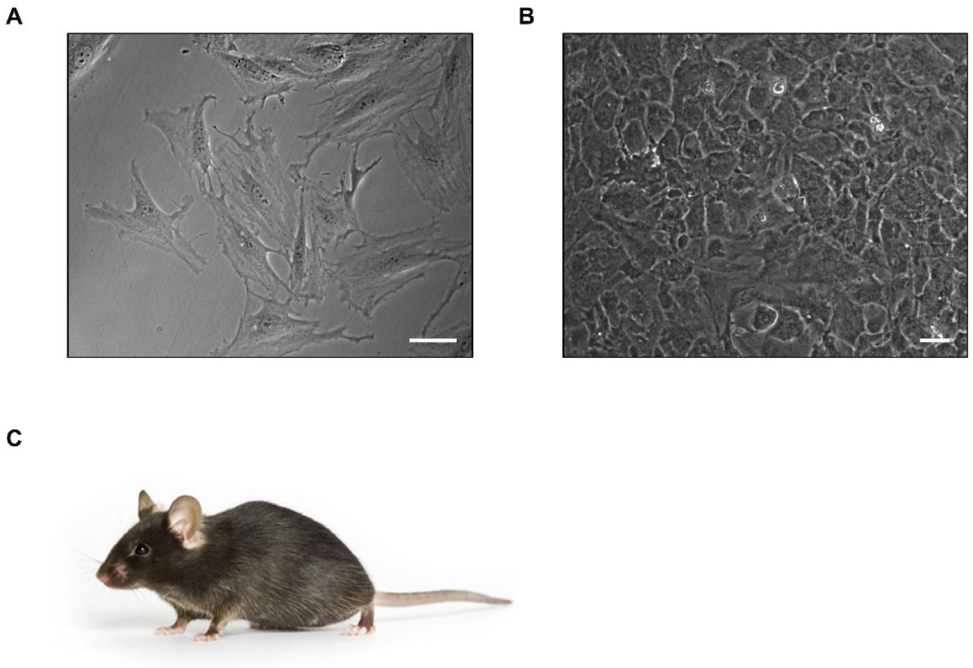

Figure 3.1: Representative images of the main biological models used in this thesis: A) H9c2 rat cardiomyoblasts (scale bar represents 50 μm); B) Cor.At cardiomyocytes (scale bar represents 30 μm); C) C57BL/6J mouse (image taken from The Jackson Laboratory website - https://www.jax.org)

EXPERIMENTAL PROCEDURES AND RESULTS

Chapter 4

4. General Equipment and Material

4.1. Equipment

- Accuri™ C6 flow cytometer *(Becton Dickinson, USA)*
- CFX™ Real-Time system *(Bio-Rad, USA)*
- CM1950 cryostat *(Leica, Germany)*
- Cytation™ 3 microplate reader *(BioTek, USA)*
- Experion Automated Electrophoresis System *(Bio-Rad, USA)*
- Nanodrop 2000 *(ThermoScientific, USA)*
- Nikon Eclipse Ti-S fluorescence microscope *(Nikon Instruments Inc., USA)*
- Potter homogenizer *(Heidolph, Germany)*
- Seahorse XFe96 analyzer *(Agilent Technologies, USA)*
- TissueLyser II *(Qiagen, Germany)*
- UVP Biospectrum 500 Imaging System *(UVP, UK)*
- Victor X3 multiplate reader *(Perkin-Elmer, USA)*
- Waters® Breeze™ system, consisting of a 1525 Binary HPLC Pump and a Waters® 2487 Dual Wavelength Absorbance Detector *(Waters, USA)*
- Z16 APO microscope *(Leica, Germany)*

4.2 Chemical reagents

Table 4.1: List of chemical reagents

Reagent	Reference	Distributor
Acetic acid	131008.1611	Panreac
ADP	A2754	Sigma-Aldrich
AMP	A1752	Sigma-Aldrich
ATP	A-2383	Sigma-Aldrich
Beta mercaptoethanol	M3148	Sigma-Aldrich
Calcium chloride	C5080	Sigma-Aldrich
D-(+)-glucose	G7021	Sigma-Aldrich
Dexamethasone	D1756	Sigma-Aldrich
DMSO	34869	Sigma-Aldrich
Doxorubicin	D1515	Sigma-Aldrich
EDTA	ED2SS	Sigma-Aldrich
Eosin	HT110132	Sigma-Aldrich
Ethanol	121086.1212	Panreac
FCCP	SC-203578	Santa Cruz Biotechnology
Glycine	MB01401	Nzytech
Guanidine hydrochloride	BP178-500	Fisher Scientific
HCl	131020.1212	Panreac
Hematoxylin	SH26	Fisher Scientific
HEPES	H3375	Sigma-Aldrich
Histomount	HS-103	National Diagnostics
Histosol	HS-100	National Diagnostics
Hoechst 33342	B2261	Sigma-Aldrich
Iodoacetate	I4386	Sigma-Aldrich
Isopropyl alcohol	190764	Sigma-Aldrich
Methanol	M/4056/17	Fisher Chemical
NAC	A9165	Sigma-Aldrich
Oligomycin	SC-203342	Santa Cruz Biotechnology
Perchloric acid	P/1280/PB15	Fisher Chemical
Pifithrin-alpha	506132	Millipore
PMSF	P7626	Sigma-Aldrich
Ponceau S	P3504	Sigma-Aldrich
Potassium hydroxide	P5958	Sigma-Aldrich
Propidium iodide	P3566	Molecular Probes
PureZOL reagent	732-6890	Bio-Rad
Resazurin	R7017	Sigma-Aldrich
RNase-free water	H20MB1001	Millipore
Sodium bicarbonate	S6014	Sigma-Aldrich
Sodium butyrate	B5887	Sigma-Aldrich
Sodium chloride	S7653	Sigma-Aldrich
Sodium dichloroacetate	34,779-5	Sigma-Aldrich

Table 4.1: Continued from previous page

Reagent	Reference	Distributor
Sodium dodecyl sulphate	1610301	Bio-Rad
Sodium hydroxide	S8045	Sigma-Aldrich
Sucrose	84100	Sigma-Aldrich
Sulforhodamine B	S9012	Sigma-Aldrich
TEMED	MB03501	Nzytech
TMRE	115532-52-0	Santa Cruz Biotechnology
TMRM	T-668	Molecular Probes
Tris base	MB01601	Nzytech
Triton X-100	X100	Sigma-Aldrich
TRIzol reagent	15596018	Life Technologies
Tween 20	P1379	Sigma-Aldrich
z-VAD-fmk	ALX-260-020-M001	Enzo Life Science

4.3 Solutions

Buffered Saline Solution (PBS, 10x)

17.6 mM KH_2PO_4

1.37 M NaCl

101 mM Na_2HPO_4

26.8 mM KCl

Stored at room temperature

Running Buffer (10x)

2 M Glycine

0.25 M Tris-HCl

0.1% (w/v) SDS

Stored at room temperature

Transfer Buffer (10x)

1.93 M Glycine

0.25 M Tris-HCl

Stored at room temperature. Transfer Buffer 1x is prepared on the day of the assay by diluting transfer buffer 10x in water, with 10% (v/v) methanol and 0.005% (w/v) SDS and kept at 4°C until used.

Washing buffer (TBS-T) (10x)

1.54 M NaCl

0.5 M Tris-HCl [pH 8.0]

1% (v/v) Tween 20

Stored at room temperature.

Microscopy medium

120 mM NaCl

3.5 mM KCl

0.4 mM KH_2PO_4

20 mM HEPES

5 mM $NaHCO_3$

1.2 mM $NaSO_4$

1.3 mM $MgCl_2$

1.3 mM $CaCl_2$

15 mM glucose

pH adjusted to 7.4, sterilized by autoclaving and by filtration (0.22 μm) and stored at 4°C.

Basal Medium

109.5 mM NaCl

5.4 mM KCl

1.8 mM $CaCl_2$

0.91 mM NaH_2PO_4

1 mM $MgCl_2$

25 mM glucose

25 mM HEPES

pH adjusted to 7.4, sterilized by autoclaving and by filtration (0.22 μm) and stored at 4°C.

STM buffer

250 mM sucrose

50 mM Tris-HCl [pH 7.4]

5 mM $MgCl_2$

Supplemented with 1 μL/mL protease inhibitor cocktail.

NET buffer

20 mM HEPES [pH 7.9]	0.2 mM EDTA
1.5 mM $MgCl_2$	20% (v/v) glycerol
0.5 M NaCl	1% (v/v) Triton-X-100

Supplemented with 1 μL/mL protease inhibitor cocktail.

RIPA buffer

50 mM Tris [pH 8]	Inhibitors:
150 mM NaCl	0.5 mM PMSF
5 mM EDTA	1 μL/mL Protease Inhibitor Cocktail
15 mM $MgCl_2$	20 mM NaF
1% (v/v) NP40	10 mM Nam
	330 nM TSA
	0.5% (w/v) DOC

Stored at 4°C (the inhibitors were added before use).

Ponceau

0.3% (w/v) Ponceau S

5% (v/v) glacial acetic acid

Stored at room temperature.

4.4 Kits

Aurum™ Total RNA Mini Kit *(Bio-Rad, Hercules, CA, USA)*

BCA Protein Assay Kit *(Thermo Fisher Scientific, Lafayette, CO, USA)*

CellTiter-Glo Luminescent Cell Viability Assay *(Promega, Madison, WI, USA)*

DNMT1 ELISA kit *(ab113469, Abcam, Cambridge, UK)*

iScript cDNA synthesis kit *(Bio-Rad, Hercules, CA, USA)*

PDH Activity Assay Kit *(Sigma-Aldrich, St. Louis, MO, USA)*

Promega Caspase-GLO 3/7 assay *(Promega, Madison, WI, USA)*

Promega Caspase-GLO 9 assay *(Promega, Madison, WI, USA)*

PureLink™ Genomic DNA MiniKit *(Invitrogen, Carlsbad, CA, USA)*

Seahorse XF Cell Mito Stress Test *(Agilent Technologies, Santa Clara, CA, USA)*

Seahorse XF Glycolysis Stress Test *(Agilent Technologies, Santa Clara, CA, USA)*

SsoFast™ EvaGreen® supermix *(Bio-Rad, Hercules, CA, USA)*

SYBR® Green supermix *(Bio-Rad, Hercules, CA, USA)*

4.5 Antibodies

Table 4.2: List of antibodies used in Western Blot, Immunostaining and Immunoprecipitation protein analysis

	Dilution	MW (kDa)	Gel (%)	Host	Reference	Manufacturer
Western Blot						
Chapter 6						
HK2	1:1000	102	10	rabbit	#2867	Cell Signaling
OXPHOS	1:1000	—	10	mouse	ab110413	Abcam
p53	1:1000	53	10	mouse	#2524	Cell Signaling
PARP-1	1:1000	116	10	rabbit	sc-7150	Santa Cruz
PDH	1:1000	43	12	rabbit	#3205	Cell Signaling
Phospho-PDH Ser293	1:5000	43	12	rabbit	ABS204	Millipore
SOD2	1:1000	25	10	mouse	ab16956	Abcam
Anti-mouse IgG, HRP-linked antibody	1:5000	—	—	—	#7076S	Cell Signaling
Anti-rabbit IgG, HRP-linked antibody	1:5000	—	—	—	#7074	Cell Signaling
Chapter 7						
AceCS1	1:10000	75	8	rabbit	#3658S	Cell Signaling
Acetyl Bmal1 (Lys538)	1:500	78	6	rabbit	AB15396	Millipore
acetyl H3 (Lys9)	1:2000	17	16	rabbit	#9649	Cell Signaling

Table 4.2: Continued from previous page

	Dilution	MW (kDa)	Gel (%)	Host	Reference	Manufacturer
Western Blot						
Chapter 7						
acetyl p53 (Lys379)	1:1000	53	12	rabbit	#2570	Cell Signaling
Alpha tubulin	1:50000	52	—	mouse	T5168	Sigma-Aldrich
Bmal1	1:5000	78	6	rabbit	ab93806	Abcam
Flag tag	1:3000	—	—	rabbit	F7425	Sigma-Aldrich
H3	1:2000	17	16	rabbit	#4499	Cell Signaling
Myc tag	1:5000	—	—	mouse	GTX628259	GeneTex
p53	1:1000	53	12	mouse	#2524S	Cell Signaling
p84	1:5000	84	—	mouse	GTX70220	GeneTex
Total acetyl-lysine	1:2000	—	10	rabbit	#9441S	Cell Signaling
Anti-mouse IgG, HRP-linked antibody	1:10000	—	—	—	AP160P	Millipore
Anti-rabbit IgG, HRP-linked antibody	1:10000	—	—	—	12-348	Millipore
Immunostaining						
5-methylcytosine	1:100	—	—	mouse	ab73938	Abcam
Anti-mouse IgG, Alexa Fluor 488-conjugated antibody	1:200	—	—	—	A11001	Invitrogen
Immunoprecipitation						
myc tag	1:250	—	—	mouse	GTX628259	GeneTex
IgG	—	—	—	mouse	sc-2025	Santa Cruz Biotechnology

4.6 Biological models

Cor.At iPSC-derived cardiomyocytes *(#Ax-C-MC02, NCardia, Germany)*

Wild-type male C57BL/6J mice *(Jackson Laboratory, USA)*

HEK293 *(CRL-1573™, ATCC, USA)*

H9c2(2-1) *(CRL-1446™, ATCC, USA)*

Hs-578T *(HTB-126™, ATCC, USA)*

MDA-MB-231 *(HTB-26™, ATCC, USA)*

4.7 Cell culture reagents and media

Antibiotic/Antimycotic Solution *(15240-062, Thermo Fisher Scientific, Lafayette, CO, USA)*

Cor.At culture medium *(#Ax-M-MC250, NCardia, Cologne, Germany)*

Dulbecco's modified Eagle's medium *(DMEM D5030, Sigma-Aldrich, St. Louis, MO, USA)*

Dulbecco's modified Eagle's medium high glucose *(DMEM D5648, Sigma-Aldrich, St. Louis, MO, USA)*

Fetal Bovine Serum *(FBS; 10270–106, Thermo Fisher Scientific, Lafayette, CO, USA)*

Fibronectin (F1141, Sigma-Aldrich, St. Louis, MO, USA)

HyClone™ Dulbecco's modified Eagle's medium *(SH30243, Fisher scientific, Hampton, NH, USA)*

Puromycin *(NCardia, Cologne, Germany)*

Trypsin-EDTA (0.05%) *(25300062, Thermo Fisher Scientific, Lafayette, CO, USA)*

4.8 Specific reagents for biological analysis

Albumin, from bovine serum *(A7030, Sigma-Aldrich, St. Louis, MO, USA)*

BioT Transfection agent *(Bioland Scientific, Paramount, CA, USA)*

Cell lysis buffer *(98035, Cell Signaling, Danvers, MA, USA)*

Clarity™ Western ECL Substrate *(170-5061, Bio-Rad, Hercules, CA, USA)*

Fluorescence Mounting Medium *(S3023, DAKO, Denmark)*

Laemmli sample loading buffer *(Bio-Rad, Hercules, CA, USA)*

Precision Plus Protein™ Standard *(161-0394, Bio-Rad, Hercules, CA, USA)*

Protease Inhibitor Cocktail *(P8340, Sigma-Aldrich, St. Louis, MO, USA)*

Protein G Sepharose® beads *(3296, Sigma-Aldrich, St. Louis, MO, USA)*

Prolab RMH 2500 standard chow *(PMI Nutrition International LLC, Brentwood, CA, USA)*

RNase *(12091-021, Invitrogen, Carlsbad, CA, USA)*

Shandon™ Cryomatrix™ embedding resin *(6769006, Thermo Fisher Scientific, Lafayette, CO, USA)*

4.9 Primers

The primers used for quantitative real-time PCR (RT-qPCR) were chosen based on several criteria: a) primers should be specific and have compatible melting temperatures; b) the product length should be approximately 80-250 bp; c) primers should have between 18 and 24 nucleotides in length as well as approximately 50% of GC content and, importantly; d) primers should hybridize at exon-exon junctions, in order to avoid the amplification of any genomic DNA in solution. These features can be used to design primers with a proper software for primer design, such as the NCBI Primer-BLAST tool (https://www.ncbi.nlm.nih.gov/tools/primer-blast/). Still, other characteristics should be kept in mind, such as for example 1) the 3′ primer end should not be complementary with any unspecific region, 2) if possible the 3′ end should be rich in GC content to enhance the annealing and 3) the sequences must be checked in order to avoid secondary structures and hybridization between the pair of primers. The primers used are identified in the Table 4.3.

Table 4.3: Sequences of primers used for the analysis of gene expression. Abbreviations: F, forward; R, reverse; Amp, amplicon; Tan, annealing temperature; MEF, mouse embryonic fibroblasts

Target	Accession Number	Sequences (5′ -3′)	Amp (bp)	Tan (°C)
Rat – H9c2				
18S	NR_046237	**F** ACTCAACACGGGAAACCTC **R** ACCAGACAAATCGCTCCAC	122	63
ACAA2	NM_130433	**F** CCTCAGTTCTTGGCTGTTCA **R** CCACCTCGACGCCTTAAC	149	63
ACOX1	NM_017340	**F** GCAGACAGCCAGGTTCTTGATG **R** ACTCGGCAGGTCATTCAGGTAT	94	63

Table 4.3: Continued from previous page

Target	Accession Number	Sequences (5′ -3′)	Amp (bp)	Tan (°C)
Rat – H9c2				
ATP6	AC_000022	**F** CCTGAGCCCTAATAATTGTATCCC **R** GTTCCTTGCGGTGAGAAGT	199	63
ATP8	AC_000022	**F** TGCCACAACTAGACACATCCACAT **R** GAGGGAGGTGCAGGAAAGGTT	112	63
CBP	NM_133381	**F** GCACCCATGCCAACAACATT **R** ACCTGGCCCTGTGAAACAC	151	63
CLS1	NM_001014258	**F** AATGTTGATCGCTGCTGTGTT **R** GCTGTATTGACCTTGCTGATGAAT	132	63
COX1	AC_000022	**F** GCCAGTATTAGCAGCAGGTATCA **R** GCCGAAGAATCAGAATAGGTGTTG	121	63
CYTB	AC_000022	**F** TACGCTATTCTACGCTCCATTC **R** GCCTCCGATTCATGTTAAGACT	189	63
DNMT1	NM_053354	**F** GGAAGGTGAGCATCGACGAA **R** TGCTGTGACCCTGGCTAGAT	101	63
EP300	XM_017595367	**F** TGGAGGCACTTTACCGACAG **R** GATCCATGGGGCTCTTCACA	111	63
GABPA	NM_001108841	**F** CGGCACCAAGCATATCAC **R** GGACCACTGTATAGGATCATAGG	130	63
GABPB1	NM_001039036	**F** GCACCGCTGTCATTTTGTCG **R** CAGAGCAGTCTCACGTCCTC	158	63
HDAC1	NM_001025409	**F** AGCCAAAGGGGTCAAAGAAGA **R** TGAGAAATTGAGGGAAAGTAAGGGA	93	63
HDAC2	NM_053447	**F** GGAGGTCGTAGGAATGTCGC **R** TTTGGCTCCTTTGGTGTCTGT	156	63
HDAC5	NM_053450	**F** CCCGTCCGTCTGTCTGTTAT **R** CCTGACATGCCATCCGACTC	139	63
Mat2A	NM_134351	**F** GGGGAAGGTCATCCAGATAAGA **R** AGCAACAGTTTCACAAGCCAC	105	63
ND1	AC_000022.2	**F** TCCTCCTAATAAGCGGCTCCTTCT **R** TGGTCCTGCGGCGTATTCG	200	63
ND6	AC_000022.2	**F** TCCTCAGTAGCCATAGCAGTTGT **R** GTTGTCTAGGGTTGGCGTTGAA	187	63
NFE2L2	NM_031789	**F** GATGACCATGAGTCGCTTGC **R** TGTCCTGCTGTATGCTGCTTA	136	63
NRF1	NM_001100708	**F** CCAAGCATTACGGACCATAGTT **R** CAGTACCAACCTGGATGAGC	197	63
POLG	NM_053528	**F** ATAATGGCCCACACCCGTTT **R** GAGTTTCCGGTACCACCCAG	102	63
PPARα	NM_013196	**F** AGACTAGCAACAATCCGCCTTT **R** TGGCAGCAGTGGAAGAATCG	136	63
SDHA	NM_130428	**F** CTATGGAGACCTACAGCATCT **R** AATCCGCACCTTGTAATCTTC	178	63
SLP2	NM_001031646	**F** GACTCAACACAATGGAGACGC **R** GCCTGAGCCACCATACTTGT	141	63

Table 4.3: Continued from previous page

Target	Accession Number	Sequences (5′ -3′)	Amp (bp)	Tan (°C)
Rat – H9c2				
SOD1	NM_017050	**F** AAGAGAGGCATGTTGGAGACC **R** CGGCCAATGATGGAATGCTC	115	63
SOD2	NM_017051	**F** CGCGACCTACGTGAACAATC **R** CTCCAGCAACTCTCCTTTGG	193	63
TAZ	NM_001025748	**F** CAAATGGGGAATTGGACGGC **R** AGGGAGTGTACTGAAGGGCT	166	63
TBP	NM_001004198	**F** CCTATCACTCCTGCCACACC **R** CAGCAAACCGCTTGGGATTA	154	63
TFAM	NM_031326	**F** AATGTGGGGCGTGCTAAGAA **R** TCGGAATACAGATAAGGCTGACAG	101	63
TFB1M	NM_181474	**F** CCCGTTACCCACCATTCGAG **R** ATTTTGTCTGTCAGCCTCAAGTC	102	63
TFB2M	NM_001008293	**F** AGTCAAAGCACTCGGAATCA **R** TTGCGTTTCCCAAAGCAGTG	151	63
UQCRC1	NM_001004250	**F** GAGACACAGGTCAGCGTATTG **R** TTTGTTCCCTTGAAAGCCAGAT	167	63
UQCRFS1	NM_001008888	**F** GGACGTGAAGCGACCCTT **R** CGAACAGAAGCAGGAACATTCAG	102	63
mouse - Cor.At				
18S	NR_003278	**F** GGACAGGATTGACAGATTGAT **R** CCAGAGTCTCGTTCGTTATC	115	60
ANT1	NM_007450	**F** TGACACTGCCAAGGGGATGC **R** GCCAGACTGCATCATCATCCT	145	63
ATM	NM_007499	**F** GAGGCCTAGGATTTCACGAAG **R** TGTTCGATCCTCATCAAGGTG	200	60
ATR	NM_019864	**F** CCTCAAACCGCTTTTTCGCA **R** ATCCGGCCTTTTGTTGAGACT	157	63
BAX	NM_007527	**F** TGCTACAGGGTTTCATCCAGG **R** TCCACGTCAGCAATCATCCT	175	63
BCL2	NM_009741	**F** ATAACGGAGGCTGGGATGC **R** GGCAGGTTTGTCGACCTCA	165	63
BPGM	NM_007563	**F** TACAAAGTGTGCGATGTG **R** CGTCTGAGATACCTTCCA	190	60
CDK1	NM_007659	**F** ACACACACGAGGTAGTGACG **R** GTCAATCTCTGAGTCGCCGT	155	63
CDK2	NM_183417	**F** CGGAGTGGTGTACAAAGCCA **R** TTCAGTCTCAGTGTCGAGCC	82	60
CHK1	NM_007691	**F** AAAGGACTGCTTGTCGCTGT **R** TCCATAGGCACCTTCTCCCA	93	60
CHK2	NM_016681	**F** TTCTTTTCATCTGCCTAAGTGGG **R** CCTCCTCTGTGGTAAGCCGA	192	62
HIF1A	NM_001313919	**F** CCTTAACCTGTCTGCCACTT **R** TAATGTTCCAATTCCTGCTGCTT	148	60

Table 4.3: Continued from previous page

Target	Accession Number	Sequences (5′ -3′)	Amp (bp)	Tan (°C)
mouse - Cor.At				
HK2	NM_013820	**F** CCTGGTTTCAAAGCGGTCGG **R** TACTGGTCAACCTTCTGCACTTG	166	63
MDM2	NM_010786	**F** TGGCGTAAGTGAGCATTC **R** CCGATAGACCTCATCATCCT	154	60
NOXA	NM_021451	**F** GGTGCCAGCAGACTTGAAGG **R** GCATTTCCATCAACCGGCG	181	63
P53	NM_011640	**F** TTCATTGGGACCATCCTGGC **R** GGCAGTCATCCAGTCTTCGG	120	63
PDK4	NM_013743	**F** GTGGACCCCGTTACCAATCA **R** GCACACTCAAAGGCATCTTGG	194	60
PUMA	NM_133234	**F** GAGCGGCGGAGACAAGAA **R** AGGAGTCCCATGAAGAGATTGT	80	60
VDAC1	NM_011694	**F** GTAACACTCGCTTCGGAAT **R** CGTCAGTTTGATACCTGGTTT	131	60
mouse - C57BL/6J and MEF				
18S	NR_003278	**F** CGCCGCTAGAGGTGAAATTC **R** CGAACCTCCGACTTTCGTTCT	101	60
ACADL	NM_007381	**F** GCGATTTCTGCCTGTGAGTT **R** CCACAAAAGCTCTGGTGACA	151	60
ACLY	NM_134037	**F** GAAGCTGACCTTGCTGAACC **R** CTGCCTCCAATGATGAGGAT	237	60
ANP	NM_008725	**F** AGAGACGGCAGTGCTCTAGG **R** AGCCCTCAGTTTGCTTTTCA	78	60
BMAL1	NM_007489	**F** GCAGTGCCACTGACTACCAAGA **R** TCCTGGACATTGCATTGCAT	201	60
BNP	NM_008726	**F** CACCCAAAAAGAGTCCTTCG **R** GCCCAAAGCAGCTTGAGATA	97	60
Catalase	NM_009804	**F** TTGACAGAGAGCGGATTCCT **R** GAGAATCGAACGGCAATAGG	151	60
CDKN1A	NM_007669	**F** CGGTGTCAGAGTCTAGGGGA **R** AGGATTGGACATGGTGCCTG	88	60
CLOCK	NM_007715	**F** ACCACAGCAACAGCAACAAC **R** GGCTGCTGAACTGAAGGAAG	66	60
CPT1α	NM_013495	**F** TGACTGGTGGGAGGAATACA **R** AGTATGGCGTGGATGGTGTT	141	60
CPT1β	NM_009948	**F** GTCGCTTCTTCAAGGTCTGG **R** AAGAAAGCAGCACGTTCGAT	232	60
CRY1	NM_007771	**F** CAGACTCACTCACTCAAGCAAGG **R** TCAGTTACTGCTCTGCCGCTGGAC	126	60
CYTL1	NM_001081106	**F** GCTGAGAGACTTCGTGGCTT **R** AGGAATACCAAGTCCCGCCT	123	60
DBP	NM_016974	**F** AATGACCTTTGAACCTGATCCCGCT **R** GCTCCAGTACTTCTCATCCTTCTGT	175	60

Table 4.3: Continued from previous page

Target	Accession Number	Sequences (5′ -3′)	Amp (bp)	Tan (°C)
mouse - C57BL/6J and MEF				
FOXO3	NM_019740	**F** ATAAGGGCGACAGCAACAG **R** CTGTGCAGGGACAGGTTGT	67	60
GPX1	NM_008160	**F** GTTTCCCGTGCAATCAGTTC **R** GGTGAGCCTTCTCACCATTC	147	60
IRF7	NM_016850	**F** CACACAGGGTGTGTCCCC **R** GGGTTCCTCGTAAACACGGT	202	60
NAMPT	NM_021524	**F** GGTCATCTCCCGATTGAAGT **R** TCAATCCAATTGGTAAGCCA	119	60
ND1	AY172335	**F** TTGTTGGTCCATACGGCATTTTAC **R** GCTAGTGTGAGGTGATAGGGTAGG	131	60
ND2	AY172335	**F** ATACTAGCAATTACTTCTATTTTCATAGGG **R** GAGGGATGGGTTGTAAGGAAG	135	60
NRF1	NM_010938	**F** CAACAGGGAAGAAACGGAAA **R** GCACCACATTCTCCAAAGGT	213	60
PDK4	NM_013743	**F** GTGGACCCCGTTACCAATCA **R** GCACACTCAAAGGCATCTTGG	194	60
PER1	NM_011065	**F** ACCAGCGTGTCATGATGACATA **R** GTGCACAGCACCCAGTTCCC	143	60
PER2	NM_011066	**F** CGCCTAGAATCCCTCCTGAGA **R** CCACCGGCCTGTAGGATCT	202	60
PPARα	NM_011144	**F** ACAAGGCCTCAGGGTACCA **R** GCCGAAAGAAGCCCTTACAG	63	60
PRG4	NM_021400	**F** ACGCCTTTTCCAAAGATCAATACT **R** TGTCAAGTTGAGAACTGTTTTGT	249	60
REV-ERBα	NM_145434	**F** AGGCTGCTCAGTTGGTTGTT **R** CTCCATCGTTCGCATCAATC	177	60
RORα	NM_013646	**F** ACCGTGTCCATGGCAGAAC **R** TTTCCAGGTGGGATTTGGAT	61	60
SDHA	NM_023281	**F** CATGGTCACTAGGGCTGGTT **R** CACGACACCCTTCTGTGATG	104	60
SIRT1	NM_019812	**F** CAGTGTCATGGTTCCTTTGC **R** CACCGAGGAACTACCTGAT	104	60
SIRT3	NM_022433	**F** ATCCCGGACTTCAGATCC **R** CAACATGAAAAAGGGCTTGG	126	60
SIRT7	NM_153056	**F** AGAACTGTGATGGGCTCCAC **R** GAAGGGCAGTACGCTCAGTC	150	60
TFAM	NM_009360	**F** CCAAAAAGACCTCGTTCAGC **R** CTTCAGCCATCTGCTCTTCC	211	60
UQCRQ	NM_025352	**F** GATCTACACATGGGGCAACC **R** GCAGGCCGTCTACTTGTCAT	85	60

Chapter 5

5. Doxorubicin-compensatory response in H9c2 cardiomyoblasts

5.1. Introduction

DOX is one of the most effective and frequently used drugs prescribed for the treatment of cancer. However, the clinical use of DOX is limited by its dose-dependent and cumulative cardiotoxicity [21], mostly expressed as cardiomyopathy and congestive heart failure [135]. Delayed onset manifestation of DOX-toxicity is a major concern, especially in pediatric patients [29, 30]. This manifestation can appear many years after the completion of the therapy and was first described in the 1990's [29, 30]. The most employed tool to prevent DOX-induced cardiotoxicity is the limitation of cumulative DOX doses, which may translate into lower cancer response rates [37].

Pathophysiologically, a panoply of mechanisms underlies DOX-cardiotoxicity, making the identification of prevention or treatment strategies difficult (section 1.2). However, the over-production of ROS, generated predominantly in cardiac mitochondria, is considered the primary initiating event in the cascade of intracellular modifications. The excessive generation of ROS causes damage to many cellular structures, and mitochondrial dysfunction is considered a hallmark of DOX-induced cardiotoxicity [371-373]. DOX exposure was also associated with persistent alterations of gene expression [188] and severe defects on functionally competent cardiac progenitor cells (CPC) [48, 374]. CPC are particularly susceptible to DOX, which is a critical factor for neovascularization and sustaining functional resiliency in cardiac tissue [374]. This capacity for cardiac regeneration is especially important during the first years of life, since regenerative potential has been described to decrease with age.

Adaptive responses have been investigated in the context of cell toxicology. This phenomenon is based on the notion that low doses of toxic agents stimulate adaptive mechanisms, resulting in less adverse effects after a subsequent larger exposure. It has been previously shown that DOX treatment *in vivo* causes an adaptive response that includes reprogramming of metabolic flux from fatty acid oxidation to glycolysis [184]. Our hypothesis is that nanomolar concentrations of DOX confer H9c2 cells protection against a second DOX treatment at higher doses, due to a mitochondrial adaptive-like effect. Therefore, the relevance of the results is that pre-treatment with low, sub-clinical doses of DOX may induce a cardiac adaptive response, thereby improving the overall success of DOX-based chemotherapies, by decreasing cardiotoxicity events.

5.2. Methods

5.2.1. H9c2 cell culture, DOX treatment and experimental design

H9c2 cells were cultured in 25 mM glucose DMEM supplemented with 1.5 g/L of sodium bicarbonate, 1% antibiotic/antimycotic solution and 10% fetal bovine serum (FBS). The cell culture was maintained at 37°C in a humidified atmosphere of 5% CO_2. H9c2 cells were passaged when cells reached approximately 80% of confluence and the medium was changed every 2-3 days. Cells were used between passage 6 and 20.

The experimental design is shown in Figure 5.1. DOX was prepared freshly in water at a 10 mM stock concentration; intermediary dilutions of this working stock were also made in water. If not indicated otherwise, cells were seeded at a density of $1.8x10^3$ cells/cm^2. One day post-seeding, H9c2 cells were exposed to DOX (10 to 25 nM) for 24 hours, after which the cells were rinsed with PBS and the culture medium replaced. After three days of recovery, H9c2 cells were passaged (CTR 1:3, DOX-treated cells 1:2), and this step was repeated again at day 6 (starting from the recovery time). In

total, four time-points were established for the post-exposure period; days 0, 3, 6, and 9 (Fig. 5.1). For the second exposure (Fig. 5.1), H9c2 cells were re-seeded on day 9 at a density of $6.0x10^3$ cells/cm^2; 24 hours later they were incubated with DOX (0.2, 0.5 and 1 μM) or iodoacetate (2 μM), an irreversible inhibitor of glyceraldehyde-3-phosphate dehydrogenase (GAPDH), for further 24 hours. DOX concentrations were chosen based on human plasma kinetics studies which reported initial peak plasma concentrations of 5 – 0.2 μM that further decline to nanomolar concentrations within one hour [9]. A similar protocol was performed with human breast cancer cell lines (Hs-578T and MDA-MB-231).

5.2.2. Sulforhodamine B (SRB) assay

Cell mass was measured by the sulforhodamine B (SRB) assay [375]. This method, developed in the 1990's [376], relies on the ability of SRB dye to bind to protein basic amino acid residues under mildly acidic conditions and its dissociation after a shift to basic conditions. The dye present in the basic solution is then used to estimate the total protein content, which is related to cell number.

H9c2 cells were seeded in 48 well-plates at $6.0x10^3$ cells/cm^2 in a final volume of 500 μL per well. At the respective time-points, the medium was removed from the microplate wells which were further rinsed with PBS, and the cells were fixed overnight with ice-cold acetic acid/methanol (1% v/v) at -20°C. Following fixation, plates were dried and incubated with 200 μL SRB 0.05% (w/v) in 1% acetic acid for 1 hour at 37°C. The unbound dye was then removed by washing the wells with 1% acetic acid and the plates were dried again. Finally, 1 mL Tris (10 mM, pH 10) was added to the plates to dissolve SRB and optical density was read at 530 nm.

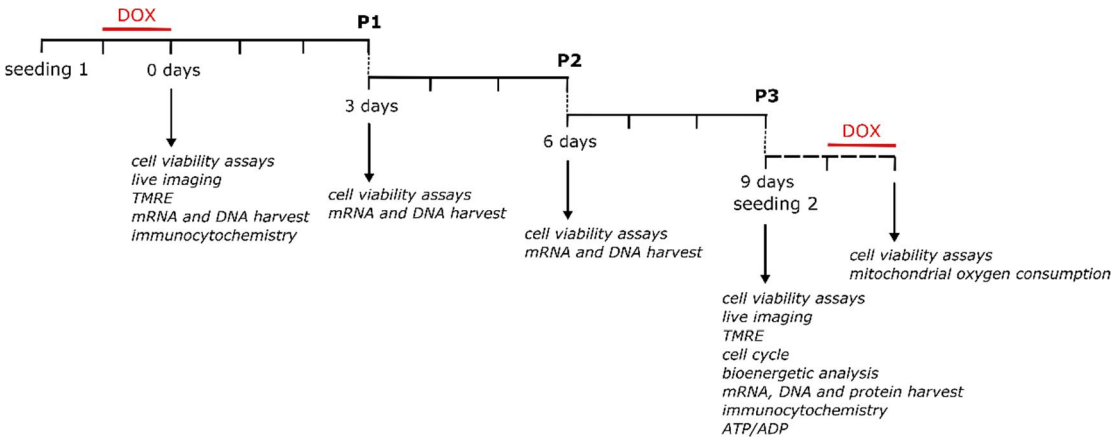

Figure 5.1: H9c2 cells experimental design. One day after seeding, H9c2 were incubated with 0, 10, 25 or 50 nM DOX for 24 bours. Following the single treatment, the cells were cultured in drug-free medium. At day 9, cells were seeded again and 24 hours later were exposed to a second 24 hours DOX treatment. Experimental procedures including SRB, live imaging, mitochondrial transmembrane potential measurement, mRNA, DNA and protein harvest, immunocytochemistry, ATP/ADP measurement, cell cycle and bioenergetics analysis were performed at different time-points, as observed in the scheme. P refers to a cell passage.

5.2.3. Metabolic cell viability determination using resazurin assay

The resazurin assay is based on the ability of viable cells to reduce resazurin into resorufin, whose fluorescence is then indicative of the cellular redox activity [377]. Cells were seeded at a density of 6.0×10^3 cells/cm^2 in 96-well plates. The working resazurin solution was prepared in cell culture medium immediately prior the assay, at a concentration of 10 μg/mL. At the proper time-point, cell medium was removed from the plate and 80 μL of resazurin solution was added in each well and incubated for 90 min (minutes) at 37°C in a humidified atmosphere of 5% CO_2. Each independent replicate had four technical replicates in the same plate. Fluorescence was measured using the excitation wavelength of 540 nm and emission of 590 nm.

5.2.4. Mitochondrial transmembrane electric potential measurement

Tetramethylrhodamine ethyl ester perchlorate ($TMRE^+$) is a cationic, lipophilic fluorescent dye that accumulates in the negatively charged mitochondrial matrix and can be used to assess changes in $\Delta\Psi m$ [378].

$TMRE^+$ stock was prepared at a concentration of 10 mg/mL in DMSO and stored at -20°C. Working stocks of 50 μM were also made by dilution in DMSO. H9c2 cells were seeded in 96-well plates at a density of $6.0x10^3$ cells/cm^2 in a final volume of 200 μL. Each sample had at least six technical replicates in the same plate. At the proper time-point the wells were washed with PBS and incubated in the dark for 1 hour at 37°C with 100 μL of basal medium supplemented with 300 nM of $TMRE^+$. The basal $TMRE^+$ fluorescence intensity was measured during 15 min in a plate reader with 549 nm excitation and 575 nm emission. Oligomycin and FCCP (final concentration of 2 μg/mL and 2.5 μM, respectively) were added to the wells to dissipate $\Delta\Psi m$ and unquench $TMRE^+$ from mitochondria, and a kinetic curve for fluorescence was generated for 10 min with 1 min intervals. Finally, Hoechst 33342 (1 μg/mL) was added to the medium and after 5 min the fluorescence was measured at an excitation wavelength of 355 nm and an emission of 465 nm. The results were calculated by the difference between the maximum and the baseline values of $TMRE^+$ in quenching mode and normalized by Hoechst intensity.

5.2.5. Live epifluorescence microscopy

To evaluate DOX-induced changes on cell morphology, cells were visualized in a Nikon eclipse Ti-S fluorescence microscope. For the analysis of $\Delta\Psi m$ and nuclear morphology, cells were incubated with the cationic fluorophore $TMRE^+$ and with the nucleic acid stain Hoechst 33342. H9c2 cells were seeded in 6 well-plates with a glass coverslip in each well, at a density of $2.2x10^3$ cells/cm^2 in a final volume of 2 mL per

well. At the proper time-points, cells were washed with PBS and incubated with the fluorescent probes in microscopy medium for 30 min (50 nM TMRE and 0.75 μg/mL Hoechst 33342), at 37°C in the dark. Images treatment and individual cellular and nuclear areas measurement was performed with ImageJ 1.49v.

5.2.6. Cell Cycle Analysis

Cell cycle analysis by flow cytometry is based on the quantification of DNA content following cell staining with a fluorescent DNA intercalating agent such as propidium iodide and reveals the proportion of cells in each of the three major phases of the cell cycle (G1, S and G2/M).

H9c2 cells were trypsinized, centrifuged at 250 xg for 3 min, washed with PBS and fixed overnight by adding 70% ice-cold ethanol (-20°C). Cells were then centrifuged at 400 xg at room temperature and ethanol was discarded. Cells were washed with filtered PBS and, after a second centrifugation, resuspended in 500 μL of a PBS/EDTA 2 mM/Tween 0.1% (v/v) solution supplemented with RNase (20 μg/mL). The samples were left at room temperature for 30 min. Finally, propidium iodide was added to the solution at a final concentration of 20 μg/mL and incubated for 30 min at 37°C. The DNA content was analyzed following 20,000 events per sample by using an Accuri™ C6 flow cytometer. The percentage of cells in G1/G0, S and G2/M was determined using FlowJo V10 software (Ashland, OR, USA).

5.2.7. Bioenergetic analysis

The mitochondrial profile was provided by Seahorse XF Cell Mito Stress Test and based on the oxygen consumption rate (OCR); and the glycolytic rate was based on

the extracellular acidification rate (ECAR) using the Seahorse XF Glycolysis Stress Test, both determined using a Seahorse XFe96 analyzer.

H9c2 were seeded in XFe96 cell culture plates ($1.5x10^4$ cells/80 μL/well) in triplicate and cultured for 24 hours at 37°C in a humidified incubator with 5% CO_2. One hour prior to the assay the plate was rinsed twice with PBS and 175 μL of the appropriate serum-free assay medium with adjusted pH to 7.4 was added (DMEM D5030 supplemented with 25 mM of glucose and 4 mM of glutamine, or DMEM D5030 supplemented only with 4 mM of glutamine for OCR and ECAR measurements, respectively) and the plate was incubated at 37°C without CO_2. A constant volume of 25 μL of the compounds was pre-loaded into the respective ports of the cartridges. For OCR measurements, the sequential addition and the respective final concentration was: 1 μM of oligomycin (Port A), 1 μM of FCCP (Port B), 1 μM of rotenone and 1 μM of antimycin (Port C). For ECAR the sequence was: 10 mM of glucose (Port A), 1 μM of oligomycin (Port B) and 50 mM of 2-deoxyglucose (2-DG; Port C). OCR and ECAR values were normalized by cell mass, determined by the SRB assay, and analyzed using Wave v2.3 software (Agilent Technologies, USA).

5.2.8. Adenine nucleotide measurement (ATP/ADP/AMP)

ATP, ADP and AMP levels were measured by HPLC. All steps were carried out on ice or at 4°C. For the nucleotides extraction, cells were rinsed with PBS, followed by the addition of 500 μl ice-cold 0.6 M $HClO_4$ to each dish. The dishes were scraped and the lysates were centrifuged for 10 min at 14,000 xg. The resulting pellet was resuspended in 500 μl of 1 M NaOH for posterior protein quantification, while the supernatant was neutralized with 3 M KOH/1.5 M Tris, and centrifuged again for 10 min at 14,000 xg. The supernatant was collected and immediately analyzed by reverse-phase high performance liquid chromatography (HPLC), at a wavelength of 254 nm. The chromatographic apparatus was a Waters® Breeze™ system, consisting of a 1525

Binary HPLC Pump and a Waters® 2487 Dual Wavelength Absorbance Detector. The column was a LiChrospher® 100 RP-18 (5 μm) LiChroCART® 125-4 (Merck) and the analysis was performed using the software Waters® Breeze™ HPLC software. An isocratic elution with 100 mM phosphate buffer (KH_2PO_4), pH 6.5 and 1.2% (v/v) methanol was performed with a flow rate of 1 mL/min. To determine the nucleotide concentrations, standard curves of ATP, ADP and AMP were previously run. The required time for each analysis was 5.5 min. The adenylate energy charge (EC) was then calculated as EC = (ATP+½ADP)/(ATP+ADP+AMP).

5.2.9. RNA isolation

RNA extraction was performed using Aurum™ Total RNA Mini Kit, according to the manufacturer's instructions. Briefly, the cell pellet was treated with 350 μL of lysis solution followed by mechanical stirring, pipetting the solution up and down several times. Next, 350 μL of 70% ethanol was added to each tube and the solution was transferred to a binding column, centrifuged for 30 seconds at 16,000 xg and washed with 700 μL of low stringency wash solution buffer. After a centrifugation step of 30 seconds at 16,000 xg, RNse-free DNase provided with the kit was added to the membrane of each column. The membrane was washed again with 700 μL of high stringency wash solution and 700 μL of low stringency wash solution, being these steps followed by centrifugation steps at 16,000 xg of 30 and 60 seconds, respectively. An additional centrifugation was done to remove residual washing solutions. Finally the RNA was eluted in 40 μL of elution solution after a centrifugation for 2 min at 16,000 xg. RNA was further stored at -80°C until use.

5.2.10. cDNA preparation and quantitative real-time PCR

The concentration and purity of the RNA samples were determined spectrophometrically using a Nanodrop 2000 by observing the A260 as well as the A260 /A280 and A260/A230 ratios. The integrity of the RNA was screened with the Experion™ Automated - Electrophoresis System in accordance with the manufacturer's instructions. For cDNA preparation, 2 μg of RNA were mixed with 8 μL of 5x iScript reaction mix and 2 μL of iScript reverse transcriptase, to a final volume of 40 μL. In this kit, the iScript reverse transcriptase is pre-blended with RNase inhibitor and the reaction mix contains a blend of oligo(dT) and random hexamer primers that allows the random amplification of targets with <1kb in length. The reaction was performed on a CFX™ Real-Time system using the following protocol: 5 min at 25°C, 30 min at 42°C and 5 min at 85°C. To ensure the quality of the RNA and exclude the presence of genomic DNA, a control sample was also prepared in which nuclease-free water was added instead of the reverse transcriptase (NRT).

The quantitative real-time PCR (RT-qPCR) is a technique based on a traditional PCR but with the particularity of being possible to measure the quantity of PCR product that is being produced in each cycle. The analysis of the exponential phase of the reaction enables to determine the absolute or relative amount of initial target.

RT-qPCR was performed using the SsoFast™ EvaGreen® Supermix, a ready-to-use cocktail composed by all the components needed to perform the reaction including the EvaGreen dye, that binds to double strand DNA (dsDNA) and allows detecting any dsDNA generated during the amplification, and a hot-start polymerase which ensures that the enzymatic activity is kept off until the initial PCR denaturation step. The RT-qPCR mixture contained 5 μL of supermix, 500 nM of each primer (Table 4.3) and 12.5 ng of cDNA sample in a total volume of 10 μL. The reaction was run on a CFX™ Real-Time system according to the following protocol: 30 seconds at 95°C, 40

cycles of 5 seconds at 95°C plus 5 seconds at the annealing temperature (Table 4.3). At the end of each cycle, EvaGreen fluorescence was recorded to enable determination of Cq. After amplification, melting temperature of the PCR products were determined by performing melting curves, and amplicon length was confirmed by agarose gel electrophoresis. For each set of primers, amplification efficiency was assessed. Relative normalized expression was determined by the CFX96 Manager software (v. 3.0; Bio-Rad), using *18S* RNA and *TBP* (TATA box binding protein) as references. All samples were analyzed in duplicate.

5.2.11. Mitochondrial DNA copy number

Total genomic DNA was extracted by PureLink™ Genomic DNA MiniKit according to the manufacturer's protocol. Briefly, the collected cells were resuspended in 200 μL of PBS and treated with 20 μL of Proteinase K and 20 μL of RNase A. After 2 min of incubation at room temperature the lysate was mixed with 200 μL of lysis/binding buffer and protein digestion was promoted by incubating at 55°C for 10 min. Then, 200 μL of 100% ethanol was added to the lysate and loaded into a spin column. After centrifugation and column washing, bounded DNA was eluted by centrifuging 40 μL of elution buffer through the column. Concentration and DNA quality was screened with Nanodrop 2000 and samples were stored at -20°C until use.

Mitochondrial DNA content was measured by RT-qPCR. Cytochrome b gene (*cytb*) was used to represent the mitochondrial DNA (mtDNA) and beta 2-microglobulin gene (*b2m*) was used to represent nuclear DNA (nDNA). Relative mtDNA copy numbers were assessed after *cytb* normalization by *b2m* gene copy number. Rat primers for *cytb* were: forward 5'-TACGCTATTCTACGCTCCATTC-3', reverse 5'-GCCTCCGATTCATGTTAAGACTA-3'; primers for *b2m* were: forward 5'-AGAGAACTCAACGGTGGCAG-3', reverse 5'- CGACCGCACACTATAGGGAC-3'. The 10 μL PCR reaction contained 5 μL of SsoFast™ EvaGreen® supermix, 500 nM of

each DNA primer and 25 ng of total genomic DNA template. Amplification program consisted in 2 min at 98°C, followed by 40 cycles of 5 seconds at 98°C and 5 seconds at 62°C. The amplification specificity was assessed at the end of the amplification by a melting curve between 65 and 95°C, using an increment of 0.5°C in each step. The reactions were performed on a CFX™96 Real-Time system. The normalized expression was calculated by the comparative quantification algorithm ΔΔCt (CFX Manager™ 3.1 software, Bio-Rad).

5.2.12. Cellular fractioning and measurement of nuclear DNA methyltransferase I (DNMT1)

Nuclear fractions were obtained according to a subcellular fractioning protocol described elsewhere [379], with slight modifications. Briefly, cells were scraped from the dishes with PBS/EDTA (0.2 g/L) and centrifuged at 200 xg for 4 min. The pellets were washed with 1 mL of cold PBS and centrifuged again at 300 xg for 7 min. The supernatant was discarded and the pellet was resuspended in 500 μL of STM buffer (section 4.3) and homogenized using a tight pestle attached to a potter homogenizer set at 500 rpm and with 50 strokes. After 30 min on ice, the cell homogenate was vortexed at maximum speed and further centrifuged at 700 xg for 15 min. The pellet was resuspended in STM (250 μL), vortexed for 15 seconds and centrifuged at 500 xg for 15 min. This last wash was repeated again but followed by a 1,000 xg centrifugation. Then, the pellet was resuspended in 250 μL of NET buffer (section 4.3), vortexed for 15 seconds and incubated on ice for 30 min. Lastly, the crude nuclear fraction was lysed by sonication (3x 10 seconds, with 20 seconds pauses) and, after a centrifugation of 9,000 xg for 30 min, the supernatant was recovered as the final nuclear fraction. Nuclear DNMT1 amounts were determined using a DNMT1 ELISA kit according to the manufacturer's instructions.

DNMT1 present in the samples binds to the bottom of coated wells containing a DNMT1 affinity substrate. The bound DNMT1 can be subsequently recognized by a specific DNMT1 antibody and measured colorimetrically.

Briefly, 6 μg protein of the enriched nuclear extract was mixed with the antibody buffer and incubated for 2 hours on the plate at 37°C. Next, blocking buffer was added followed by another incubation step of 30 minutes. The plate was then washed and sequentially incubated at room temperature with the capture and detection antibodies for 1 hour period each. Finally, color development was added, followed by a stop solution. The absorbance was read at 450 nm. All samples were analyzed in duplicate.

5.2.13. Immunostaining

For immunocytochemistry, H9c2 cells were seeded in 6 well-plates with a glass coverslip in each well, at a density of $8.0x10^3$ cells/cm^2 and in a final volume of 2 mL per well. The wells were washed twice with filtered PBS and fixed with 4% paraformaldehyde in PBS for 15 min. Then, cells were washed three times with PBS-T (PBS + 0.05% (v/v) Tween 20) and permeabilized with 0.2% (v/v) Triton X-100 in PBS (2 min, room temperature). Cells were washed twice with PBS-T and treated with HCl 2 N (20 minutes, room temperature) to denature the DNA and allow binding of the primary antibody to methylated DNA. After five washes with PBS-T, cells were blocked with 3% BSA in PBS-T (30 min, 37°C). The anti-5-methylcytosine antibody (1:100 in blocking solution) was added and incubated for 5 hours at 4°C (Table 4.2). Cells were then rinsed with PBS-T three times for 5 min. Primary antibody was detected using Alexa Fluor-488 conjugated secondary antibody (1:200 in blocking solution) after 2 hours incubation at room temperature in the dark. Next, cells were incubated with Hoechst 33342 in PBS-T (3 μg/mL) for 10 min at room temperature, followed by two washes with PBS-T for 2 min, and mounted with Fluorescence

Mounting Medium. Images were taken on the following day with a Nikon eclipse Ti-S fluorescence microscope.

5.2.14. Statistical analysis

Statistical analyses were performed using SPSS version 23.0 (IBM, NY, USA) and GraphPad Prism 6 (GraphPad Software, Inc., La Jolla, CA, USA). Nonparametric Mann-Whitney U-test and Kruskal-Wallis H-test followed by Dunn's post hoc analysis were used. The data is presented as mean ± SEM. Differences were considered statistically significant at $p<0.05$.

5.3. Results

5.3.1. Effects of DOX pre-treatment on cell viability

In our experimental design, we tested therapeutically relevant concentrations of DOX [9] and investigated the long-term effects of that treatment after a prolonged recovery time. For this, H9c2 cells were treated with DOX for 24 hours, after which the cells were washed, and kept in culture for nine days more, being passaged twice (Fig. 5.2 A). The SRB assay was used to investigate the effects of DOX on cell mass, at four distinct time-points (Fig. 5.2 B). After the initial treatment with DOX (10 - 50 nM) (0 days of recovery), no significant differences were observed on cell mass between control group and DOX-treated cells. However, at the second time-point (3 days) significant loss of total cell mass was observed, which seemed to gradually recover at the two last time points.

Then, we evaluated the effects of the less toxic DOX concentrations (10 and 25 nM) on metabolic viability (Fig. 5.2 C). Even though 25 nM DOX significantly decreased resazurin reduction at days 3, 6 and 9, an overall improvement of cell viability was

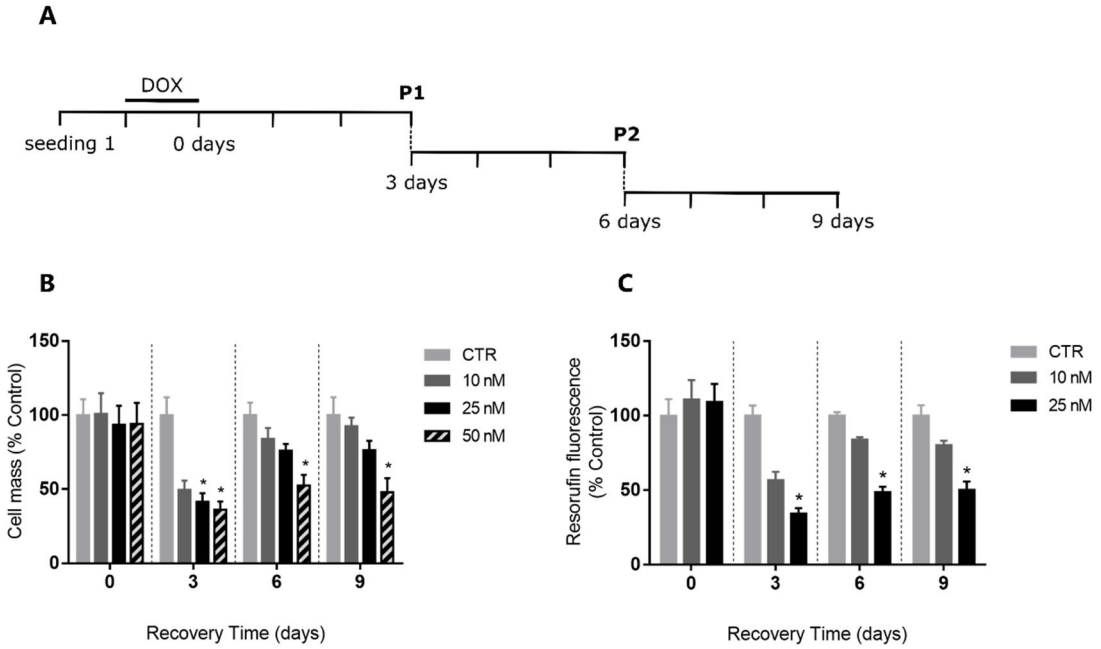

Figure 5.2: Effect of DOX pre-treatment on H9c2 viability. A) Cells were incubated with 10, 25 and 50 nM DOX for 24 hours. Following the single treatment, the cells were cultured in drug-free media until day 9. P refers to a cell passage. B) Cell mass and C) metabolic viability were determined by using the SRB and resazurin methods, respectively, at days 0, 3, 6 and 9. Data are expressed as mean ± SEM of 4 independent experiments; *$p < 0.05$, compared to control.

observed over time. The concentrations of 10 and 25 nM were selected for the next follow-up experiments.

5.3.2. DOX treatment resulted in hypertrophy and cell cycle arrest

To determine alterations on H9c2 cell morphology and $\Delta\Psi m$ after 0 and 9 days of recovery, control and 25 nM DOX-treated cells (milder morphological changes were observed in cells treated with 10 nM DOX) were labeled with Hoechst and $TMRE^+$ and visualized by fluorescence microscopy (Fig. 5.3 A). Immediately after the initial 24 hours treatment with DOX, no morphological differences were found between groups (Fig. 5.3 A). However, at day 9, significantly larger nuclei were observed in 25 nM DOX-treated cells compared to non-treated cells (Fig. 5.3 C). Also, treated cells were hypertrophied, with average total cellular area significantly larger than in the

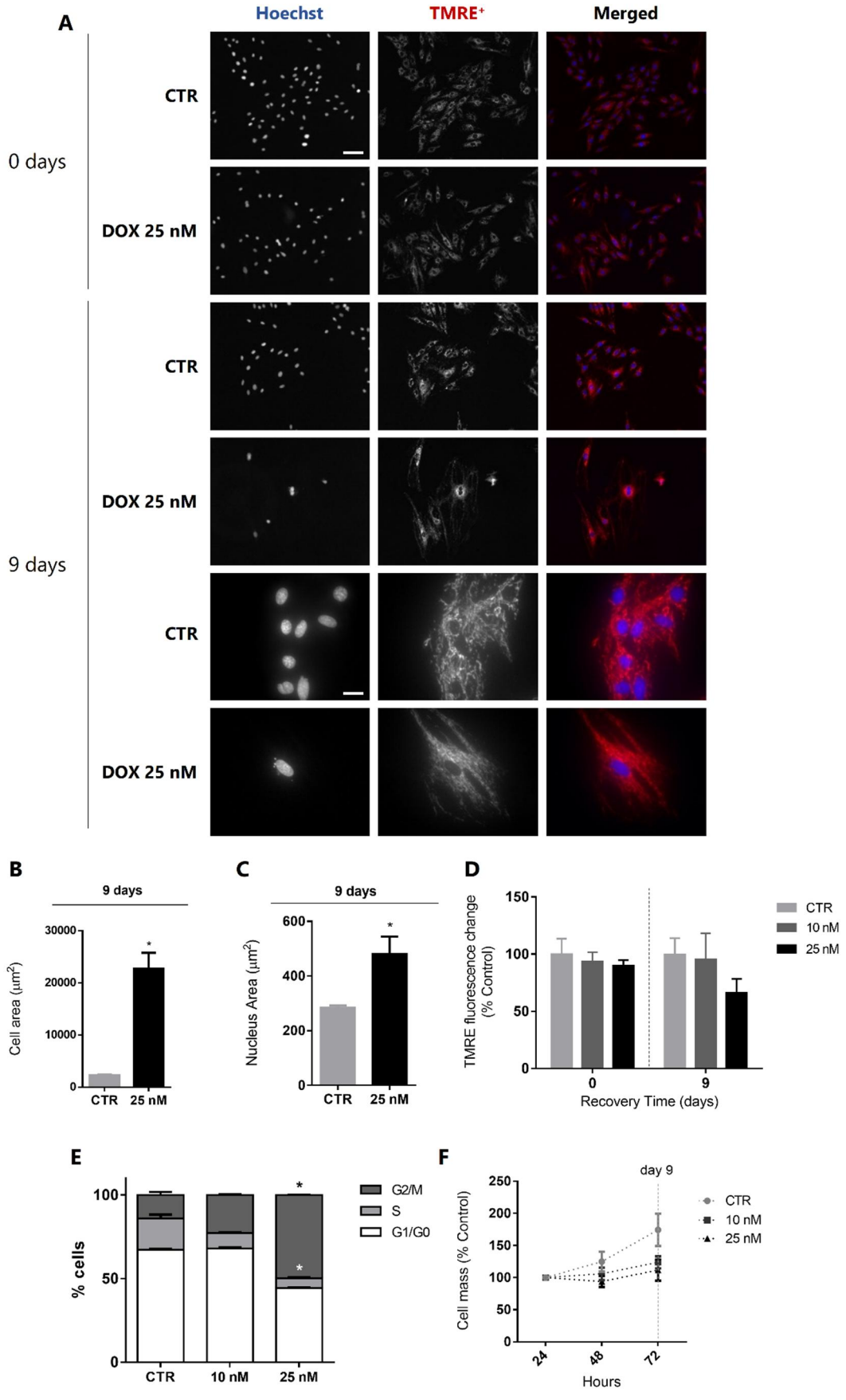

(Legend on the next page)

Figure 5.3: DOX effects on H9c2 cells morphology and cell cycle. (A) At 0 and 9 days of recovery time were collected epifluorescence microscopy images of nuclei and polarized mitochondria in H9c2 cells control and treated with 25 nM DOX for 24 hours. Scale bar; 100 and 25 μm. (B-C) At day 9, the nuclear and cellular sizes were measured and expressed as percentage of controls. Error bars indicate SEM from measurements of multiple cells of 3 independent experiments. (D) TMRE+ accumulation was measured in a plate reader at day 0 and 9 and data is represented as mean ± SEM percentage of control for each specific time-point from four independent experiments. (E) Cell cycle was analyzed by flow cytometry using propidium iodide in untreated and DOX-treated cells at day 9. Data are expressed as percentage of cells in G2/M, S and G1/G0 ± SEM from at least 3 independent experiments. (F) At day 6 cells were seeded and cell mass was evaluated by SRB from day 7 to day 9. Data are expressed as mean ± SEM of 3 independent experiments; *$p < 0.05$, compared to control.

controls (Fig. 5.3 B). For the analyses of ΔΨm, the membrane permeable cation $TMRE^+$ was used, which accumulates in the mitochondrial matrix depending on the ΔΨm. High accumulation of the dye inside mitochondria leads to fluorescence quenching, which means the total dye fluorescence decreases as the organelles accumulate $TMRE^+$. DOX effect on ΔΨm in H9c2 cells was analyzed using the quenching approach. Our results showed no significant changes on ΔΨm in DOX-treated H9c2 cells, compared to controls (Fig. 5.3 D). We next evaluated DOX persistent effects on cell cycle, also at the last time-point. At day 9, DOX treatment induced a cell cycle arrest in G2/M (Fig. 5.3 E). Unlike control cells, in which the majority of H9c2 cells (≈ 67%) were in G1/G0 phase, DOX-treated cells had a dose-dependent increase of cells in G2/M and a reduction in the population of cells in S and G1/G0. As a consequence, DOX-treated cells exhibited a slower proliferation rate, observed by the growth curve performed from day 7 to day 9 (Fig. 5.3 F).

5.3.3. DOX decreased extracellular acidification and reduced basal respiration of H9c2 cells

DOX cardiotoxicity has been previously shown to alter cellular metabolic fluxes [184, 186]. Our next step was to evaluate whether DOX altered the OCR and ECAR in

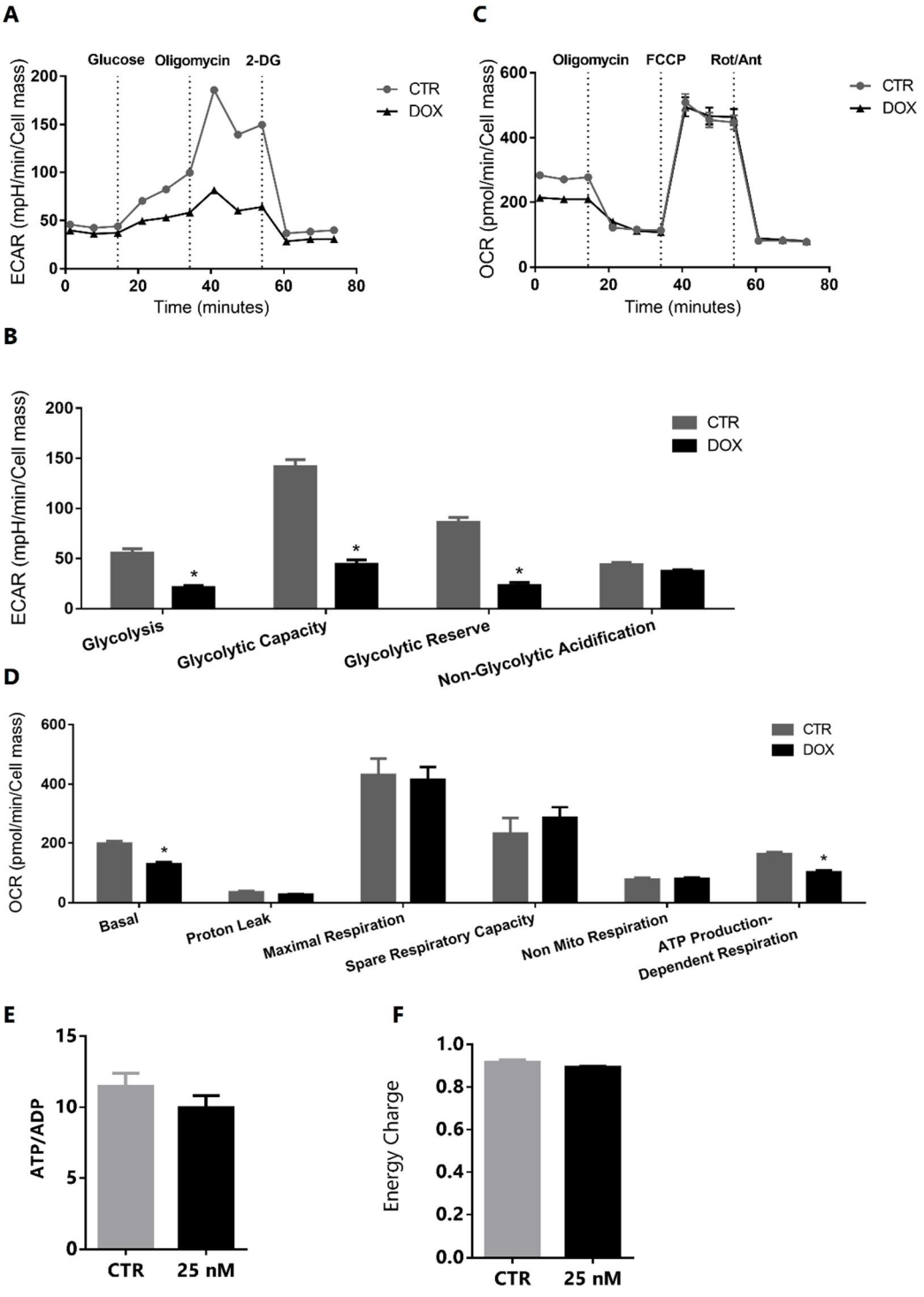

Figure 5.4: Effects of DOX on H9c2 cells extracellular acidification rate (ECAR), oxygen consumption rate (OCR) and ATP/ADP levels. Cells incubated with 0 and 25 nM DOX were evaluated in terms of ECAR (A-B) and OCR (C-D). *(Continues on the next page)*

Several parameters were analyzed in both cases: cell basal respiration (measurement prior to oligomycin addition minus non-mitochondrial OCR, described below), proton leak (minimal measurement after oligomycin injection minus non-mitochondrial OCR), maximal respiration (maximal measurement after FCCP addition minus non-mitochondrial OCR), spare respiratory capacity (maximal measurement after FCCP addition minus basal respiration), non-mitochondrial respiration (minimal measurement after rotenone and antimycin A addition), respiration associated to ATP synthesis (measurement prior to oligomycin addition minus minimal measurement after oligomycin injection), glycolysis (maximal measurement after glucose injection minus non-glycolytic acidification, described below), glycolytic capacity (maximal measurement after oligomycin injection minus non-glycolytic acidification), glycolytic reserve (maximal measurement after oligomycin injection minus maximal measurement after glucose injection) and non-glycolytic acidification (measurement prior to glucose addition). (E-F) ATP/ADP and energy charge were calculated after quantification by high-performance liquid chromatography. Data are expressed as mean ± SEM of at least 4 independent experiments; *$p < 0.05$, compared to control.

nanomolar treatments. At day 9, OCR and ECAR were measured using a Seahorse XFe96 Extracellular Flux analyzer. Cells treated with 25 nM DOX had decreased glycolysis compared to control cells (~ 60% less ECAR), as well as decreased glycolytic capacity and reserve, indicative of impaired glycolytic metabolism (Fig. 5.4 A-B). Regarding OCR measurements, basal respiration and ATP synthesis-related respiration were significantly decreased in DOX-treated cells, the latter most likely resulting from the first observation (Fig. 5.4 C-D). However, other parameters including maximal respiration and spare respiration capacity were not altered (Fig. 5.4 C-D). Similarly, neither the ratio ATP/ADP nor energy charge were altered by the treatment (Fig. 5.4 E-F).

5.3.4. Sublethal DOX treatment was associated with transcriptional alterations of mitochondrial-relevant genes

Because gene expression changes were previously described in a persistent model of cardiomyopathy [188], we examined if DOX treatment would induce changes in mRNA expression in H9c2 cells throughout the time course of the treatment (Fig. 5.5). Several functional categories of genes were analyzed, namely oxidative

phosphorylation (OxPhos) subunits (Fig. 5.5 A), mitochondrial biogenesis (Fig. 5.5 B), cardiolipin metabolism (Fig. 5.5 C), antioxidant defenses (Fig. 5.5 D), cell metabolism (Fig. 5.5 E) and epigenetic modulators (Fig. 5.5 F).

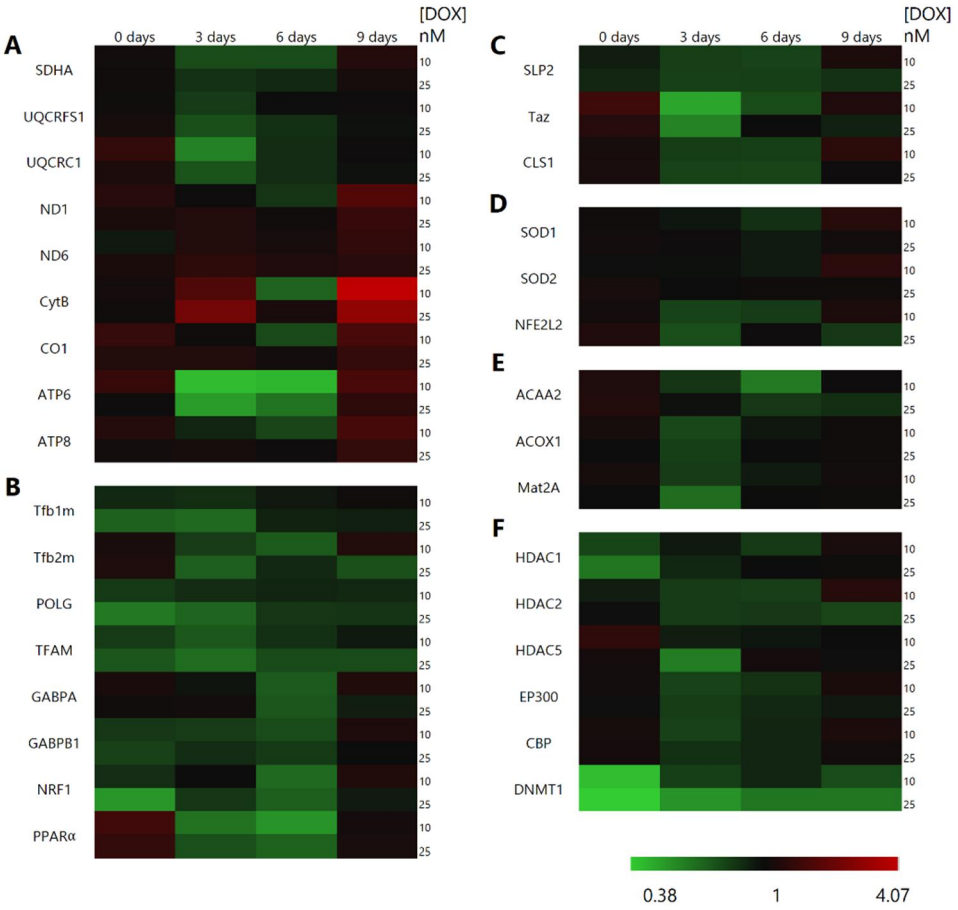

Figure 5.5: Heat map diagram of average gene expression detected by quantitative real-time PCR, belonging to the following categories: OxPhos subunits (A), mitochondrial biogenesis (B), cardiolipin metabolism (C), antioxidants (D), cell metabolism (E) and epigenetic modulators (F). Green indicates down-regulation and red indicates upregulation. Each column represents a day of recovery time, namely 0, 3, 6 and 9 days. Gene expression was quantified for both DOX concentrations, 10 and 25 nM. Data are expressed as mean of 4 independent experiments and compared to control.

These genes were chosen based on previous reports demonstrating persistent alterations on gene expression profiles after DOX exposure [188, 210]. It is worth noting that gene expression alterations varied according to the time-point analyzed,

and it was not always possible to find clear patterns of gene expression along the protocol. Also, the analyzed transcripts did not present a dose-dependent response most of the times, suggesting that, in this model, the different pharmacological concentrations may induce different cellular responses. Interestingly, the results revealed a general increase in the expression of genes encoded by the mtDNA, including *ND1*, *ND6*, *cytb*, *CO1*, *ATP6* and *ATP8* (Fig. 5.5 A). Among the overexpressed mtDNA-encoded genes, *ND1*, *cytb*, *CO1* and *ATP8* were particularly overexpressed ($p< 0.05$) in 10 nM DOX-treated cells (Fig. 5.6 A).

5.3.5. DOX induced DNMT1 downregulation associated with expression of mitochondrial-encoded genes

Since there was a tendency for an increased abundance of mitochondrial transcripts, we then analyzed mtDNA copy number to infer a possible relationship between them. mtDNA content was monitored by measuring the relative copy number of mitochondrial encoded gene *cytb* compared to the nuclear gene *b2m*, using RT-qPCR (Fig. 5.6 B). The copy number of mtDNA was not significantly different between treatments at any of the time-points (day 0: p-value = 0.124; day 3: p-value = 0.084; day 6: p-value = 0.664; day 9: p-value = 0.146). Additionally, we confirmed the gene expression levels of two important mitochondrial-related proteins usually associated with mtDNA content, the mitochondrial transcription factor A (TFAM) and the mitochondrial-specific polymerase gamma (POLγ). TFAM is involved in mtDNA packaging and mitochondrial gene expression regulation and POLγ is essential for mtDNA replication and maintenance. Both tfam and polg transcript levels decreased in DOX-treated cells (mostly at day 0 and 3) (Fig. 5 C-D). Interestingly, DNMT1 gene, encoding the primary DNA methyltransferase responsible for the maintenance of DNA methylation patterns during cell replication, was downregulated in all four time-points, although more expressively at day 0 and 6 (Fig. 5.6 E).

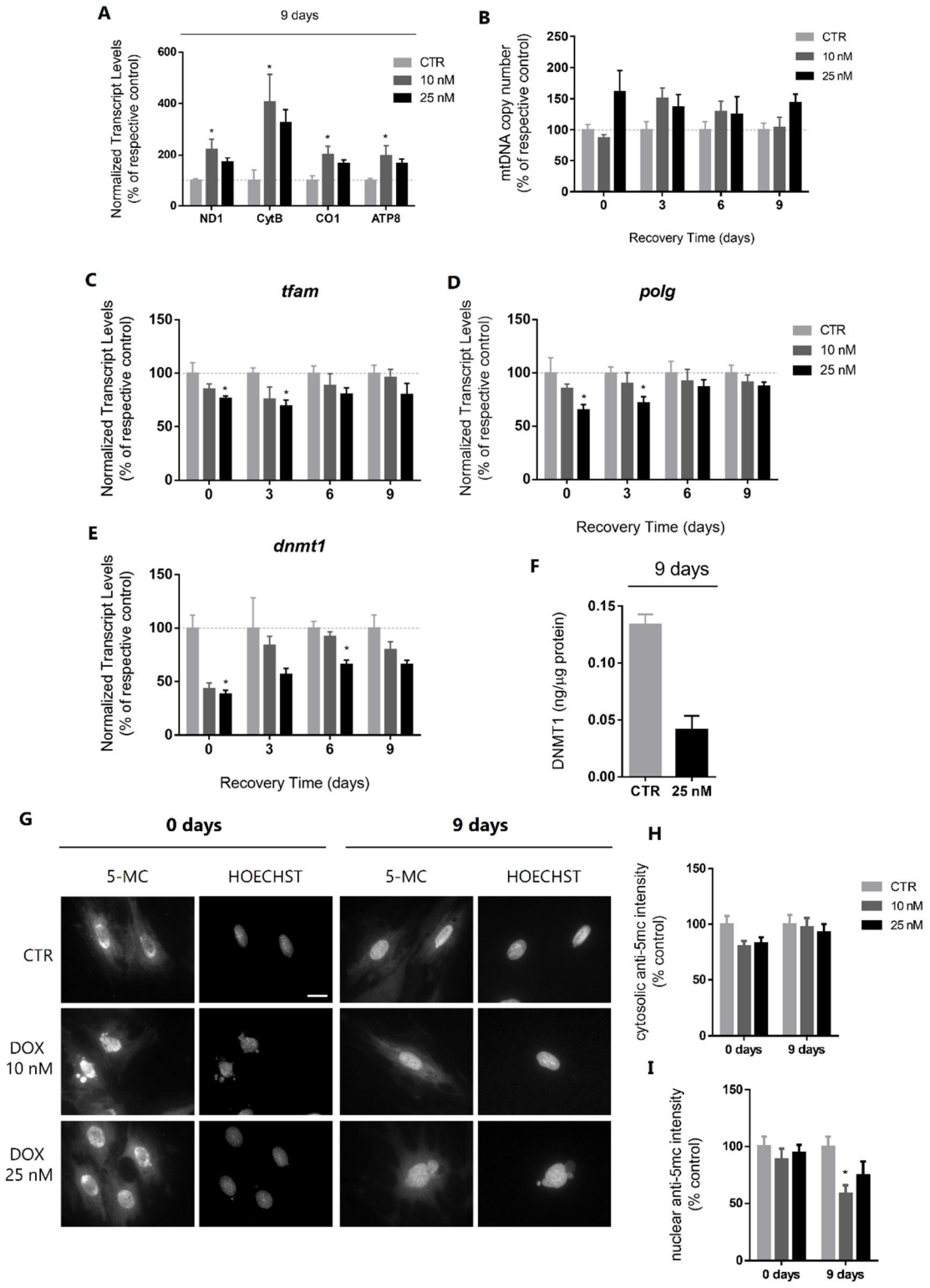

(Legend on the next page)

Figure 5.6: Effect of DOX on gene expression, mitochondrial DNA copy number, DNMT1 protein levels and DNA methylation. RT-PCR was used to measure: (A) Expression of mtDNA-encoded genes ND1, CytB, CO1, ATP8, after 9 days of recovery after DOX exposure; (B) mtDNA copy number and (C-E) expression of the nuclear-encoded genes tfam, polg and dnmt1. Data are expressed as mean ± SEM of 4-7 independent experiments (F) Nuclear DNMT1 protein levels were also quantified at day 9. Data are expressed as mean ± SEM of three independent experiments. (G) Immunocytochemistry staining of control and DOX-treated H9c2 cells labeled with an antibody against 5-mc and counterstained with Hoechst 33342, after 0 and 9 days of recovery. Scale bar; 20 μm. Cytosolic (H) and nuclear (I) DNA methylation relative to control samples were quantified. Data are expressed as mean ± SEM from measurements of multiple cells of three independent experiments; *$p < 0.05$ compared to control.

Nuclear DNMT1 protein levels were assessed by a commercial ELISA kit and a similar tendency (although not statistically significant) was observed, with DOX-treated cells presenting lower levels of DNMT1 (Fig. 5.6 F). Immunocytochemistry examination of H9c2 cells labeled with anti-5-mc antibody revealed loss of signal in 10 nM DOX-treated cells, as well as the presence of micronuclei in 10 and 25 nM DOX-treated cells (Fig. 5.6 G-I). Recent evidence suggests the presence of methylated cytosine in mtDNA, namely within the D-loop region, a hypervariable region where the main regulatory elements for mtDNA replication and expression are located [380, 381]. Also, DNMT1 seems to modulate mitochondrial transcription through the regulation of mtDNA methylation [66, 382]. Our findings suggest that in response to low DOX concentration, a DNMT1-based mechanism of mtDNA expression regulation seems to happen, although this was not directly measured.

5.3.6. Nanomolar DOX-mediated mitochondrial adaptation protected against a subsequent DOX treatment

Considering the mitochondrial data obtained so far, our next question was whether the apparent mitochondrial adaptation of DOX-treated cells could lead to an increased resistance to a second-hit stressor. To assess this, after nine days of recovery, H9c2

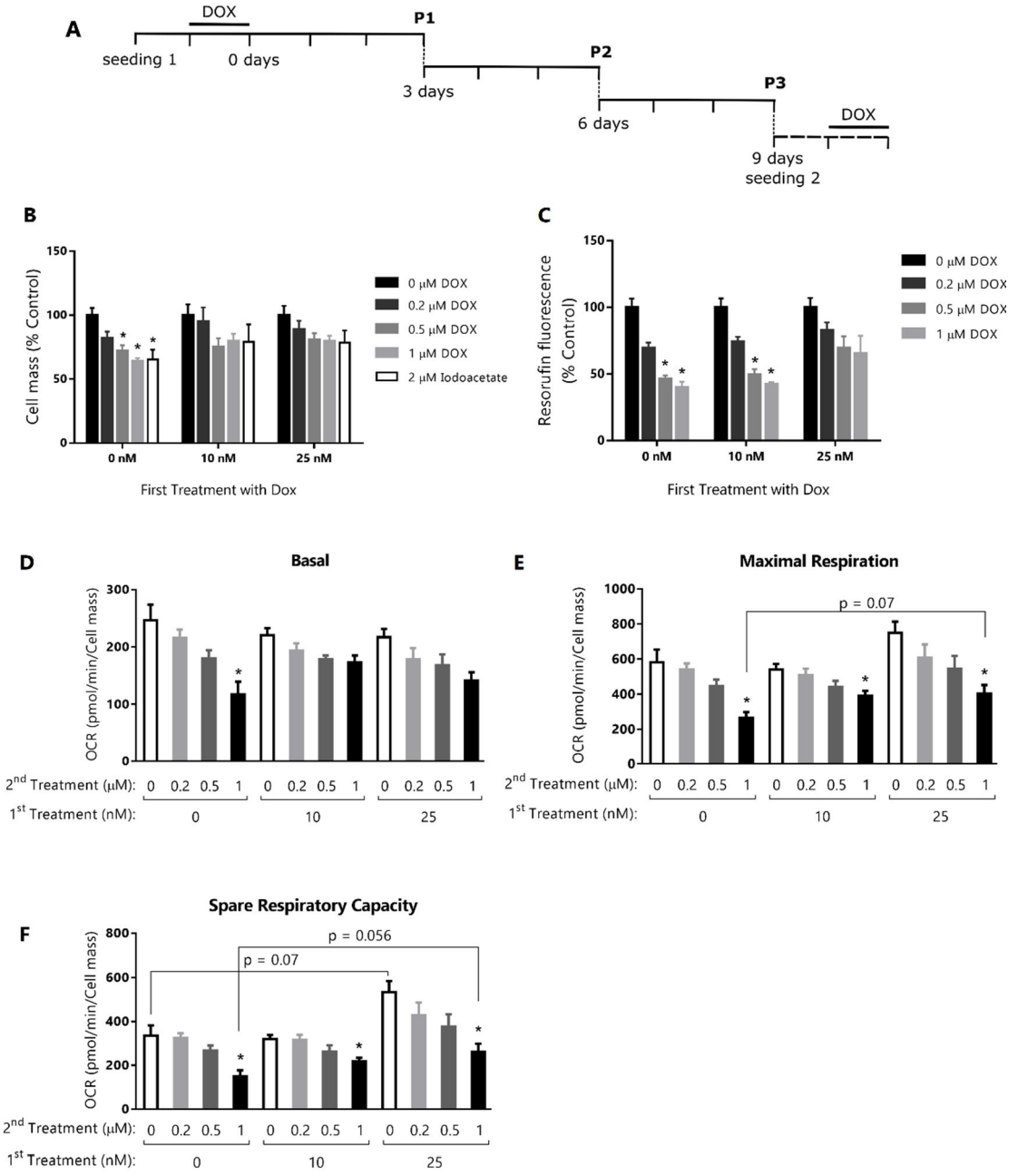

Figure 5.7: Effect of pre-treatment with DOX on H9c2 cells response to second-hit stress. A) After the initial protocol, cells were seeded again and exposed to DOX (0.2, 0.5 and 1 μM) or iodoacetate (2 μM) for 24 hours. P refers to a cell passage. Toxicity was evaluated by SRB as the post-treatment percentage of cell mass (B) and by metabolic reduction of resazurin (C). Data are expressed as mean ± SEM of 4-6 independent experiments. (D-F) Seahorse XFe96 analyzer was used to evaluate mitochondrial respiration rates and determine several respiratory parameters including basal respiration (D), maximal respiration (E) and spare respiratory capacity (F). These results are expressed as mean ± SEM of 4 independent experiments. *$p < 0.05$ compared to 0 μM DOX control.

cells were again treated with DOX for 24 hours, but this time with higher concentrations (0.2, 0.5 and 1 μM)(Fig. 5.7 A), and cytotoxicity was measured by the SRB and resazurin methods (Fig. 5.7 B,C). Although there was a decrease in cell mass for all the four treatments, the effect was less pronounced for the 10 and 25 nM pre-treated cells, comparing with control cells (for 1 μM DOX, cell mass decreased ~20% in DOX pre-treated cells in contrast to ~36% in control cells) (Fig. 5.7 B). Similarly, the decrease of metabolic activity was much less pronounced in the 25 nM DOX pre-treated cells when compared with the 0 nM DOX control (Fig. 5.7 C). The pre-treatment also improved the resistance of H9c2 against iodoacetate, an inhibitor of glycolysis (~13 % improvement of cell viability in DOX pre-treated cells compared to DOX-naïve cells), consistent with the reduced glycolytic metabolism observed in 25 nM DOX-treated cells (Fig. 5.7 B). The impact of the preconditioning on mitochondrial

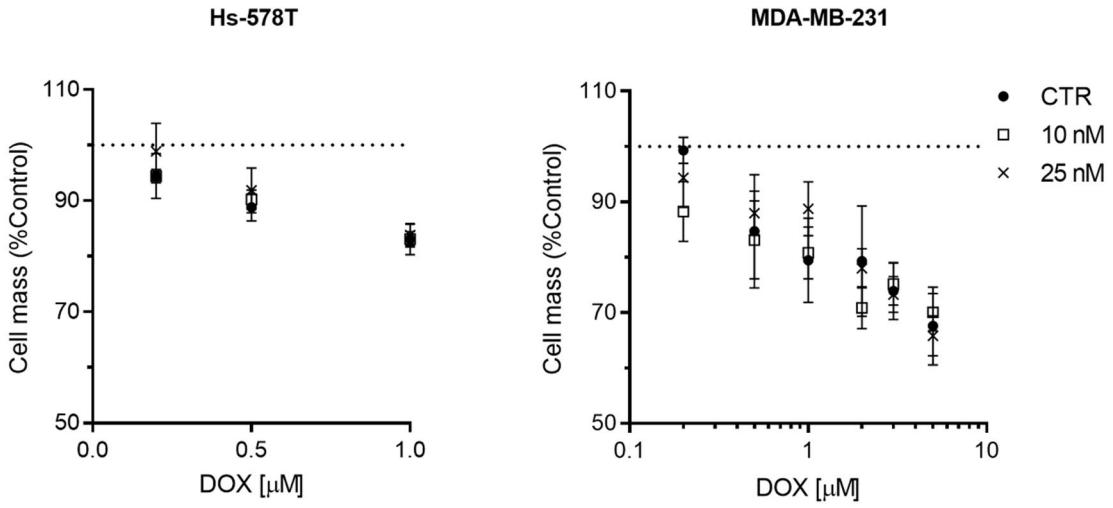

Figure 5.8: Effect of pre-treatment with DOX on human breast cancer Hs-578T and MDA-MB-231 total cell mass. Toxicity was evaluated by SRB as the post-treatment percentage of cell mass. Data are expressed as mean ± SEM of 3-4 independent experiments.

adaptation was further validated by mitochondrial oxygen consumption rate measurements (Fig. 5.7 D-F). Basal respiration rates did not change significantly (Fig. 5.7 D); however, maximal respiration (Fig. 5.7 E) and spare respiratory capacity (Fig. 5.7 F) showed higher levels in 25 nM DOX cells compared with the non-pre-treated cells. In order to discard the possibility that this preconditioning treatment with DOX could induce cross-resistance also in tumor cells, we performed the same protocol in Hs-578T and MDA-MB-231 cell lines, models of human breast/mammary gland carcinoma (Fig. 5.8). No differences were observed in cell mass after the second exposure to DOX between control, 10 nM- and 25 nM-treated groups.

5.4. Discussion

It has previously been shown that DOX treatment *in vivo* induces mitochondrial/metabolic reprogramming [184]. In the current investigation, we aimed to study the delayed response of H9c2 cells to nanomolar doses of DOX and the possible induction of an adaptive response, increasing the tolerance to a subsequent higher dose. We confirmed decreased cytotoxicity after clinically relevant DOX treatment in cells that were previously treated with DOX at low clinical doses, supporting the hypothesis of a protective mechanism.

We first demonstrated increased cell cycle arrest in G2/M and hypertrophy in nanomolar DOX-treated H9c2 cells. Similar hypertrophic behavior has been previously observed in H9c2 cells, as well as in animal models of DOX-induced cardiomyopathy [208, 383, 384]. Oyama et al. reported that H_2O_2 and 1 μM DOX (2 hours) also induced cell cycle arrest in G2/M with increased p21 expression, a well-established regulator of the cell cycle [385]. Their findings implicate H9c2 cell hypertrophy as a late event secondary to cell cycle arrest. Activation of p53 by DOX usually results in the overexpression of the p53-target gene *Bax*, leading to

overexpression of the corresponding proapoptotic protein BAX, which translocates to the mitochondrial membrane leading to apoptosis. Alternatively, under stress conditions, such as DNA damage or oxidative stress, upregulation of p53 activity results in increased p21 transcription that leads to cell cycle arrest [386, 387]. These biological responses can either give time for DNA repair and cell survival, or can lead to a senescence-like phenotype [388, 389], which could eventually lead to mitotic catastrophe and cell death. Thus, the possible beneficial effects of preconditioning can be counterbalanced with less positive outcomes that need to be carefully noted and taken into account.

Other authors have previously reported a shift of energy production in DOX damaged hearts [184, 366]. In our model, nanomolar DOX treatment inhibited glycolysis, in accordance with the lower proliferative behavior, but did not cause major effects on maximal mitochondrial respiration capacity or total ATP levels. In addition, gene expression analysis showed an increase in mitochondrial transcripts after nine days of recovery, and these increased levels seem to be independent from mtDNA content, as confirmed by mtDNA copy number, and from *tfam* and *polg* levels.

Evidence for the existence of 5-methylcytosines (5-mc) and 5-hydroxycytosines (5-hmc) and their influence on mtDNA function are becoming stronger due to the improvement and development of sensitive techniques capable of detecting low-levels of methylation in the mtDNA, supporting the presence of dynamic mitochondrial epigenetic mechanisms of gene regulation. However, it is still not clear how these modifications functionally affect mtDNA even though it is very likely that they influence mitochondrial gene expression and biogenesis. Shock et al. reported not only the presence of 5-mc and 5-hmc in mammalian mtDNA, but also a mitochondrial DNMT1 that binds to the mtDNA and regulates the expression of particular mitochondrial genes [66]. Interestingly, we observed a decrease in DNMT1 mRNA levels after DOX treatment, which was similar to previous reports [390, 391].

This DNMT1 down-regulation was most pronounced at day 0, right after the exposure to DOX, and resolved over time. We hypothesize that DNMT1 could be involved in the regulation of mitochondrial gene expression. Actually, although not mitochondrial specific, the total 5-mc signal obtained from immunocytochemistry analysis was lower in DOX-treated cells compared to controls. Similar results have been previously reported, in which chronic DOX exposure was followed by a global decrease of DNA methylation in cardiac tissue [209]. We speculate a possible reduction in the levels of mtDNA methylation caused by the lack of DNMT1, which could result in upregulation of some mitochondrial genes and maintenance of mitochondrial functions. In fact, hypomethylation of mtDNA was already suggested as a cause for the increased expression of mtDNA-encoded genes [392]. More recently, and strengthening our hypothesis, a downregulation in the expression of DNMT1 accompanied by mtDNA hypomethylation was observed under conditions of oxidative stress [67]. However, it is worth mentioning that our study has some limitations that have been considered for data analyses, one being the failure to confirm mtDNA methylation. Our immunocytochemistry experiments revealed some 5-mc-positive signal in the cytoplasm of H9c2 cells, which may suggest mitochondrial staining, although this needs to be explored in further detail.

Based on the transcriptional and metabolic alterations observed in DOX-treated cells, we proposed that preconditioning H9c2 cells could increase resistance to a second, more severe exposure. An adaptive response to DOX has previously been shown in non-cancer cells [393], although the underlying mechanisms were not clarified. More recently, a study reported that the pre-treatment with low-dose radiation was able to attenuate DOX-induced cardiotoxicity [394]. Here again, the molecular consequences of the stimulation with low-dose radiation were not totally clear, but the authors proposed that the radiation could lead to a small increase of ROS that promote the upregulation of antioxidant defenses.

In the present study we exposed the preconditioned cells to a further 24 hours incubation with either DOX (0.2, 0.5 and 1 μM) or iodoacetate (2 μM), known to irreversibly inhibit the glycolytic enzyme GAPDH. H9c2 cells previously incubated with DOX were significantly more resistant to the second treatment, demonstrated by a lesser decrease in cell mass and metabolic viability. Supporting the role of mitochondria on the cellular adaptation, the oxygen consumption rate results showed an improvement of mitochondrial function with the pre-treatment with DOX. This illustrates a paradoxical beneficial effect of DOX pre-exposure and supports the hypothesis that the capability of proliferating cardiac cells to adapt after DOX exposure can be an advantage to further stresses. However, our data does not provide direct evidence whether the adaptation is a result of epigenetic regulation, protective mechanisms including ROS-induced signaling pathways and pro-survival signaling or, more likely, a combination of multiple factors. Moreover, it is also possible that the first exposure could initially select the more resilient cells that later proliferate and are better able to withstand DOX-induced mitochondrial toxicity.

In conclusion, we demonstrated that exposure of H9c2 cells to nanomolar concentrations of DOX increases the resistance of these cells against a subsequent and more stressful dose through a process of mitochondrial adaptation, possibly epigenetic-linked [395, 396]. This strategy could be particularly important for cardiac protection in patients with childhood cancers, considerably ameliorating the DOX-induced cardiomyopathy while maintaining the anticancer treatment effectiveness.

Chapter 6

6. Doxorubicin triggers bioenergetic failure and p53 activation in mouse stem cell-derived cardiomyocytes

6.1. Introduction

Most of the previous studies aimed at elucidating *in vitro* mechanisms behind DOX cardiotoxicity relied on the H9c2 cell line as a biological model [34, 136-138, 140, 349, 397-400]. However, this cell line has several limitations that can be overcome by using stem cell-derived cardiomyocyte cultures that maintain the capacity to beat in culture, which is relevant for cardiotoxic studies since cardiomyocyte contractility is highly dependent on cellular ATP levels [401]. In this study, we used Cor.At cells, produced through *in vitro* differentiation of mouse iPSC coupled with puromycin selection of cardiomyocytes [402]. Cor.At cells have limited proliferative capacity similar to primary cells, as determined through BrdU incorporation assays [358], and can be transplanted into mouse hearts. These cells express all relevant cardiac ion channels (K^+, Ca^{2+}, Na^+) [361] and the gap junction channel protein connexin-43 [403], the predominant connexin expressed by cardiomyocytes [404]. This is an indication of the ability for electric coupling of these cells, as shown in immunostaining, and enables the cells to beat synchronously in culture. Patch clamp analysis, as well as multi-electrode array (MEA) recordings, demonstrated the normal electrophysiological properties of these cells, and DOX treatment in Cor.At cardiomyocytes significantly decreased overall beating rate and induced an irregular beating pattern similar to other compounds that induce arrhythmia [361]. Overall, the data obtained so far suggest that these cells present some advantages to study DOX cardiotoxicity. Still, no

information is available on how mitochondrial stress responses and metabolism respond to DOX treatment in the Cor.At cardiomyocyte cell system. This limitation hinders a more complete picture of the mechanisms underlying DOX toxicity in beating mouse stem cell-derived cardiomyocytes. Our objective is thus to investigate mitochondrial stress responses triggered by DOX on Cor.AT cells, focusing on oxidative phosphorylation, regulation of pyruvate oxidation, and p53 signaling.

6.2. Methods

6.2.1. Cor.At cell culture, DOX treatment and experimental design

Frozen Cor.At cardiomyocytes were rapidly thawed by gentle agitation in a 37°C water bath and immediately transferred into 50 mL centrifuge tubes filled with 8 mL Cor.At Culture Medium. The cryotube was rinsed with an additional 1 mL of medium to collect remaining cells and pipetted into the same centrifuge tube. The cells were then centrifuged at 200 xg for 5 min and the pellet was carefully resuspended in

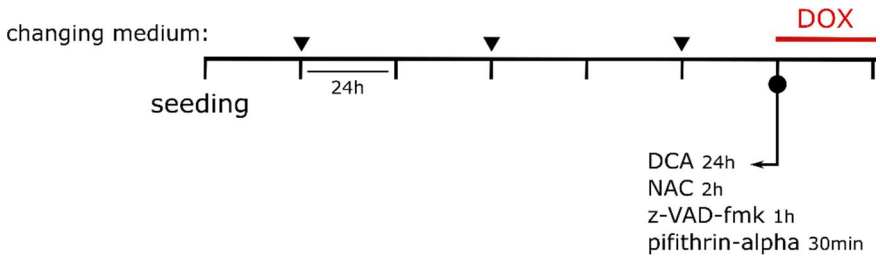

Figure 6.1: Cor.At experimental design. Cor.At were thawed and seeded in fibronectin coated culture-plates. The medium was replaced every two days. After 6 days in culture cells were exposed to DOX (0, 0.5 μM, 1 μM) for 24 hours. For the pre-incubation experiments, DCA, NAC, z-VAD-fmk and pifithrin-alpha were added prior DOX exposure and were kept in the medium for controlled periods.

culture medium containing puromycin. Cells were counted and seeded on fibronectin-coated culture plates at a density of $1x10^5$ cells/cm^2 and incubated at 37°C in 5% CO_2/95% air for 1 week before experiments were performed, with the culture

medium being replaced every two days (Fig. 6.1). Cells were then incubated with DOX (0, 0.5 or 1 μM) for 24 hours. For the pre-incubation experiments, the following compounds were added to cells prior to DOX treatment: 50 μM z-VAD-fmk for 1 hour, 100 μM NAC for 2 hours, 30 μM pifithrin-alpha for 30 min, 3 mM dichloroacetate (DCA) for 24 hours.

6.2.2. Sulforhodamine B (SRB) assay

SRB assay was performed as described on section 5.2.2 with slight modifications. Cor.At were seeded in 96 well-plates at a concentration of $1.0x10^5$ cells/cm^2. At the end of DOX treatment, cells were fixed overnight and then incubated with 100 μL 0.05% (w/v) SRB solution. Dye bound to cellular proteins was extracted with 200 μL Tris (10 mM, pH 10) and absorbance was read at 530 nm.

6.2.3. Live epifluorescence microscopy

Cell morphology and contractile function were analyzed by epifluorescence microscopy. Cor.At were seeded in 96-well plates and, after DOX treatment, cells were washed with PBS and incubated for 30 min in microscopy medium with the cationic fluorophore $TMRM^+$ (tetramethylrhodamine methyl ester; 100 nM) and Hoechst 33342 (1 μg/mL). After incubation, cells were imaged in a Nikon Eclipse Ti-S microscope and analyzed with ImageJ 1.49v.

6.2.4. Bioenergetic analysis

Oxygen consumption rate (OCR) and extracellular acidification rate (ECAR) were determined using a Seahorse XFe96 analyzer and the Seahorse XF Cell Mito Stress Test. Cor.At were seeded into Seahorse XFe96 well plates at a density of $1.0x10^4$

cells/well/80 μL. One hour prior the assay the plate was rinsed twice with PBS, 175 μL of Cor.At culture medium was added and cells were incubated for 1 hour at 37°C without CO_2. Cor.At medium was used in the assay, including in the preparation of the loaded compounds. A constant volume of 25 μL of each compound was pre-loaded into the respective ports of the cartridge (Port A: oligomycin, final concentration: 1 μM; Port B: FCCP, final concentration: 4 μM; Port C: a mix of rotenone/antimycin A, final concentration: 2 μM). Measurements were performed in five to six replicates. OCR and ECAR values were normalized to the cell mass, determined by the SRB assay, and analyzed using Wave v2.3 software (Agilent Technologies, USA).

6.2.5. RNA and protein isolation

PureZOL Reagent was used to isolate RNA and protein fractions from the same sample. For this purpose, Cor.At cells were cultured in 6 multiwell plates. After aspiration of the culture medium, 1 mL of PureZOL was added to each well, the reagent was mixed by pipetting up and down, and incubated at room temperature for 5 min, to allow the disruption of nucleoprotein complexes. The content was transferred to a 1.5 mL microtube and 0.2 mL of chloroform was added, followed by vigorous mixing for 15 seconds. The samples were incubated for 5 min and centrifuged at 12,000 xg for 15 min at 4°C, to separate the sample into 3 phases: aqueous phase (RNA), interphase (DNA) and organic phase (protein).

RNA extraction: The aqueous phase was immediately transferred to a new microtube and 0.5 mL of isopropyl alcohol was added and incubated for 5 min at room temperature, for RNA precipitation. Another centrifugation was performed at 12,000 xg for 10 min at 4°C and the supernatant was discarded. To wash the RNA white pellet, 1 mL of 75% ethanol was used, followed by vortexing and centrifugation at

7,500 xg for 5 min at 4°C. Supernatant was again discarded, and the pellet dried for 5 min. Lastly, the pellet was resuspended in 20 μL of RNase-free water and stored at -80°C.

Protein extraction: After the removal of the aqueous phase, 0.3 mL of 100% ethanol was added to the microtube containing the two other phases. After 3 min at room temperature, the samples were centrifuged at 2,000 xg for 5 min at 4°C and the supernatant transferred for a new Eppendorf tube. To precipitate the proteins, 1.5 mL of isopropyl alcohol was added and incubated for 10 min at room temperature, followed by centrifugation at 12,000 xg for 10 min at 4°C. After discarding the supernatant, the pellet was washed with 2 mL of 0.3 M guanidine hydrochloride in 10% ethanol, incubated 20 min at room temperature, centrifuged at 7,500 xg for 5 min at 4°C, and the supernatant was discarded. These steps were performed 3 times. Then, 2 mL of ethanol was added, and the sample was vortexed and centrifuged at 7,500 xg for 5 min at 4°C. After discarding the supernatant, the pellet was dried for 10 min and resuspended in 50 μL of 1% SDS at 50°C. The protein was quantified by the BCA method using bovine serum albumin (BSA) as a standard.

6.2.6. Western Blotting

Samples were heated at 55°C (for OXPHOS) or 95°C for 5 min in a 2x Laemmli sample loading buffer, and equivalent amounts of protein (30 μg) were separated in SDS-polyacrylamide gel electrophoresis and electrophoretically transferred to a poly-vinylidene difluoride (PVDF) membrane. After membrane blocking with 5% non-fat dry milk in TBS-T for 90 min at room temperature under continuous stirring, membranes were incubated overnight at 4°C, under stirring, with the primary antibodies (Table 4.2). Once incubation was complete, membranes were incubated with horseradish peroxidase (HRP)-conjugated secondary antibodies for 1 hour at

room temperature under continuous agitation (Table 4.2). Membranes were washed again and incubated with Clarity Western ECL Substrate, for 5 min maximum at room temperature. Band intensity was analyzed in a UVP Biospectrum 500 Imaging System. Before blocking, the membranes were stained with Ponceau S reagent to confirm equal protein loading in each membrane. Ponceau S labels a wide range of proteins independently of drug treatment, being a reliable method for protein normalization in western blotting [405]. Band density was measured using the ImageJ 1.45S software (NIH, USA).

6.2.7. cDNA preparation and quantitative real-time PCR

cDNA preparation and RT-qPCR were performed as described on section 5.2.9. Primers and annealing temperatures are specified on Table 4.3.

6.2.8. ATP levels

Cell viability based on ATP measurement was assessed using CellTiter-Glo Luminescent Cell Viability Assay. The assay is based on the premise that, in the presence of Mg^{2+}, O_2 and ATP, luciferase converts luciferin into oxyluciferin and emits yellow-green light whose signal is then proportional to the amount of present ATP.

Briefly, Cor.At were seeded in a white 96-well plate and, at the day of the assay, the medium was removed from the wells, replaced by 50 µL of fresh medium and 50 µL of the Cell Titer-Glo® reagent was added and mixed for 2 min on an orbital shaker to promote cell lysis. The plate was incubated for 10 min and the luminescent signal was recorded using Cytation™ 3 microplate reader.

6.2.9. Caspase activity

Caspase-9 and -3/7-like activities were evaluated using the Promega Caspase-GLO assays: Caspase-Glo 9 and Caspase-Glo 3/7. These assays provide luminogenic caspase substrates (DEVD and LEHD derivatives for caspase-3/7 and caspase-9, respectively) that following caspase cleavage release a substrate for luciferase, resulting in luciferase reaction and production of light. The signal generated is then proportional to the present caspase activity.

Cor.At were seeded in white-walled 96-well plates and the assay was performed at the end of DOX treatment, following the instructions provided by the manufacturer. Luminescence was measured in Cytation™ 3 microplate reader.

6.2.10. PDH activity

PDH activity was measured using a commercial assay kit according to manufacturer's instructions. Briefly, $9x10^5$ Cor.At cells were lysed in 100 μL PDH assay buffer. For that, cells were sonicated 3 x 5 seconds, with 30 seconds intervals, in PDH assay buffer and further left for 10 min on ice. The cell lysate was then centrifuged (10,000 xg, 5 min) and the pellet was discarded. From the resultant supernatant, 10 μL were used per reaction. After the addition of the reaction mixture, consisting of assay buffer, PDH substrate and developer, the absorbance was measured continuously at 450 nm every 1 min for 80 min total, while the plate was incubated at 37°C. Only measurements within the linear range of the assay were used for PDH activity calculation and sample blanks were used for each sample correction. The results were expressed as amount of NADH (nmole) generated per reaction time and sample volume.

6.2.11. Statistical analysis

Data were expressed as mean±SEM for the number of experiments indicated in the figure legends. Comparisons were performed using Mann-Whitney U-test when comparing 2 conditions, Kruskal-Wallis H-test followed by Dunn's post hoc analysis was used for multiple conditions comparison. For parametric analysis, multiple comparisons were performed using one-way ANOVA followed by Bonferroni post-hoc test. Significance was accepted with p value <0.05.

6.3. Results

6.3.1. DOX induced dose-dependent morphological and functional changes associated with mitochondrial depolarization and apoptotic hallmarks

To evaluate DOX cardiotoxicity, cardiomyocytes were incubated with 0, 0.5 or 1 μM DOX, and cell morphology and mass were evaluated after 24 hours of treatment (Fig. 6.2). Alterations of cell morphology were apparent for both DOX concentrations, with the highest concentration (1 μM) inducing more evident changes (Fig. 6.2 A), accompanied by desynchronization of cardiomyocyte beating, possibly due to lower intercellular surface contacts due to DOX toxicity (data observed with live cell imaging). Average nuclear area was significantly decreased for 1 μM DOX, being 50% lower in average when compared to control, and 37% lower when compared to 0.5 μM DOX (Fig. 6.2 B). This mostly resulted from a decrease in the number of cells with larger nuclei and a correspondent increase in cells with smaller ones (Fig. 6.2 C). However, cell protein mass was not significantly affected by DOX at the concentrations used (Fig. 6.2 D). The ATP levels, on the other hand, were significantly reduced after DOX treatment (Fig. 6.2 E). Morphological changes accompanied alterations in mitochondrial polarization, assessed by $TMRM^+$ labeling intensity, and

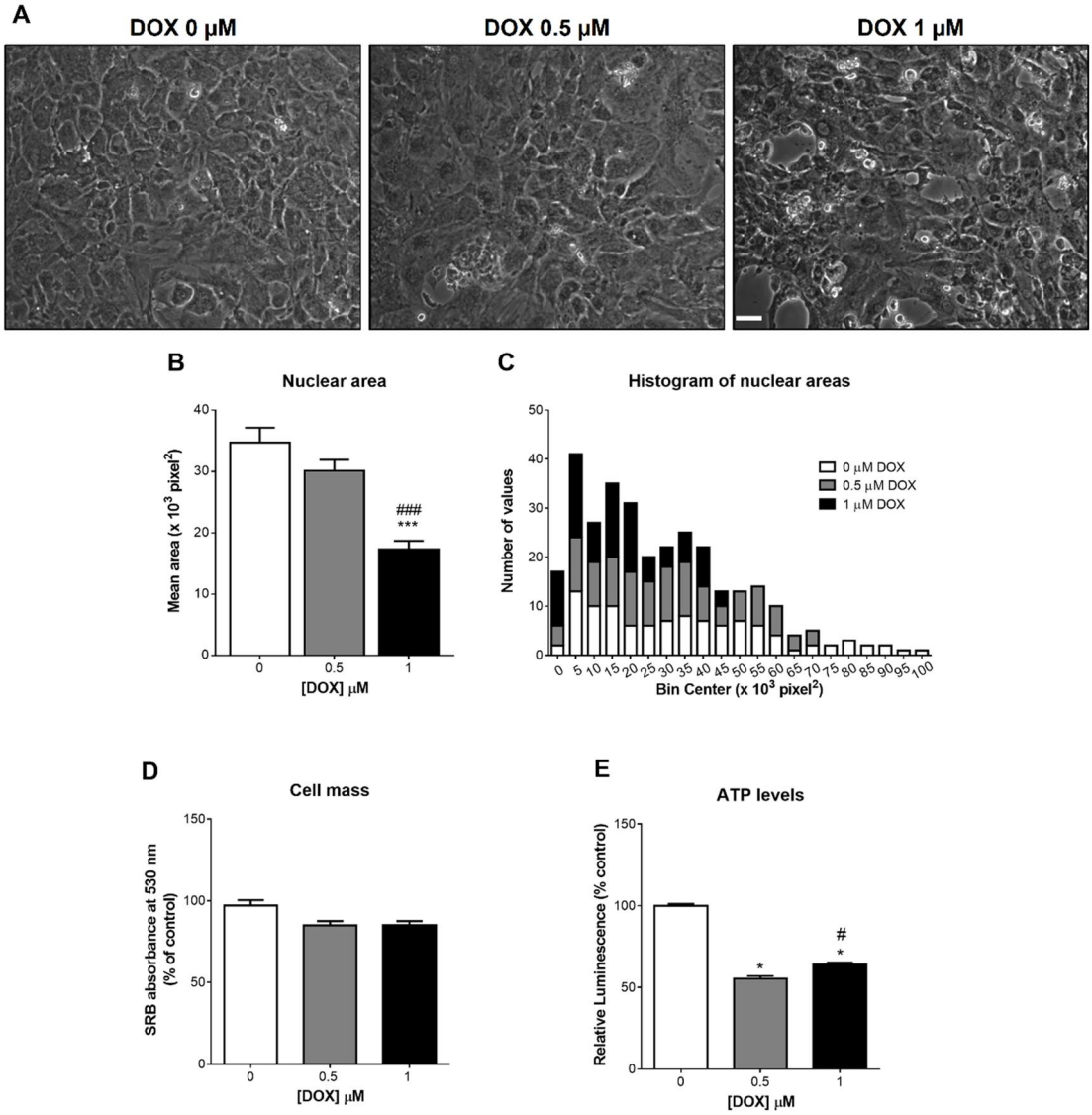

Figure 6.2: Morphological alterations induced by DOX in cultured cardiomyocytes. A) Images are representative of cells cultured in control conditions or treated with DOX (0, 0.5 or 1 μM) for 24 hours. Scale bar represents 30 μm. B-C) Nuclear areas were measured using ImageJ software and presented as B) mean±SEM of about 100 nuclei per condition, from at least 3 independent experiments, or C) as a histogram to show frequency distribution of nuclear areas. D) Cell mass was estimated using the sulforhodamine B (SRB) assay. Data are the mean±SEM of 4 independent experiments. E) Cell viability based on ATP levels was assessed by CellTiter-Glo® assay. Results represent the mean±SEM of 4 independent experiments. *p<0.05, ***p<0.001 compared to 0 μM DOX, #p<0.05, ###p<0.001 compared to 0.5 μM DOX

by increased nuclear apoptotic morphology, analyzed after labelling with Hoechst 33342 (Fig. 6.3 A). At 0.5 μM, DOX treatment resulted in a small increase in the number

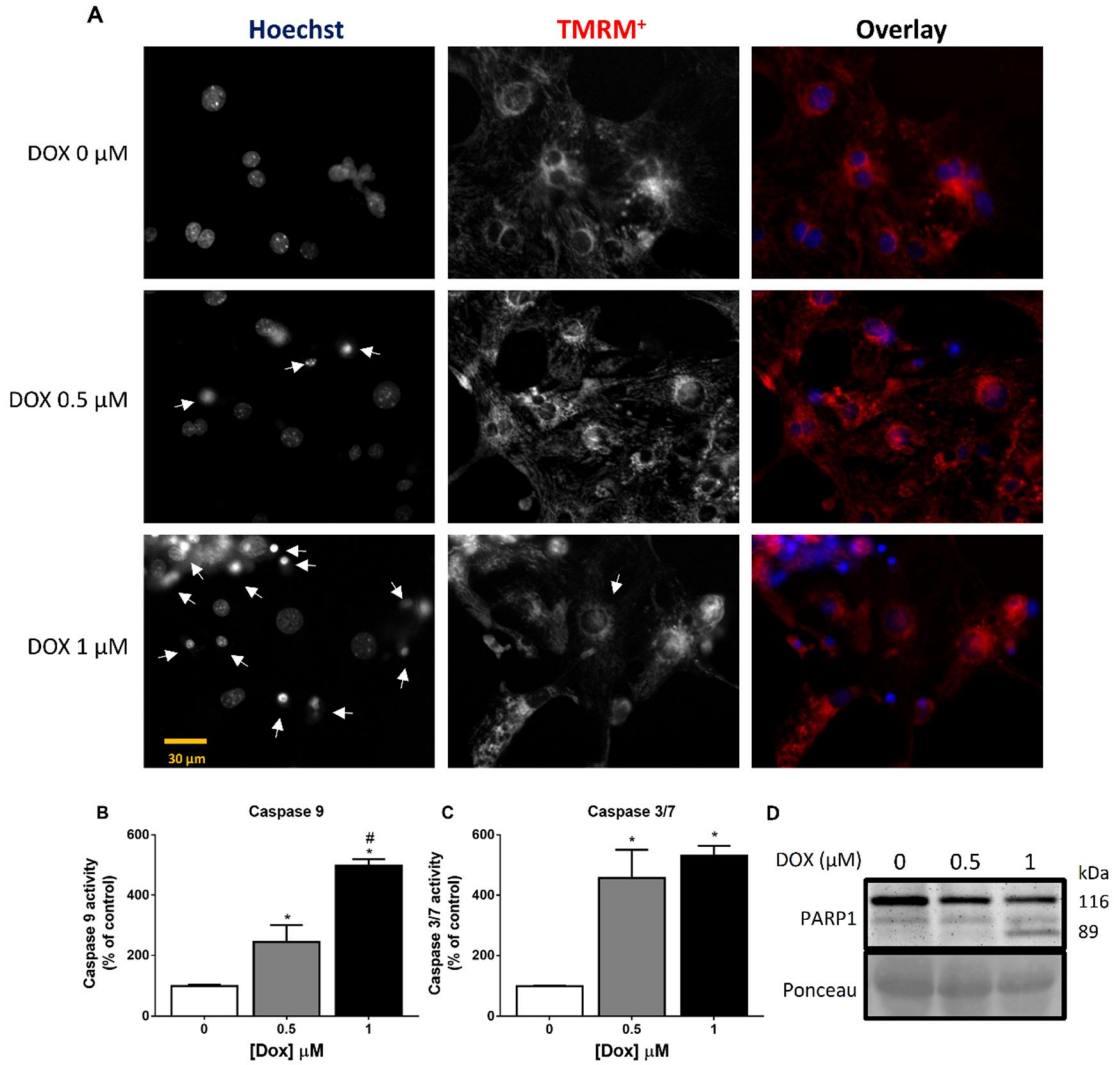

Figure 6.3: Analysis of apoptotic hallmarks in cultured cardiomyocytes exposed to DOX (0, 0.5 or 1 µM) for 24 hours. A) Nuclear morphology, mitochondrial polarization and mitochondrial network arrangement were analyzed by fluorescence microscopy using Hoechst 33342 and TMRM+. Arrows in the Hoechst panels correspond to apoptotic nuclei. Arrows in the TMRM+ panel correspond to depolarized mitochondrial network. Scale bar represents 30 µm. B,C) Activities of caspases -9 and -3/7 were evaluated using Caspase-GLO kits from Promega, as described in Material and Methods. D) PARP cleavage was analyzed by western blotting. Data are representative from 3-4 independent experiments. *p<0.05 compared to 0 µM DOX, #p<0.05, compared to 0.5 µM DOX.

of apoptotic nuclei and appeared to increase perinuclear mitochondrial polarization, which can be an early feature of apoptosis that precedes caspase activation [406-410]. In accordance, the activities of caspases -9 and -3/7 were also significantly increased

under these conditions (Fig. 6.3 B,C). In comparison with control conditions, caspase-9 activity was increased by ~2.4 fold in cells treated with 0.5 μM DOX, (Fig. 6.3 B), whereas caspase-3/7 activity increased by ~4.6 fold (Fig. 6.3 C). In cells treated with 1 μM DOX, an increase in the number of apoptotic nuclei and a decrease in mitochondrial polarization was observed, together with increased activities of caspases -9 (~5 fold) and -3/7 (~5.3 fold), and increased protein content of the PARP-1 fragment (Fig. 6.3 D) resulting from caspase-3-mediated PARP-1 cleavage.

6.3.2. DOX induced p53-associated caspase activation and decreased SOD2 protein content

DOX cardiotoxicity has been described to be mediated by p53 and oxidative stress [136, 411]. In our cell model, both drug concentrations increased p53 (Fig.6.4 A) and decreased SOD2 (Fig. 6.4 B) protein contents. The levels of p53 were increased by ~4.6 fold in cells treated with 0.5 μM DOX and ~3.6 fold with cells treated with 1 μM DOX. SOD2 protein levels were decreased by ~30% for 0.5 μM DOX concentration and ~37% for 1 μM DOX. Activation of caspases by DOX was completely prevented by pre-incubation with the non-selective caspase inhibitor z-VAD-fmk (Fig. 6.4 C,D). Pre-incubation with pifithrin alpha (Pfα), a p53 inactivator that blocks p53-dependent transcriptional activation and apoptosis [412], partially prevented caspase-9 activation by DOX at 1 μM (Fig. 6.4 C), and completely prevented caspase 3/7 activation by DOX at 0.5 and 1 μM (Fig. 6.4 D). The antioxidant N-acetyl cysteine (NAC) did not present significant protective effects against DOX-induced caspase activation in this cell model (Fig. 6.4 C,D). At the concentrations used in this study, Pfα, NAC and zVAD

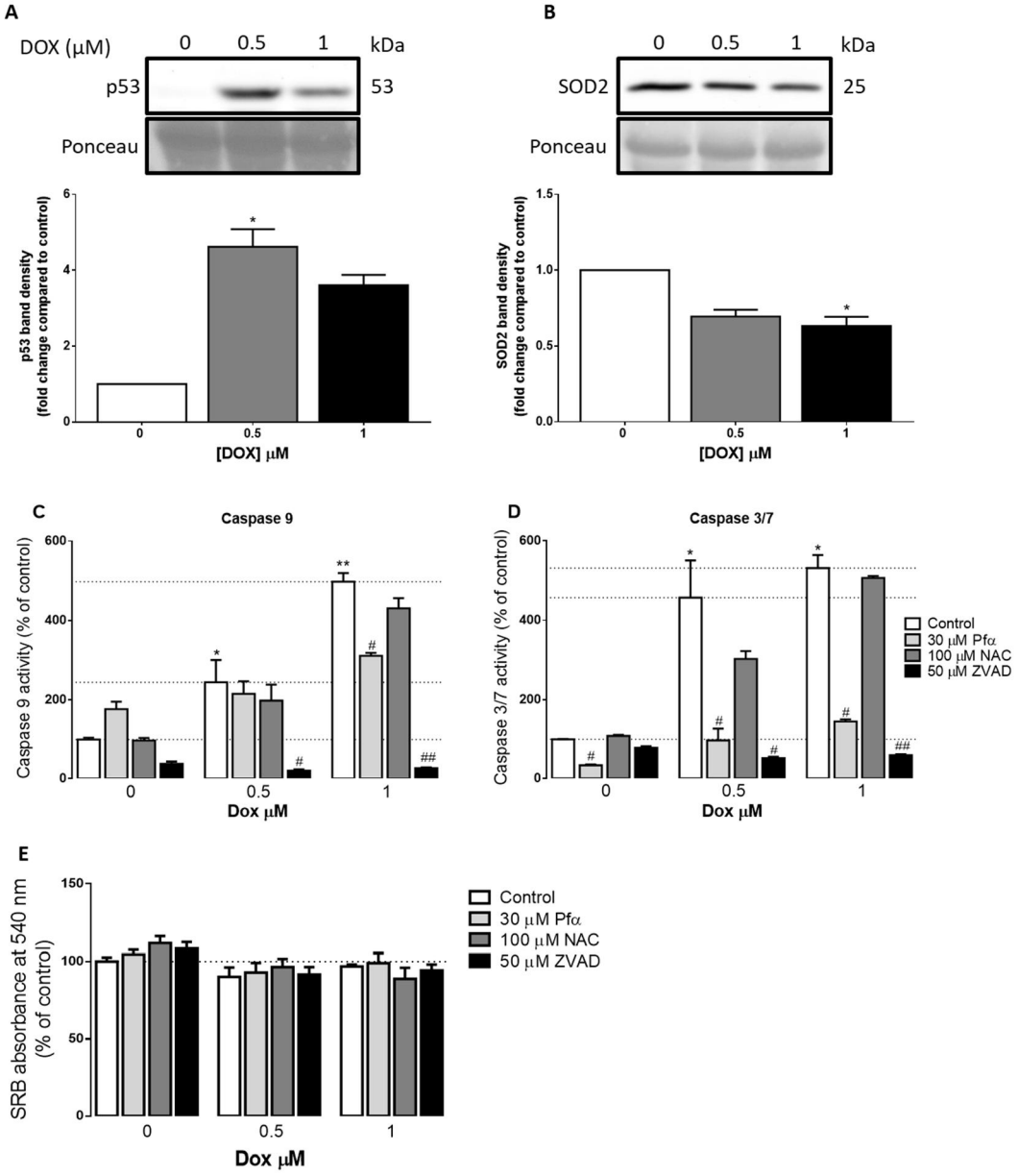

Figure 6.4: Involvement of p53, ROS and caspases in DOX toxicity in cultured cardiomyocytes. Cells were incubated with DOX (0, 0.5 or 1 μM) for 24 hours, the protein fraction was extracted with Purezol (Bio-Rad) and the total levels of A) p53 and B) SOD2 were analyzed by western blotting. Involvement of p53, ROS and caspases were analyzed in cells pre-exposed to 30 μM pifithrin alfa (Pfα), 100 μM N-acetyl-cysteine (NAC) or the non-selective caspase inhibitor zVAD-fmk (ZVAD) before treatment with doxorubicin. C) Caspase-9 and D) Caspase-3/7 activities were analyzed using Promega Caspase-GLO assays, as described in Material and Methods. E) None of the used compounds (Pfα, z-VAD-fmk and NAC) affected significantly cell mass, using the SRB analysis. Data are the mean±SEM from 4 independent experiments. *p<0.05, **p<0.01, compared to control. #p<0.05, ##p<0.01, compared to cells treated only with DOX.

did not induce a significant decrease in cardiomyocyte cell mass, in the presence or in the absence of DOX (Fig. 6.4 E).

6.3.3. DOX dose-dependently affected p53 target transcripts associated with mitochondria-dependent apoptosis and DNA-damage response.

Since DOX-induced cardiomyocyte apoptosis seems to be dependent on p53, we next evaluated the mRNA levels of p53-target genes as well as other genes associated with the regulation of the p53 pathway (Fig. 6.5). DOX effects on gene transcription were dependent on the drug concentration. The lower DOX concentration (0.5 μM) induced an increase in transcripts for the p53 target genes *Puma* (~4.6 fold) (Fig. 6.5 C), *Noxa* (~17.5 fold) (Fig. 6.5 D) and *Bax* (~2.1 fold) (Fig. 6.5 E), which are proapoptotic, and also *Mdm2* (~2.6 fold) (Fig. 6.5 B), a gene directly related with the regulation of the p53 pathway [413]. The levels of *p53* also showed a non-statistical increase (~1.7 fold) with 0.5 μM DOX (Fig. 6.5 A). For the higher DOX concentration, the levels of all transcripts were similar to the control situation, except for *Noxa*, which also showed a non-statistically significant tendency to increase (~3.5 fold) (Fig. 6.5 D) and *Bax*, which was significantly decreased (-70%) (Fig. 6.5 E). The mRNA levels of the antiapoptotic gene *Bcl-2* were decreased in cells exposed to both DOX concentrations (-58% for 0.5 μM DOX and -88% for 1 μM DOX) (Fig. 6.5 F). Since p53 activation is associated with DNA damage, we also evaluated transcripts associated with p53-related DNA damage response (Fig. 6.5 G-L). From the genes studied, *Atm* and *Cdk2* transcription was not affected by any of the DOX concentrations tested (Fig. 6.5 J,L). The expression of *Atr* (-63%)(Fig. 6.5 G), *Chk2* (-42%)(Fig. 6.5 H) and *Cdk1* (-80%)(Fig. 6.5 I) was significantly decreased in cells treated with 1 μM DOX, in comparison with control cells. The expression of *Chk1* (Fig. 6.5 K) decreased (-50%) for both DOX

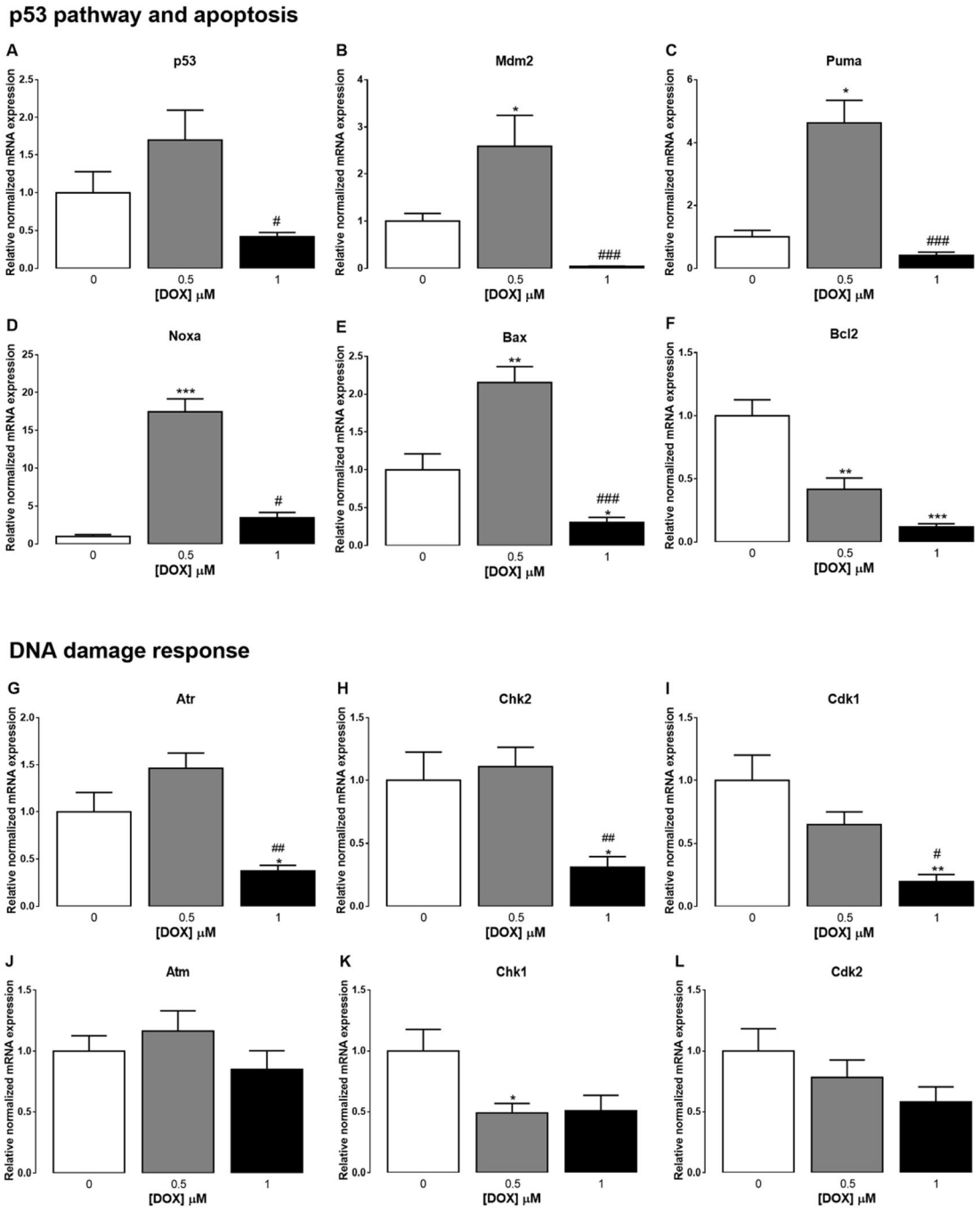

Figure 6.5: Effect of DOX on the levels of p53-associated transcripts involved in apoptosis and DNA damage response in cultured cardiomyocytes. Cells were incubated with DOX (0, 0.5 or 1 μM) for 24 hours, total RNA was extracted with Purezol, converted into cDNA, and analyzed by RT-qPCR. Data are the mean±SEM from 7 independent experiments. *p<0.05, **p<0.01, ***p<0.001, compared to control. #p<0.05, ##p<0.01, ###p<0.001 compared to cells treated with 0.5 μM DOX.

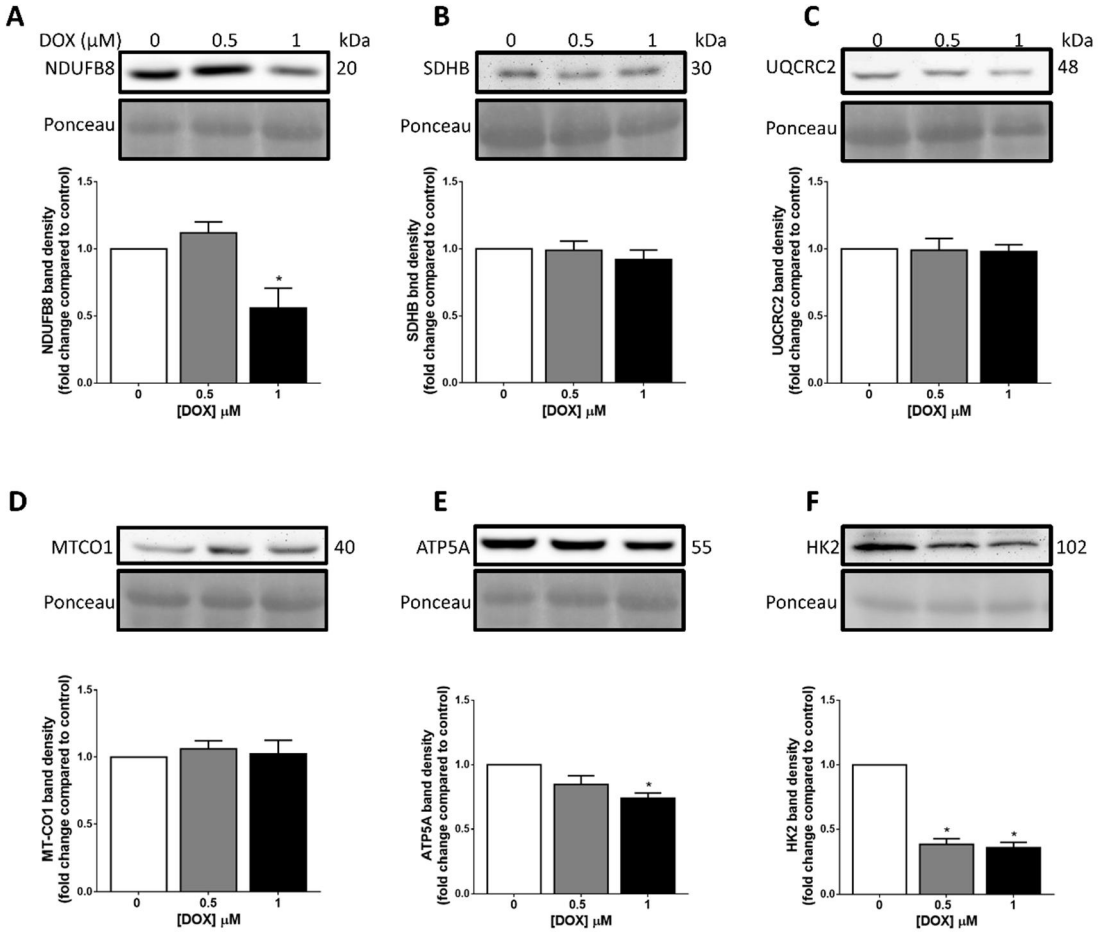

Figure 6.6: Effect of DOX on the protein content of A-E) OxPhos subunits and F) hexokinase 2 (HK2) in cultured cardiomyocytes. Cells were incubated with DOX (0, 0.5 or 1 μM) for 24 hours, the protein fraction was extracted with Purezol, and analyzed by western blotting, as described in Material and Methods. Data are the mean±SEM from 4 independent experiments. *p<0.05 compared to control.

concentrations, although the difference was only statistically significant for cells treated with 0.5 μM DOX.

6.3.4. DOX altered proteins and transcripts associated with mitochondrial bioenergetics

Since the results suggested that DOX treatment resulted in mitochondrial dysfunction in our cell model, we next evaluated the protein content of several OxPhos subunits, as well as the glycolytic enzyme hexokinase-2 (HK2) (Fig. 6.6). Decreases in protein

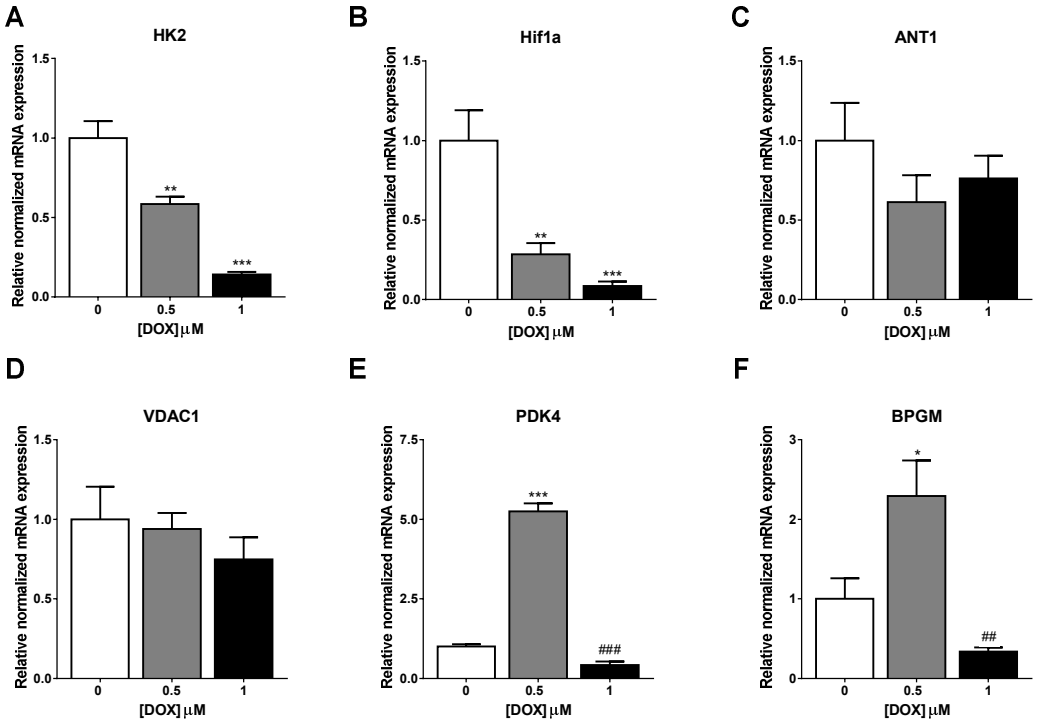

Figure 6.7: Effect of DOX on transcripts associated with bioenergetic regulation in cultured cardiomyocytes. Cells were incubated with DOX (0, 0.5 or 1 μM) for 24 hours, total RNA was extracted with Purezol, converted into cDNA, and analyzed by RT-qPCR, as described in Material and Methods. Data are the mean±SEM from 5-7 independent experiments. *p<0.05, **p<0.01, ***p<0.001 compared to control. ##p<0.01, ###p<0.001 compared to cells treated with 0.5 μM DOX.

content of OxPhos subunits NDUFB8 (complex I) (Fig. 6.6 A) and ATP5A (ATP synthase) (Fig. 6.6 E) were only observed in cells treated with 1 μM DOX, by ~44% and ~26%, respectively. However, HK2 protein content (Fig. 6.6 F) was decreased by ~60% in cells treated with both DOX concentrations. Since DOX may interfere with DNA and affect gene transcription, we measured the abundance of mRNAs encoding genes involved in mitochondrial bioenergetics. We observed a dose-dependent decrease in *Hk2* and *Hif1α* transcripts (Fig. 6.7 A,B). Interestingly, the two DOX concentrations used had a different impact on *Pdk4* and *Bpgm* transcripts, which were only increased after treatment with 0.5 μM DOX (Fig. 6.7 E,F), by ~5.3 and ~2.3 fold, respectively. *Ant1* and *Vdac1* transcripts were not significantly affected by any of the DOX concentrations

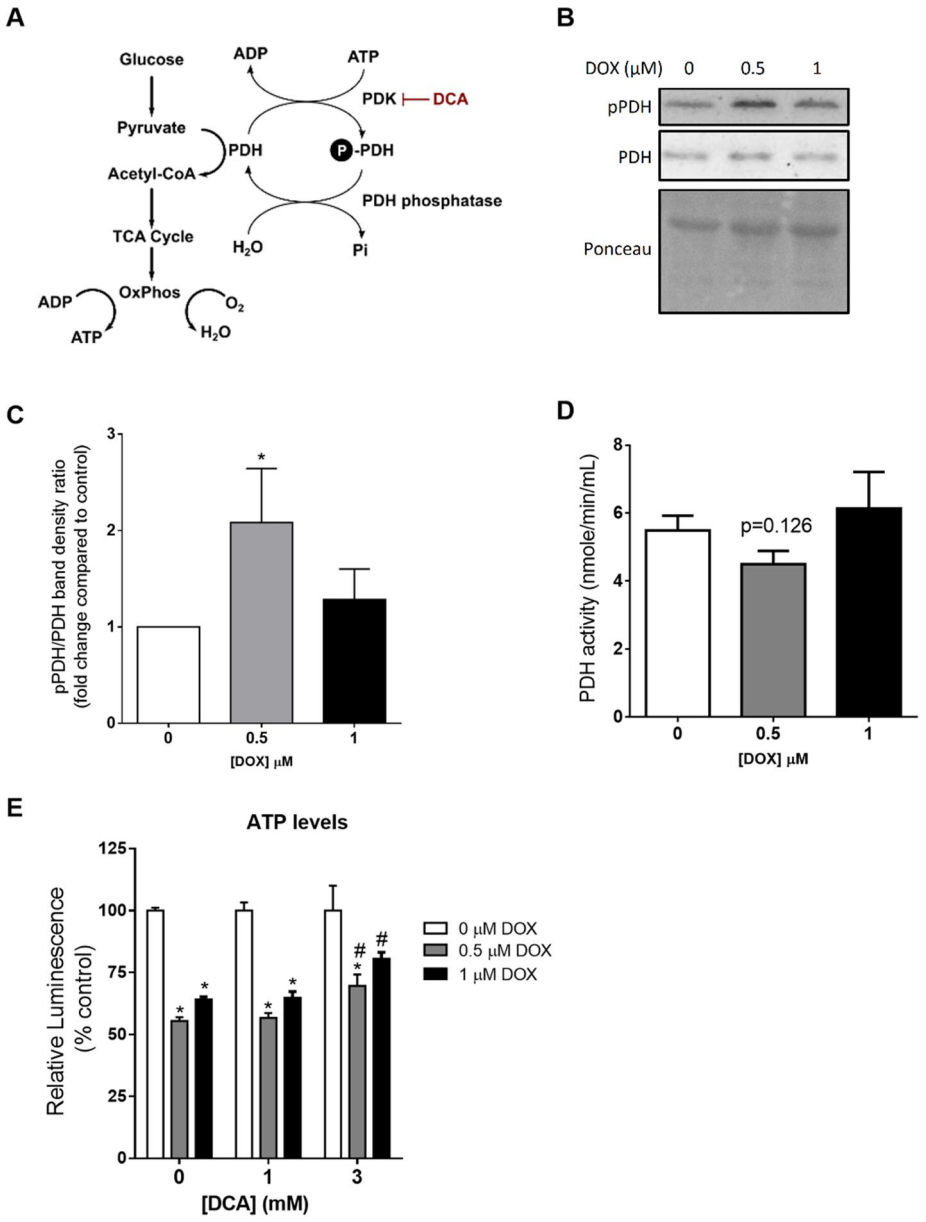

Figure 6.8: Involvement of PDH in DOX toxicity in Cor.At cardiomyocytes. A) PDH is central to metabolic flexibility, linking glycolytic flux to mitochondrial respiration. PDH activity is highly regulated, being inhibited by phosphorylation mediated by PDKs. By inhibiting PDK, DCA is known to restore the active form of PDH, increasing the conversion of pyruvate into acetyl-CoA. B-C) Exposure to 0.5 μM DOX increased the phosphorylation of PDH and D) seemed to decrease PDH activity. Data are the mean±SEM from 4-6 independent experiments. E) Pre-incubation with DCA followed by 24 h incubation with DOX (0, 0.5 or 1 μM) partially recovered ATP levels, estimated using the CellTiter-Glo® assay after. Data are the mean±SEM from 4 independent experiments. *p<0.05 compared to control (0 μM DOX). #p<0.05 compared to cells non-pretreated with DCA.

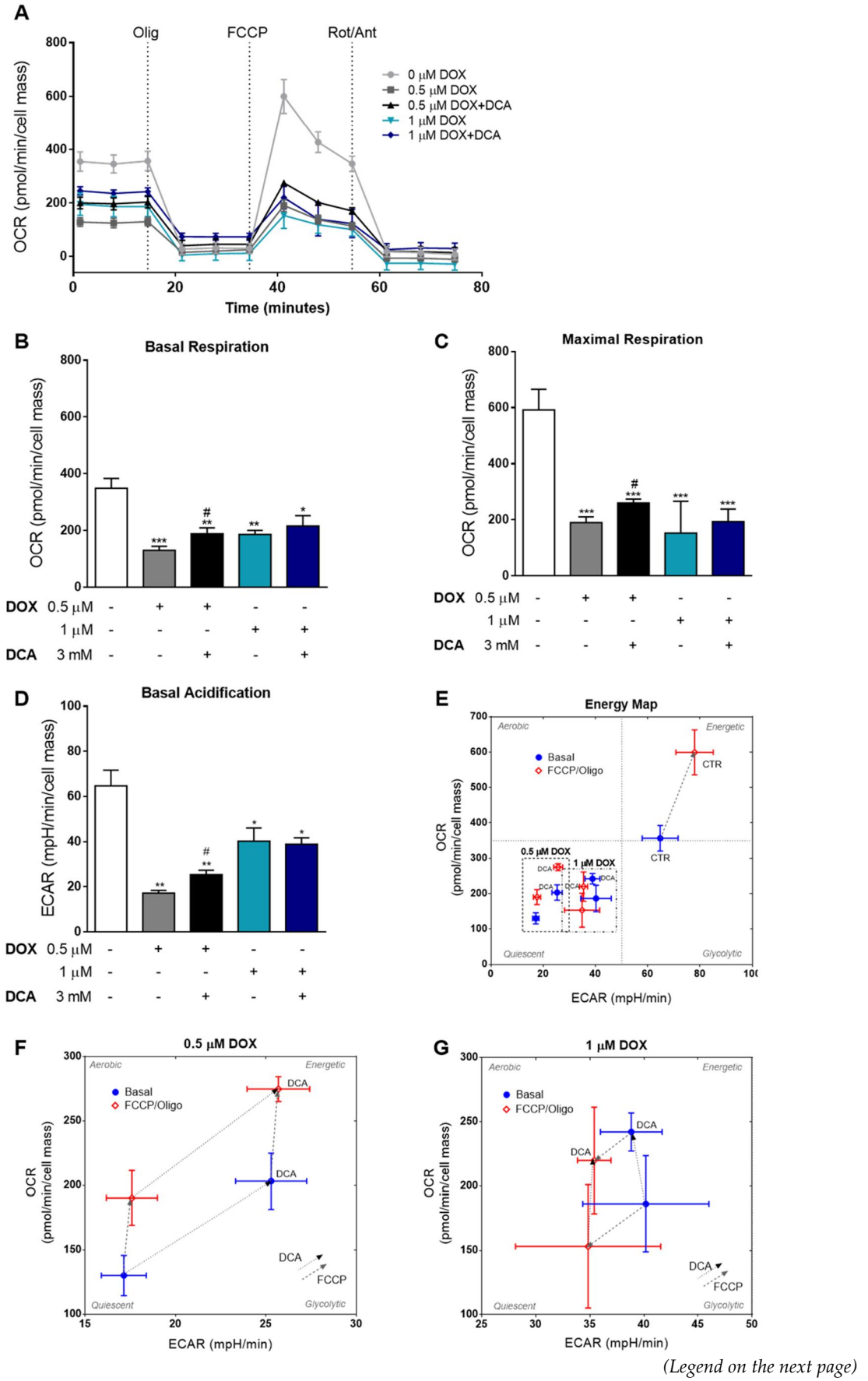

(Legend on the next page)

Figure 6.9: The effect of DCA on mitochondrial bioenergetics in DOX-treated Cor.At cardiomyocytes. A-G) The effect of 3 mM DCA on mitochondrial bioenergetics, based on the oxygen consumption rate (OCR) and extracellular acidification rate (ECAR), was assessed with a Seahorse XFe96 instrument using the mitochondrial stress test. Pre-treatment with DCA increased PDH activity and enhanced mitochondrial respiration (B-C) Basal and maximal respirations were calculated based on the responses to oligomycin, FCCP and rotenone/antimycin A. D) Basal acidification corresponds to ECAR under basal conditions. E-G) Energy maps show the correlation between OCR and ECAR in basal conditions in the absence and presence of DOX, and the shifts induced by exposure to FCCP (and oligomycin), or by pre-exposure to DCA. Data are the mean±SEM from 6 independent experiments. *p<0.05, **p<0.01, ***p<0.01 compared to control. #p<0.05 compared to cells treated only with 0.5 μM DOX.

used (Fig. 6.7 C,D). These results suggest a selective and dose-dependent impact of DOX over gene transcription. The increase in *PDK4* transcription suggests that DOX may have led to metabolic alterations through a decrease in PDH activity, which would result in decreased flux of pyruvate to the TCA cycle and the OXPHOS (Fig. 6.8 A) [414]. Thus, we evaluated the levels of phospho-PDH and PDH activity (Fig. 6.8 B-D). In agreement with the increase in *PDK4* transcript levels, treatment with 0.5 μM DOX induced an increase in phospho-PDH levels (Fig. 6.8 B-C), which seems to result in decreased PDH activity, although the results did not reach statistical significance due to a limitation in the number of cells available for this particular experiment (Fig. 6.8 D).

Next, we measured ATP levels, and evaluated bioenergetic parameters by simultaneously following Oxygen Consumption Rate (OCR) and Extracellular Acidification Rate (ECAR) using the Seahorse Extracellular Flux Analyzer (Fig. 6.9 A-G). DOX induced decreases in basal respiration by ~63% for 0.5 μM DOX and by ~47% for 1 μM DOX (Fig 6.9 B), in maximal respiration by ~68% for 0.5 μM DOX and by ~74% for 1 μM DOX (Fig 6.9 C), and in basal acidification by ~74% for 0.5 μM DOX and by ~37% for 1 μM DOX (Fig 6.9 D). Basal acidification reflects the activity of several components, including lactic acid production by glycolysis and TCA cycle. In an attempt to reverse this effect, cells were pre-treated with the PDK inhibitor DCA, in order to decrease PDH phosphorylation by PDKs and improve its activity. DCA (3

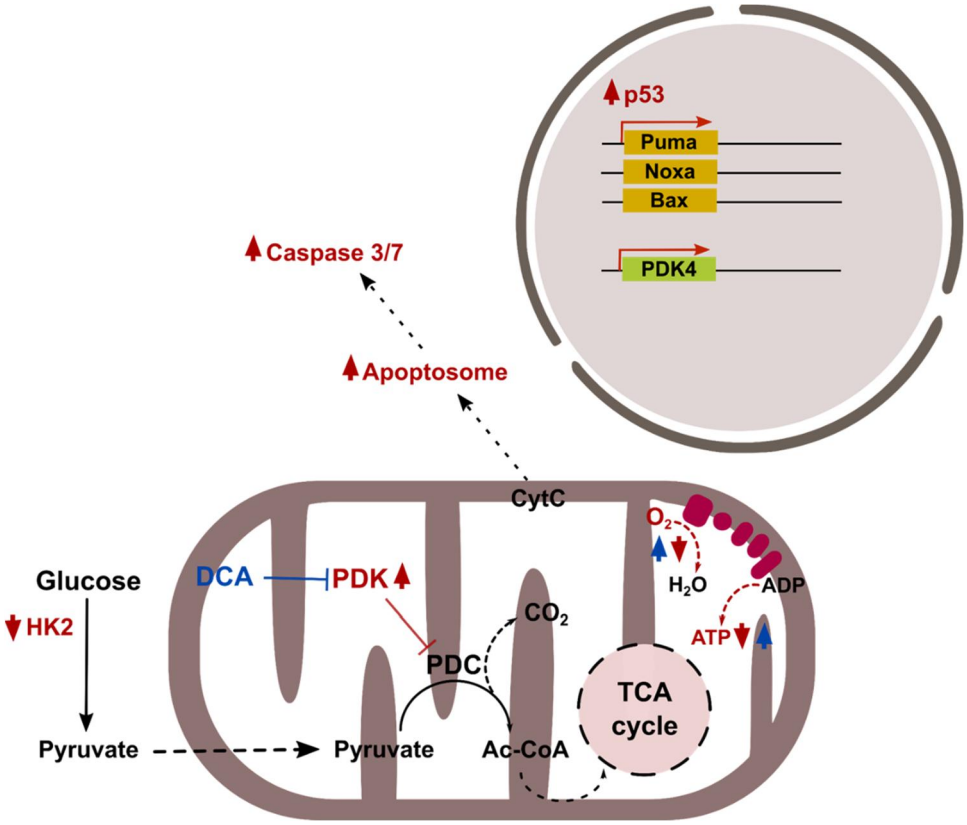

Figure 6.10: Schematic illustration showing the proposed mechanism of DOX-induced cardiotoxicity in Cor.At cells. DOX treatment leads to p53-associated caspase activation and apoptosis, decreased HK2 levels and reduced mitochondrial respiration (red) in Cor.AT cardiomyocytes. Cells treated with 0.5 μM DOX presented increased PDK4 transcripts, followed by increased PDH phosphorylation and inactivation (red). DCA, an inhibitor of PDK, ameliorated the impact of DOX treatment by activating PDH and partially restoring mitochondrial respiration and ATP levels (blue).

mM) pre-treatment partially inhibited the negative effects of DOX on ATP levels, recovering ~14% of the lost ATP levels for 0.5 μM DOX and ~16% for 1 μM DOX (Fig 6.8 E). No protection was observed for 1 mM DCA. Pre-treatment with 3 mM DCA ameliorated the loss of basal (~17%) and maximal (~12%) respirations in cells incubated with 0.5 μM DOX, but not with 1 μM DOX (Fig 6.9 B,C), suggesting that the loss of PDH activity partially contributes to bioenergetic dysfunction associated with DOX cardiotoxicity and may be reversible for lower doses of this drug. DCA pre-treatment also decreased the loss of basal acidification in cells incubated with 0.5 μM DOX (~13%) (Fig 6.9 D). To better understand the energetic shifts induced by DOX

and DCA treatments, and the impact in the capacity of cells to respond to mitochondrial stress, the Seahorse results are also shown in the form of energy maps (Fig. 6.9 E-G). In a control situation, Cor.At cells responded to mitochondrial stress induced by acute FCCP+oligomycin exposure by adopting a more pseudo-energetic phenotype, with increased OCR and ECAR (Fig. 6.9 E). DOX-treated cells presented decreased ECAR and OCR, becoming more energetically quiescent. DCA pre-treatment had different effects in cells exposed to the two DOX concentrations. To facilitate the visualization, zoomed energy maps corresponding to 0.5 μM DOX (Fig. 6.9 F), and 1 μM DOX (Fig. 6.9 G) conditions are also presented. Acute mitochondrial stress by exposure to FCCP+oligomycin induced a transition to a more pseudo-energetic phenotype in cells exposed to 0.5 μM DOX, but cells exposed to 1 μM DOX became more energetically quiescent after this acute mitochondrial stress. Pre-treatment with DCA induced a transition to a more energetic phenotype in cells exposed to 0.5 μM DOX, whereas cells exposed to 1 μM DOX seemed to become more aerobic. The results are summarized in Figure 6.10.

6.4. Discussion

DOX is a widely used anticancer drug whose clinically used dosages are limited by delayed cardiotoxicity. Even though several *in vivo* and *in vitro* models have been used to study DOX cardiotoxicity, cardiac cells that maintain the capacity to beat in culture, such as Cor.At mouse iPSC-derived cardiomyocytes, are particularly helpful to uncover the mechanisms of DOX-induced cardiotoxicity.

Mouse stem cell-derived cardiomyocytes have been a useful tool for toxicity screening assays of compounds interfering with ion channels function, contractility and cardiomyocyte metabolism [360, 415]. However, these cells may still present critical differences compared to human counterparts, due to species specificities in

cardiomyocyte function [416] which demand caution when extrapolating to clinical applications. Physiological and biochemical differences between mouse and human cardiomyocyte function include a ~10 times faster heart rate in the mouse, different ion channel-mediated repolarization, differences in the role of the regulatory molecule phospholamban, and in the expression and location of structural proteins [416]. Nonetheless, the presence of the contractile component in iPSCs-derived mouse cardiomyocytes makes these cells more bioenergetically demanding compared to other commonly used non-contractile models of cardiac cells, thus allowing a more sensitive detection of mitochondrial drug liabilities.

The objective of this work was to investigate the mechanisms underlying DOX toxicity in beating cardiomyocytes, focusing on mitochondria stress-related and metabolic pathways. For this purpose, we used Cor.At cardiomyocytes treated with 0.5 or 1 μM DOX, and investigated the morphological, functional and biochemical changes associated with mitochondrial bioenergetics, DNA-damage response and apoptosis. These concentrations fall within the range found in plasma of patients administered DOX [9] and are thus clinically relevant.

DOX induced dose-dependent alterations in cell morphology and ATP levels without affecting total cell mass. The higher DOX concentration (1 μM) induced a decrease in nuclear area, consistent with apoptotic nuclear pyknosis, contrary to what was observed in H9c2 cells for the same conditions, in which DOX induced nuclear hypertrophy [34]. Morphological changes accompanied alterations in mitochondrial polarization, and chromatin condensation and fragmentation. At the lower concentration (0.5 μM), DOX induced the appearance of a few apoptotic nuclei and seemed to increase perinuclear mitochondrial polarization, which can be an early feature of apoptosis [406-410]. Electrophysiologically, DOX has previously been reported to affect beat period, spike amplitude and corrected field potential duration in a time and dose-dependent manner [361, 417]. A 24 hours DOX exposure in human

iPSC-derived cardiomyocytes induced arrhythmic beating at 10 μM DOX and caused a complete arrest of heart beating at 100 μM [417]. Interestingly, DOX showed both acute and chronic electrophysiological effects with abnormal beating patterns worsening with prolonged time after treatment [132]. In our model, and in line with these previous studies, DOX (0.5 and 1 μM) did not have a major impact on cardiomyocytes beating for the 24 hours exposure; however, the beating stopped completely when cells were exposed to DOX for 48 hours.

Under these conditions, the activities of caspases -9 and -3/7 were also significantly increased. At the highest DOX concentration, an increase in apoptotic nuclei and a decrease in mitochondrial polarization, together with increased activities of caspases -9 and -3/7, and increased protein content of the caspase-3 cleavage PARP-1 fragment were observed. These results suggest the involvement of the mitochondrial apoptotic pathway and are in accordance with previous studies in different biological models [96, 136, 138, 140].

Both DOX concentrations used in this work induced an increase in p53 and a decrease in SOD2 protein contents. The transcription factor p53 is sensitive to redox changes and coordinates multiple cell responses including the decision between cell survival and cell death, namely through the blockade of cell cycle progression in response to DNA damage [418]. The levels of p53 protein increase after exposure to stress signals, and it may act through transcription-dependent and independent mechanisms, namely regulating mitochondrial apoptotic signaling [419].

Transcriptional regulation by p53 activates or represses the transcription of target genes [420]. However, the transcriptional response of p53 is transient, primarily through the induction of short-lived mRNAs [421]. Transcription-mediated effects involve upregulation of proapoptotic genes, such as *Puma*, *Noxa* and *Bax*, and downregulation of antiapoptotic genes, such as *Bcl-2* [420]. Transcription-

independent effects include direct interaction with Bax [422] or with SOD2 [423, 424]. The latter interaction leads to a reduction of superoxide anion scavenging activity, with a subsequent decrease in mitochondrial membrane potential and activation of apoptosis [423, 424]. However, transcription-mediated effects may also be in place, since it was described that p53 represses SOD2 gene expression [425]. DOX effects on SOD2 protein amount and activity seem to be dependent on the experimental model, dose and duration of DOX treatment. Sub-chronic DOX exposure decreased SOD2 activity in rat hearts [426], while acute DOX exposure induced an increase in SOD2 activity [96]. Differential effects of DOX in SOD2 content observed across different experimental models may be related with the fact that p53 can both suppress and induce SOD2 expression, depending on the balance of promoter and enhancer binding transcription factors, and SOD2 activity may also affect p53 activation [427].

Activation of caspases by DOX was completely prevented by pre-incubation with the non-selective caspase inhibitor z-VAD-fmk. Moreover, pre-exposure to pifithrin alpha (Pfα), a p53 inactivator that blocks p53-dependent transcriptional activation and apoptosis [412], partially prevented caspase-9 activation by DOX at 1 μM, and completely prevented caspase 3/7 activation by DOX at 0.5 and 1 μM. Pfα *per se* showed a tendency to increase caspase-9 activity, which may explain why no protection was observed for the lower DOX concentration, contrary to what was observed in H9c2 cells [136]. In addition, the antioxidant NAC did not significantly protect against DOX-induced caspase activation in this cell model. In our study, DOX increased p53-associated caspase activity and decreased SOD2 content, although increased ROS generation did not seem to occur upstream of caspase activation. The present results further reinforce the role of p53 in DOX-induced activation of caspases-3 and -9 in cardiomyocytes, as previously measured in H9c2 cardiomyoblasts [136], suggesting that DOX-induced p53-mediated cytotoxicity is common for both H9c2 cardiomyoblasts, which show proliferative activity, and the cells used in the present study, which do not proliferate in culture.

In accordance with the increase in p53 protein content and apoptotic hallmarks, DOX dose-dependently affected p53 target transcripts associated with mitochondria-dependent apoptosis and DNA-damage response. Nuclear-localized p53 activates genes that arrest cell growth and repair DNA damage, such as *Atm*, *Atr*, *Chk1*, *Chk2*, *Cdk1* and *Cdk2* [420, 428]. At the higher DOX concentration, a significant decrease in *Cdk1*, *Atr* and *Chk2* transcripts was observed, whereas at the lower concentration there was an increase in *Mdm2*, *Puma*, *Noxa* and *Bax* transcripts, and a decrease in *Bcl-2* and *Chk1*. These results suggest that cells responded to DOX-induced DNA damage through activation of p53 transcriptional activity, which led to mitochondrial-mediated apoptosis, in a dose-dependent manner.

In the present work, DOX treatment altered proteins and transcripts associated with mitochondrial bioenergetics and decreased ATP levels and basal and maximal oxygen consumption rates. At the higher DOX concentration, a decrease in protein content of Complex I and ATP synthase subunits and HK2 was observed, together with a significant decrease in *Hk2* transcripts. Complex I and ATP synthase activity and/or protein expression were also previously shown to be decreased in DOX-exposed animals [96, 426]. At the lower concentration, there was a decrease in *Hk2* and *Hif1α* transcripts and an increase in *Pdk4* and *Bpgm* transcripts. For the higher DOX concentration, there was a significant decrease in *Hk2* and *Hif1α* transcripts. Increases in transcripts observed with the lower DOX concentration were generally not seen for the higher DOX concentration, probably due to the higher rate of apoptosis observed. In previous studies with mice exposed to a single dose of DOX, genes related to glucose metabolism, including *Hk2*, *Pdk4*, *fructose-2,6-bisphosphate 2-phosphatase*, and especially *Bpgm*, were suggested to be involved in DOX-induced cardiac injury [133]. HK2, BPGM, and PDK4 are rate-limiting enzymes that control glucose metabolism. Since DOX administration has been shown to significantly decrease glucose and ATP levels in the heart [133], these metabolic genes may be involved in the regulation of

glucose and energy generation, contributing to remodel heart metabolism in the presence of that anthracycline.

In the present study, the decrease in HK2 levels observed after incubation with both DOX concentrations may result in a decrease in the glycolytic rate, which could contribute to the observed decrease in basal acidification rate measured by using the Extracellular Flux Analyzer. HK2 is primarily expressed in skeletal and cardiac muscles and is regulated by insulin or ischemia [429]. Hexokinases regulate the use of glucose for catabolic processes, regulate reduced glutathione levels through generation of NADPH, and modulate cell death by interacting with the voltage-dependent anion channel (VDAC), which is a regulator of the mitochondrial permeability transition pore [429]. Modulation of HK2 levels alters cardiomyocyte energy levels and contractility [401]. Decrease in HK2 levels results in decreased cardiac function and altered remodeling after ischemia/reperfusion injury [401] and HK2 knockdown resulted in exaggerated cardiac hypertrophy through increased ROS production [430]. In contrast, overexpression of HK2 increases both ATP levels and O_2 consumption in cardiomyocytes, as well as cellular contractility [401].

Hif1a has been shown to be significantly downregulated in hearts of mice exposed to DOX [133]. Hypoxia and HIF-1 increase virtually all the enzymes in the glycolytic pathway, including HK2, as well as glucose transporters [431]. Thus, the observed decrease in the levels of Hif1a transcripts is in agreement with the decrease in HK2 protein and transcript levels, and with the decrease in basal acidification rate, and our results suggest a concerted cellular response to decrease glucose consumption after DOX exposure, which may result from a metabolic remodeling or from lower energetic demands of treated cells.

BPGM is an enzyme known to regulate hemoglobin oxygen affinity in erythrocytes and placental cells. It participates in glycolysis by converting 1,3-bisphosphoglycerate

(1,3-BPG) to 2,3-bisphosphoglycerate (2,3-BPG), which acts as an allosteric effector influencing oxygen and hemoglobin dissociation curve, especially in erythrocytes [432]. This enzyme is expressed in various tissues and cells, including the heart. BPGM was previously suggested to play a central role in DOX-induced cardiac injury [133]. Although the role of BPGM in cardiovascular diseases including DOX-induced cardiotoxicity remains unclear, the protein levels of BPGM were found to be significantly decreased after DOX administration in the heart and in cultured cardiomyocytes, consistently with our results, suggesting that BPGM may play a core role in DOX-induced cardiomyopathy [133].

PDK4 regulates the metabolic flux between glycolysis and mitochondrial OXPHOS by phosphorylating and inactivating pyruvate dehydrogenase (PDH), resulting in decreased conversion of pyruvate into acetyl-CoA [433], conserving glucose and promoting FAO [434]. DOX was previously shown to upregulate the expression of FoxO1 in H9c2 cells [435] and FoxO1 and FoxO3 in rat hearts [436], which are known to mediate PDK4 upregulation [437-439]. Since cardiomyocytes have high energy demands, failure to oxidize enough carbohydrates leads to cardiac inefficiency [440]. Transgenic mice overexpressing PDK4 in the heart present decreased glucose catabolism and increased FAO, suggesting that increased cardiac PDK expression is sufficient to promote a loss in metabolic flexibility and exacerbate cardiomyopathy [441]. A metabolic shift to FAO would require active complex I, which is known to be compromised by DOX treatment [217, 442]. In addition, for cells in culture to be able to shift their metabolism to increased FAO, fatty acids would have to be available in the culture medium or in intracellular storages. In our conditions, the increase in PDK4 levels seems to contribute to PDH inactivation. In the presence of DOX, cells seem to suffer a generalized bioenergetic failure.

Pre-treatment with DCA ameliorated the impact of DOX treatment on ATP levels and mitochondrial respiration, suggesting that PDH may be an interesting therapeutic

target to avoid DOX cardiotoxic side-effects. Since tumor cells are mostly reliant on glycolysis for energy, activation of PDH may also contribute to improve cancer chemotherapy [414, 443]. However, other strategies to overcome PDH deficiency, besides the use of DCA, may have to be developed, since co-treatment of DOX+DCA may affect the efficacy of anti-tumor chemotherapy [444]. In conclusion, the DOX concentrations used in the present study differentially affected several proteins and transcripts associated with mitochondrial bioenergetics, and induced p53-dependent caspase activation, affecting the expression of p53 target transcripts associated with mitochondria-dependent apoptosis and DNA-damage response. The highest concentration induced a high degree of apoptosis, with increased nuclear apoptotic morphology, PARP1 cleavage and decrease of some OXPHOS protein subunits. This may be relevant for more severe DOX treatments. Interestingly, cells treated with the lowest DOX concentration seem to be more mildly affected, presenting metabolic remodeling associated with an increase in PDK4 transcript levels, phosphorylation of PDH and downregulation of PDH activity. This led to a decrease in basal and maximal oxygen consumption rates (OCR) and in basal acidification rate, which were partially recovered by pre-treatment with the PDK inhibitor DCA.

The results suggest that the higher DOX concentration mainly induces p53-dependent apoptosis, whereas for the lower DOX concentration the cardiotoxic effects involve the adoption of a quiescent energetic phenotype that is improved by indirect stimulation of PDH activity with DCA, unveiling PDH as a possible therapeutic target to ameliorate the effects of DOX cardiotoxicity.

Chapter 7

7. Doxorubicin persistently rewires cardiac circadian homeostasis

7.1. Introduction

The burden of DOX-associated cardiotoxicity is heavy and the understanding of its molecular basis is critical for defining better prevention and treatment measures. Children are particularly vulnerable to suffer from post-treatment side effects and care attention needs to be provided not only during treatment or shortly after, but also during long-term follow-up [27]. Persistent deleterious and chronic effects on the cardiovascular system compromise the quality of life and can result in heart failure. The numbers of long-term cardiotoxicity have not been totally determined due to the high variability among studies in terms of follow-up periods and setting the threshold for cardiac dysfunction. However, it was estimated that 10% of children receiving a cumulative dose of 300 mg/m^2 or higher eventually experience heart failure during the 20 years after anthracycline therapy [445]. In another cohort, the relative hazard of congestive heart failure associated with anthracycline treatment was more than 5-fold higher at doses of 250 mg/m^2 or more, compared with survivors who have not been exposed to anthracyclines [446]. The reasons for this persistency of effects have not yet been totally clarified even though several hypotheses have been described (section 1.3), including mtDNA mutations with further perpetuation of defects on respiratory subunits encoded by mtDNA [207], impaired cardiac progenitor cells function and neovascularization [48], persistent altered transcript levels [188, 208] or even altered DNA methylation landscape [209].

Cardiovascular physiology and cardiac pathologies, including myocardial infarction and sudden cardiac death, exhibit a 24 hours periodicity [307, 308, 447]. The observation of the rhythmic cardiac behaviors led to the acknowledgment of the circadian clock as a relevant factor in the development of cardiac diseases, as well as a therapeutic target. The intrinsic biological clock works in response to Earth's 24 hours rotation that forced life to develop mechanisms to anticipate the time of the day in which a certain biological process should occur more efficiently and with more benefits for the organism. These daily oscillations are mostly controlled by transcriptional and translational feedback loops but are also driven by the interplay with cellular metabolism and energy status. One such example is NAD^+-dependent sirtuin activity that fluctuates dependently on the clock-driven NAD^+ biosynthesis [277]. For example, SIRT3 activity rhythmicity is known for generating oscillations on the acetylation of key mitochondrial proteins [290], while SIRT1 binds the core clock proteins BMAL1:CLOCK in a rhythmic manner promoting deacetylation of clock proteins, histones, and proteins involved in metabolic and apoptotic processes [266, 269, 280]. Disturbances of the circadian rhythms and the desynchronization between the central pacemaker (located in the suprachiasmatic nucleus) and peripheral clocks are associated with several diseases [447-449]. Mice exposed to unusual light-dark (LD) cycles, similarly to what occurs to shift workers, present altered metabolic efficiency and substrate utilization, as well as depressed cardiac function [448]. While circadian disruptions are deleterious for the normal heart function [312, 318], NAD^+ and SIRT1 seem to protect the myocardium against ageing and oxidative stress [323, 450].

Accumulating evidence suggests that DOX may interfere with sirtuin pathways. This line of study started with the observation that resveratrol, a sirtuin activator, shows promising results in the prevention of DOX-induced cardiotoxicity [435, 451-453]. Some recent *in vivo* and *in vitro* studies observed reduced SIRT1 [454-456] and SIRT3 [384, 397] mRNA expression and protein levels after DOX administration.

Additionally, the metabolic shifts resultant from cardiac DOX exposure have also shown to alter mitochondrial pathways for ATP production that could ultimately result in dysregulated NAD^+/NADH ratios and NAD^+ levels, important linkers with the circadian regulation [457, 458].

The present study investigates whether DOX exposure in young mice could persistently interfere with the long-term transcriptional and signaling circadian homeostasis, and how the metabolic and energetic failure induced by a sub-chronic DOX treatment is integrated at the level of the circadian machinery.

7.2. Methods

7.2.1. Animal care

Animals and protocols were reviewed and approved by the Institutional Animal Care and Use Committee (IACUC) of the University of California, Irvine.

Wild-type male C57BL/6J mice with three weeks of age were purchased from Jackson Laboratory (Bar Harbor, ME, USA) and acclimated for 1 week prior the initiation of experiments. Animals were housed with *ad libitum* standard chow (Prolab® RMH 2500) and water access, under controlled temperature (24-25°C), humidity and 12 hours artificial light/dark cycle (12:12 LD). Animals were monitored daily by both the laboratory and University Lab Animal Resources (ULAR) veterinary staff. Cages (5 mice per cage) were cleaned weekly to maintain a clean environment.

7.2.2. Experimental design

C57BL/6J mice were randomly divided into two groups: SAL and DOX treatment. One group received a total of 20 mg/kg of DOX (intraperitoneal injection of 5 mg/kg in

0.9% saline solution, for 4 weeks), while the control group received the equivalent volume of the vehicle saline solution during the same period of time. To avoid local tissue damage, a different region of the peritoneal cavity was injected each week. Animals were injected during the light phase (~ZT 5), considering that best tolerability to DOX in mice was observed near the middle of the light phase [331, 332], and were weighted weekly before the injections to adjust DOX dose. Two weeks prior to sacrifice, the cages were moved into another room under strict 12:12 LD conditions. The animals were sacrificed by CO_2 inhalation followed by cervical dislocation 6 weeks after the final DOX injection, at 4 different time-points (ZT 3, ZT 9, ZT 15 and ZT 21)(Fig. 7.1). Extraction of the heart was quickly performed, followed by washing in PBS and weighing. The left ventricle carefully extracted and flash frozen in liquid nitrogen. Heart ventricles were then kept at -80°C. No mortality was observed during the experiment.

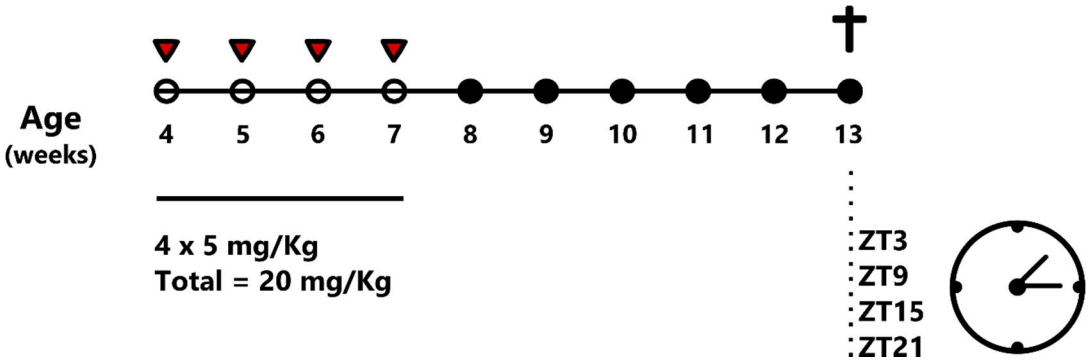

Figure 7.1: Timeline for the DOX protocol on C57BL/6J mice. Young animals were assigned into DOX and SAL groups. DOX animal received a total of 20 mg/kg DOX by intraperitoneal injection and were allowed to recovery for a 6 weeks period after which the animals were sacrificed at 4 different daylight hours (2 light periods: ZT3 and ZT9; 2 dark periods: ZT15 and ZT21).

7.2.3. Cell culture and transfection

HEK293 (Human Embryonic Kidney) cells were cultured in 25 mM glucose DMEM (HyClone™ DMEM, Fisher scientific) supplemented with 10% FBS (26140, Thermo

Fisher Scientific) and 1% Penicillin- Streptomycin (15070, Thermo Fisher Scientific), in 0.1% gelatin-coated dishes. The culture was maintained at 37°C in a humidified atmosphere of 5% CO_2 and cells were passaged when reaching 80-90% of confluence.

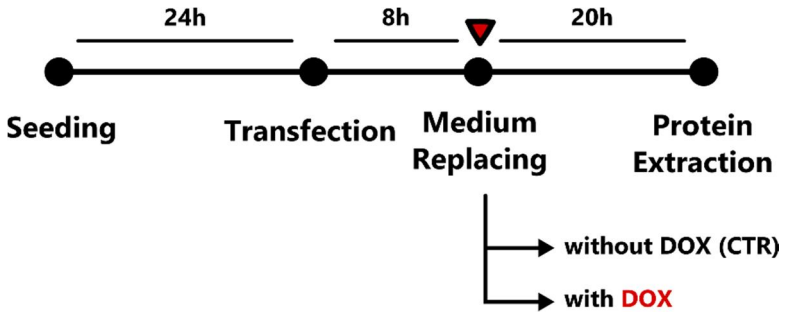

Figure 7.2: HEK293 experimental design. Transfection was initiated 24 hours after seeding and the transfection mixture containing the transfecting agent and plasmids were incubated with the cells for 8 hours. After this period the cells were allowed to grow for 20 hours in normal growth conditions or in the presence of DOX (0.05, 0.5 and 1 μM).

One day after seeding ($2.5x10^4$ cells/cm^2), cells were transfected with the plasmids (indicated below) using BioT Transfection agent according to the manufacturer's recommendations. Briefly, for each 100mm dish, 15 μL of transfection agent was mixed with 500 μL of FBS-free medium and, after 5 minutes, this mixture was added to plasmids already prepared. The mixture was incubated for 5 min and added to the cells in culture. After 8 hours of transfection period, the transfection medium was replaced by normal culture medium with 0, 0.05, 0.5 or 1 μM DOX for 20 hours (Fig. 7.2). After this period, cells were collected for protein extraction. The total amount of DNA for each transfection was kept constant using an empty expression vector. The plasmids myc-CLOCK/pSG5, myc-Bmal1/pCS2 and flag-SIRT1/pcDNA were previously described [459].

Wild-type and $SIRT1^{-/-}$ MEFs were cultured in 25 mM glucose DMEM supplemented with 10% FBS (26140, Thermo Fisher Scientific) and 1% Penicillin/Streptomycin (15070,

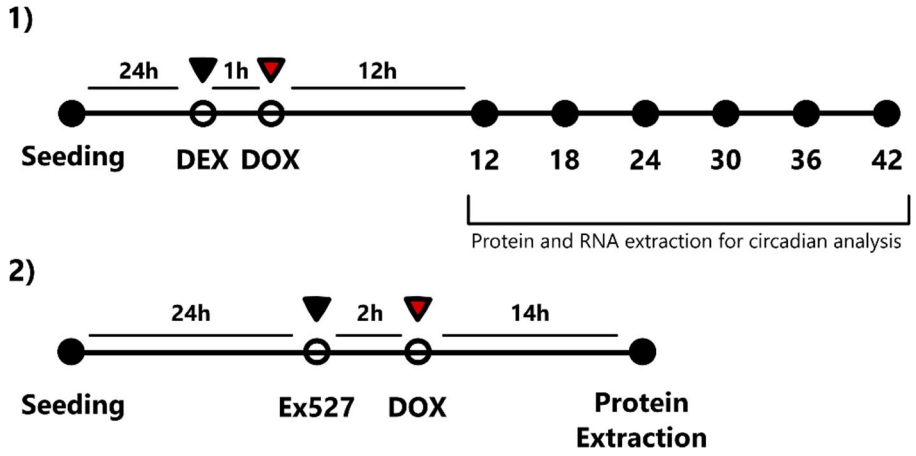

Figure 7.3: MEFs experimental design. 1) MEFs were synchronized with dexamethasome (DEX) for 1 hour prior DOX exposure. After 12 hours the medium was replaced and DOX washed out. Cell harvest was performed in six time-points (CT 12, 18, 24, 39, 36 and 42). 2) Two hours before DOX exposure, the SIRT1 inhibitor Ex527 was added to MEFs medium. After 14 hours of DOX incubation (and 16 hours with Ex527) cells were washed and collected for protein extraction.

Thermo Fisher Scientific) and under standard cell culture conditions (37°C, 5% CO_2). These MEFs were previously generated from wild-type or homozygous SIRT1$^{-/-}$ sibling mice [266]. Two different experimental designs were followed for either 1) circadian protein/RNA analysis or 2) total protein extraction without synchronization. For experimental design 1): 24 hours prior the synchronization, cells were seeded at a concentration of 1.1x10^4 cells/cm^2 in standard 60mm dishes and incubated under normal growth conditions. The synchronization was performed by 1 hour incubation with 100 nM dexamethasone (DEX) [460], prepared in serum-free medium (Fig. 7.3). The medium was then washed out and new serum-containing medium with DOX was added. At this point, CT 0 (circadian time 0) was defined and cells were kept for 12 hours in culture before the first collection at CT 12. In total, six time-points (from CT 12 to CT 42, 6 hours interval) were considered for cells collection. For experimental design 2): Cells were seeded at the concentration of 1.1x10^4 cells/cm^2 in 150mm dishes. Twenty-four hours after seeding, MEFs were incubated with 50 μM Ex527, a sirtuin inhibitor more selective for SIRT1 (Fig. 7.3). In the conditions where Ex527 was not used, the same volume of ethanol (vehicle) was added to the medium.

7.2.4. Sulforhodamine B assay

SRB assay was performed as described on section 5.2.2 with slight modifications. HEK293 were seeded in 48 well-plates at a concentration of $2.5x10^4$ cells/cm^2. At the end of DOX treatment (0.05, 0.5 and 1 μM; 20 hours), cells were fixed overnight and then incubated with 200 μL 0.05% (w/v) SRB solution. WT MEFs were seeded at $1.1x10^4$ cells/cm^2 and exposed to DEX for 1 hour followed by DOX (up to 1 μM) incubation for 12 hours, after which cells were fixed or kept in culture for 30 hours in DOX-free medium before fixation. Dye bound to cellular proteins was extracted with 1 mL Tris (10 mM, pH 10) and absorbance was read at 530 nm.

7.2.5. RNA extraction

Total RNA was extracted from MEF cells and frozen left ventricles with TRIzol reagent. Briefly, 1 mL of TRIzol was added to ~15 mg of heart tissue and the tubes were transferred into a precooled (-20°C) TissueLyser II adapter (Qiagen, Germany). The tissue was homogenized by 2 pulses of 2 min and an oscillation frequency of 25 Hz in a TissueLyser II (Qiagen, Germany). Then, 200 μL of chloroform was added and, after vortexing and a 3 min incubation, the tubes were centrifuged for 10 min at 12,000 xg (4°C). The upper aqueous phase was transferred to a new tube and the extraction step was repeated a second time with 200 μL of chloroform. Later, 500 μL of isopropyl alcohol was used to precipitate RNA during 2 hours at -20°C. Finally, the tubes were centrifuged at 12,000 xg for 10 minutes (4°C), and the pellet was washed with 1 mL of 70% ethanol. After a final centrifugation (12,000 xg, 10 min, 4°C), RNA was air dried and resuspended in 40 μL of nuclease-free water and stored at -80°C. For RNA extraction from MEFs the protocol was very similar, although the homogenization step was not required and the volumes used were half of the ones used for tissues.

TRIzol (500 μL) was directly added to each 60mm cell dish. RNA quantity and quality were assessed using a NanoDrop 2000 spectrophotometer.

7.2.6. cDNA preparation and quantitative real-time PCR

For gene expression analysis by RT-qPCR, 1 μg mRNA was retrotranscribed into cDNA using iScript RT supermix according to manufacturer's instructions and as described on section 5.2.9. For a 10 μL RT-qPCR, 12.5 ng of cDNA was mixed with primers (0.4 μM each), and 5 μL of SsoAdvanced universal SYBR® Green supermix. The reaction was run on a CFX96 Real-Time System and included a first incubation of 30 seconds at 95°C, followed by 40 cycles of 15 seconds at 95°C and 40 seconds at 60°C. Gene expression changes were evaluated by the ΔΔCt method and all samples were analyzed in duplicate. All values are relative to those of *18S* RNA levels. Primers sequences used for gene expression analysis are listed in Table 4.3.

7.2.7. Protein extraction

Cells and tissues were lysed in RIPA buffer (section 4.3). Briefly, 1 mL of RIPA supplemented with the inhibitors was added either directly to the culture plates, after a first wash with PBS, or to approximately 20 mg of ventricular tissue. Cell lysate was then transferred to an Eppendorf tube. Tubes were placed at 4°C, rocking for 30 min and vortexed every 5 min. Lysates were then sonicated 3 x 10 seconds and centrifuged at 18,000 xg for 20 min (4°C) and the pellet was discarded. Protein content was measured using BCA assay and using BSA as standard. Protein was kept at -80°C until use.

7.2.8. Immunoprecipitation

Immunoprecipitation allows the small-scale affinity purification or enrichment of an antigen, in this case a protein, by using a specific antibody that may or may not be immobilized in a solid support such as magnetic particles or beaded resins. The complex antibody/antigen is then pulled out and the protein of interest can be separated by immunoblotting.

Same amount of protein (around 500 – 1000 μg) per condition was precleared with 30 μL of prewashed Protein G Sepharose® beads for one hour at 4°C. The IgG control consisted of a pool with all samples and the same final protein amount, and it was processed the same way as the experimental samples. Subsequently, tubes were centrifuged at 100 xg for 5 min at 4°C and the supernatant was transferred to a new tube. Around 20 μL of this protein extract was kept for posterior input analysis. The myc tag antibody and the negative IgG control (Table 4.2) were added to the tubes and incubated at 4°C, overnight. After the incubation, 40 μL Protein G Sepharose® was added and rocked at 4°C for 2 hours. The beads were then collected by centrifugation (100 xg, 5 min at 4°C) and washed 3 times for 10 min with RIPA buffer. In this step, the immune complexes in the lysate were retrieved by the IgG-binding proteins attached to the beaded support. After the last wash and centrifugation, 30 μL of Laemmli without β-mercaptoethanol was added to the beads followed by boiling at 95°C, during 10 min. After a final 4 min centrifugation at room temperature, 25 μL was recovered from each tube, mixed with β-mercaptoethanol (5% final concentration) and incubated at 95°C for 10 min. Protein was electrophoresed and separated on SDS-polyacrylamide gels (as described on section 7.2.9). The antibodies utilized in the immune-detection are listed on table 4.2 and included Anti-acetyl BMAL1 (Lys538), anti-flag, anti-myc and the Millipore HRP-conjugated anti-rabbit and anti-mouse IgG secondary antibodies.

7.2.9. Western Blotting

Western blotting was mostly performed as described on section 6.2.6. After denaturation at 95°C for 5 min in Laemmli buffer, 20-30 μg protein lysate was loaded into SDS-polyacrylamide gels and proteins were transferred to nitrocellulose or pre-activated PVDF membranes. After blocking with 5% non-fat dry milk on TBS-T for 1:30 hours at room temperature, membranes were incubated overnight at 4°C with the primary antibody directed against the respective protein (listed in Table 4.2), under continuous stirring. The antibody against acetyl-AceCS1 was kindly provided by John M. Denu (University of Wisconsin, USA). Once incubation was completed, membranes were washed and incubated at room temperature with anti-rabbit or anti-mouse HRP-conjugated secondary antibodies. Clarity™ Western ECL Substrate was used for chemiluminescence detection. Band intensities were calculated with ImageJ.

7.2.10. RNA sequencing

RNA was extracted from ZT 9 and ZT 21 left ventricles of 3 animals per group (group 1: SAL ZT 9; group 2: SAL ZT 21; group 3: DOX ZT 9; group 4: DOX ZT 21), using the standard PureZOL protocol. Briefly, approximately 15 mg of frozen tissue was homogenized immediately after adding 1 mL PureZOL, using a tight pestle attached to a potter homogenizer set at 400 rpm. After a 5 min incubation at room temperature, samples were centrifuged at 12,000 xg for 10 min at 4°C to remove solid insoluble debris and 200 μL of chloroform was added to each tube, followed by mixing and 3 min incubation at room temperature. The samples were centrifuged at 12,000 xg for 10 min at 4°C and the aqueous phase was transferred to a new tube. Chloroform was added a second time and the separation step was repeated. For RNA precipitation, 500 μL isopropyl alcohol was added followed by 2 hours incubation at -20°C. Once the precipitation step was completed, another centrifugation was performed at 12,000

xg for 10 min at 4°C, the supernatant was discarded and the RNA pellet was washed with 1 mL ethanol 70%. After a last centrifugation, the RNA pellet was air-dried and was finally resuspended in 30 μL H2O nuclease-free water. An additional cleanup step was performed with RNeasy Mini Kit (Qiagen) spin columns. RNA quantity and integrity were assessed by Nanodrop 2000 and Experion RNA StdSens kit. High quality RNA was essential for the success of the RNA sequencing. Only samples with RNA quality indicator (RQI) above 8 (on a 1-10 scale), 260/280 ≈ 2 and 260/230 ≥ 1.8 were used in the sequencing experiment. RNA was kept at -80°C until processed.

RNA sequencing experiments were performed in the Genomics Unit of the CNIC, Madrid. Library preparation and sequencing were performed with 200 ng of total RNA as starting material. Libraries were prepared using the NEBNext Ultra RNA Library preparation kit (New England Biolabs, USA) and sequenced on Illumina HiSeq2500 with 60-bp single end reads each. Data processing was performed in the Next Gen sequencing Unit at Biocant, Cantanhede. First, rRNA reads were removed from received reads using RiboPicker [461]. The remaining reads were mapped using Bowtie2 [462] against the reference transcriptome of *Mus musculus* (version GRCm38.p5). Read count was performed by eXpress (bio.math.berkeley.edu/eXpress) for each condition. The mapped reads (~ 10 million aligned reads) allowed the detection of more than 70% of annotated *Mus musculus* protein-coding genes. Gene name and description for each reference transcript were extracted from the *Mus musculus* transcriptome (version GRCm38.p5). The R package EdgeR was used; the criteria for selection of differentially expressed genes for use in subsequent pathway analysis included false discovery rate (FDR) < 0.05 and Log2FC > 0.585 (fold change > 1.5) for DOX *vs* SAL, or Log2FC > 1 (fold change > 2) for ZT9 *vs* ZT21.

7.2.11. Histological staining

Mice hearts were quickly harvested, rinsed with PBS, embedded in cryomatrix and frozen in liquid nitrogen. Later, frozen hearts were sliced 10 μm thick in a Leica CM1950 cryostat at -20°C. Sections were collected on Fisherbrand Superfrost microscope slides (Fisher Scientific, USA) and stored at -80°C. Histological sections were processed with hematoxylin and eosin (HE) by using standard procedures. Briefly, the slides were dried at 37°C for 1 hour and then, after several incubations with decreasing alcohol solutions (100%, 90%, 70%; 2 min each) and water for 5 min, tissues were stained with HE for 10 seconds each. Both stainings were followed by a rinse in tap water (30 seconds). Finally, the slides were incubated with increasing alcohol percentages (70%, 90%, 100%) and kept in histosol for 2 x 2 min. After drying for approximately 1 hour the slides were sealed with histomount and cover-sliped. Images were collected using a Leica Z16 APO microscope.

7.2.12. Statistical analysis

Statistical analyses were performed using SPSS version 23.0 (IBM, NY, USA) and GraphPad Prism 6 (GraphPad Software, Inc., La Jolla, CA, USA). Normality was assessed with Shapiro-Wilk test, and parametric or non-parametric statistical tests were chosen accordingly. The Student's t test or the analysis of variances (ANOVA) followed by Bonferroni multiple comparison post hoc test were used when normality was observed. Otherwise, the nonparametric Mann-Whitney U-test or Kruskal-Wallis H-test followed by Dunn's post hoc analysis were used. The data is presented as mean ± SEM. Differences were considered statistically significant at $p<0.05$.

7.3. Results

7.3.1. Juvenile mouse model of persistent DOX-induced cardiac dysfunction

7.3.1.1. DOX treatment affected mice body weight and induced cardiac injury

Juvenile C57BL/6J mice with 4 weeks of age received injections of saline or DOX during 4 consecutive weeks. Six weeks after the final injection, animals were sacrificed and hearts collected. Even though both groups gained weight during the period of study, DOX sub-chronic treatment caused a significant slower weight gain in pups over time, as seen by the differences of body mass values between groups (final difference: 19.6%; Table 7.1; Fig. 7.4 A). While saline animals presented a 2-fold increase in body mass from the beginning to the end of the experiment, that increase was only of 1.7-fold for DOX group. A reduction of heart mass was observed at the end of the experiment in DOX-injected animals compared to controls (Table 7.1; Fig. 7.4 B). However, heart mass over body mass ratio showed a significant increase (1.13-fold) (Table 7.1; Fig. 7.4 C), mostly a reflection of the lower body weight in DOX treated animals.

Table 7.1: Body and heart mass profile of mice subjected to DOX sub-chronic protocol

Treatment	Initial body mass (g)		Final body mass (g)		Heart mass		HM:BM (x100)	
	Mean	SEM	Mean	SEM	Mean	SEM	Mean	SEM
Saline (n = 20)	14.050	0.486	28.695	0.430	0.145	0.003	0.499	0.008
DOX (n = 20)	13.555	0.375	23.073***	0.447	0.129***	0.003	0.563***	0.013

***p<0.001 *vs* saline group; HM:BM – heart mass to body mass ratio; SEM – standard error of mean

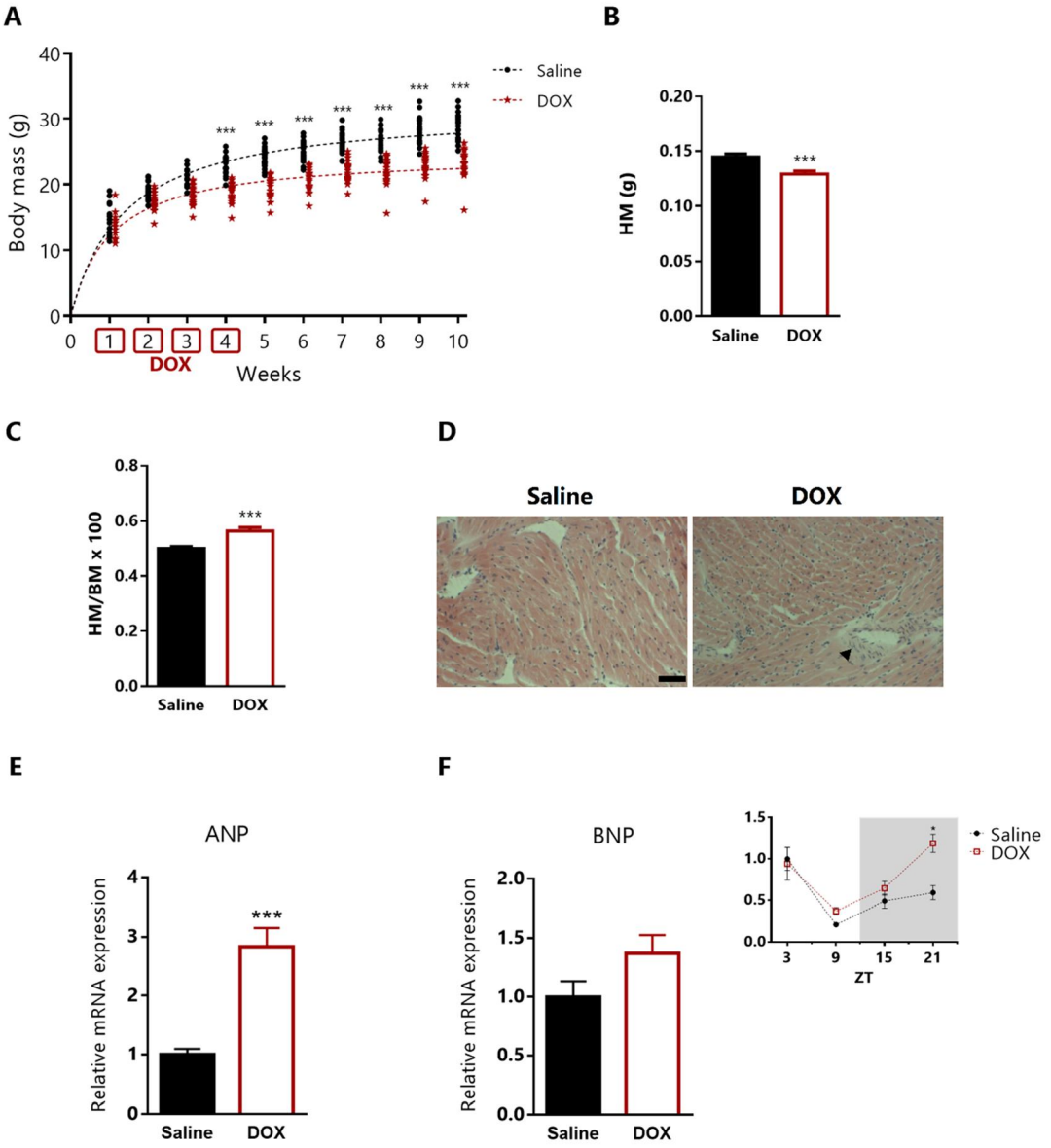

Figure 7.4: Weight, histochemical and transcriptional analysis of saline- and DOX-injected young mice. A) Mice body weight recorded along the 10-weeks experiment (4 weeks of treatment plus 6 weeks of recovery). Lines represent the weight curve based on the means of each group over time. B) Heart weight in grams and C) heart-to-body-weight ratio in saline and DOX-injected animals 6 weeks after the end of treatment. D) Representative images of heart sections stained with HE. Scale bar represents 100 μm. E) Total *ANP* and F) total and circadian *BNP* mRNA levels were assessed by RT-qPCR. Error bars indicate SEM. *p<0.05, ***p<0.001 DOX *vs* saline. n=20 per group, n=5 per group and ZT (zeitgeber time, light-dark cycle).

Hearts from saline and DOX animals were harvested and processed for histochemical analysis. Sections stained with HE appeared morphologically normal with no obvious signs of damage, even though gross observations suggest mild fibrotic changes (Fig. 7.4 D). The analysis of the expression of the cardiac injury biomarkers, brain natriuretic peptide (*BNP*) and atrial natriuretic peptide (*ANP*), showed increased transcription levels in DOX treated animals (Fig. 7.4 E,F). While *ANP* mRNA levels significantly increased 2.8-fold in DOX animals (Fig. 7.4 E), no statistically difference was observed in total *BNP* levels between saline and DOX (1.4-fold difference) (Fig. 7.4 F). Interestingly, *BNP* transcript levels exhibited a daily oscillatory profile among the animals sacrificed at 4 different time-points with DOX animals showing significant increased *BNP* expression at ZT 21 (Fig. 7.4 F).

7.3.1.2. DOX treatment impacted total and rhythmic gene expression

To clarify whether sub-chronic DOX early-life exposure leads to persistent alteration of gene expression, we investigated the circadian oscillations and total transcript levels of key clock and metabolic genes by RT-qPCR (Fig. 7.5). To investigate these differences, saline and DOX-treated mice were sacrificed every 6 hours over the circadian cycle (ZT 3, 9, 15, 21) and left ventricles were subjected to gene expression analysis. The mRNA expression of clock genes including *Bmal1*, *CLOCK*, *Per2*, *Cry1* and *DBP* were unaffected by the treatment (Fig. 7.5 A-D,F), whereas *Rev-erbα* gene expression showed a significant dampening at ZT 9 (Fig. 7.5 E). *Nampt* and *Cpt1α* (carnitine palmitoyl transferase 1 alpha) genes also showed an oscillatory expression pattern, as previously described [277, 463]. While no alterations were observed in *Nampt* expression with treatment, DOX led to a *Cpt1α* peak in expression at ZT 3 (Fig. 7.5 G-H). Cpt1α is involved in long-chain fatty acids transport across the OMM and its availability is related with fatty acid oxidation capacity [464]. Considering the described effects of DOX on mitochondrial function and oxidative stress in the cardiac

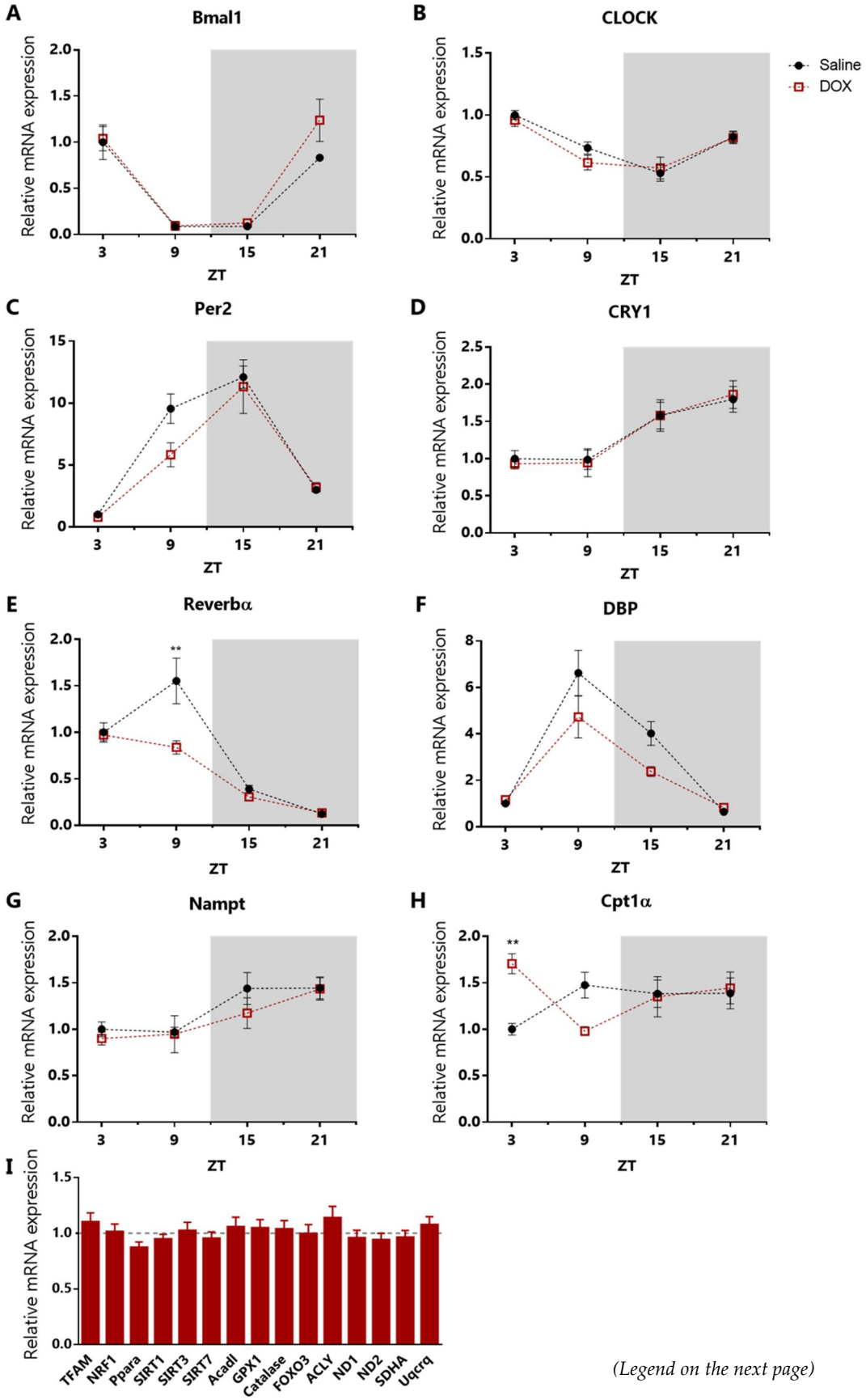

(Legend on the next page)

Figure 7.5: Impact of DOX treatment on the expression of circadian molecular clock, metabolic and mitochondrial-related genes in the heart. A-F) Circadian expression levels of the core clock genes (*Bmal1*, *CLOCK*, *Per2*, *Cry1*, *Rev-erbα*, *DBP*), G) *Nampt* and H) *Cpt1α* were determined by RT-qPCR. I) Total mRNA levels of important metabolic and mitochondrial genes were assessed by RT-qPCR. Error bars indicate SEM. **p<0.01 DOX *vs* saline. n=20 per group, n=5 per group and ZT (zeitgeber time, light-dark cycle).

tissue, mRNA expression of genes belonging to mitochondrial biogenesis, electron transport chain and antioxidant pathways were analyzed, as well as *SIRT1*, *3* and *7* (Fig. 7.5 I). None of the analyzed genes presented neither significant total gene expression alterations nor changes in the expression pattern over the 4 time-points. In order to better characterize the effects of DOX on mice transcriptome, RNA-sequencing was performed in 4 different groups of mice (saline ZT 9, saline ZT 21, DOX ZT 9 and DOX ZT 21) to unveil alterations on saline *versus* DOX animals and to detect changes on gene oscillation between those 2 time-points. Global transcriptome profiling identified 54 transcripts differentially expressed in DOX mice compared to the vehicle control (FDR < 0.05). From these 54 genes, only 5 were downregulated after DOX treatment (*Tmem150c*, *Inmt*, *Pfkfb1*, *Aldob* and *Ppl*) (Fig. 7.6 A) and the biological process most significantly enriched among the upregulated transcripts was innate immune response ($p < 10^{-4}$), indicative of inflammatory response. In this category, genes including interferon regulatory factor 7 (*Irf7*), interferon-induced protein with tetratricopeptide repeats (*Ifit1-3*), toll-like receptor 13 (*Tlr13*), 2′-5′ oligoadenylate synthetase 1A (*Oas1a*) or 2′-5′ oligoadenylate synthetase-like 1 (*Oasl1*) were overexpressed. Hierarchical clustering and heatmap analysis of the six replicates indicated the reproducible nature of the analysis and highlighted the transcriptional changes between the treatments (Fig. 7.6 B). However, it was possible to observe variability between the 6 DOX animal patterns, possibly due to different individual recovery responses during the following period.

For the identification of alterations on the oscillation patterns between ZT 9 and ZT 21, a comparison of gene expression was performed between both ZT for the same

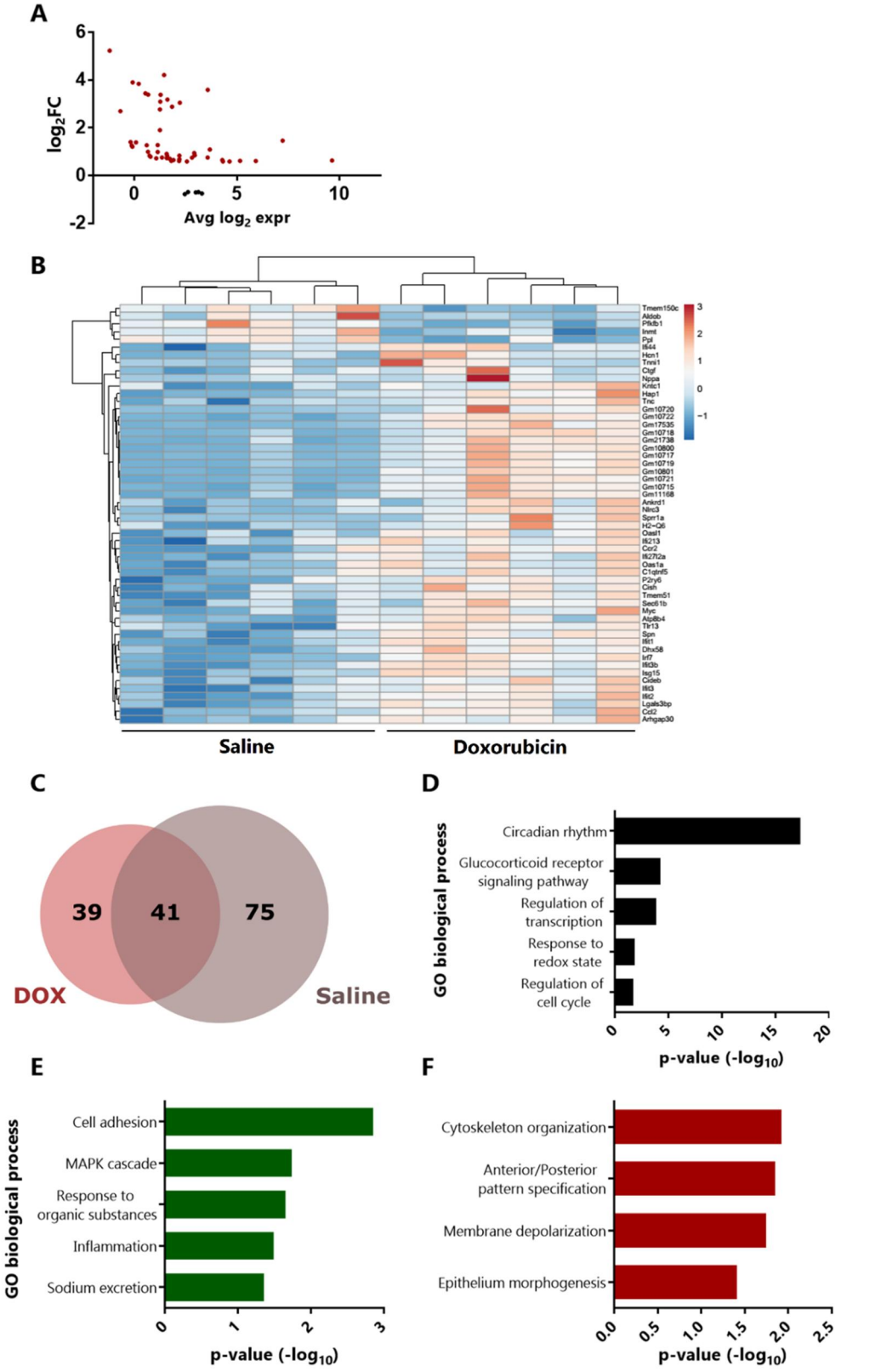

(Legend on the next page)

Figure 7.6: RNA sequencing analysis and identification of oscillatory transcripts upon DOX treatment. A) MA plot of DOX differentially expressed genes compared with vehicle-treated mice (red dots: overexpressed genes; black dots: underexpressed genes). log2FC: log2 fold change; avg log2exp: average log2 expression. B) Gene expression heatmap view of saline and DOX mice groups (n=6). Each row represents a gene, and each column represents each of the 12 animals analyzed. C) Venn diagram of detected oscillators between ZT 9 and ZT 21, for saline and DOX. D-F) Enrichment analysis (gene ontology, biological process) of oscillating genes in both conditions (D), uniquely in salines (E) and uniquely in DOX-treated mice (F), represented as negative of log10 of p-value after Bonferroni correction.

condition (saline ZT 9 *vs* saline ZT 21, and DOX ZT 9 *vs* DOX ZT 21). While in the saline group 116 genes presented significant oscillation between both time-points, this number was lower for DOX-treated mice, with 80 genes oscillating (FDR < 0.05). From these genes, 41 were commonly detected in both groups, while 39 and 75 were found to oscillate exclusively in DOX and saline groups, respectively (Fig. 7.6 C). Gene ontology analysis of the commonly oscillating genes showed a strong enrichment for circadian rhythm, followed by circadian-related pathways, including regulation of glucocorticoid receptor signaling pathway, regulation of transcription, response to redox state and regulation of cell cycle (Fig. 7.6 D), indicating that the peripheral core clock machinery was not affected by the treatment. Saline oscillators (that stopped oscillating after DOX treatment) were enriched for biological processes including cell adhesion, regulation of MAPK cascade, response to organic substances, inflammatory response, and sodium excretion (Fig. 7.3 E). Although not statistically significant, other biological processes, such as regulation of blood vessel size, vasoconstriction and heart rate, were also identified. On the other hand, the top DOX specific oscillating pathways included cytoskeleton organization, anterior/posterior pattern specification, regulation of membrane depolarization and epithelial morphogenesis (Fig. 7.6 F). Even though the oscillation of gene expression between 2 time-points is not enough to categorize a gene as circadian, several oscillating genes in the murine left ventricle were already described as circadian according to Circadian Expression Profiles Data Base (CircaDB, http://circadb.hogeneschlab.org/). Among the differentially expressed genes, mRNA levels of some particular genes were confirmed

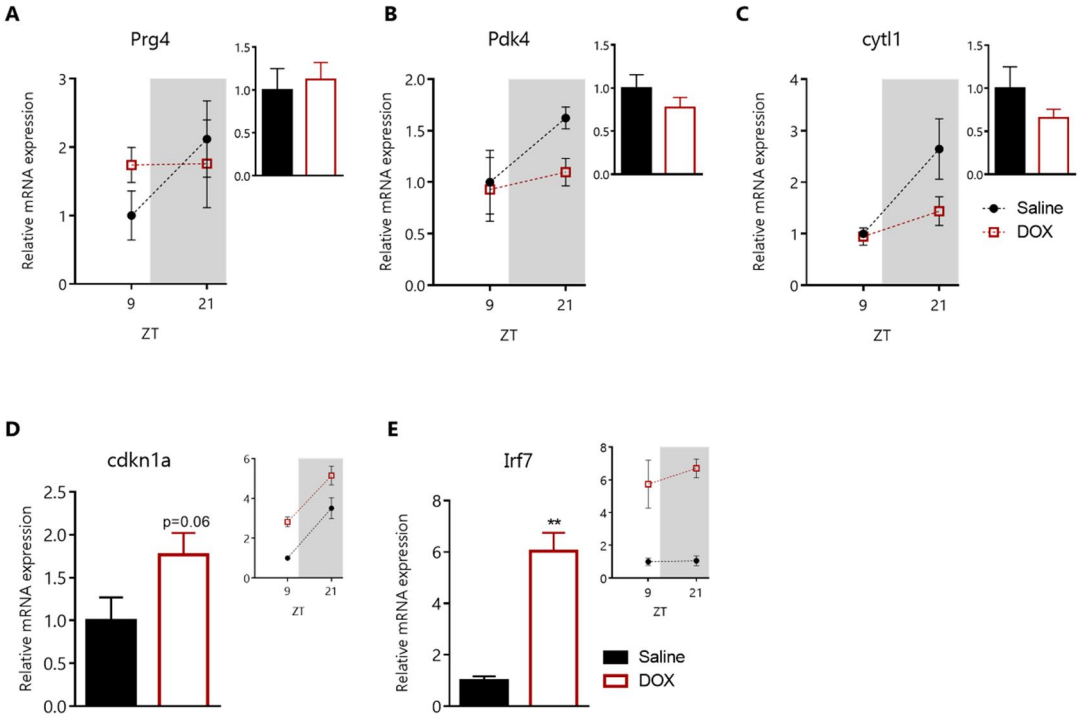

Figure 7.7: Gene expression profiles in saline and DOX mice heart. Total and oscillating (ZT9 and ZT 21) mRNA levels of *Prg4* (A), *Pdk4* (B), *cytl1* (C), *cdkn1a* (D) and *Irf7* (E), determined by RT-qPCR. Error bars indicate SEM. **p<0.01 DOX *vs* saline. n=6 per group, n=3 per group and ZT (zeitgeber time, light-dark cycle).

by RT-qPCR using the same RNA samples used for RNA-sequencing analysis (Fig. 7.7). *Prg4* and *cytl1* loss of oscillation after DOX treatment was confirmed, even though not statistically significant, due to the low number of biological replicates (n=3) (Fig. 7.7 A,C). However, *pdk4*, found to have increased oscillation in DOX mice, did not show this same pattern when analyzed by RT-qPCR (Fig. 7.7 B). Interestingly, *cdkn1a* (involved in cell cycle arrest and DNA damage response) and *Irf7* (involved in immune system processes) mRNA analysis reinforced RNA sequencing results and

showed to be overexpressed in DOX-treated animals in comparison to saline mice, by 1.7-fold and 6.0-fold, respectively (Fig. 7.7 D,E).

7.3.1.3. SIRT1-mediated oscillatory deacetylation was altered upon DOX treatment

Previous publications reported a reduction of SIRT1 protein and mRNA levels in *in vitro* and *in vivo* models of DOX-induced cardiac injury [454-456]. However, DOX effects on SIRT1 deacetylase activity are still not totally clear. SIRT1 is known to interact with a number of proteins, including PGC-1α [465], LKB1 [454], p53 [466], Per2, H3 and Bmal1 [278]. In the current study, it was investigated whether the early DOX treatment would mediate changes in the acetylation levels of 2 SIRT1 targets, H3K9 and Bmal1. Both proteins are crucial in the maintenance of circadian processes. Bmal1 deacetylation mediated by SIRT1 is required for the regulation of circadian transcription, whereas H3K9 acetylation and deacetylation cycles promotes rhythmic induction of gene activation and gene silencing [278]. SIRT1, in turn, functions as a metabolic sensor, because of its dependency on the NAD^+, helping the cell to respond to stress conditions. The results from western blotting performed on saline and DOX samples collected at ZT 9 and ZT 21 showed that the acetylation levels of H3K9 were altered in response to DOX treatment (Fig. 7.8 A,B). While the levels of H3K9 acetylation were similar for both time-points in saline samples, DOX induced significant changes between ZT 9 and ZT 21, with higher acetylation at ZT 21 (Fig. 7.8 B). Regarding Bmal1 Lys538 acetylation, it was observed that DOX reverted the oscillatory acetylation tendency observed in the respective saline controls (Fig. 7.8 A,D). Importantly, Bmal1 itself presented opposite patterns of protein levels in both groups with DOX decreasing Bmal1 at ZT 21 (Fig. 7.8 A,D). SIRT1 levels did not

change between conditions for the respective time-points, although a significant difference was observed in DOX ZT 21 compared with saline ZT 9 (Fig. 7.8 A).

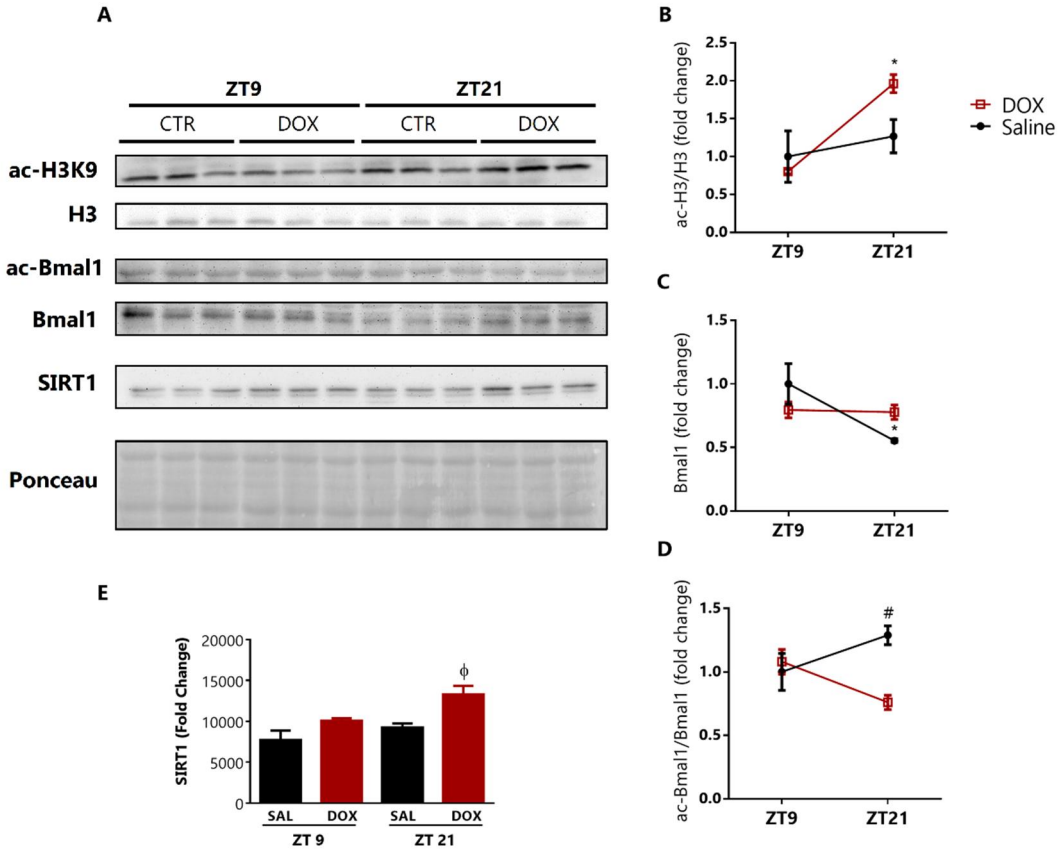

Figure 7.8: Western blotting analysis of SIRT1 and SIRT1 deacetylation targets. A) Total protein expression and acetylation levels of H3K9 and Bmal1 at ZT 9 and ZT 21. B-D) Oscillatory levels of the ratio acetylated H3K9/total H3K9 (A), total Bmal1 (B) and the ratio acetylated Bmal1/total Bmal1 (D). E) Total SIRT1 protein levels. Error bars indicate SEM. *p<0.05 ZT 21 *vs* ZT 9; #p<0.05 saline *vs* DOX at ZT 21; Φ p<0.05 DOX ZT 21 *vs* CTR ZT 9. n=3 per group and ZT.

7.3.2. *In vitro* effects of DOX on the circadian expression and SIRT1-mediated acetylation

7.3.2.1. DOX altered transcripts patterns on Mouse Embryonic Fibroblasts (MEFs)

In order to have a deeper perception of DOX effects on the circadian clock, mouse embryonic fibroblasts (MEFs) from WT mice were incubated with DOX for posterior

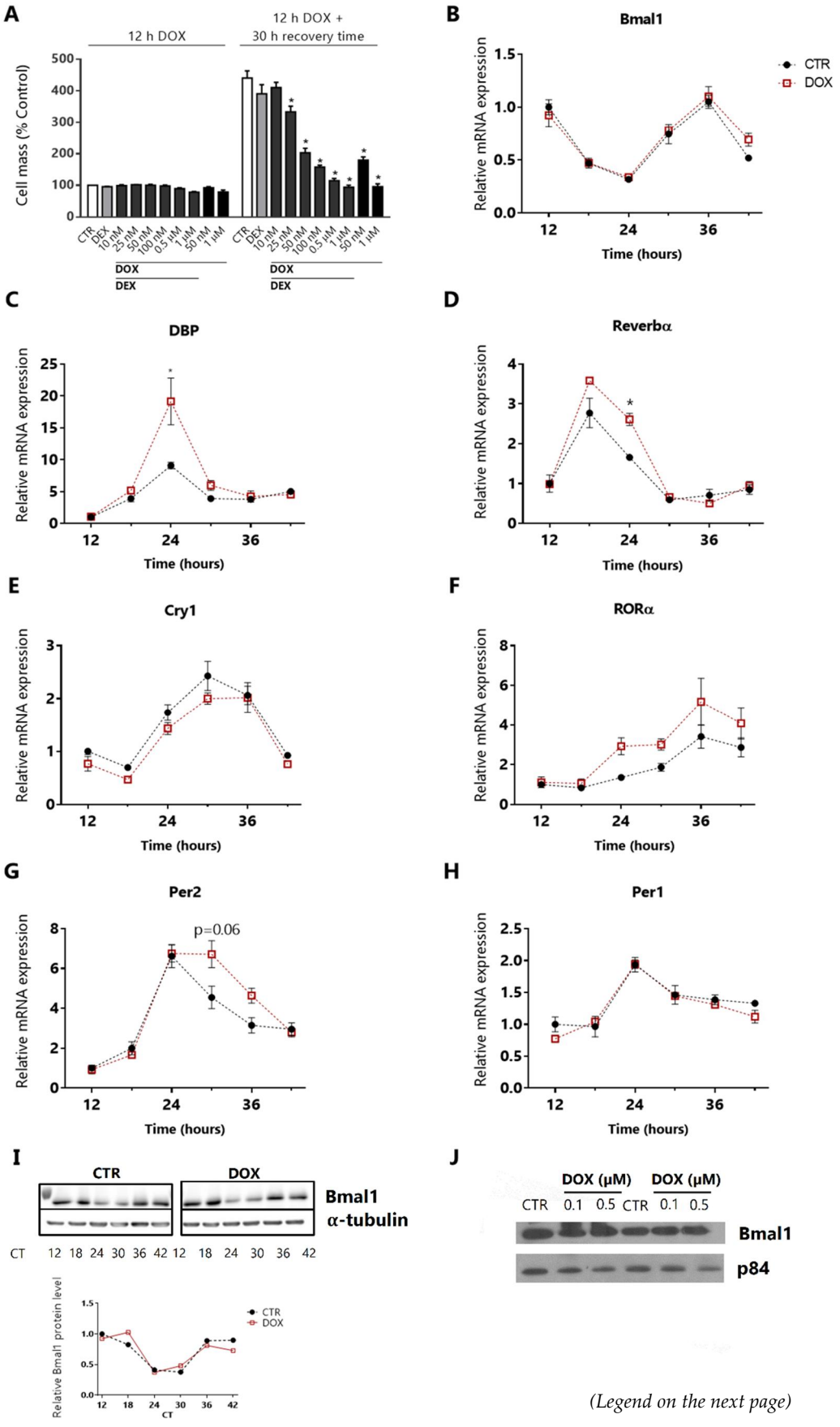

(Legend on the next page)

Figure 7.9: Impact of DOX treatment on WT MEFs circadian molecular clock. A) SRB analysis of MEFs synchronized with DEX (dexamethasone; 100 nM) and treated with DOX (10 nM- 1μM) for 12 hours. Results express protein content right after the treatment and after 30 hours of recovery time in DOX-free medium. n = 3 per condition. B-H) Circadian expression levels of *Bmal1* (B), *DBP* (C), *Rev-erbα* (D), *Cry1 I*, *Per1* (F), *Per2* (G) and *RORα* (H) was determined by RT-qPCR. n = 3 per group (CTR and 50 nM DOX) and CT (circadian-time). I-J) Bmal1 protein content was determined by western blotting. I) *Bmal1* oscillatory protein of control and 0.1 μM DOX-treated MEFs. J) Total Bmal1 protein of control and cells treated with 0.1 and 0.5 μM DOX, assayed in duplicate. Error bars indicate SEM. *p<0.05 DOX *vs* control.

mRNA expression and protein analysis. *In vitro* cell culture is naturally desynchronized and the corticosteroid DEX was used to synchronize the circadian clocks [460]. Circadian gene expression in cultured cells was proved to be induced by serum shock [467] and later by DEX [460], that was shown to induce *Per1* expression. Given the cytotoxicity of DOX and considering that gene expression analysis should be performed before triggering severe cell death events, SRB (as a measure of cell mass) was used to assess the suitable DOX concentration to be used in the assay. After the 1 hour pre-incubation with DEX (Fig. 7.3 1) the cells were exposed to DOX (concentrations ranging from 10 nM to 1 μM) for 12 hours. No effects were observed on cell mass after the 12 hours period of incubation (Fig. 7.9 A). However, after 30 hours of recovery time in drug free medium it was possible to observe a very significant decrease in cell mass in DOX treated cells, possibly by affecting cell proliferation (Fig. 7.9 A). Even though statistically significant, 50 nM DOX was chosen for the following assays since it seemed an adequate concentration to affect cell function while still allowing cell proliferation during the 30 hours period. DEX incubated alone or in combination with DOX did not alter cell viability. Cells were initially collected after DOX incubation period, which means 12 hours after DEX synchronization, and continued to be collected every 6 hours for a 30 hours period. Gene expression analysis of core clock and metabolic genes was performed for all time-points (Fig. 7.9 and Fig. 7.10). Overall, the circadian patterns confirmed the efficacy of DEX synchronization. From the clock mRNA transcripts, including *Bmal1*, *DBP*, *Rev-erbα*, *Cry1*, *Per1*, *Per2* and *RORα*, only *DBP* and *Rev-erbα* presented an

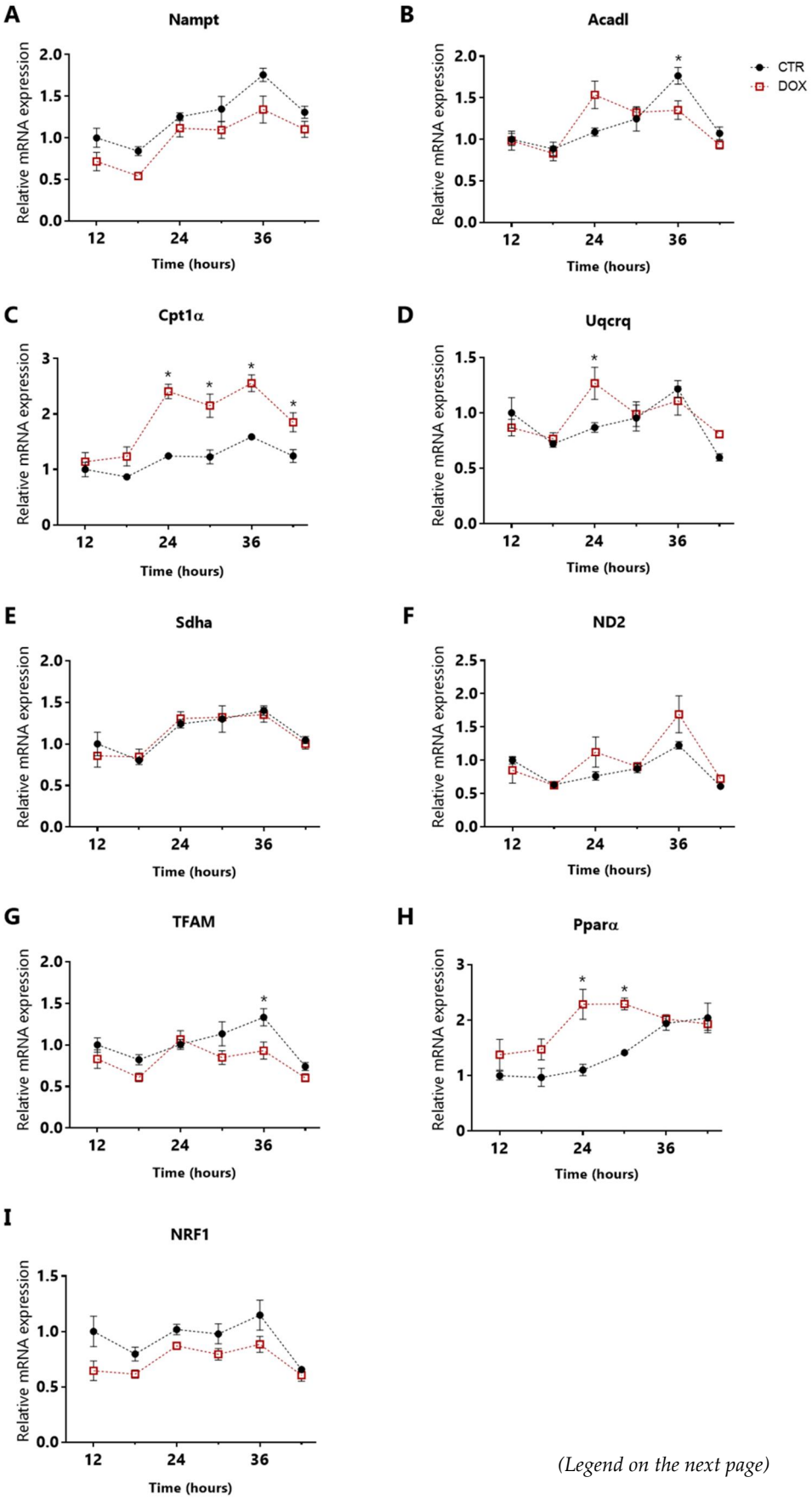

(Legend on the next page)

Figure 7.10: DOX effects on gene expression of metabolic and mitochondrial proteins, in WT MEFs. A-J) Circadian gene expression of metabolic genes over the circadian time: *Nampt* (A), *Acadl* (B), *Cpt1α* (C), *Cpt1β* (D), *Uqcrq I*, *Sdha* (F), *ND2* (G), *TFAM* (H), *Pparα* (I), *NRF1* (J). Error bars indicate SEM. *p<0.05 DOX *vs* control. n=5 per group and CT (circadian-time).

increased peak of expression at CT 24 compared with the respective controls, whereas *Per2* expression showed a prolonged peak in mRNA levels that instead of declining at CT 30 continued at maximal levels (Fig. 7.9 A-H). Since no differences in Bmal1 transcription were observed after treatment, the circadian and total Bmal1 protein levels were confirmed by western blotting using higher DOX concentrations (Fig. 7.9 I-J). Neither the total Bmal1 protein levels (DOX 0.1 and 0.5 μM) nor the differential protein expression over time (DOX 0.1 μM) were affected by DOX. Interestingly, multiple gene expression alterations were detected on the metabolic panel of genes (Fig. 7.10). The more notorious were the up-regulations of *Cpt1α* and *Pparα*, both related with fatty acid metabolism (Fig. 7.10 C,I). Additionally, *Acadl* suffered a phase-shift, *Uqcrq* was up-regulated at CT 24 and *TFAM* was overall under-expressed with a significant alteration at CT 36.

7.3.2.2. DOX exposure resulted in increased SIRT1-mediated deacetylation

To test the *in vitro* ability of SIRT1 to deacetylate Bmal1 after DOX treatment, expression vectors encoding flag-tagged murine SIRT1, and myc-tagged murine Bmal1 and CLOCK were co-transfected into HEK293 cells, good transfection hosts (Fig. 7.11). But first, DOX (0.05, 0.5 and 1 μM) cytotoxicity was screened on HEK293 using the SRB technique and only 1 μM DOX (20 hours exposure) significantly decreased HEK293 cell mass (Fig. 7.11 A). Bmal1 acetylation levels were measured after immunoprecipitation with anti-myc and further western blotting with acetyl-Bmal1 antibody (Fig. 7.11 B). In order to have acetylated levels of Bmal1, the

acetyltransferase CLOCK was used to counteract SIRT1 deacetylase activity. The efficiency of the transfection was confirmed by western blotting with anti-myc and anti-flag antibodies and comparison with the input signal. SIRT1 transfected cells presented lower levels of acetyl-Bmal1, and DOX seemed to dose-dependently reduce Bmal1 acetylation compared with non-treated cells. To confirm these results, WT and *SIRT1*$^{-/-}$ (knockout) MEFs were treated with DOX (1 and 2 μM) and the acetylation levels of Bmal1 and acetyl-CoA synthase 1 (AceCS1), another SIRT1 target [269], were measured (Fig. 7.12 A). Again, both DOX treatments led to a reduction of Bmal1

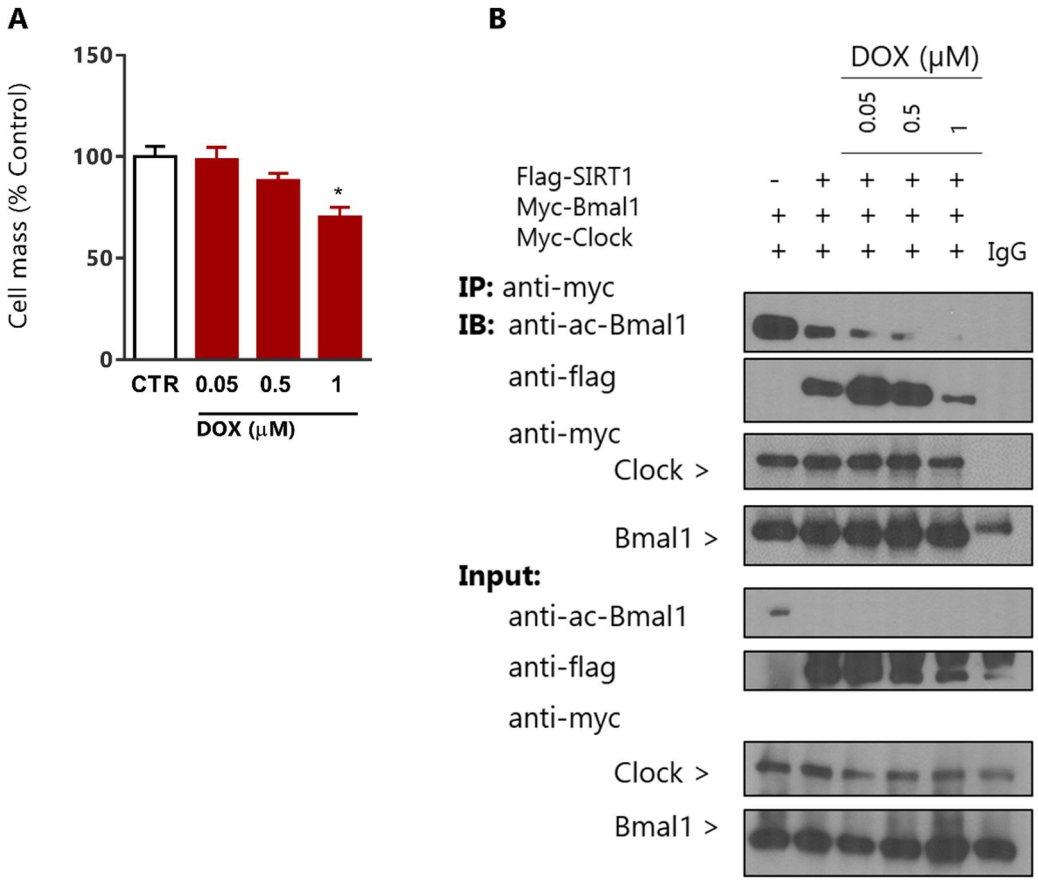

Figure 7.11: Bmal1 acetylation levels in HEK293 cells. A) SRB analysis of HEK293 cells treated with DOX (0.05, 0.5 and 1 μM) for 20 hours. Results express protein content right after the treatment. n = 4 per condition. B) HEK293 were co-transfected with expression vectors (flag-SIRT1, myc-Bmal1, myc-CLOCK) and treated with DOX (0, 0.05, 0.5, 1 μM). The protein extracts were immunoprecipitated with an anti-myc antibody and the levels of Bmal1 acetylated were assessed. IP, immunoprecipitation; IB, immunoblotting; IgG, immunoglobulin G. Error bars indicate SEM. *p<0.05 DOX *vs* control.

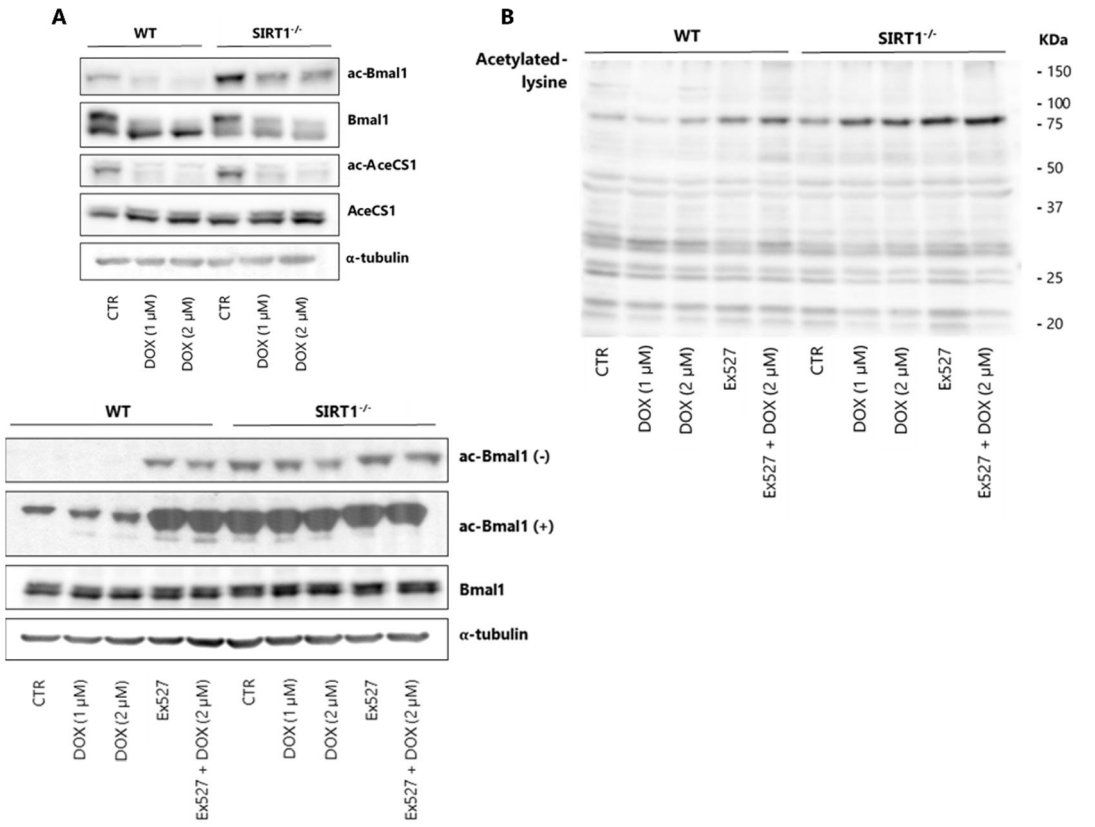

Figure 7.12: Acetylation levels in DOX-treated WT and *SIRT1* knockout MEFs. A-B) Total protein lysates of MEFs treated with DOX (1 and 2 μM; 14 hours) and pre-treated with Ex527 (50 μM) were resolved by SDS-PAGE. A) Total Bmal1, acetyl-Bmal1, total AceCS1, acetyl-AceCS1, α-tubulin and B) total acetyl-lysine were detected by western blotting. (-) short exposure time; (+) long exposure time.

acetylation compared with control cells. Decreased acetyl-Bmal1 levels were also observed in DOX-treated *SIRT1*$^{-/-}$ cells, but band-intensities were significantly higher than in WT MEFs. Thus, even though SIRT1-mediated Bmal1 deacetylation may be affected by DOX, it does not seem to be the only mechanism affecting the acetylation levels. Other sirtuins may be involved as well, since the Ex527 inhibitor, used at a concentration (50 μM) which is not totally selective for SIRT1 [468], considerably increased acetyl-Bmal1 intensity in both WT and *SIRT1*$^{-/-}$ cells. Similarly, acetyl-AceCS1 decreased with DOX treatment in both cell lines, suggesting that SIRT1 activity may not be the only reason for the reduction of AceCS1 acetylation. Interestingly, Bmal1 phosphorylation state (detected as upper and lower bands in

Bmal1 western blotting) seemed to be altered with DOX exposure. Global lysine acetylation was not dramatically impacted by DOX, even though some particular bands were more intense with the treatment (Fig. 7.12 B). Similarly, SIRT1 ablation increased some band intensities but did not cause major alterations in the overall profile.

7.4. Discussion

Even though advances have been made in the comprehension of the molecular mechanisms behind the cardiotoxicity of DOX, the complexity and multi-factorial nature of the problem has hampered the success of therapeutic strategies aiming the reduction of DOX-related heart injury. This is particularly relevant for late onset chronic manifestations, since cardiotoxicity can be developed as late as 15 years after treatment completion and most of the times it is difficult to keep track of children's health trajectories for so long. In this sense, it is important to clarify the impact of DOX in children and young adult hearts in order to understand how to manage preventive approaches. In this study, we investigated whether a sub-chronic DOX regimen in juvenile mice would interfere with the normal transcriptional oscillation and circadian-related acetylation patterns observed in the murine hearts 6 weeks after finishing the treatment, and the results were supported by *in vitro* testing. Multiple lines of evidence support the role of disrupted internal clock in the development of a number of pathologies [253]. We believe that the multiplicity of disturbed pathways induced by DOX, mostly as a result of mitochondrial injury and DNA damage response, may interfere with cellular energy state and subsequently unbalance the circadian rhythms of the heart.

In this protocol, the cumulative administration dose of 20 mg/kg DOX in juvenile mice induced a decrease in body weight gain during the initial weeks, while the treatment was occuring, but also during the following weeks of recovery time, never reaching

the values of the control group. Moreover, at the end of the experimental design, heart weight in DOX group was lower compared with saline controls, while the ratio heart/body weight, an index of cardiac hypertrophy, was higher in DOX animals. These persistent phenomena have been reported by many others [208, 469, 470]. Some authors justify the reduced heart weight as a result of cardiomyocyte loss by cell death processes, whereas the loss of body mass may be a consequence of decreased appetite and food consumption [203, 208, 469]. Although other experiments should have been performed in order to confirm the increased myocardial collagen deposition in DOX-treated animals, HE staining allowed to observe an increase in fibroblasts number suggesting the presence of a mild DOX-induced myocardial fibrosis, as previously reported [203, 471]. Other indicators of cardiac injury included the higher mRNA levels of cardiac *ANP* and *BNP*. Both natriuretic peptides are mainly synthesized in the heart (ANP in the atria, BNP in the atria and ventricles) and increased plasma ANP and BNP concentrations are useful predictive markers of heart failure [472, 473]. Functionally, ANP and BNP possess diuretic, natriuretic and vasodilatory properties [474] and up-regulation of ANP and BNP have previously been reported in murine models of DOX-induced cardiotoxicity [370, 475] and in pediatric patients [85, 476]. Overall, the designed protocol was successful in establishing a juvenile model of DOX-induced cardiotoxicity with persistent repercussions later in life.

To address the impact of DOX exposure on the cardiac circadian expression, mice from both groups (saline and DOX) were sacrificed at 4 different times of the day, two during the light phase and the other two during the dark phase. Gene expression analysis by RT-qPCR revealed no major alterations on the master clock. From the 6 circadian genes analyzed, only *Rev-erbα* was differently expressed at ZT 9. Rev-erbα works as a repressor of Bmal1 transcription upon binding to the RORE region located in Bmal1 promoter region [244]. Additionally, Rev-erbα also regulates the expression of other metabolic genes, coordinating the circadian rhythm and metabolism [477]. The stabilization of Rev-erbα protein seems to directly affect mitochondria by

enhancing their respiration and antioxidant defenses [478], whereas conditions of oxidative stress and inflammation modulate Rev-erbα transcription [479]. All the other metabolic and mitochondrial-related genes, with the exception of *Cpt1α*, also showed no differences in circadian and total expression compared with the respective controls. Thus, at least for this panel of genes, the recovery time given to the animals after the treatment seemed to rebalance the normal mRNA levels. In order to have a global overview of the transcriptional alterations caused by DOX, and considering that previous studies confirmed persistent alteration in gene expression profiles [188], we next performed a deep sequencing approach. Regardless of the ZT, DOX treatment did not lead to modulation of metabolic pathways, including glycolysis and fatty acid metabolism, as reported by other [188], but instead resulted in the up-regulation of genes involved in the inflammatory response, including *IRF7* and *IFIT1-3*. The family of interferon regulatory factors, to which IRF7 belongs (together with 8 other members – IRF1-9), are known to be involved in host defending mechanisms including response to viral infection and DNA-damaging agents. IRF7 has also been associated with TNF-related apoptosis-inducing ligands and extrinsic apoptotic pathway [480]. In agreement with our results, IRF7 was previously shown to be activated by several DNA-damaging chemotherapeutic agents including DOX [481]. DOX induces IRF7 phosphorylation and translocation to the nucleus where it works as a transcription factor and mediator of DNA damage signaling pathways [481]. Other members of the IRF family, including the IRF3 pathway, are activated in response to DOX or UV radiation [482]. These regulatory factors are also implicated in cell cycle arrest and apoptosis. It is then not surprising that *cdkn1a* (encoding p21) was also up-regulated in DOX animals. p21 is a cyclin-dependent kinase inhibitor that can interact and inactivate various cyclin-dependent kinases that control cell cycle phase transitions, resulting in cell cycle arrest usually to prevent the accumulation of mutations or to allow the function of DNA repair machinery. The p21 up-regulation in response to DOX treatment was reported in several other studies [388, 483-485]. Additionally,

IRF1 seems to be essential for DNA damage-induced cell cycle arrest [486], whereas antisense IRF1 transfection suppresses p21 induction and rescue cell growth [487]. In fact, p21 induction was found to be dependent on both p53 and IRF1, suggesting a cooperative work in response to genotoxic stress [486].

The circadian homeostasis is crucial for the normal body physiology and, even though some extent of plasticity can be achieved under more stressing conditions, extreme situations can contribute to the misalignment of the normal rhythmicity. Here we chose 2 ZT, 12 hours apart, to analyze the total RNA expression and variation between those 2 time-points to identify possible alterations in the oscillatory expression patterns. We observed that the treatment did not alter the expression of the core circadian components but contributed to changes in the oscillation of genes participating in important cell functions, with emphasis to cell adhesion (stopped oscillating with DOX) and cytoskeleton organization (started oscillating with DOX). Importantly, these results are referents to mRNA levels between ZT9 and ZT21, which means that no full conclusions can be taken from the overall circadian behavior. Yet, it is possible to conclude that the cardiac damage caused by DOX significantly affects the mRNA rhythmicity in the heart, flattening or accentuating the expression levels in the analyzed ZTs. Similarly, our results on MEFs confirmed the effect on multiple cyclic gene expression profiles. Obviously, the effects on this model were more expressive when compared with the murine model, not only because of the lack of complexity of the model but also because of the acute analysis in comparison with the sub-chronic treatment involving a recovery period. Still, when examining SIRT1 protein levels and the acetylation of 2 of its targets (H3K9 and Bmal1) in the animal model, we found indications of altered acetylation patterns and possibly acetylation-related activity. We have focused on SIRT1-mediated acetylation because of its linking role between redox state, metabolism and the circadian regulation [278]. Among SIRT1 targets are the circadian repressor PER2, whose deacetylation promotes PER2 degradation, and Bmal1, that requires rhythmic acetylation to recruit CRY1 to

CLOCK-Bmal1 complex and therefore promote the activation and repression of circadian transcription [267, 268]. Also, several reports described the benefits of SIRT1 on ameliorating DOX side effects [435, 455], while others observed reduced SIRT1 levels in response to DOX treatment [370, 397, 455]. Corroborating the *in vivo* observations, both MEFs and HEK293 confirmed the decreased acetylated states of Bmal1 and AceCS1. The latter participates in the biosynthesis of acetyl-CoA, using acetate as substrate, and its cyclic acetylation mediated by SIRT1 contributes for the rhythmicity of acetyl-CoA cellular levels [269, 488]. Since AceCS1 deacetylation is required for AceCS1 activation, we speculate whether DOX may have an actual impact on the nucleocytosolic acetyl-CoA pool that is used for *de novo* synthesis of fatty acids or histone acetylation, which would be interesting to explore further. Additionally, SIRT3 was reported to deacetylate and activate the mitochondrial AceCS2 and, given the mitochondrial-targeted nature of DOX, future studies should also elucidate the role of this drug on AceCS2 activity [488]. In turn, the loss of oscillation in Bmal1 acetylation between ZT 9 and ZT 21 in mice and the increased Bmal1 deacetylation observed in the cell culture treatments may eventually affect the downstream expression of clock-controlled genes since Bmal1 deacetylation leads to repression of target genes expression. Importantly, even in SIRT1 knockout MEFs it was possible to observe a reduction of acetylation in DOX-treated cells, which suggests that other sirtuins may be involved. An overall increase in lysine-acetylated proteins was observed in H9c2 cardiomyoblasts and in hearts of DOX-treated mice, with those differences attributed to reduced SIRT1 and SIRT3 levels [397]. However, although a general increase in acetylation may be possible in response to signaling pathways or metabolic remodeling, our results suggest that DOX treatment also leads to a selective increase of sirtuin activity. Another report observed increased H3 deacetylation induced by DOX, suggesting activation of SIRT1, and it was considered whether it could be a compensatory mechanism to respond to oxidative stress [489].

In conclusion, the present study reveals that DOX treatment in mice during the first weeks of age has detrimental effects on oscillatory molecular mechanisms including gene expression rhythmicity and acetylation profiles, which are biologically related. If confirmed in humans, these results suggest that treatment with cardiotoxic agents during childhood may compromise the circadian mechanisms and daily rhythmicity of the heart, which can contribute to the manifestation of cardiovascular disease later in life.

Chapter 8

8. Final considerations and Future perspectives

Doxorubicin is a powerful agent in the fight against cancer. However, more than a decade after its discovery, several clinical studies started to report cardiotoxic side effects. Since then, multiple efforts have been made aiming to understand the molecular causes of the problem, as well as to develop strategies to reduce the myocardial toxicity. Unfortunately, none of these objectives have been entirely accomplished and DOX-induced cardiotoxicity is still the main bottleneck of the anticancer treatment. The persistence of the effects and the progressive cardiac deterioration add another layer of complexity considering that cardiotoxicity is often not detected until years after completion of the treatment.

In the present thesis, we aimed to approach the problematic of DOX-associated cardiotoxicity at three different levels: delineate possible protective measures of the proliferative cardiac population, identify metabolic alterations in cardiomyocytes acutely exposed to DOX, and evaluate the persistent DOX effects in a murine model at the transcriptional and circadian level.

The first objective of this thesis consisted in evaluating the long term effects of a pre-exposure to non-lethal DOX doses on an extensively studied cell line of proliferative cardiomyoblasts. Phenomena like hormesis and adaptative responses have gained special attention in the last years. These mechanisms rely on the fact that low doses of some toxic agents can stimulate adaptative responses, resulting in less adverse effects after a subsequent higher exposure. Thus, we hypothesized that a nanomolar dose of

DOX could have a similar effect and attenuate the damage of a further exposure at clinically relevant concentrations. Our data confirmed this hypothesis since pre-exposed cells seemed to be more resistant than the naïve counterpartners. Whether this effect is caused by an apparent mitochondrial adaptation or by DOX effects on the cell cycle and replication is still not totally clarified. Still, we observed an improvement in mitochondrial activity. In the future it would be interesting to explore some particular aspects: 1) DOX pre-exposure in H9c2 resulted in cell cycle arrest in G2/M. In proliferating cells, DOX is known for inducing DNA damage through intercalation into DNA and inhibition of TopII. Thus, it is plausible that if replication rate is affected, DOX-induced DNA damage may also be reduced. Importantly, even though cell cycle arrest may be essential for DNA repair it is important to confirm if DOX is not inducing irreversible cell cycle arrest and if the capacity of differentiate towards a cardiac phenotype was not impaired; 2) Our data, supported with previous observations [390, 391], suggest DOX effects on DNMT1 levels. Additionally, the persistent mitochondrial transcriptional changes observed after DOX treatment seem to be independent from mtDNA copy number and mitochondrial transcriptional machinery. These preliminary data suggest a relationship between the mitochondrial mRNA levels and DNMT1 function. We observed reduced DNA methylation signal by immunocytochemistry but, being aware of the limitations of this technique, it would be relevant to confirm these results using a more sensitive and informative approach.

The second aim was to recapitulate the acute effects of DOX in a more reliable model of cardiomyocytes. Over the past years, H9c2 have been the most used *in vitro* model to study the impact of DOX on cardiac-derived cells [34, 137, 138, 140, 150, 349, 397, 490]. This model has multiple advantages over other cardiac-derived models, including being easily manipulated and the possibility of being kept in culture for long periods. However, it lacks features that are very important when studying an energy-demanding organ like the heart. For this reason, we decided to use iPSC-

derived mouse cardiomyocytes to study the stress responses and mitochondrial and metabolic alterations caused by a 24 hours exposure to DOX. The treatment proved to affect differently the cells according to the concentration of drug. While the higher concentration clearly induced an apoptotic process, the lower concentration led to a reshape of mitochondrial metabolism. Importantly, even though mouse iPSC-derived cardiomyocytes are a perfectly valid model to obtain insight into the bioenergetics effects of DOX, it would be important to reinforce the results using iPSC-derived human cardiomyocytes. The results from both chapters (Chapters 5 and 6) demonstrated a negative impact of DOX over the glycolytic pathway. Increased glucose uptake and utilization is observed in failing hearts in an attempt to respond to the high ATP demands [491]. However, upon DOX treatment, cells seem to undergo energetic failure and none of the different pathways for ATP supply (glycolysis, mitochondrial oxidative phosphorylation and phosphotransferase reactions catalyzed by creatine kinase) are sufficient to respond to the energetic needs [183]. Still, these observations were not verified in all DOX-induced toxicity studies, possibly due to the high variability of models and doses. Moreover, it was observed that 0.5 μM DOX exposure induced the inhibition of PDH through the overexpression of PDK4, and pre-treatment with DCA, a PDK inhibitor, ameliorated the mitochondrial respiration. The pyruvate dehydrogenase complex converts pyruvate into acetyl-CoA. In the future, it would be interesting to not only study the effect of DOX on the acetyl-CoA pool but also understand if the reduction of this metabolite in the mitochondrial compartment would lead to alterations in the acetylation levels of mitochondrial enzymes. For instance, it is already known that under particular conditions, such as fasting, high-fat diet or ethanol exposure, the patterns of mitochondrial protein acetylation are modified [492]. According to our results PDH activity is decreased and that might be eventually translated into lower acetyl-CoA levels that influence protein acetylation.

Altered acetylation was also observed in Chapter 7 as a result of DOX treatment in mice, MEF and HEK293. Whether these alterations are a consequence of metabolic remodeling (caused by dysregulated NAD^+ fluctuations or acetyl-CoA depletion) or transcriptional reprogramming is still not clear. Nevertheless, the results from Chapter 7 highlighted some persistent effects of DOX on murine heart and unveiled repercussions on the rhythmicity of cardiac molecular mechanisms. However, the analysis the cardiac transcriptome over the 24 hours period would be crucial to take more clear conclusions regarding the effects on the circadian gene expression. Even though our results allow to observe that multiple genes were oscillating differently between groups, more time-points are required to take circadian conclusions. In the future it would also be interesting to confirm if NAD^+ content (total and oscillation) was altered by DOX treatment and unbalance of the NADH/NAD^+ homeostasis. Also, our results suggest the involvement of more sirtuins than SIRT1 in the deacetylation of described SIRT1 targets (Bmal1 and AceCS1). This result is hard to explain since no literature was found to support this conclusion. Even though the analysis of SIRT1 activity is still experimentally challenging it would be important to confirm the contribution of this circadian-metabolism linking sirtuin.

Overall the results obtained in this thesis added knowledge to the mechanisms of DOX action. One challenge is still the variability of results obtained with different models, which hampers the setting of clear preventive measures. While *in vitro* models have the advantage of reducing the complexity of the model and interference of other external factors, animal models are more realistic approaches. This work contributed to the recognition of the hormetic behavior of DOX, the understanding of how naturally beating cells react to higher or lower DOX acute exposures and the finding that DOX exposure early in life still has a deleterious cardiac impact during adulthood and that oscillatory transcriptional and acetylation processes are affected. Still, complementary work and a deeper understanding of DOX-induced cardiotoxicity is

still required for the validation of conclusions and the development of additional preventive measures.

References

1. Arcamone F, *et al.* (1969) Adriamycin, 14-hydroxydaunomycin, a new antitumor antibiotic from S. peucetius var. caesius. *Biotechnology and bioengineering* 11(6):1101-1110.

2. Bonadonna G, *et al.* (1969) Clinical evaluation of adriamycin, a new antitumour antibiotic. *British medical journal* 3(5669):503-506.

3. Bonadonna G, *et al.* (1970) Phase I and preliminary phase II evaluation of adriamycin (NSC 123127). *Cancer research* 30(10):2572-2582.

4. Smith LA, *et al.* (2010) Cardiotoxicity of anthracycline agents for the treatment of cancer: systematic review and meta-analysis of randomised controlled trials. *BMC cancer* 10:337.

5. Lipshultz SE, *et al.* (2013) Treatment-related cardiotoxicity in survivors of childhood cancer. *Nature reviews. Clinical oncology* 10(12):697-710.

6. Cagel M, *et al.* (2017) Doxorubicin: nanotechnological overviews from bench to bedside. *Drug discovery today* 22(2):270-281.

7. Peterson C & Trouet A (1978) Transport and storage of daunorubicin and doxorubicin in cultured fibroblasts. *Cancer research* 38(12):4645-4649.

8. Dalmark M & Storm HH (1981) A Fickian diffusion transport process with features of transport catalysis. Doxorubicin transport in human red blood cells. *The Journal of general physiology* 78(4):349-364.

9. Greene RF, *et al.* (1983) Plasma pharmacokinetics of adriamycin and adriamycinol: implications for the design of in vitro experiments and treatment protocols. *Cancer research* 43(7):3417-3421.

10. Speth PA, *et al.* (1988) Clinical pharmacokinetics of doxorubicin. *Clinical pharmacokinetics* 15(1):15-31.

11. Licata S, *et al.* (2000) Doxorubicin metabolism and toxicity in human myocardium: role of cytoplasmic deglycosidation and carbonyl reduction. *Chemical research in toxicology* 13(5):414-420.

12. Tacar O, *et al.* (2013) Doxorubicin: an update on anticancer molecular action, toxicity and novel drug delivery systems. *The Journal of pharmacy and pharmacology* 65(2):157-170.

13. Kiyomiya K, *et al.* (2001) Mechanism of specific nuclear transport of adriamycin: the mode of nuclear translocation of adriamycin-proteasome complex. *Cancer research* 61(6):2467-2471.

14. Yang F, *et al.* (2014) Doxorubicin, DNA torsion, and chromatin dynamics. *Biochimica et biophysica acta* 1845(1):84-89.

15. Ashley N & Poulton J (2009) Mitochondrial DNA is a direct target of anti-cancer anthracycline drugs. *Biochemical and biophysical research communications* 378(3):450-455.

16. Coldwell K, *et al.* (2010) Detection of adriamycin-DNA adducts by accelerator mass spectrometry. *Methods in molecular biology (Clifton, N.J.)* 613:103-118.

17. Kellner U, *et al.* (2002) Culprit and victim -- DNA topoisomerase II. *The Lancet. Oncology* 3(4):235-243.

18. Nitiss JL (2009) Targeting DNA topoisomerase II in cancer chemotherapy. *Nature reviews. Cancer* 9(5):338-350.

19. Mai Y, *et al.* (2016) An oxidative stress-based mechanism of doxorubicin cytotoxicity suggests new therapeutic strategies in ABC-DLBCL. 128(24):2797-2807.

20. Doroshow JH, *et al.* (2001) Oxidative DNA base modifications in peripheral blood mononuclear cells of patients treated with high-dose infusional doxorubicin. *Blood* 97(9):2839-2845.

21. Von Hoff DD, *et al.* (1979) Risk factors for doxorubicin-induced congestive heart failure. *Annals of internal medicine* 91(5):710-717.

22. Swain SM, *et al.* (2003) Congestive heart failure in patients treated with doxorubicin: a retrospective analysis of three trials. *Cancer* 97(11):2869-2879.

23. Dobbs NA, *et al.* (1995) Gender affects doxorubicin pharmacokinetics in patients with normal liver biochemistry. *Cancer chemotherapy and pharmacology* 36(6):473-476.

24. Krischer JP, *et al.* (1997) Clinical cardiotoxicity following anthracycline treatment for childhood cancer: the Pediatric Oncology Group experience. *Journal of clinical oncology : official journal of the American Society of Clinical Oncology* 15(4):1544-1552.

25. Henderson IC, *et al.* (1989) Randomized clinical trial comparing mitoxantrone with doxorubicin in previously treated patients with metastatic breast cancer. *Journal of clinical oncology : official journal of the American Society of Clinical Oncology* 7(5):560-571.

26. Giantris A, *et al.* (1998) Anthracycline-induced cardiotoxicity in children and young adults. *Critical reviews in oncology/hematology* 27(1):53-68.

27. Bansal N, *et al.* (2017) Chemotherapy-induced cardiotoxicity in children. *Expert opinion on drug metabolism & toxicology* 13(8):817-832.

28. Yeh ET, *et al.* (2004) Cardiovascular complications of cancer therapy: diagnosis, pathogenesis, and management. *Circulation* 109(25):3122-3131.

29. Goorin AM, *et al.* (1990) Initial congestive heart failure, six to ten years after doxorubicin chemotherapy for childhood cancer. *The Journal of pediatrics* 116(1):144-147.

30. Lipshultz SE, *et al.* (1991) Late cardiac effects of doxorubicin therapy for acute lymphoblastic leukemia in childhood. *The New England journal of medicine* 324(12):808-815.

31. Harake D, *et al.* (2012) Cardiotoxicity in childhood cancer survivors: strategies for prevention and management. *Future cardiology* 8(4):647-670.

32. Ewer MS & Ewer SM (2010) Cardiotoxicity of anticancer treatments: what the cardiologist needs to know. *Nature reviews. Cardiology* 7(10):564-575.

33. Torti FM, *et al.* (1986) Cardiotoxicity of epirubicin and doxorubicin: assessment by endomyocardial biopsy. *Cancer research* 46(7):3722-3727.

34. Sardao VA, *et al.* (2009) Morphological alterations induced by doxorubicin on H9c2 myoblasts: nuclear, mitochondrial, and cytoskeletal targets. *Cell biology and toxicology* 25(3):227-243.

35. Ascensao A, *et al.* (2005) Moderate endurance training prevents doxorubicin-induced in vivo mitochondriopathy and reduces the development of cardiac apoptosis. *American journal of physiology. Heart and circulatory physiology* 289(2):H722-731.

36. Yusuf SW, *et al.* (2008) The diagnosis and management of cardiovascular disease in cancer patients. *Current problems in cardiology* 33(4):163-196.

37. Wouters KA, *et al.* (2005) Protecting against anthracycline-induced myocardial damage: a review of the most promising strategies. *British journal of haematology* 131(5):561-578.

38. Okuda S, *et al.* (1986) Adriamycin-induced nephropathy as a model of chronic progressive glomerular disease. *Kidney international* 29(2):502-510.

39. Paczek L, *et al.* (1992) Intraglomerular proteinase activity in adriamycin-induced nephropathy. *Nephron* 60(1):81-86.

40. Vogl TJ, *et al.* (2011) Liver, gastrointestinal, and cardiac toxicity in intermediate hepatocellular carcinoma treated with PRECISION TACE with drug-eluting beads: results from the PRECISION V randomized trial. *AJR. American journal of roentgenology* 197(4):W562-570.

41. Peters JH, *et al.* (1981) Tissue distribution of doxorubicin and doxorubicinol in rats receiving multiple doses of doxorubicin. *Cancer chemotherapy and pharmacology* 7(1):65-69.

42. Kim HD, *et al.* (1994) Quantitative study on the relation between structural and functional properties of the hearts from three different mammals. *The Anatomical record* 238(2):199-206.

43. Goormaghtigh E, *et al.* (1987) Study of the adriamycin-cardiolipin complex structure using attenuated total reflection infrared spectroscopy. *Biochemistry* 26(6):1789-1794.

44. Doroshow JH, *et al.* (1980) Enzymatic defenses of the mouse heart against reactive oxygen metabolites: alterations produced by doxorubicin. *The Journal of clinical investigation* 65(1):128-135.

45. Zhou P & Pu WT (2016) Recounting Cardiac Cellular Composition. *Circulation research* 118(3):368-370.

46. Bearzi C, *et al.* (2007) Human cardiac stem cells. *Proceedings of the National Academy of Sciences of the United States of America* 104(35):14068-14073.

47. Le T & Chong J (2016) Cardiac progenitor cells for heart repair. *Cell death discovery* 2:16052.

48. Huang C, *et al.* (2010) Juvenile exposure to anthracyclines impairs cardiac progenitor cell function and vascularization resulting in greater susceptibility to stress-induced myocardial injury in adult mice. *Circulation* 121(5):675-683.

49. Ettema TJ (2016) Evolution: Mitochondria in the second act. *Nature* 531(7592):39-40.

50. Lee C, *et al.* (2015) The mitochondrial-derived peptide MOTS-c promotes metabolic homeostasis and reduces obesity and insulin resistance. *Cell metabolism* 21(3):443-454.

51. Lee C, *et al.* (2013) Humanin: a harbinger of mitochondrial-derived peptides? *Trends in endocrinology and metabolism: TEM* 24(5):222-228.

52. Mootha VK, *et al.* (2003) Integrated analysis of protein composition, tissue diversity, and gene regulation in mouse mitochondria. *Cell* 115(5):629-640.

53. Sickmann A, *et al.* (2003) The proteome of Saccharomyces cerevisiae mitochondria. *Proceedings of the National Academy of Sciences of the United States of America* 100(23):13207-13212.

54. Pagliarini DJ, *et al.* (2008) A mitochondrial protein compendium elucidates complex I disease biology. *Cell* 134(1):112-123.

55. Matilainen O, *et al.* (2017) Mitochondria and Epigenetics - Crosstalk in Homeostasis and Stress. *Trends in cell biology* 27(6):453-463.

56. Acin-Perez R & Enriquez JA (2014) The function of the respiratory supercomplexes: the plasticity model. *Biochimica et biophysica acta* 1837(4):444-450.

57. Genova ML & Lenaz G (2013) A critical appraisal of the role of respiratory supercomplexes in mitochondria. *Biological chemistry* 394(5):631-639.

58. Signes A & Fernandez-Vizarra E (2018) Assembly of mammalian oxidative phosphorylation complexes I-V and supercomplexes. *Essays in biochemistry* 62(3):255-270.

59. Bezawork-Geleta A, *et al.* (2017) Mitochondrial Complex II: At the Crossroads. *Trends in biochemical sciences* 42(4):312-325.

60. Davies KM, *et al.* (2011) Macromolecular organization of ATP synthase and complex I in whole mitochondria. *Proceedings of the National Academy of Sciences of the United States of America* 108(34):14121-14126.

61. Cogliati S, *et al.* (2016) Mitochondrial Cristae: Where Beauty Meets Functionality. *Trends in biochemical sciences* 41(3):261-273.

62. Guzy RD, *et al.* (2008) Loss of the SdhB, but Not the SdhA, subunit of complex II triggers reactive oxygen species-dependent hypoxia-inducible factor activation and tumorigenesis. *Molecular and cellular biology* 28(2):718-731.

63. Murphy MP (2009) How mitochondria produce reactive oxygen species. *The Biochemical journal* 417(1):1-13.

64. Jones DP (2006) Redefining oxidative stress. *Antioxidants & redox signaling* 8(9-10):1865-1879.

65. Andreyev AY, *et al.* (2005) Mitochondrial metabolism of reactive oxygen species. *Biochemistry. Biokhimiia* 70(2):200-214.

66. Shock LS, *et al.* (2011) DNA methyltransferase 1, cytosine methylation, and cytosine hydroxymethylation in mammalian mitochondria. *Proceedings of the National Academy of Sciences of the United States of America* 108(9):3630-3635.

67. Saini SK, *et al.* (2017) DNA Methyltransferase1 (DNMT1) Isoform3 methylates mitochondrial genome and modulates its biology. *Scientific reports* 7(1):1525.

68. Vasington FD & Murphy JV (1962) Ca ion uptake by rat kidney mitochondria and its dependence on respiration and phosphorylation. *The Journal of biological chemistry* 237:2670-2677.

69. Rizzuto R, *et al.* (2012) Mitochondria as sensors and regulators of calcium signalling. *Nature reviews. Molecular cell biology* 13(9):566-578.

70. Hajnoczky G, *et al.* (1995) Decoding of cytosolic calcium oscillations in the mitochondria. *Cell* 82(3):415-424.

71. Rizzuto R, *et al.* (1998) Close contacts with the endoplasmic reticulum as determinants of mitochondrial Ca2+ responses. *Science (New York, N.Y.)* 280(5370):1763-1766.

72. Crompton M (1999) The mitochondrial permeability transition pore and its role in cell death. *The Biochemical journal* 341 (Pt 2):233-249.

73. Jendrach M, *et al.* (2008) Short- and long-term alterations of mitochondrial morphology, dynamics and mtDNA after transient oxidative stress. *Mitochondrion* 8(4):293-304.

74. Twig G, *et al.* (2008) Fission and selective fusion govern mitochondrial segregation and elimination by autophagy. *The EMBO journal* 27(2):433-446.

75. Vincent AE, *et al.* (2017) Mitochondrial Nanotunnels. *Trends in cell biology* 27(11):787-799.

76. Doroshow JH (1983) Anthracycline antibiotic-stimulated superoxide, hydrogen peroxide, and hydroxyl radical production by NADH dehydrogenase. *Cancer research* 43(10):4543-4551.

77. Pawlowska J, *et al.* (2003) Differential ability of cytostatics from anthraquinone group to generate free radicals in three enzymatic systems: NADH dehydrogenase, NADPH cytochrome P450 reductase, and xanthine oxidase. *Oncology research* 13(5):245-252.

78. Doroshow JH & Davies KJ (1986) Redox cycling of anthracyclines by cardiac mitochondria. II. Formation of superoxide anion, hydrogen peroxide, and hydroxyl radical. *The Journal of biological chemistry* 261(7):3068-3074.

79. Polyakov N, *et al.* (2018) Redox-Active Quinone Chelators: Properties, Mechanisms of Action, Cell Delivery, and Cell Toxicity. *Antioxidants & redox signaling* 28(15):1394-1403.

80. Kehrer JP (2000) The Haber-Weiss reaction and mechanisms of toxicity. *Toxicology* 149(1):43-50.

81. Bohnson VL & Robertson AC (1923) THE CATALYTIC DECOMPOSITION OF HYDROGEN PEROXIDE BY FERRIC SALTS. II. *Journal of the American Chemical Society* 45(11):2493-2503.

82. Thomas CE & Aust SD (1986) Release of iron from ferritin by cardiotoxic anthracycline antibiotics. *Archives of biochemistry and biophysics* 248(2):684-689.

83. Simunek T, *et al.* (2009) Anthracycline-induced cardiotoxicity: overview of studies examining the roles of oxidative stress and free cellular iron. *Pharmacological reports : PR* 61(1):154-171.

84. Lipshultz SE, *et al.* (2010) Assessment of dexrazoxane as a cardioprotectant in doxorubicin-treated children with high-risk acute lymphoblastic leukaemia: long-term follow-up of a prospective, randomised, multicentre trial. *The Lancet. Oncology* 11(10):950-961.

85. Lipshultz SE, *et al.* (2012) Changes in cardiac biomarkers during doxorubicin treatment of pediatric patients with high-risk acute lymphoblastic leukemia: associations with long-term echocardiographic outcomes. *Journal of clinical oncology : official journal of the American Society of Clinical Oncology* 30(10):1042-1049.

86. Choi HS, *et al.* (2010) Dexrazoxane for preventing anthracycline cardiotoxicity in children with solid tumors. *Journal of Korean medical science* 25(9):1336-1342.

87. Sterba M, *et al.* (2013) Oxidative stress, redox signaling, and metal chelation in anthracycline cardiotoxicity and pharmacological cardioprotection. *Antioxidants & redox signaling* 18(8):899-929.

88. Jirkovská-Vávrová A, *et al.* (2015) Synthesis and analysis of novel analogues of dexrazoxane and its open-ring hydrolysis product for protection against anthracycline cardiotoxicity in vitro and in vivo. *Toxicology Research* 4(4):1098-1114.

89. Massion PB, *et al.* (2003) Nitric oxide and cardiac function: ten years after, and continuing. *Circulation research* 93(5):388-398.

90. Vasquez-Vivar J, *et al.* (1997) Endothelial nitric oxide synthase-dependent superoxide generation from adriamycin. *Biochemistry* 36(38):11293-11297.

91. Turko IV & Murad F (2002) Protein nitration in cardiovascular diseases. *Pharmacological reviews* 54(4):619-634.

92. Yamakura F, *et al.* (1998) Inactivation of human manganese-superoxide dismutase by peroxynitrite is caused by exclusive nitration of tyrosine 34 to 3-nitrotyrosine. *The Journal of biological chemistry* 273(23):14085-14089.

93. Radi R, *et al.* (2002) Peroxynitrite reactions and formation in mitochondria. *Free radical biology & medicine* 33(11):1451-1464.

94. Ahsan H (2013) 3-Nitrotyrosine: A biomarker of nitrogen free radical species modified proteins in systemic autoimmunogenic conditions. *Human immunology* 74(10):1392-1399.

95. Mukhopadhyay P, *et al.* (2009) Role of superoxide, nitric oxide, and peroxynitrite in doxorubicin-induced cell death in vivo and in vitro. *American journal of physiology. Heart and circulatory physiology* 296(5):H1466-1483.

96. Ascensao A, *et al.* (2011) Acute exercise protects against calcium-induced cardiac mitochondrial permeability transition pore opening in doxorubicin-treated rats. *Clinical science (London, England : 1979)* 120(1):37-49.

97. Chacon E, *et al.* (1992) A digitized-fluorescence-imaging study of mitochondrial Ca2+ increase by doxorubicin in cardiac myocytes. *The Biochemical journal* 281 (Pt 3):871-878.

98. Lebrecht D, *et al.* (2010) Respiratory chain deficiency precedes the disrupted calcium homeostasis in chronic doxorubicin cardiomyopathy. *Cardiovascular*

pathology : the official journal of the Society for Cardiovascular Pathology 19(5):e167-174.

99. McCormack JG & Denton RM (1993) Mitochondrial Ca2+ transport and the role of intramitochondrial Ca2+ in the regulation of energy metabolism. *Developmental neuroscience* 15(3-5):165-173.

100. Glancy B & Balaban RS (2012) Role of mitochondrial Ca2+ in the regulation of cellular energetics. *Biochemistry* 51(14):2959-2973.

101. Boucek RJ, Jr., *et al.* (1987) The major metabolite of doxorubicin is a potent inhibitor of membrane-associated ion pumps. A correlative study of cardiac muscle with isolated membrane fractions. *The Journal of biological chemistry* 262(33):15851-15856.

102. Olson RD, *et al.* (2005) Doxorubicin cardiac dysfunction: effects on calcium regulatory proteins, sarcoplasmic reticulum, and triiodothyronine. *Cardiovascular toxicology* 5(3):269-283.

103. Pereira GC, *et al.* (2011) Drug-induced cardiac mitochondrial toxicity and protection: from doxorubicin to carvedilol. *Current pharmaceutical design* 17(20):2113-2129.

104. Bernardi P, *et al.* (2006) The mitochondrial permeability transition from in vitro artifact to disease target. *The FEBS journal* 273(10):2077-2099.

105. Baines CP, *et al.* (2007) Voltage-dependent anion channels are dispensable for mitochondrial-dependent cell death. *Nature cell biology* 9(5):550-555.

106. Kokoszka JE, *et al.* (2004) The ADP/ATP translocator is not essential for the mitochondrial permeability transition pore. *Nature* 427(6973):461-465.

107. Crompton M, *et al.* (1988) Inhibition by cyclosporin A of a Ca2+-dependent pore in heart mitochondria activated by inorganic phosphate and oxidative stress. *The Biochemical journal* 255(1):357-360.

108. Basso E, *et al.* (2005) Properties of the permeability transition pore in mitochondria devoid of Cyclophilin D. *The Journal of biological chemistry* 280(19):18558-18561.

109. Baines CP, *et al.* (2005) Loss of cyclophilin D reveals a critical role for mitochondrial permeability transition in cell death. *Nature* 434(7033):658-662.

110. Giorgio V, *et al.* (2009) Cyclophilin D modulates mitochondrial F0F1-ATP synthase by interacting with the lateral stalk of the complex. *The Journal of biological chemistry* 284(49):33982-33988.

111. Perez MJ & Quintanilla RA (2017) Development or disease: duality of the mitochondrial permeability transition pore. *Developmental biology* 426(1):1-7.

112. Alavian KN, *et al.* (2014) An uncoupling channel within the c-subunit ring of the F1FO ATP synthase is the mitochondrial permeability transition pore. 111(29):10580-10585.

113. Jonas EA, *et al.* (2015) Cell death disguised: The mitochondrial permeability transition pore as the c-subunit of the F(1)F(O) ATP synthase. *Pharmacological research* 99:382-392.

114. Hansson MJ, *et al.* (2008) Calcium-induced generation of reactive oxygen species in brain mitochondria is mediated by permeability transition. *Free radical biology & medicine* 45(3):284-294.

115. Halestrap AP, *et al.* (2004) Mitochondrial permeability transition pore opening during myocardial reperfusion--a target for cardioprotection. *Cardiovascular research* 61(3):372-385.

116. Zorov DB, *et al.* (2014) Mitochondrial reactive oxygen species (ROS) and ROS-induced ROS release. *Physiological reviews* 94(3):909-950.

117. Gharanei M, *et al.* (2013) Doxorubicin induced myocardial injury is exacerbated following ischaemic stress via opening of the mitochondrial permeability transition pore. *Toxicology and applied pharmacology* 268(2):149-156.

118. Montaigne D, *et al.* (2011) Doxorubicin induces mitochondrial permeability transition and contractile dysfunction in the human myocardium. *Mitochondrion* 11(1):22-26.

119. Oliveira PJ & Wallace KB (2006) Depletion of adenine nucleotide translocator protein in heart mitochondria from doxorubicin-treated rats--relevance for mitochondrial dysfunction. *Toxicology* 220(2-3):160-168.

120. Kerr JF, *et al.* (1972) Apoptosis: a basic biological phenomenon with wide-ranging implications in tissue kinetics. *British journal of cancer* 26(4):239-257.

121. Pena-Blanco A & Garcia-Saez AJ (2018) Bax, Bak and beyond - mitochondrial performance in apoptosis. *The FEBS journal* 285(3):416-431.

122. Shamas-Din A, *et al.* (2011) BH3-only proteins: Orchestrators of apoptosis. *Biochimica et biophysica acta* 1813(4):508-520.

123. Gross A, *et al.* (1998) Enforced dimerization of BAX results in its translocation, mitochondrial dysfunction and apoptosis. *The EMBO journal* 17(14):3878-3885.

124. Wei MC, *et al.* (2000) tBID, a membrane-targeted death ligand, oligomerizes BAK to release cytochrome c. *Genes & development* 14(16):2060-2071.

125. Llambi F, *et al.* (2011) A unified model of mammalian BCL-2 protein family interactions at the mitochondria. *Molecular cell* 44(4):517-531.

126. Crawford ED & Wells JA (2011) Caspase substrates and cellular remodeling. *Annual review of biochemistry* 80:1055-1087.

127. Bratton SB & Salvesen GS (2010) Regulation of the Apaf-1-caspase-9 apoptosome. *Journal of cell science* 123(Pt 19):3209-3214.

128. Karch J, *et al.* (2013) Bax and Bak function as the outer membrane component of the mitochondrial permeability pore in regulating necrotic cell death in mice. *eLife* 2:e00772.

129. Caelles C, *et al.* (1994) p53-dependent apoptosis in the absence of transcriptional activation of p53-target genes. *Nature* 370(6486):220-223.

130. Marchenko ND & Moll UM (2014) Mitochondrial death functions of p53. *Molecular & cellular oncology* 1(2):e955995.

131. Zhang YW, *et al.* (2009) Cardiomyocyte death in doxorubicin-induced cardiotoxicity. *Archivum immunologiae et therapiae experimentalis* 57(6):435-445.

132. Maillet A, *et al.* (2016) Modeling Doxorubicin-Induced Cardiotoxicity in Human Pluripotent Stem Cell Derived-Cardiomyocytes. *Scientific reports* 6:25333.

133. Wei SN, *et al.* (2015) Microarray and Co-expression Network Analysis of Genes Associated with Acute Doxorubicin Cardiomyopathy in Mice. *Cardiovascular toxicology* 15(4):377-393.

134. Yang Y, *et al.* (2015) Effects of PPARalpha/PGC-1alpha on the energy metabolism remodeling and apoptosis in the doxorubicin induced mice cardiomyocytes in vitro. *International journal of clinical and experimental pathology* 8(10):12216-12224.

135. Minotti G, *et al.* (2004) Anthracyclines: molecular advances and pharmacologic developments in antitumor activity and cardiotoxicity. *Pharmacological reviews* 56(2):185-229.

136. Sardao VA, *et al.* (2009) Doxorubicin-induced mitochondrial dysfunction is secondary to nuclear p53 activation in H9c2 cardiomyoblasts. *Cancer chemotherapy and pharmacology* 64(4):811-827.

137. Branco AF, *et al.* (2012) Differentiation-dependent doxorubicin toxicity on H9c2 cardiomyoblasts. *Cardiovascular toxicology* 12(4):326-340.

138. Deus CM, *et al.* (2015) Stimulating basal mitochondrial respiration decreases doxorubicin apoptotic signaling in H9c2 cardiomyoblasts. *Toxicology* 334:1-11.

139. Youn HJ, *et al.* (2005) Induction of caspase-independent apoptosis in H9c2 cardiomyocytes by adriamycin treatment. *Molecular and cellular biochemistry* 270(1-2):13-19.

140. Moreira AC, *et al.* (2014) Mitochondrial apoptosis-inducing factor is involved in doxorubicin-induced toxicity on H9c2 cardiomyoblasts. *Biochimica et biophysica acta* 1842(12 Pt A):2468-2478.

141. Chen Q, *et al.* (2011) Activation of mitochondrial mu-calpain increases AIF cleavage in cardiac mitochondria during ischemia-reperfusion. *Biochemical and biophysical research communications* 415(4):533-538.

142. Wang L, *et al.* (2001) Preconditioning limits mitochondrial Ca(2+) during ischemia in rat hearts: role of K(ATP) channels. *American journal of physiology. Heart and circulatory physiology* 280(5):H2321-2328.

143. Lim CC, *et al.* (2004) Anthracyclines induce calpain-dependent titin proteolysis and necrosis in cardiomyocytes. *The Journal of biological chemistry* 279(9):8290-8299.

144. Konorev EA, *et al.* (2008) Differences in doxorubicin-induced apoptotic signaling in adult and immature cardiomyocytes. *Free radical biology & medicine* 45(12):1723-1728.

145. Pointon AV, *et al.* (2010) Doxorubicin in vivo rapidly alters expression and translation of myocardial electron transport chain genes, leads to ATP loss and caspase 3 activation. *PloS one* 5(9):e12733.

146. Ueno M, *et al.* (2006) Doxorubicin induces apoptosis by activation of caspase-3 in cultured cardiomyocytes in vitro and rat cardiac ventricles in vivo. *Journal of pharmacological sciences* 101(2):151-158.

147. Lee BS, *et al.* (2013) Protective effect of survivin in Doxorubicin-induced cell death in h9c2 cardiac myocytes. *Korean circulation journal* 43(6):400-407.

148. Xiao J, *et al.* (2012) Kaempferol protects against doxorubicin-induced cardiotoxicity in vivo and in vitro. *Toxicology* 292(1):53-62.

149. Capranico G, *et al.* (1992) Different patterns of gene expression of topoisomerase II isoforms in differentiated tissues during murine development. *Biochimica et biophysica acta* 1132(1):43-48.

150. Lyu YL, *et al.* (2007) Topoisomerase IIbeta mediated DNA double-strand breaks: implications in doxorubicin cardiotoxicity and prevention by dexrazoxane. *Cancer research* 67(18):8839-8846.

151. Vejpongsa P, *et al.* (2013) Abstract 11619: Topoisomerase 2ß Expression in Peripheral Blood Predicts Susceptibility to Anthracycline-Induced Cardiomyopathy. *Circulation* 128(suppl_22):A11619-A11619.

152. Vejpongsa P & Yeh ET (2014) Topoisomerase 2beta: a promising molecular target for primary prevention of anthracycline-induced cardiotoxicity. *Clinical pharmacology and therapeutics* 95(1):45-52.

153. Zhang S, *et al.* (2012) Identification of the molecular basis of doxorubicin-induced cardiotoxicity. *Nature medicine* 18(11):1639-1642.

154. Li H, *et al.* (1998) Cleavage of BID by caspase 8 mediates the mitochondrial damage in the Fas pathway of apoptosis. *Cell* 94(4):491-501.

155. Green DR & Llambi F (2015) Cell Death Signaling. *Cold Spring Harbor perspectives in biology* 7(12).

156. Niu J, *et al.* (2009) Cardiac-targeted expression of soluble fas attenuates doxorubicin-induced cardiotoxicity in mice. *The Journal of pharmacology and experimental therapeutics* 328(3):740-748.

157. Nakamura T, *et al.* (2000) Fas-mediated apoptosis in adriamycin-induced cardiomyopathy in rats: In vivo study. *Circulation* 102(5):572-578.

158. Vanden Berghe T, *et al.* (2014) Regulated necrosis: the expanding network of non-apoptotic cell death pathways. *Nature reviews. Molecular cell biology* 15(2):135-147.

159. Feoktistova M & Leverkus M (2015) Programmed necrosis and necroptosis signalling. *The FEBS journal* 282(1):19-31.

160. Shin HJ, *et al.* (2015) Doxorubicin-induced necrosis is mediated by poly-(ADP-ribose) polymerase 1 (PARP1) but is independent of p53. *Scientific reports* 5:15798.

161. Dhingra R, *et al.* (2014) Bnip3 mediates doxorubicin-induced cardiac myocyte necrosis and mortality through changes in mitochondrial signaling. *Proceedings of the National Academy of Sciences of the United States of America* 111(51):E5537-5544.

162. Hoyer-Hansen M, *et al.* (2007) Control of macroautophagy by calcium, calmodulin-dependent kinase kinase-beta, and Bcl-2. *Molecular cell* 25(2):193-205.

163. Kanamori H, *et al.* (2009) Functional significance and morphological characterization of starvation-induced autophagy in the adult heart. *The American journal of pathology* 174(5):1705-1714.

164. Sishi BJ, *et al.* (2013) Autophagy upregulation promotes survival and attenuates doxorubicin-induced cardiotoxicity. *Biochemical pharmacology* 85(1):124-134.

165. Kawaguchi T, *et al.* (2012) Prior starvation mitigates acute doxorubicin cardiotoxicity through restoration of autophagy in affected cardiomyocytes. *Cardiovascular research* 96(3):456-465.

166. Nishida K, *et al.* (2008) Crosstalk between autophagy and apoptosis in heart disease. *Circulation research* 103(4):343-351.

167. Levine B, *et al.* (2008) Bcl-2 family members: dual regulators of apoptosis and autophagy. *Autophagy* 4(5):600-606.

168. Lu L, *et al.* (2009) Adriamycin-induced autophagic cardiomyocyte death plays a pathogenic role in a rat model of heart failure. *International journal of cardiology* 134(1):82-90.

169. Smuder AJ, *et al.* (2013) Doxorubicin-induced markers of myocardial autophagic signaling in sedentary and exercise trained animals. *Journal of applied physiology (Bethesda, Md. : 1985)* 115(2):176-185.

170. Harris DA & Das AM (1991) Control of mitochondrial ATP synthesis in the heart. *The Biochemical journal* 280 (Pt 3):561-573.

171. Anonymous (*Blood*.

172. Bers DM (2002) Cardiac excitation-contraction coupling. *Nature* 415(6868):198-205.

173. Aon MA & Cortassa S (2012) Mitochondrial network energetics in the heart. *Wiley interdisciplinary reviews. Systems biology and medicine* 4(6):599-613.

174. Neubauer S (2007) The failing heart--an engine out of fuel. *The New England journal of medicine* 356(11):1140-1151.

175. Lopaschuk GD, *et al.* (1991) Glycolysis is predominant source of myocardial ATP production immediately after birth. *The American journal of physiology* 261(6 Pt 2):H1698-1705.

176. Kolwicz SC, Jr., *et al.* (2013) Cardiac metabolism and its interactions with contraction, growth, and survival of cardiomyocytes. *Circulation research* 113(5):603-616.

177. Stanley WC, *et al.* (2005) Myocardial substrate metabolism in the normal and failing heart. *Physiological reviews* 85(3):1093-1129.

178. Kaijser L & Berglund B (1992) Myocardial lactate extraction and release at rest and during heavy exercise in healthy men. *Acta physiologica Scandinavica* 144(1):39-45.

179. Wentz AE, *et al.* (2010) Adaptation of myocardial substrate metabolism to a ketogenic nutrient environment. *The Journal of biological chemistry* 285(32):24447-24456.

180. Jeyaseelan R, *et al.* (1997) Molecular mechanisms of doxorubicin-induced cardiomyopathy. Selective suppression of Reiske iron-sulfur protein, ADP/ATP translocase, and phosphofructokinase genes is associated with ATP depletion in rat cardiomyocytes. *The Journal of biological chemistry* 272(9):5828-5832.

181. Chaudhari U, *et al.* (2017) Metabolite signatures of doxorubicin induced toxicity in human induced pluripotent stem cell-derived cardiomyocytes. *Amino acids* 49(12):1955-1963.

182. Xia Y, *et al.* (2017) LCZ696 improves cardiac function via alleviating Drp1-mediated mitochondrial dysfunction in mice with doxorubicin-induced dilated cardiomyopathy. *Journal of molecular and cellular cardiology* 108:138-148.

183. Tokarska-Schlattner M, *et al.* (2006) Alterations in myocardial energy metabolism induced by the anti-cancer drug doxorubicin. *Comptes rendus biologies* 329(9):657-668.

184. Carvalho RA, *et al.* (2010) Metabolic remodeling associated with subchronic doxorubicin cardiomyopathy. *Toxicology* 270(2-3):92-98.

185. Tan G, *et al.* (2011) Potential biomarkers in mouse myocardium of doxorubicin-induced cardiomyopathy: a metabonomic method and its application. *PloS one* 6(11):e27683.

186. Strigun A, *et al.* (2012) Doxorubicin increases oxidative metabolism in HL-1 cardiomyocytes as shown by 13C metabolic flux analysis. *Toxicological sciences : an official journal of the Society of Toxicology* 125(2):595-606.

187. Wakasugi S, *et al.* (1993) Myocardial substrate utilization and left ventricular function in adriamycin cardiomyopathy. *Journal of nuclear medicine : official publication, Society of Nuclear Medicine* 34(9):1529-1535.

188. Berthiaume JM & Wallace KB (2007) Persistent alterations to the gene expression profile of the heart subsequent to chronic Doxorubicin treatment. *Cardiovascular toxicology* 7(3):178-191.

189. Abdel-aleem S, *et al.* (1997) Acute and chronic effects of adriamycin on fatty acid oxidation in isolated cardiac myocytes. *Journal of molecular and cellular cardiology* 29(2):789-797.

190. Yuan H, *et al.* (2016) A PGC-1alpha-Mediated Transcriptional Network Maintains Mitochondrial Redox and Bioenergetic Homeostasis against Doxorubicin-Induced Toxicity in Human Cardiomyocytes: Implementation of TT21C. *Toxicological sciences : an official journal of the Society of Toxicology* 150(2):400-417.

191. Buja LM & Vela D (2008) Cardiomyocyte death and renewal in the normal and diseased heart. *Cardiovascular pathology : the official journal of the Society for Cardiovascular Pathology* 17(6):349-374.

192. Patterson M, *et al.* (2017) Frequency of mononuclear diploid cardiomyocytes underlies natural variation in heart regeneration. 49(9):1346-1353.

193. Mollova M, *et al.* (2013) Cardiomyocyte proliferation contributes to heart growth in young humans. *Proceedings of the National Academy of Sciences of the United States of America* 110(4):1446-1451.

194. Alkass K, *et al.* (2015) No Evidence for Cardiomyocyte Number Expansion in Preadolescent Mice. *Cell* 163(4):1026-1036.

195. Vranas S, *et al.* (2017) Small size at birth predicts decreased cardiomyocyte number in the adult ovine heart. 8(5):618-625.

196. van Berlo JH, *et al.* (2014) c-kit+ cells minimally contribute cardiomyocytes to the heart. *Nature* 509(7500):337-341.

197. Noseda M, *et al.* (2015) The Quest for the Adult Cardiac Stem Cell. *Circulation journal : official journal of the Japanese Circulation Society* 79(7):1422-1430.

198. Ott HC, *et al.* (2007) The adult human heart as a source for stem cells: repair strategies with embryonic-like progenitor cells. *Nature clinical practice. Cardiovascular medicine* 4 Suppl 1:S27-39.

199. Hu S, *et al.* (2014) The influence of disease and age on human cardiac stem cells. *Annals of clinical biochemistry* 51(Pt 5):582-590.

200. Simpson DL, *et al.* (2012) A strong regenerative ability of cardiac stem cells derived from neonatal hearts. *Circulation* 126(11 Suppl 1):S46-53.

201. Godoy LY, *et al.* (1997) Anthracycline-induced cardiotoxicity in children with malignancies. *Acta paediatrica Japonica : Overseas edition* 39(2):188-193.

202. Strolin Benedetti M, *et al.* (2005) Differences in absorption, distribution, metabolism and excretion of xenobiotics between the paediatric and adult populations. *Expert opinion on drug metabolism & toxicology* 1(3):447-471.

203. Zhu W, *et al.* (2008) A mouse model for juvenile doxorubicin-induced cardiac dysfunction. *Pediatric research* 64(5):488-494.

204. Aihara Y, *et al.* (2000) Doxorubicin represses CARP gene transcription through the generation of oxidative stress in neonatal rat cardiac myocytes: possible role of serine/threonine kinase-dependent pathways. *Journal of molecular and cellular cardiology* 32(8):1401-1414.

205. Jeyaseelan R, *et al.* (1997) A novel cardiac-restricted target for doxorubicin. CARP, a nuclear modulator of gene expression in cardiac progenitor cells and cardiomyocytes. *The Journal of biological chemistry* 272(36):22800-22808.

206. Johnson D, *et al.* (1997) Cardiovascular responses to dynamic submaximal exercise in children previously treated with anthracycline. *American heart journal* 133(2):169-173.

207. Lebrecht D, *et al.* (2005) Tissue-specific mtDNA lesions and radical-associated mitochondrial dysfunction in human hearts exposed to doxorubicin. *The Journal of pathology* 207(4):436-444.

208. Richard C, *et al.* (2011) Oxidative stress and myocardial gene alterations associated with Doxorubicin-induced cardiotoxicity in rats persist for 2 months after treatment cessation. *The Journal of pharmacology and experimental therapeutics* 339(3):807-814.

209. Nordgren KKS, *et al.* (2017) Editor's Highlight: The Altered DNA Methylome of Chronic Doxorubicin Exposure in Sprague Dawley Rats. *Toxicological sciences : an official journal of the Society of Toxicology* 159(2):470-479.

210. Ferreira A, *et al.* (2017) Altered mitochondrial epigenetics associated with subchronic doxorubicin cardiotoxicity. *Toxicology* 390:63-73.

211. Gut P & Verdin E (2013) The nexus of chromatin regulation and intermediary metabolism. *Nature* 502(7472):489-498.

212. Menna P, *et al.* (2008) Cardiotoxicity of antitumor drugs. *Chemical research in toxicology* 21(5):978-989.

213. Stohr W, *et al.* (2006) Comparison of epirubicin and doxorubicin cardiotoxicity in children and adolescents treated within the German Cooperative Soft Tissue Sarcoma Study (CWS). *Journal of cancer research and clinical oncology* 132(1):35-40.

214. van Dalen EC, *et al.* (2004) Cumulative incidence and risk factors of mitoxantrone-induced cardiotoxicity in children: a systematic review. *European journal of cancer (Oxford, England : 1990)* 40(5):643-652.

215. Kotwinski P, *et al.* (2016) Body Surface Area and Baseline Blood Pressure Predict Subclinical Anthracycline Cardiotoxicity in Women Treated for Early Breast Cancer. *PloS one* 11(12):e0165262.

216. Iarussi D, *et al.* (1994) Protective effect of coenzyme Q10 on anthracyclines cardiotoxicity: control study in children with acute lymphoblastic leukemia and non-Hodgkin lymphoma. *Molecular aspects of medicine* 15 Suppl:s207-212.

217. Oliveira PJ, *et al.* (2004) Carvedilol-mediated antioxidant protection against doxorubicin-induced cardiac mitochondrial toxicity. *Toxicology and applied pharmacology* 200(2):159-168.

218. Santos DL, *et al.* (2002) Carvedilol protects against doxorubicin-induced mitochondrial cardiomyopathy. *Toxicology and applied pharmacology* 185(3):218-227.

219. Kalay N, *et al.* (2006) Protective effects of carvedilol against anthracycline-induced cardiomyopathy. *Journal of the American College of Cardiology* 48(11):2258-2262.

220. Liao JK (2002) Beyond lipid lowering: the role of statins in vascular protection. *International journal of cardiology* 86(1):5-18.

221. Acar Z, *et al.* (2011) Efficiency of atorvastatin in the protection of anthracycline-induced cardiomyopathy. *Journal of the American College of Cardiology* 58(9):988-989.

222. Chotenimitkhun R, *et al.* (2015) Chronic statin administration may attenuate early anthracycline-associated declines in left ventricular ejection function. *The Canadian journal of cardiology* 31(3):302-307.

223. Henninger C & Fritz G (2017) Statins in anthracycline-induced cardiotoxicity: Rac and Rho, and the heartbreakers. *Cell death & disease* 8(1):e2564.

224. Marty M, *et al.* (2006) Multicenter randomized phase III study of the cardioprotective effect of dexrazoxane (Cardioxane) in advanced/metastatic breast cancer patients treated with anthracycline-based chemotherapy. *Annals of oncology : official journal of the European Society for Medical Oncology* 17(4):614-622.

225. Swain SM & Vici P (2004) The current and future role of dexrazoxane as a cardioprotectant in anthracycline treatment: expert panel review. *Journal of cancer research and clinical oncology* 130(1):1-7.

226. Elbl L, *et al.* (2006) Late anthracycline cardiotoxicity protection by dexrazoxane (ICRF-187) in pediatric patients: echocardiographic follow-up. *Supportive care in cancer : official journal of the Multinational Association of Supportive Care in Cancer* 14(2):128-136.

227. Deng S, *et al.* (2014) Dexrazoxane may prevent doxorubicin-induced DNA damage via depleting both topoisomerase II isoforms. *BMC cancer* 14:842.

228. Duncan EJ, *et al.* (2014) Epigenetics, plasticity, and evolution: How do we link epigenetic change to phenotype? *Journal of experimental zoology. Part B, Molecular and developmental evolution* 322(4):208-220.

229. Stein R, *et al.* (1982) Clonal inheritance of the pattern of DNA methylation in mouse cells. *Proceedings of the National Academy of Sciences of the United States of America* 79(1):61-65.

230. Miranda TB & Jones PA (2007) DNA methylation: the nuts and bolts of repression. *Journal of cellular physiology* 213(2):384-390.

231. Jones PA & Liang G (2009) Rethinking how DNA methylation patterns are maintained. *Nature reviews. Genetics* 10(11):805-811.

232. Hendrich B & Tweedie S (2003) The methyl-CpG binding domain and the evolving role of DNA methylation in animals. *Trends in genetics : TIG* 19(5):269-277.

233. Okano M, *et al.* (1999) DNA methyltransferases Dnmt3a and Dnmt3b are essential for de novo methylation and mammalian development. *Cell* 99(3):247-257.

234. Iacobazzi V, *et al.* (2013) Mitochondrial DNA methylation as a next-generation biomarker and diagnostic tool. *Molecular genetics and metabolism* 110(1-2):25-34.

235. Tahiliani M, *et al.* (2009) Conversion of 5-methylcytosine to 5-hydroxymethylcytosine in mammalian DNA by MLL partner TET1. *Science (New York, N.Y.)* 324(5929):930-935.

236. Xiao M, *et al.* (2012) Inhibition of alpha-KG-dependent histone and DNA demethylases by fumarate and succinate that are accumulated in mutations of FH and SDH tumor suppressors. *Genes & development* 26(12):1326-1338.

237. Letouze E, *et al.* (2013) SDH mutations establish a hypermethylator phenotype in paraganglioma. *Cancer cell* 23(6):739-752.

238. Killian JK, *et al.* (2013) Succinate dehydrogenase mutation underlies global epigenomic divergence in gastrointestinal stromal tumor. *Cancer discovery* 3(6):648-657.

239. Castro-Vega LJ, *et al.* (2014) Germline mutations in FH confer predisposition to malignant pheochromocytomas and paragangliomas. *Human molecular genetics* 23(9):2440-2446.

240. Hebbes TR, *et al.* (1988) A direct link between core histone acetylation and transcriptionally active chromatin. *The EMBO journal* 7(5):1395-1402.

241. Braunstein M, *et al.* (1993) Transcriptional silencing in yeast is associated with reduced nucleosome acetylation. *Genes & development* 7(4):592-604.

242. Dawson MA, *et al.* (2012) Targeting epigenetic readers in cancer. *The New England journal of medicine* 367(7):647-657.

243. Marmorstein R & Roth SY (2001) Histone acetyltransferases: function, structure, and catalysis. *Current opinion in genetics & development* 11(2):155-161.

244. Buhr ED & Takahashi JS (2013) Molecular components of the Mammalian circadian clock. *Handbook of experimental pharmacology* (217):3-27.

245. Guo H, *et al.* (2006) Suprachiasmatic regulation of circadian rhythms of gene expression in hamster peripheral organs: effects of transplanting the pacemaker. *The Journal of neuroscience : the official journal of the Society for Neuroscience* 26(24):6406-6412.

246. Stephan FK & Zucker I (1972) Circadian rhythms in drinking behavior and locomotor activity of rats are eliminated by hypothalamic lesions. *Proceedings of the National Academy of Sciences of the United States of America* 69(6):1583-1586.

247. Eastman CI, *et al.* (1984) Suprachiasmatic nuclei lesions eliminate circadian temperature and sleep rhythms in the rat. *Physiology & behavior* 32(3):357-368.

248. Drucker-Colin R, *et al.* (1984) Fetal suprachiasmatic nucleus transplants: diurnal rhythm recovery of lesioned rats. *Brain research* 311(2):353-357.

249. Baeza-Raja B, *et al.* (2013) p75 neurotrophin receptor is a clock gene that regulates oscillatory components of circadian and metabolic networks. *The Journal of neuroscience : the official journal of the Society for Neuroscience* 33(25):10221-10234.

250. Duffy JF, *et al.* (2011) Sex difference in the near-24-hour intrinsic period of the human circadian timing system. *Proceedings of the National Academy of Sciences of the United States of America* 108 Suppl 3:15602-15608.

251. Stokkan KA, *et al.* (2001) Entrainment of the circadian clock in the liver by feeding. *Science (New York, N.Y.)* 291(5503):490-493.

252. Damiola F, *et al.* (2000) Restricted feeding uncouples circadian oscillators in peripheral tissues from the central pacemaker in the suprachiasmatic nucleus. *Genes & development* 14(23):2950-2961.

253. Bechtold DA, *et al.* (2010) Circadian dysfunction in disease. *Trends in pharmacological sciences* 31(5):191-198.

254. Zee PC, *et al.* (2013) Circadian rhythm abnormalities. *Continuum (Minneapolis, Minn.)* 19(1 Sleep Disorders):132-147.

255. Hatori M, *et al.* (2012) Time-restricted feeding without reducing caloric intake prevents metabolic diseases in mice fed a high-fat diet. *Cell metabolism* 15(6):848-860.

256. Panda S, *et al.* (2002) Coordinated transcription of key pathways in the mouse by the circadian clock. *Cell* 109(3):307-320.

257. Gekakis N, *et al.* (1998) Role of the CLOCK protein in the mammalian circadian mechanism. *Science (New York, N.Y.)* 280(5369):1564-1569.

258. Busino L, *et al.* (2007) SCFFbxl3 controls the oscillation of the circadian clock by directing the degradation of cryptochrome proteins. *Science (New York, N.Y.)* 316(5826):900-904.

259. Hirano A, *et al.* (2013) FBXL21 regulates oscillation of the circadian clock through ubiquitination and stabilization of cryptochromes. *Cell* 152(5):1106-1118.

260. Kurabayashi N, *et al.* (2006) Phosphorylation of mCRY2 at Ser557 in the hypothalamic suprachiasmatic nucleus of the mouse. *Chronobiology international* 23(1-2):129-134.

261. Reppert SM & Weaver DR (2002) Coordination of circadian timing in mammals. *Nature* 418(6901):935-941.

262. Berger SL & Sassone-Corsi P (2016) Metabolic Signaling to Chromatin. *Cold Spring Harbor perspectives in biology* 8(11).

263. Aguilar-Arnal L & Sassone-Corsi P (2013) The circadian epigenome: how metabolism talks to chromatin remodeling. *Current opinion in cell biology* 25(2):170-176.

264. Doi M, *et al.* (2006) Circadian regulator CLOCK is a histone acetyltransferase. *Cell* 125(3):497-508.

265. Etchegaray JP, *et al.* (2003) Rhythmic histone acetylation underlies transcription in the mammalian circadian clock. *Nature* 421(6919):177-182.

266. Nakahata Y, *et al.* (2008) The NAD+-dependent deacetylase SIRT1 modulates CLOCK-mediated chromatin remodeling and circadian control. *Cell* 134(2):329-340.

267. Asher G, *et al.* (2008) SIRT1 regulates circadian clock gene expression through PER2 deacetylation. *Cell* 134(2):317-328.

268. Hirayama J, *et al.* (2007) CLOCK-mediated acetylation of BMAL1 controls circadian function. *Nature* 450(7172):1086-1090.

269. Sahar S, *et al.* (2014) Circadian control of fatty acid elongation by SIRT1 protein-mediated deacetylation of acetyl-coenzyme A synthetase 1. *The Journal of biological chemistry* 289(9):6091-6097.

270. Katada S & Sassone-Corsi P (2010) The histone methyltransferase MLL1 permits the oscillation of circadian gene expression. *Nature structural & molecular biology* 17(12):1414-1421.

271. Brown SA (2016) Circadian Metabolism: From Mechanisms to Metabolomics and Medicine. *Trends in endocrinology and metabolism: TEM* 27(6):415-426.

272. Sancar G & Brunner M (2014) Circadian clocks and energy metabolism. *Cellular and molecular life sciences : CMLS* 71(14):2667-2680.

273. Dallmann R, *et al.* (2012) The human circadian metabolome. *Proceedings of the National Academy of Sciences of the United States of America* 109(7):2625-2629.

274. Edery I (2000) Circadian rhythms in a nutshell. *Physiological genomics* 3(2):59-74.

275. Bailey SM, *et al.* (2014) Circadian regulation of metabolism. *The Journal of endocrinology* 222(2):R75-96.

276. Eckel-Mahan KL, *et al.* (2012) Coordination of the transcriptome and metabolome by the circadian clock. *Proceedings of the National Academy of Sciences of the United States of America* 109(14):5541-5546.

277. Nakahata Y, *et al.* (2009) Circadian control of the NAD+ salvage pathway by CLOCK-SIRT1. *Science (New York, N.Y.)* 324(5927):654-657.

278. Masri S & Sassone-Corsi P (2014) Sirtuins and the circadian clock: bridging chromatin and metabolism. *Science signaling* 7(342):re6.

279. Bellet MM, *et al.* (2016) Histone Deacetylase SIRT1 Controls Proliferation, Circadian Rhythm, and Lipid Metabolism during Liver Regeneration in Mice. *The Journal of biological chemistry* 291(44):23318-23329.

280. Bellet MM, *et al.* (2013) Pharmacological modulation of circadian rhythms by synthetic activators of the deacetylase SIRT1. *Proceedings of the National Academy of Sciences of the United States of America* 110(9):3333-3338.

281. Aguilar-Arnal L, *et al.* (2015) NAD(+)-SIRT1 control of H3K4 trimethylation through circadian deacetylation of MLL1. *Nature structural & molecular biology* 22(4):312-318.

282. Masri S, *et al.* (2014) Partitioning circadian transcription by SIRT6 leads to segregated control of cellular metabolism. *Cell* 158(3):659-672.

283. Feldman JL, *et al.* (2013) Activation of the protein deacetylase SIRT6 by long-chain fatty acids and widespread deacylation by mammalian sirtuins. *The Journal of biological chemistry* 288(43):31350-31356.

284. Asher G, *et al.* (2010) Poly(ADP-ribose) polymerase 1 participates in the phase entrainment of circadian clocks to feeding. *Cell* 142(6):943-953.

285. Bai P, *et al.* (2011) PARP-1 inhibition increases mitochondrial metabolism through SIRT1 activation. *Cell metabolism* 13(4):461-468.

286. Wellen KE & Thompson CB (2012) A two-way street: reciprocal regulation of metabolism and signalling. *Nature reviews. Molecular cell biology* 13(4):270-276.

287. Pietrocola F, *et al.* (2015) Acetyl coenzyme A: a central metabolite and second messenger. *Cell metabolism* 21(6):805-821.

288. Weinert BT, *et al.* (2014) Acetylation dynamics and stoichiometry in Saccharomyces cerevisiae. *Molecular systems biology* 10:716.

289. Mauvoisin D, *et al.* (2014) Circadian clock-dependent and -independent rhythmic proteomes implement distinct diurnal functions in mouse liver. *Proceedings of the National Academy of Sciences of the United States of America* 111(1):167-172.

290. Peek CB, *et al.* (2013) Circadian clock NAD+ cycle drives mitochondrial oxidative metabolism in mice. *Science (New York, N.Y.)* 342(6158):1243417.

291. Yamazaki S, *et al.* (1994) Circadian rhythms of adenosine triphosphate contents in the suprachiasmatic nucleus, anterior hypothalamic area and caudate putamen of the rat--negative correlation with electrical activity. *Brain research* 664(1-2):237-240.

292. Cela O, *et al.* (2016) Clock genes-dependent acetylation of complex I sets rhythmic activity of mitochondrial OxPhos. *Biochimica et biophysica acta* 1863(4):596-606.

293. Neufeld-Cohen A, *et al.* (2016) Circadian control of oscillations in mitochondrial rate-limiting enzymes and nutrient utilization by PERIOD proteins. *Proceedings of the National Academy of Sciences of the United States of America* 113(12):E1673-1682.

294. Jacobi D, *et al.* (2015) Hepatic Bmal1 Regulates Rhythmic Mitochondrial Dynamics and Promotes Metabolic Fitness. *Cell metabolism* 22(4):709-720.

295. Masri S, *et al.* (2013) Circadian acetylome reveals regulation of mitochondrial metabolic pathways. *Proceedings of the National Academy of Sciences of the United States of America* 110(9):3339-3344.

296. Baeza J, *et al.* (2016) Mechanisms and Dynamics of Protein Acetylation in Mitochondria. *Trends in biochemical sciences* 41(3):231-244.

297. Putker M & O'Neill JS (2016) Reciprocal Control of the Circadian Clock and Cellular Redox State - a Critical Appraisal. *Molecules and cells* 39(1):6-19.

298. Tamaru T, *et al.* (2013) ROS stress resets circadian clocks to coordinate pro-survival signals. *PloS one* 8(12):e82006.

299. O'Neill JS & Reddy AB (2011) Circadian clocks in human red blood cells. *Nature* 469(7331):498-503.

300. Rhee SG & Kil IS (2016) Mitochondrial H2O2 signaling is controlled by the concerted action of peroxiredoxin III and sulfiredoxin: Linking mitochondrial function to circadian rhythm. *Free radical biology & medicine* 99:120-127.

301. Kil IS, *et al.* (2012) Feedback control of adrenal steroidogenesis via H2O2-dependent, reversible inactivation of peroxiredoxin III in mitochondria. *Molecular cell* 46(5):584-594.

302. Palacios OM, *et al.* (2009) Diet and exercise signals regulate SIRT3 and activate AMPK and PGC-1alpha in skeletal muscle. *Aging* 1(9):771-783.

303. Hirschey MD, *et al.* (2010) SIRT3 regulates mitochondrial fatty-acid oxidation by reversible enzyme deacetylation. *Nature* 464(7285):121-125.

304. Lamia KA, *et al.* (2009) AMPK regulates the circadian clock by cryptochrome phosphorylation and degradation. *Science (New York, N.Y.)* 326(5951):437-440.

305. Lemberger T, *et al.* (1996) Expression of the peroxisome proliferator-activated receptor alpha gene is stimulated by stress and follows a diurnal rhythm. *The Journal of biological chemistry* 271(3):1764-1769.

306. Yang X, *et al.* (2006) Nuclear receptor expression links the circadian clock to metabolism. *Cell* 126(4):801-810.

307. Tsimakouridze EV, *et al.* (2015) Therapeutic applications of circadian rhythms for the cardiovascular system. *Frontiers in pharmacology* 6:77.

308. Mistry P, *et al.* (2017) Cardiac Clocks and Preclinical Translation. *Heart failure clinics* 13(4):657-672.

309. Lee KW, *et al.* (2005) High pulse pressure and nondipping circadian blood pressure in patients with coronary artery disease: Relationship to thrombogenesis and endothelial damage/dysfunction. *American journal of hypertension* 18(1):104-115.

310. Sack RL, *et al.* (1992) Melatonin rhythms in night shift workers. *Sleep* 15(5):434-441.

311. James FO, *et al.* (2004) Controlled exposure to light and darkness realigns the salivary cortisol rhythm in night shift workers. *Chronobiology international* 21(6):961-972.

312. Knutsson A, *et al.* (1986) Increased risk of ischaemic heart disease in shift workers. *Lancet (London, England)* 2(8498):89-92.

313. Virag JA & Lust RM (2014) Circadian influences on myocardial infarction. *Frontiers in physiology* 5:422.

314. Hardeland R, *et al.* (2003) Circadian rhythms, oxidative stress, and antioxidative defense mechanisms. *Chronobiology international* 20(6):921-962.

315. Galano A, *et al.* (2013) On the free radical scavenging activities of melatonin's metabolites, AFMK and AMK. *Journal of pineal research* 54(3):245-257.

316. Storch KF, *et al.* (2002) Extensive and divergent circadian gene expression in liver and heart. *Nature* 417(6884):78-83.

317. Martino T, *et al.* (2004) Day/night rhythms in gene expression of the normal murine heart. *Journal of molecular medicine (Berlin, Germany)* 82(4):256-264.

318. Kohsaka A, *et al.* (2014) The circadian clock maintains cardiac function by regulating mitochondrial metabolism in mice. *PloS one* 9(11):e112811.

319. Tsai JY, *et al.* (2010) Direct regulation of myocardial triglyceride metabolism by the cardiomyocyte circadian clock. *The Journal of biological chemistry* 285(5):2918-2929.

320. Vukolic A, *et al.* (2010) Role of mutation of the circadian clock gene Per2 in cardiovascular circadian rhythms. *American journal of physiology. Regulatory, integrative and comparative physiology* 298(3):R627-634.

321. Bonney S, *et al.* (2013) Cardiac Per2 functions as novel link between fatty acid metabolism and myocardial inflammation during ischemia and reperfusion injury of the heart. *PloS one* 8(8):e71493.

322. Sun YY, *et al.* (2014) Period 2 is essential to maintain early endothelial progenitor cell function in vitro and angiogenesis after myocardial infarction in mice. *Journal of cellular and molecular medicine* 18(5):907-918.

323. Mericskay M (2016) Nicotinamide adenine dinucleotide homeostasis and signalling in heart disease: Pathophysiological implications and therapeutic potential. *Archives of cardiovascular diseases* 109(3):207-215.

324. Hershberger KA, *et al.* (2017) Role of NAD(+) and mitochondrial sirtuins in cardiac and renal diseases. *Nature reviews. Nephrology* 13(4):213-225.

325. Mori V, *et al.* (2014) Metabolic profiling of alternative NAD biosynthetic routes in mouse tissues. *PloS one* 9(11):e113939.

326. Hsu CP, *et al.* (2009) Nicotinamide phosphoribosyltransferase regulates cell survival through NAD+ synthesis in cardiac myocytes. *Circulation research* 105(5):481-491.

327. Levi F, *et al.* (2010) Circadian timing in cancer treatments. *Annual review of pharmacology and toxicology* 50:377-421.

328. Gachon F, *et al.* (2006) The circadian PAR-domain basic leucine zipper transcription factors DBP, TEF, and HLF modulate basal and inducible xenobiotic detoxification. *Cell metabolism* 4(1):25-36.

329. Inoue N, *et al.* (1999) Circadian variation of hepatic glutathione S-transferase activities in the mouse. *Xenobiotica; the fate of foreign compounds in biological systems* 29(1):43-51.

330. Canal P, *et al.* (1991) Chronopharmacokinetics of doxorubicin in patients with breast cancer. *European journal of clinical pharmacology* 40(3):287-291.

331. Granda TG, *et al.* (2001) Experimental chronotherapy of mouse mammary adenocarcinoma MA13/C with docetaxel and doxorubicin as single agents and in combination. *Cancer research* 61(5):1996-2001.

332. Sothern RB, *et al.* (1989) Control of a murine plasmacytoma with doxorubicin-cisplatin: dependence on circadian stage of treatment. *Journal of the National Cancer Institute* 81(2):135-145.

333. To H, *et al.* (2003) Dosing time dependency of doxorubicin-induced cardiotoxicity and bone marrow toxicity in rats. *The Journal of pharmacy and pharmacology* 55(6):803-810.

334. Borniger JC, *et al.* (2017) Time-of-Day Dictates Transcriptional Inflammatory Responses to Cytotoxic Chemotherapy. *Scientific reports* 7:41220.

335. Dierickx P, *et al.* (2017) Circadian networks in human embryonic stem cell-derived cardiomyocytes. 18(7):1199-1212.

336. Leonardo-Mendonca RC, *et al.* (2015) The benefits of four weeks of melatonin treatment on circadian patterns in resistance-trained athletes. *Chronobiology international* 32(8):1125-1134.

337. Burke TM, *et al.* (2013) Combination of light and melatonin time cues for phase advancing the human circadian clock. *Sleep* 36(11):1617-1624.

338. Chen Z, *et al.* (2012) Identification of diverse modulators of central and peripheral circadian clocks by high-throughput chemical screening. *Proceedings of the National Academy of Sciences of the United States of America* 109(1):101-106.

339. Chun SK, *et al.* (2014) Identification and validation of cryptochrome inhibitors that modulate the molecular circadian clock. *ACS chemical biology* 9(3):703-710.

340. Lee J, *et al.* (2016) Identification of a novel circadian clock modulator controlling BMAL1 expression through a ROR/REV-ERB-response element-dependent mechanism. *Biochemical and biophysical research communications* 469(3):580-586.

341. Kusunose N, *et al.* (2015) Mitomycin C modulates the circadian oscillation of clock gene period 2 expression through attenuating the glucocorticoid signaling in mouse fibroblasts. *Biochemical and biophysical research communications* 467(1):157-163.

342. Dojo K, *et al.* (2017) Carbachol Induces Phase-dependent Phase Shifts of Per1 Transcription Rhythms in Cultured Suprachiasmatic Nucleus Slices. *Journal of biological rhythms* 32(2):101-108.

343. Logan RW, *et al.* (2014) Circadian rhythms and addiction: mechanistic insights and future directions. *Behavioral neuroscience* 128(3):387-412.

344. Zhou P, *et al.* (2014) Disturbances in the murine hepatic circadian clock in alcohol-induced hepatic steatosis. *Scientific reports* 4:3725.

345. Summa KC, *et al.* (2015) Chronic Alcohol Exposure and the Circadian Clock Mutation Exert Tissue-Specific Effects on Gene Expression in Mouse Hippocampus, Liver, and Proximal Colon. *Alcoholism, clinical and experimental research* 39(10):1917-1929.

346. Hwang JW, *et al.* (2014) Circadian clock function is disrupted by environmental tobacco/cigarette smoke, leading to lung inflammation and injury via a SIRT1-BMAL1 pathway. *FASEB journal : official publication of the Federation of American Societies for Experimental Biology* 28(1):176-194.

347. Narishige S, *et al.* (2014) Effects of caffeine on circadian phase, amplitude and period evaluated in cells in vitro and peripheral organs in vivo in PER2::LUCIFERASE mice. *British journal of pharmacology* 171(24):5858-5869.

348. Burke TM, *et al.* (2015) Effects of caffeine on the human circadian clock in vivo and in vitro. *Science translational medicine* 7(305):305ra146.

349. Coelho AR, *et al.* (2017) Berberine-induced cardioprotection and Sirt3 modulation in doxorubicin-treated H9c2 cardiomyoblasts. *Biochimica et biophysica acta. Molecular basis of disease* 1863(11):2904-2923.

350. Kimes BW & Brandt BL (1976) Properties of a clonal muscle cell line from rat heart. *Experimental cell research* 98(2):367-381.

351. Branco AF, *et al.* (2015) Gene Expression Profiling of H9c2 Myoblast Differentiation towards a Cardiac-Like Phenotype. *PloS one* 10(6):e0129303.

352. Lenco J, *et al.* (2015) Proteomic investigation of embryonic rat heart-derived H9c2 cell line sheds new light on the molecular phenotype of the popular cell model. *Experimental cell research* 339(2):174-186.

353. Branco AF, *et al.* (2011) Isoproterenol cytotoxicity is dependent on the differentiation state of the cardiomyoblast H9c2 cell line. *Cardiovascular toxicology* 11(3):191-203.

354. Menard C, *et al.* (1999) Modulation of L-type calcium channel expression during retinoic acid-induced differentiation of H9C2 cardiac cells. *The Journal of biological chemistry* 274(41):29063-29070.

355. Sipido KR & Marban E (1991) L-type calcium channels, potassium channels, and novel nonspecific cation channels in a clonal muscle cell line derived from embryonic rat ventricle. *Circulation research* 69(6):1487-1499.

356. Mejia-Alvarez R, *et al.* (1994) Simultaneous expression of cardiac and skeletal muscle isoforms of the L-type Ca2+ channel in a rat heart muscle cell line. *The Journal of physiology* 478 (Pt 2):315-329.

357. Watkins SJ, *et al.* (2011) The H9C2 cell line and primary neonatal cardiomyocyte cells show similar hypertrophic responses in vitro. *In vitro cellular & developmental biology. Animal* 47(2):125-131.

358. Kolossov E, *et al.* (2006) Engraftment of engineered ES cell-derived cardiomyocytes but not BM cells restores contractile function to the infarcted myocardium. *The Journal of experimental medicine* 203(10):2315-2327.

359. Gan L, *et al.* (2014) Transcriptome analysis in cardiomyocyte-specific differentiation of murine embryonic stem cells reveals transcriptional regulation network. *Gene expression patterns : GEP* 16(1):8-22.

360. Himmel HM (2013) Drug-induced functional cardiotoxicity screening in stem cell-derived human and mouse cardiomyocytes: effects of reference compounds. *Journal of pharmacological and toxicological methods* 68(1):97-111.

361. Abassi YA, *et al.* (2012) Dynamic monitoring of beating periodicity of stem cell-derived cardiomyocytes as a predictive tool for preclinical safety assessment. *British journal of pharmacology* 165(5):1424-1441.

362. Pasqualini FS, *et al.* (2015) Structural phenotyping of stem cell-derived cardiomyocytes. *Stem cell reports* 4(3):340-347.

363. Doevendans PA, *et al.* (1998) Cardiovascular phenotyping in mice. *Cardiovascular research* 39(1):34-49.

364. Blank S, *et al.* (1989) Biochemical characteristics of mammalian myocardia. *Journal of molecular and cellular cardiology* 21(4):367-373.

365. Barth E, *et al.* (1992) Ultrastructural quantitation of mitochondria and myofilaments in cardiac muscle from 10 different animal species including man. *Journal of molecular and cellular cardiology* 24(7):669-681.

366. Zhao Y, *et al.* (2014) Redox proteomic identification of HNE-bound mitochondrial proteins in cardiac tissues reveals a systemic effect on energy metabolism after doxorubicin treatment. *Free radical biology & medicine* 72:55-65.

367. Ruan Y, *et al.* (2015) SIRT1 suppresses doxorubicin-induced cardiotoxicity by regulating the oxidative stress and p38MAPK pathways. *Cellular physiology and biochemistry : international journal of experimental cellular physiology, biochemistry, and pharmacology* 35(3):1116-1124.

368. Henninger C, *et al.* (2015) Chronic heart damage following doxorubicin treatment is alleviated by lovastatin. *Pharmacological research* 91:47-56.

369. Yarana C, *et al.* (2018) Extracellular Vesicles Released by Cardiomyocytes in a Doxorubicin-Induced Cardiac Injury Mouse Model Contain Protein Biomarkers of Early Cardiac Injury. *Clinical cancer research : an official journal of the American Association for Cancer Research* 24(7):1644-1653.

370. Yuan YP, *et al.* (2018) CTRP3 protected against doxorubicin-induced cardiac dysfunction, inflammation and cell death via activation of Sirt1. *Journal of molecular and cellular cardiology* 114:38-47.

371. Berthiaume JM & Wallace KB (2007) Adriamycin-induced oxidative mitochondrial cardiotoxicity. *Cell biology and toxicology* 23(1):15-25.

372. Serrano J, *et al.* (1999) Cardioselective and cumulative oxidation of mitochondrial DNA following subchronic doxorubicin administration. *Biochimica et biophysica acta* 1411(1):201-205.

373. Zhou S, *et al.* (2001) Doxorubicin-induced persistent oxidative stress to cardiac myocytes. *Toxicology letters* 121(3):151-157.

374. De Angelis A, *et al.* (2010) Anthracycline cardiomyopathy is mediated by depletion of the cardiac stem cell pool and is rescued by restoration of progenitor cell function. *Circulation* 121(2):276-292.

375. Vichai V & Kirtikara K (2006) Sulforhodamine B colorimetric assay for cytotoxicity screening. *Nature protocols* 1(3):1112-1116.

376. Skehan P, *et al.* (1990) New colorimetric cytotoxicity assay for anticancer-drug screening. *Journal of the National Cancer Institute* 82(13):1107-1112.

377. Silva FS, *et al.* (2016) Determination of Metabolic Viability and Cell Mass Using a Tandem Resazurin/Sulforhodamine B Assay. *Current protocols in toxicology* 68:2.24.21-22.24.15.

378. Brand MD & Nicholls DG (2011) Assessing mitochondrial dysfunction in cells. *The Biochemical journal* 435(2):297-312.

379. Dimauro I, *et al.* (2012) A simple protocol for the subcellular fractionation of skeletal muscle cells and tissue. *BMC research notes* 5:513.

380. Abhyankar A, *et al.* (2009) Comparative sequence analysis of the non-protein-coding mitochondrial DNA of inbred rat strains. *PloS one* 4(12):e8148.

381. Bellizzi D, *et al.* (2013) The control region of mitochondrial DNA shows an unusual CpG and non-CpG methylation pattern. *DNA research : an international journal for rapid publication of reports on genes and genomes* 20(6):537-547.

382. He B, *et al.* (2018) Melatonin-induced increase of lipid droplets accumulation and in vitro maturation in porcine oocytes is mediated by mitochondrial quiescence. 233(1):302-312.

383. Merten KE, *et al.* (2006) Calcineurin activation is not necessary for Doxorubicin-induced hypertrophy in H9c2 embryonic rat cardiac cells: involvement of the phosphoinositide 3-kinase-Akt pathway. *The Journal of pharmacology and experimental therapeutics* 319(2):934-940.

384. Pillai VB, *et al.* (2016) Sirt3 protects mitochondrial DNA damage and blocks the development of doxorubicin-induced cardiomyopathy in mice. *American journal of physiology. Heart and circulatory physiology* 310(8):H962-972.

385. Oyama K, *et al.* (2011) Hydrogen peroxide induces cell cycle arrest in cardiomyoblast H9c2 cells, which is related to hypertrophy. *Biological & pharmaceutical bulletin* 34(4):501-506.

386. Garner E & Raj K (2008) Protective mechanisms of p53-p21-pRb proteins against DNA damage-induced cell death. *Cell cycle (Georgetown, Tex.)* 7(3):277-282.

387. Venkatakrishnan CD, *et al.* (2008) HSP27 regulates p53 transcriptional activity in doxorubicin-treated fibroblasts and cardiac H9c2 cells: p21 upregulation and G2/M phase cell cycle arrest. *American journal of physiology. Heart and circulatory physiology* 294(4):H1736-1744.

388. Maejima Y, *et al.* (2008) Induction of premature senescence in cardiomyocytes by doxorubicin as a novel mechanism of myocardial damage. *Aging cell* 7(2):125-136.

389. Eom YW, *et al.* (2005) Two distinct modes of cell death induced by doxorubicin: apoptosis and cell death through mitotic catastrophe accompanied by senescence-like phenotype. *Oncogene* 24(30):4765-4777.

390. Yokochi T & Robertson KD (2004) Doxorubicin inhibits DNMT1, resulting in conditional apoptosis. *Molecular pharmacology* 66(6):1415-1420.

391. Krushkal J, *et al.* (2016) Concerted changes in transcriptional regulation of genes involved in DNA methylation, demethylation, and folate-mediated one-carbon metabolism pathways in the NCI-60 cancer cell line panel in response to cancer drug treatment. *Clinical epigenetics* 8:73.

392. Yamazaki M, *et al.* (2016) Fructose consumption induces hypomethylation of hepatic mitochondrial DNA in rats. *Life sciences* 149:146-152.

393. Anuszewska EL & Koziorowska JH (1999) Capability of adriamycin and busulfan to induce adaptive response in vitro. *Archivum immunologiae et therapiae experimentalis* 47(1):51-54.

394. Jiang X, *et al.* (2018) Low dose radiation prevents doxorubicin-induced cardiotoxicity. *Oncotarget* 9(1):332-345.

395. Boettcher M, *et al.* (2010) High-definition DNA methylation profiles from breast and ovarian carcinoma cell lines with differing doxorubicin resistance. *PloS one* 5(6):e11002.

396. Ramachandran K, *et al.* (2016) Role of DNA Methylation in Cabazitaxel Resistance in Prostate Cancer. *Anticancer research* 36(1):161-168.

397. Cheung KG, *et al.* (2015) Sirtuin-3 (SIRT3) Protein Attenuates Doxorubicin-induced Oxidative Stress and Improves Mitochondrial Respiration in H9c2 Cardiomyocytes. *The Journal of biological chemistry* 290(17):10981-10993.

398. Li D, *et al.* (2013) Doxorubicin-induced apoptosis in H9c2 cardiomyocytes by NF-kappaB dependent PUMA upregulation. *European review for medical and pharmacological sciences* 17(17):2323-2329.

399. Gergely S, *et al.* (2015) High Throughput Screening Identifies a Novel Compound Protecting Cardiomyocytes from Doxorubicin-Induced Damage. *Oxidative medicine and cellular longevity* 2015:178513.

400. Lou Y, *et al.* (2015) Resveratrol prevents doxorubicin-induced cardiotoxicity in H9c2 cells through the inhibition of endoplasmic reticulum stress and the activation of the Sirt1 pathway. *International journal of molecular medicine* 36(3):873-880.

401. Wu R, *et al.* (2011) Reduction in hexokinase II levels results in decreased cardiac function and altered remodeling after ischemia/reperfusion injury. *Circulation research* 108(1):60-69.

402. Kolossov E, *et al.* (2005) Identification and characterization of embryonic stem cell-derived pacemaker and atrial cardiomyocytes. *FASEB journal : official publication of the Federation of American Societies for Experimental Biology* 19(6):577-579.

403. Frank S, *et al.* (2014) Cellular radiation response of mouse embryonic stem cell derived cardiomyocytes. *Scientific Report 2013*, (GSI Helmholtzzentrum für Schwerionenforschung, Darmstadt), Vol 2014-1, p 222 p.

404. Severs NJ, *et al.* (2004) Gap junction alterations in human cardiac disease. *Cardiovascular research* 62(2):368-377.

405. Romero-Calvo I, *et al.* (2010) Reversible Ponceau staining as a loading control alternative to actin in Western blots. *Analytical biochemistry* 401(2):318-320.

406. Sanchez-Alcazar JA, *et al.* (2000) Increased mitochondrial cytochrome c levels and mitochondrial hyperpolarization precede camptothecin-induced apoptosis in Jurkat cells. *Cell death and differentiation* 7(11):1090-1100.

407. Giovannini C, *et al.* (2002) Mitochondria hyperpolarization is an early event in oxidized low-density lipoprotein-induced apoptosis in Caco-2 intestinal cells. *FEBS letters* 523(1-3):200-206.

408. Iijima T, *et al.* (2003) Mitochondrial hyperpolarization after transient oxygen-glucose deprivation and subsequent apoptosis in cultured rat hippocampal neurons. *Brain research* 993(1-2):140-145.

409. Liu MJ, *et al.* (2005) Methyl protodioscin induces G2/M arrest and apoptosis in K562 cells with the hyperpolarization of mitochondria. *Cancer letters* 224(2):229-241.

410. Cao J, *et al.* (2007) Curcumin induces apoptosis through mitochondrial hyperpolarization and mtDNA damage in human hepatoma G2 cells. *Free radical biology & medicine* 43(6):968-975.

411. Carvalho FS, *et al.* (2014) Doxorubicin-induced cardiotoxicity: from bioenergetic failure and cell death to cardiomyopathy. *Medicinal research reviews* 34(1):106-135.

412. Komarov PG, *et al.* (1999) A chemical inhibitor of p53 that protects mice from the side effects of cancer therapy. *Science (New York, N.Y.)* 285(5434):1733-1737.

413. Stindt MH, *et al.* (2011) MDM2 promotes SUMO-2/3 modification of p53 to modulate transcriptional activity. *Cell cycle (Georgetown, Tex.)* 10(18):3176-3188.

414. Zhang W, *et al.* (2015) Targeting Tumor Metabolism for Cancer Treatment: Is Pyruvate Dehydrogenase Kinases (PDKs) a Viable Anticancer Target? *International journal of biological sciences* 11(12):1390-1400.

415. Lagerqvist EL, *et al.* (2015) Comparing mouse and human pluripotent stem cell derived cardiac cells: Both systems have advantages for pharmacological and toxicological screening. *Journal of pharmacological and toxicological methods* 74:17-25.

416. Rajamohan D, *et al.* (2013) Current status of drug screening and disease modelling in human pluripotent stem cells. *BioEssays : news and reviews in molecular, cellular and developmental biology* 35(3):281-298.

417. Koci B, *et al.* (2017) An impedance-based approach using human iPSC-derived cardiomyocytes significantly improves in vitro prediction of in vivo cardiotox liabilities. *Toxicology and applied pharmacology* 329:121-127.

418. Vousden KH & Ryan KM (2009) p53 and metabolism. *Nature reviews. Cancer* 9(10):691-700.

419. Speidel D (2010) Transcription-independent p53 apoptosis: an alternative route to death. *Trends in cell biology* 20(1):14-24.

420. Riley T, *et al.* (2008) Transcriptional control of human p53-regulated genes. *Nature reviews. Molecular cell biology* 9(5):402-412.

421. Melanson BD, *et al.* (2011) The role of mRNA decay in p53-induced gene expression. *RNA (New York, N.Y.)* 17(12):2222-2234.

422. Chipuk JE, *et al.* (2004) Direct activation of Bax by p53 mediates mitochondrial membrane permeabilization and apoptosis. *Science (New York, N.Y.)* 303(5660):1010-1014.

423. Robbins D & Zhao Y (2012) Oxidative Stress Induced by MnSOD-p53 Interaction: Pro- or Anti-Tumorigenic? *Journal of signal transduction* 2012:101465.

424. Candas D & Li JJ (2014) MnSOD in oxidative stress response-potential regulation via mitochondrial protein influx. *Antioxidants & redox signaling* 20(10):1599-1617.

425. Drane P, *et al.* (2001) Reciprocal down-regulation of p53 and SOD2 gene expression-implication in p53 mediated apoptosis. *Oncogene* 20(4):430-439.

426. Marques-Aleixo I, *et al.* (2015) Physical exercise prior and during treatment reduces sub-chronic doxorubicin-induced mitochondrial toxicity and oxidative stress. *Mitochondrion* 20:22-33.

427. Dhar SK, *et al.* (2010) Nuclear factor kappaB- and specificity protein 1-dependent p53-mediated bi-directional regulation of the human manganese superoxide dismutase gene. *The Journal of biological chemistry* 285(13):9835-9846.

428. Zannini L, *et al.* (2014) CHK2 kinase in the DNA damage response and beyond. *Journal of molecular cell biology* 6(6):442-457.

429. Calmettes G, *et al.* (2015) Hexokinases and cardioprotection. *Journal of molecular and cellular cardiology* 78:107-115.

430. Wu R, *et al.* (2012) Hexokinase II knockdown results in exaggerated cardiac hypertrophy via increased ROS production. *EMBO molecular medicine* 4(7):633-646.

431. Ke Q & Costa M (2006) Hypoxia-inducible factor-1 (HIF-1). *Molecular pharmacology* 70(5):1469-1480.

432. Cho J, *et al.* (2008) Dephosphorylation of 2,3-bisphosphoglycerate by MIPP expands the regulatory capacity of the Rapoport-Luebering glycolytic shunt. *Proceedings of the National Academy of Sciences of the United States of America* 105(16):5998-6003.

433. Patel MS & Korotchkina LG (2006) Regulation of the pyruvate dehydrogenase complex. *Biochemical Society transactions* 34(Pt 2):217-222.

434. Sugden MC, *et al.* (2000) Fibre-type specific modification of the activity and regulation of skeletal muscle pyruvate dehydrogenase kinase (PDK) by prolonged starvation and refeeding is associated with targeted regulation of PDK isoenzyme 4 expression. *The Biochemical journal* 346 Pt 3:651-657.

435. Liu MH, *et al.* (2016) Resveratrol inhibits doxorubicin-induced cardiotoxicity via sirtuin 1 activation in H9c2 cardiomyocytes. *Experimental and therapeutic medicine* 12(2):1113-1118.

436. Kavazis AN, *et al.* (2014) Effects of short-term endurance exercise training on acute doxorubicin-induced FoxO transcription in cardiac and skeletal muscle. *Journal of applied physiology (Bethesda, Md. : 1985)* 117(3):223-230.

437. Puthanveetil P, *et al.* (2010) The increase in cardiac pyruvate dehydrogenase kinase-4 after short-term dexamethasone is controlled by an Akt-p38-forkhead box other factor-1 signaling axis. *Endocrinology* 151(5):2306-2318.

438. Piao L, *et al.* (2013) FOXO1-mediated upregulation of pyruvate dehydrogenase kinase-4 (PDK4) decreases glucose oxidation and impairs right ventricular function in pulmonary hypertension: therapeutic benefits of dichloroacetate. *Journal of molecular medicine (Berlin, Germany)* 91(3):333-346.

439. Puthanveetil P, *et al.* (2013) FoxO1 is crucial for sustaining cardiomyocyte metabolism and cell survival. *Cardiovascular research* 97(3):393-403.

440. Zhang S, *et al.* (2014) The pivotal role of pyruvate dehydrogenase kinases in metabolic flexibility. *Nutrition & metabolism* 11(1):10.

441. Zhao G, *et al.* (2008) Overexpression of pyruvate dehydrogenase kinase 4 in heart perturbs metabolism and exacerbates calcineurin-induced cardiomyopathy. *American journal of physiology. Heart and circulatory physiology* 294(2):H936-943.

442. Davies KJ & Doroshow JH (1986) Redox cycling of anthracyclines by cardiac mitochondria. I. Anthracycline radical formation by NADH dehydrogenase. *The Journal of biological chemistry* 261(7):3060-3067.

443. Sutendra G & Michelakis ED (2013) Pyruvate dehydrogenase kinase as a novel therapeutic target in oncology. *Frontiers in oncology* 3:38.

444. Heshe D, *et al.* (2011) Dichloroacetate metabolically targeted therapy defeats cytotoxicity of standard anticancer drugs. *Cancer chemotherapy and pharmacology* 67(3):647-655.

445. van Dalen EC, *et al.* (2006) Clinical heart failure in a cohort of children treated with anthracyclines: a long-term follow-up study. *European journal of cancer (Oxford, England : 1990)* 42(18):3191-3198.

446. Mulrooney DA, *et al.* (2009) Cardiac outcomes in a cohort of adult survivors of childhood and adolescent cancer: retrospective analysis of the Childhood Cancer Survivor Study cohort. *BMJ (Clinical research ed.)* 339:b4606.

447. Litinski M, *et al.* (2009) Influence of the Circadian System on Disease Severity. *Sleep medicine clinics* 4(2):143-163.

448. West AC, *et al.* (2017) Misalignment with the external light environment drives metabolic and cardiac dysfunction. 8(1):417.

449. Young ME & Bray MS (2007) Potential role for peripheral circadian clock dyssynchrony in the pathogenesis of cardiovascular dysfunction. *Sleep medicine* 8(6):656-667.

450. Alcendor RR, *et al.* (2007) Sirt1 regulates aging and resistance to oxidative stress in the heart. *Circulation research* 100(10):1512-1521.

451. Wang S, *et al.* (2012) Inhibition of AMP-activated protein kinase alpha (AMPKalpha) by doxorubicin accentuates genotoxic stress and cell death in mouse embryonic fibroblasts and cardiomyocytes: role of p53 and SIRT1. *The Journal of biological chemistry* 287(11):8001-8012.

452. Osman AM, *et al.* (2013) Chemosensetizing and cardioprotective effects of resveratrol in doxorubicin- treated animals. *Cancer cell international* 13:52.

453. Zhang C, *et al.* (2011) Resveratrol attenuates doxorubicin-induced cardiomyocyte apoptosis in mice through SIRT1-mediated deacetylation of p53. *Cardiovascular research* 90(3):538-545.

454. Wang S, *et al.* (2017) Cardioprotective effects of fibroblast growth factor 21 against doxorubicin-induced toxicity via the SIRT1/LKB1/AMPK pathway. *Cell death & disease* 8(8):e3018.

455. Cui L, *et al.* (2017) Erythropoietin activates SIRT1 to protect human cardiomyocytes against doxorubicin-induced mitochondrial dysfunction and toxicity. *Toxicology letters* 275:28-38.

456. Zhu JN, *et al.* (2017) Activation of miR-34a-5p/Sirt1/p66shc pathway contributes to doxorubicin-induced cardiotoxicity. *Scientific reports* 7(1):11879.

457. Heart EA, *et al.* (2016) Mechanisms of Doxorubicin Toxicity in Pancreatic beta-Cells. *Toxicological sciences : an official journal of the Society of Toxicology* 152(2):395-405.

458. Wang B, *et al.* (2014) NAD(+) administration decreases doxorubicin-induced liver damage of mice by enhancing antioxidation capacity and decreasing DNA damage. *Chemico-biological interactions* 212:65-71.

459. Travnickova-Bendova Z, *et al.* (2002) Bimodal regulation of mPeriod promoters by CREB-dependent signaling and CLOCK/BMAL1 activity. *Proceedings of the National Academy of Sciences of the United States of America* 99(11):7728-7733.

460. Balsalobre A, *et al.* (2000) Resetting of circadian time in peripheral tissues by glucocorticoid signaling. *Science (New York, N.Y.)* 289(5488):2344-2347.

461. Schmieder R, *et al.* (2012) Identification and removal of ribosomal RNA sequences from metatranscriptomes. *Bioinformatics (Oxford, England)* 28(3):433-435.

462. Langmead B & Salzberg SL (2012) Fast gapped-read alignment with Bowtie 2. *Nature methods* 9(4):357-359.

463. Filiano AN, *et al.* (2013) Chronic ethanol consumption disrupts the core molecular clock and diurnal rhythms of metabolic genes in the liver without affecting the suprachiasmatic nucleus. *PloS one* 8(8):e71684.

464. Bonnefont JP, *et al.* (2004) Carnitine palmitoyltransferases 1 and 2: biochemical, molecular and medical aspects. *Molecular aspects of medicine* 25(5-6):495-520.

465. Nemoto S, *et al.* (2005) SIRT1 functionally interacts with the metabolic regulator and transcriptional coactivator PGC-1{alpha}. *The Journal of biological chemistry* 280(16):16456-16460.

466. Cheng HL, *et al.* (2003) Developmental defects and p53 hyperacetylation in Sir2 homolog (SIRT1)-deficient mice. *Proceedings of the National Academy of Sciences of the United States of America* 100(19):10794-10799.

467. Balsalobre A, *et al.* (1998) A serum shock induces circadian gene expression in mammalian tissue culture cells. *Cell* 93(6):929-937.

468. Gertz M, *et al.* (2013) Ex-527 inhibits Sirtuins by exploiting their unique NAD+-dependent deacetylation mechanism. *Proceedings of the National Academy of Sciences of the United States of America* 110(30):E2772-2781.

469. Ghibu S, *et al.* (2012) General oxidative stress during doxorubicin-induced cardiotoxicity in rats: absence of cardioprotection and low antioxidant efficiency of alpha-lipoic acid. *Biochimie* 94(4):932-939.

470. Sacco G, *et al.* (2003) Chronic cardiotoxicity of anticancer anthracyclines in the rat: role of secondary metabolites and reduced toxicity by a novel anthracycline with impaired metabolite formation and reactivity. *British journal of pharmacology* 139(3):641-651.

471. O'Connell JL, *et al.* (2017) Short-term and long-term models of doxorubicin-induced cardiomyopathy in rats: A comparison of functional and histopathological changes. *Experimental and toxicologic pathology : official journal of the Gesellschaft fur Toxikologische Pathologie* 69(4):213-219.

472. Langenickel T, *et al.* (2000) Differential regulation of cardiac ANP and BNP mRNA in different stages of experimental heart failure. *American journal of physiology. Heart and circulatory physiology* 278(5):H1500-1506.

473. Takei Y, *et al.* (2011) B-type natriuretic peptide (BNP), not ANP, is the principal cardiac natriuretic peptide in vertebrates as revealed by comparative studies. *General and comparative endocrinology* 171(3):258-266.

474. Del Ry S, *et al.* (2014) Natriuretic peptide system and the heart. *Frontiers of hormone research* 43:134-143.

475. Piotrowska I, *et al.* (2017) Early transcriptional alteration of histone deacetylases in a murine model of doxorubicin-induced cardiomyopathy. 12(6):e0180571.

476. Ekstein S, *et al.* (2007) N-terminal-proB-type natriuretic peptide as a marker for acute anthracycline cardiotoxicity in children. *Journal of pediatric hematology/oncology* 29(7):440-444.

477. Cho H, *et al.* (2012) Regulation of circadian behaviour and metabolism by REV-ERB-alpha and REV-ERB-beta. *Nature* 485(7396):123-127.

478. Sengupta S, *et al.* (2016) The circadian gene Rev-erbalpha improves cellular bioenergetics and provides preconditioning for protection against oxidative stress. *Free radical biology & medicine* 93:177-189.

479. Yang G, *et al.* (2014) Oxidative stress and inflammation modulate Rev-erbalpha signaling in the neonatal lung and affect circadian rhythmicity. *Antioxidants & redox signaling* 21(1):17-32.

480. Huang Y, *et al.* (2009) Type I interferons and interferon regulatory factors regulate TNF-related apoptosis-inducing ligand (TRAIL) in HIV-1-infected macrophages. *PloS one* 4(4):e5397.

481. Kim TK, *et al.* (2000) Chemotherapeutic DNA-damaging drugs activate interferon regulatory factor-7 by the mitogen-activated protein kinase kinase-4-cJun NH2-terminal kinase pathway. *Cancer research* 60(5):1153-1156.

482. Kim T, *et al.* (1999) Activation of interferon regulatory factor 3 in response to DNA-damaging agents. *The Journal of biological chemistry* 274(43):30686-30689.

483. Siu WY, *et al.* (1999) G1 versus G2 cell cycle arrest after adriamycin-induced damage in mouse Swiss3T3 cells. *FEBS letters* 461(3):299-305.

484. Lupertz R, *et al.* (2010) Dose- and time-dependent effects of doxorubicin on cytotoxicity, cell cycle and apoptotic cell death in human colon cancer cells. *Toxicology* 271(3):115-121.

485. Terrand J, *et al.* (2011) p21(WAF1/Cip1/Sdi1) knockout mice respond to doxorubicin with reduced cardiotoxicity. *Toxicology and applied pharmacology* 257(1):102-110.

486. Tanaka N, *et al.* (1996) Cooperation of the tumour suppressors IRF-1 and p53 in response to DNA damage. *Nature* 382(6594):816-818.

487. Miyazaki M, *et al.* (2004) Involvement of interferon regulatory factor 1 and S100C/A11 in growth inhibition by transforming growth factor beta 1 in human hepatocellular carcinoma cells. *Cancer research* 64(12):4155-4161.

488. Hallows WC, *et al.* (2006) Sirtuins deacetylate and activate mammalian acetyl-CoA synthetases. *Proceedings of the National Academy of Sciences of the United States of America* 103(27):10230-10235.

489. Danz ED, *et al.* (2009) Resveratrol prevents doxorubicin cardiotoxicity through mitochondrial stabilization and the Sirt1 pathway. *Free radical biology & medicine* 46(12):1589-1597.

490. Rharass T, *et al.* (2016) Oxidative stress does not play a primary role in the toxicity induced with clinical doses of doxorubicin in myocardial H9c2 cells. *Molecular and cellular biochemistry* 413(1-2):199-215.

491. Ingwall JS (2009) Energy metabolism in heart failure and remodelling. *Cardiovascular research* 81(3):412-419.

492. Anderson KA & Hirschey MD (2012) Mitochondrial protein acetylation regulates metabolism. *Essays in biochemistry* 52:23-35.